

DOCTOR OF PHILOSOPHY

Modelling and simulation of biomass  
gasification in a circulating fluidized bed  
reactor

Mohamed Hassan

2013

Aston University

**Some pages of this thesis may have been removed for copyright restrictions.**

If you have discovered material in AURA which is unlawful e.g. breaches copyright, (either yours or that of a third party) or any other law, including but not limited to those relating to patent, trademark, confidentiality, data protection, obscenity, defamation, libel, then please read our [Takedown Policy](#) and [contact the service](#) immediately

# **MODELLING AND SIMULATION OF BIOMASS GASIFICATION IN A CIRCULATING FLUIDIZED BED REACTOR**

**MOHAMED IBRAHIM OSMAN HASSAN**

**Doctor of Philosophy**

**ASTON UNIVERSITY**

**June 2013**

© Mohamed Hassan, 2013

Mohamed Hassan asserts his moral right to be identified as the author of this thesis

This copy of the thesis has been supplied on condition that anyone who consults it is understood to recognise that its copyright rests with its author and that no quotation from the thesis and no information derived from it may be published without proper acknowledgement.

# Aston University

Modelling and simulation of biomass gasification in a circulating fluidized bed reactor

Mohamed Ibrahim Osman Hassan

Doctor of Philosophy

2013

## Thesis summary

Computational Fluid Dynamics (CFD) has found great acceptance among the engineering community as a tool for research and design of processes that are practically difficult or expensive to study experimentally. One of these processes is the biomass gasification in a Circulating Fluidized Bed (CFB). Biomass gasification is the thermo-chemical conversion of biomass at a high temperature and a controlled oxygen amount into fuel gas, also sometime referred to as syngas. Circulating fluidized bed is a type of reactor in which it is possible to maintain a stable and continuous circulation of solids in a gas-solid system.

The main objectives of this thesis are four folds: (i) Develop a three-dimensional predictive model of biomass gasification in a CFB riser using advanced Computational Fluid Dynamic (CFD) (ii) Experimentally validate the developed hydrodynamic model using conventional and advanced measuring techniques (iii) Study the complex hydrodynamics, heat transfer and reaction kinetics through modelling and simulation (iv) Study the CFB gasifier performance through parametric analysis and identify the optimum operating condition to maximize the product gas quality.

Two different and complimentary experimental techniques were used to validate the hydrodynamic model, namely pressure measurement and particle tracking. The pressure measurement is a very common and widely used technique in fluidized bed studies, while, particle tracking using PEPT, which was originally developed for medical imaging, is a relatively new technique in the engineering field. It is relatively expensive and only available at few research centres around the world.

This study started with a simple poly-dispersed single solid phase then moved to binary solid phases. The single solid phase was used for primary validations and eliminating unnecessary options and steps in building the hydrodynamic model. Then the outcomes from the primary validations were applied to the secondary validations of the binary mixture to avoid time consuming computations. Studies on binary solid mixture hydrodynamics is rarely reported in the literature. In this study the binary solid mixture was modelled and validated using experimental data from the both techniques mentioned above. Good agreement was achieved with the both techniques.

According to the general gasification steps the developed model has been separated into three main gasification stages; drying, devolatilization and tar cracking, and partial combustion and gasification. The drying was modelled as a mass transfer from the solid phase to the gas phase. The devolatilization and tar cracking model consist of two steps; the devolatilization of the biomass which is used as a single reaction to generate the biomass gases from the volatile materials and tar cracking. The latter is also modelled as one reaction to generate gases with fixed mass fractions. The first reaction was classified as a heterogeneous reaction while the second reaction was classified as homogenous reaction. The partial combustion and gasification model consisted of carbon combustion reactions and carbon and gas phase reactions. The partial combustion considered was for C, CO, H<sub>2</sub> and CH<sub>4</sub>. The carbon gasification reactions used in this study is the Boudouard reaction with CO<sub>2</sub>, the reaction with H<sub>2</sub>O and Methanation (Methane forming reaction) reaction to generate methane. The other gas phase reactions considered in this study are the water gas shift reaction, which is modelled as a reversible reaction and the methane steam reforming reaction.

The developed gasification model was validated using different experimental data from the literature and for a wide range of operating conditions. Good agreement was observed, thus confirming the capability of the model in predicting biomass gasification in a CFB to a great accuracy. The developed model has been successfully used to carry out sensitivity and parametric analysis. The sensitivity analysis included: study of the effect of inclusion of various combustion reaction; and the effect of radiation in the gasification reaction. The developed model was also used to carry out parametric analysis by changing the following gasifier operating conditions: fuel/air ratio; biomass flow rates; sand (heat carrier) temperatures; sand flow rates; sand and biomass particle sizes; gasifying agent (pure air or pure steam); pyrolysis models used; steam/biomass ratio. Finally, based on these parametric and sensitivity analysis a final model was recommended for the simulation of biomass gasification in a CFB riser.

**Keywords: biomass gasification, computational fluid dynamic, two-fluid model, circulating fluidized bed, simulation**

(وَيَسْأَلُونَكَ عَنِ الرُّوحِ قُلِ الرُّوحُ مِنْ أَمْرِ رَبِّي وَمَا أُوتِيتُمْ مِنَ الْعِلْمِ إِلَّا قَلِيلًا )

(They ask thee concerning the Spirit (of inspiration). Say: "The Spirit (cometh) by command of my Lord of knowledge it is only a little that is communicated to you (O men!))

[Holy Quran ( Al-Isra (85)]

This thesis is dedicated to:

*My parents;*

*My wife;*

*My Children*

## **ACKNOWLEDGEMENTS**

Firstly, I would like to thank GOD for the health which sustain us to do every single motion.

Then I would like to express my deepest appreciation to my supervisor Dr. Yassir Makkawi for his patience, support and advices. I thank him for his patience in explaining the knowledge; for his support on both an academic and a personal level; for his advices and guidance which helped me in all the time of research and writing of this thesis.

## Table of Contents

1. Chapter 1: Introduction and Background .....	20
1.1. Background.....	20
1.1.1. Biomass .....	20
1.1.2. Biomass gasification .....	20
1.1.3. Circulating fluidized bed (CFB).....	21
1.1.4. Modelling of multiphase flow .....	23
1.2. Objectives .....	25
1.3. Summary of chapters .....	26
2. Chapter 2: Experimental settings and procedure .....	29
2.1. Introduction .....	29
2.2. Cold flow Circulating Fluidized Bed (CFB).....	29
2.2.1. Riser .....	30
2.2.2. Return leg (downer) .....	31
2.2.3. Rotameters .....	32
2.2.4. Cyclone.....	33
2.3. Operating procedure .....	34
2.4. Pressure measurements and data logging .....	36
2.5. Particle tracking.....	37
2.6. Experimental raw data Analysis .....	39
2.7. Conclusion .....	41
3. Chapter 3: Hydrodynamics simulations and validations .....	42
3.1. Introduction .....	42
3.2. Literature review.....	42
3.2.1. Hydrodynamic experimental investigation in CFB.....	43
3.2.2. Simulating Fluidized Bed Hydrodynamics .....	44
3.2.3. Exit and entrance effect.....	54
3.2.4. Acceleration, fully developed and deceleration zones in the riser.....	55
3.3. Developing CFB hydrodynamic model .....	56
3.3.1. Simulation Geometry.....	56
3.3.2. Mesh, grid and time step setting.....	57
3.3.3. Model equations.....	58
3.3.4. Model constitutive equations .....	59
3.3.5. Gas-Solid momentum exchange .....	60
3.3.6. Solid pressure model and radial distribution function.....	61
3.3.7. Radial distribution function .....	62
3.3.8. Boundary conditions.....	63

3.4.	Validation and verification of the hydrodynamic model for one solid phase .....	63
3.4.1.	Validation using pressure measurements.....	64
3.4.2.	Meshing (cell size) and solution time step .....	75
3.4.3.	Hydrodynamic model validation using PEPT technique.....	77
3.4.4.	Interesting hydrodynamic features of the CFB gasifier .....	79
3.4.5.	Final Hydrodynamic model.....	81
3.5.	Conclusion .....	82
4.	Chapter 4: Modeling of biomass Gasification (reactive system).....	84
4.1.	Introduction .....	84
4.2.	Literature review.....	84
4.2.1.	Fundamentals of biomass gasification.....	84
4.2.2.	Modelling of the biomass drying .....	90
4.2.3.	Modelling of the biomass devolatilization .....	92
4.2.4.	Modelling of the biomass partial combustion and gasification .....	98
4.3.	Proposed gasification reactions model .....	102
4.3.1.	The Laminar finite rate model.....	102
4.3.2.	Drying model.....	103
4.3.3.	Devolatilization and tar cracking model .....	104
4.3.4.	Partial combustion and gasification model .....	107
4.3.5.	Heat transfer model.....	110
4.4.	Conclusion .....	112
5.	Chapter 5: Simulation of a CFB biomass gasifier .....	117
5.1.	Introduction .....	117
5.2.	Literature review.....	117
5.2.1.	One-dimensional CFD models .....	117
5.2.2.	Two-dimensional CFD models .....	120
5.2.3.	Three-dimensional CFD models.....	122
5.2.4.	Other non-CFD models .....	123
5.2.5.	Conclusion of the literature review .....	132
5.3.	The base case .....	133
5.3.1.	Reactor geometry, solids properties and operating conditions.....	134
5.3.2.	Properties, initial and boundary conditions of the biomass and gases .....	135
5.4.	Preliminary mass and energy balance.....	138
5.4.1.	Mass Balance .....	139
5.4.2.	Energy Balance.....	143
5.5.	Simulation results for the base case.....	147
5.5.1.	Hot flow hydrodynamic predictions of the CFB riser .....	147
5.5.2.	Temperature distribution prediction in the CFB riser.....	151

5.5.3.	Reactions and product gases in the CFB riser .....	153
5.5.4.	Time series data of product gas composition .....	156
5.6.	.....	158
5.7.	Conclusions .....	158
6.	Chapter 6: Model sensitivity analysis and comparisons.....	160
6.1.	Literature review.....	160
6.1.1.	Studies on comparison of gasification models.....	160
6.1.2.	Options on modeling the combustion reactions .....	163
6.1.3.	Studies on modeling the heat of radiation .....	165
6.1.4.	Conclusion of the literature review .....	167
6.2.	Results of the model sensitivity analysis .....	168
6.2.1.	Effect of combustion reactions .....	168
6.2.2.	Effect of radiation on the model predictions.....	173
6.3.	Interim conclusion on the sensitivity analysis .....	175
6.4.	Results of model comparisons .....	176
6.5.	Conclusion .....	178
7.	Chapter 7: Parametric analysis of the gasifier model.....	179
7.1.	Introduction: .....	179
7.2.	Literature review.....	179
7.2.2.	Studies on the Effect of temperature .....	185
7.2.3.	Studies on the effect of biomass feed rate .....	187
7.2.4.	Studies on the effect of inert solid and biomass size .....	188
7.2.5.	Conclusion of the literature review .....	193
7.3.	Results of parameters variations .....	194
7.3.1.	Variations of the air ratio .....	194
7.3.2.	Variation of the biomass feed rate.....	197
7.3.3.	Variations of gasifier temperature.....	199
7.3.4.	Variation of the sand (heat carrier) flow rate.....	203
7.3.5.	Variations of the sand size .....	205
7.3.6.	Variation of the biomass size .....	207
7.3.7.	Operating with pure air.....	209
7.3.8.	Operating with pure steam .....	211
7.3.9.	Variations of steam/biomass ratio .....	213
7.4.	Conclusions .....	217
8.	Chapter 8: Achievements, conclusions and Recommendations .....	220
8.1.	Introduction: .....	220
8.2.	Summary of the achievements .....	220
8.3.	Conclusions .....	222

8.3.1.	The hydrodynamic and heat transfer models.....	222
8.3.2.	The reactive model.....	223
8.3.3.	Parametric analysis.....	224
8.4.	Recommendations .....	224
8.4.1.	The effect of the high temperature on the CFB hydrodynamics .....	224
8.4.2.	Developing new heat transfer coefficient for dilute gas-solid flow .....	225
8.4.3.	Modeling of devolatilization.....	225
	References.....	226
	Appendix A: Sample of raw PEPT data .....	238
	Appendix B: User Defined Function for the heterogeneous reactions .....	239

## List of Tables

Table 2.1 Rotameters specifications.....	33
Table 2.2 The experiments operating conditions in the CFB riser used in the PEPT system experiment .....	38
Table 3.1 Drag force models .....	47
Table 3.2 Turbulence formulations which have been tested (Hartge et al., 2009).....	50
Table. 3.3. The setting of the mesh .....	58
Table 3.4 Constitutive equations .....	60
Table 3.5 Various forms of the radial distribution function .....	62
Table 3.6 The final proposed hydrodynamic model for the CFB riser .....	81
Table 4.1 Arrhenius law constants for calculating the rate of wood devolatilization (Grønli and Melaaen, 2000) .....	94
Table 4.2 Pyrolysis gases fractions as reported in the literature .....	94
Table 4.3 Kinetic constants for one-stage global pyrolysis reaction for different materials (Basu, 2010a).....	95
Table 4.4 Composition of wood gas from the primary pyrolysis step (Gerber et al., 2010)....	96
Table 4.5 Composition of intermediate and inert tar for secondary pyrolysis models 1 and 2 used by (Gerber et al., 2010).....	96
Table 4.6 Wood gas composition from secondary pyrolysis for model 1 and model 2 used by (Gerber et al., 2010).....	97
Table 4.7 Kinetic constants for combustion reactions .....	99
Table 4.8 Arrhenius law constants for heterogeneous gasification reactions .....	100
Table 4.9 Kinetic constants for heterogeneous reactions from the literature .....	102
Table 4.10 The composition of the gas (Ragland et al., 1991).....	106
Table 4.11 Composition of the gases released during tar cracking (Gerber et al., 2010) ..	106
Table 4.12 The kinetic constants gas shift and methane reforming reactions .....	110
Table 4.13 Summary of the mass transfer model for biomass drying .....	114
Table 4.14 Summary of the reactions and the rate of reactions used in this study for the simulation of the CFB biomass gasification .....	114
Table 5.1 Summary of recent studies on modeling of biomass gasification in bubbling and circulating fluidized beds .....	128
Table 5.2 The properties of the biomass fuel and sand .....	135
Table 5.3: The constants used in calculating the specific heat capacities of the gas components for $300 \leq T < 1000$ .....	137
Table 5.4: The constants used in calculating the specific heat capacities of the gas components for $1000 \leq T < 5000$ .....	137
Table: 5.5 Composition of the biomass used in the simulation of the base case (Telmo et al., 2010).....	137
Table: 5.6 The composition of the gas (Ragland et al., 1991).....	138
Table 5.7 The tar from the primary de-volatilization step (Gerber et al., 2010).....	138
Table 5.8 Composition of the gases released during tar cracking (Gerber et al., 2010)....	138
Table 5.9. Mass flow rate calculations based on biomass composition given by Ragland et al. (1991) Assumed biomass federate of 2 g/s. ....	139
Table. 5.10. Mass balance calculation of the volatiles produced from biomass pyrolysis....	140
Table 5.11 Proposed gasification reactions, heat of reactions, heat required for drying.....	140
Table.5.12. Material balance calculations for Heterogeneous and homogeneous reactions .....	143
Table 5.13 Overall material balance and HHV calculations for the 2 g/s biomass gasification .....	144

Table 5.14 Estimated heat of reactions and drying during the gasification of 2 g/s biomass feed.....	145
Table 5.15 Total heat in.....	146
Table 5.16 Total heat out.....	146
Table 5.17 The CFB gasifier operating conditions considered in the base case .....	147
Table 6.1 Comparison of prediction and experimental product gas composition (Miao et al., 2013).....	163
Table 6.2 Operating conditions for the results shown in Fig. 6.5.....	169
Table 6.3 operating conditions for the simulation results shown in Fig. 6.6. the velocities of gas sand and biomass were calculated using volume weighted and time average.....	171
Table 6.4 Operating conditions.....	173
Table 7.1 Summary of studies on parametric analysis of biomass gasification in circulating and bubbling fluidized beds (CFB and BFB) .....	189
Table 7.2. Operating conditions for the simulation results shown in Fig. 7.7. The velocities of gas sand and biomass shown in this Table were calculated using volume weighted and time average.....	197
Table 7.3. operating conditions for Fig. 7.8. the velocities of gas sand and biomass were calculated using volume weighted and time average.....	199
Table 7.4. Operating conditions for the results shown in Fig. 7.9. The velocities of gas, sand and biomass were calculated using volume weighted and time average. ....	202
Table 7.5 Operating conditions for the results shown in Fig. 7.11. The velocities of the gas, sand and biomass phases were calculated using volume weighted and time average. ....	205
Table 7.6 operating conditions for Fig. 7.12 the velocities of gas sand and biomass were calculated using volume weighted and time average.....	207
Table 7.7 operating conditions for Fig. 7.13. the velocities of gas sand and biomass were calculated using volume weighted and time average.....	209
Table 7.8 Operating conditions for the results shown in Fig. 7.14. The velocities of gas sand and biomass were calculated using volume weighted and time average. ....	211
Table 7.9 operating conditions for Fig. 7.15 the velocities of gas sand and biomass were calculated using volume weighted and time average.....	213
Table 7.10 Operating conditions for the simulation results shown in Fig. 7.16. The velocities of gas sand and biomass were calculated using volume weighted and time average. ....	215
Table 7.11 operating conditions for Fig. 7.17. The velocities of gas sand and biomass were calculated using volume weighted and time average.....	217
Table. 8.1. Proposed hydrodynamic model constitutive relations.....	223

## List of Figures

Fig.1.1. Main types of a circulating fluidized bed biomass gasifier (a) single loop system (Chan et al., 2009c) (b) Two loop system (Pfeifer and Hofbauer, 2008) .....	23
Fig. 2.1. Details of the circulating fluidized bed arrangement, dimensions and attached instrumentations .....	30
Fig. 2.2. The distance between the pressure taps in the riser of the CFB. ....	31
Fig. 2.3. Receiving tank for transferring solids between the downer and riser sides of the CFB .....	32
Fig. 2.4 . The two rotameters supplying air to the CFB system. ....	33
Fig. 2.5. Dimensions of the main cyclone attached to the CFB system. ....	34
Fig. 2.6. The Pressure Transducers connected to the pressure taps in the CFB riser. ....	36
Fig. 2.7. (a) The schematic of the PEPT setup (All dimensions are in cm). (b) PEPT equipment in Birmingham university .....	38
Fig. 2.8. Example of raw time-series pressure data produced at four different selected locations along the riser height. The operating conditions are for Run#1 given in Table 2.2. ....	39
Fig.2.9. Time average pressure vs. height in the CFB riser. The operating conditions are for Run#1 given in Table 2.2.....	40
Fig. 2.10. PET data of particle vertical velocity (glass beads) recorded during 60 seconds of the CFB operation. ....	40
Fig. 2.11. PEPT data of particle vertical velocity (glass bead) recorded during 1.2s of the CFB operation. ....	41
Fig. 3.1. Comparison of time-averaged voidage distributions for CFB based on different drag models (Zhou et al., 2011).....	44
Fig. 3.2. Distributions of simulated and measured bed density in a bubbling fluidized bed (Wang et al., 2013).....	48
Fig. 3.3. Comparison of time averaged distribution of solids inside a CFB riser using different turbulence models (Hartge et al., 2009).....	51
Fig. 3.4. Distributions of instantaneous particle volume fraction in a bubbling fluidized bed (a) mixture turbulence model (b) disperse turbulence model (Wang et al., 2013).....	52
Fig. 3.5. Schematic drawing of 2-D riser with inlet and initial conditions (Benyahia et al., 2000).....	53
Fig. 3.6. Schematic diagram of a circulating fluidized bed reactor (Sabbaghan et al., 2004).....	56
Fig. 3.7. simulation geometry .....	57
Fig. 3.8. Experimental and simulation pressure verses height for four different glass beads sizes.....	64
Fig. 3.9. Laminar and different turbulence models against experimental data. Using 755 $\mu$ m glass beads, 600 lit/min gas flow and 36.42g/s solid mass flow.....	65
Fig. 3.10. Comparison of the different gas-solid drag models (momentum exchange) tested in the simulation of a monodispersed solid mixture. (a) particle size of 755 $\mu$ m glass beads, 600 lit/min gas flow (velocity of 4.71 m/s) and 36.42 g/s solid mass flow (b) particle used of 409 $\mu$ m glass beads, 405 lit/min gas flow (velocity of 3.18 m/s) and 23.0 g/s solid mass flow. ...	66
Fig. 3.11. Validation and sensitivity analysis of the model to the gas-solid and solid-solid momentum exchange coefficient for the case of a polydispersed binary mixture of glass beads. Phase 1 of $d_s = 755 \mu\text{m}$ , $\rho_s = 2500 \text{ kg/m}^3$ ) and Phase 2 of $d_s = 376 \mu\text{m}$ , $\rho_s = 2500 \text{ kg/m}^3$ with the mixing ratio of 83 wt% to 17 wt% respectively. The CFB riser was operating at a fluidization velocity of 3.6 m/s and a total solid feeding rate of 35 g/s. ....	67
Fig. 3.12. Pressures verses height for different granular temperature models. Using 755 $\mu$ m glass beads, 600 lit/min gas flow and 36.42g/s solid mass flow.....	68
Fig. 3.13. Different friction correlations with experiment pressure data along the riser. Using 755 $\mu$ m glass beads, 600 lit/min gas flow and 36.42g/s solid mass flow .....	71

Fig. 3.14. Pressures verses height for different radial distribution correlations. Using 755 $\mu$ m glass beads, 600 lit/min gas flow and 36.42g/s solid mass flow.....	72
Fig. 3.15. Comparison of different radial distribution functions for a polydispersed solid mixture as function of the total mixture solid concentration. Calculation carried out with respect to the larger size for a mixture of particles size ratio of $d_1 : d_2 = 755 : 400$ .....	73
Fig. 3.16. Sensitivity analysis of the model to the radial distribution function the case of a polydispersed binary mixture of glass beads. Phase 1 of $d_s = 755 \mu\text{m}$ , $\rho_s = 2500 \text{ kg/m}^3$ ) and Phase 2 of $d_s = 376 \mu\text{m}$ , $\rho_s = 2500 \text{ kg/m}^3$ with the mixing ratio of 83 wt% to 17 wt% respectively. The CFB riser was operating at a fluidization velocity of 3.6 m/s and a total solid feeding rate of 35 g/s.....	74
Fig. 3.17. Pressures verses height for different solids pressure correlations. Using 755 $\mu$ m glass beads, 600 lit/min gas flow and 36.42 g/s solid mass flow.....	75
Fig.3.18. Time step sensitivity analysis for the same operating conditions. Using 755 $\mu$ m glass beads, 600 lit/min gas flow and 36.42g/s solid mass flow. ....	76
Fig. 3.19. Grid sensitivity analysis using three different grid sizes. Using 755 $\mu$ m glass beads, 600 lit/min gas flow and 36.42g/s solid mass flow .....	77
Fig. 3.20. PEPT experiment result using glass beads ( $d_s = 755 \mu\text{m}$ , $\rho_s = 2500 \text{ kg/m}^3$ ) with total air flow of 600 lit/min. (a) Vertical velocity of the radioactive particle (m/s) verses time ms. (b) Vertical position of the radioactive particle (cm) verses time (ms).....	78
Fig. 3.21. Comparison of predicted and measured solid velocity for the case of a polydispersed binary mixture of glass beads ( $d_s = 755 \mu\text{m}$ , $\rho_s = 2500 \text{ kg/m}^3$ ) and wood ( $d_s = 1000 \mu\text{m}$ , $\rho_s = 585 \text{ kg/m}^3$ ).....	79
Fig. 3.22. Acceleration, developed and deceleration zones for two solids. ....	80
Fig. 3.23. Radial profiles of solid distribution and velocity for a binary mixture (wood and sand) at two different heights in the CFB riser .....	81
Fig. 4.1. Potential paths for gasification (Basu, 2010b).....	85
Fig. 4.2. Stages of gasification and temperature distribution in various types of biomass thermochemical conversion reactors (a) downdraft gasifier (b) throated-type downdraft gasifier (d) bubbling fluidized-bed gasifier (d) circulating fluidized bed reactor. Figs (a)–(c) are reported by (Basu, 2010b) and (d) is reported by (Makkawi, 2013). ....	86
Fig. 4.3. Schematic description of devolatilization (pyrolysis) in a biomass particle (Basu, 2010b).....	88
Fig. 4.4 . One-component mechanism of primary wood pyrolysis proposed by Shafizadeh and Chin (1977). ....	92
Fig. 4.5. Kinetic scheme used in the devolatilization model of (Grønli and Melaaen, 2000). .	93
Fig. 4.6. The bath of the biomass in the first step of devolatilization (Makkawi, 2013). ....	105
Fig. 4.7. The bath of the biomass in the secondary step of devolatilization (tar cracking) ..	107
Fig. 5.1. Example of uncoupled CFB gasification process simulated using ASPEN Plus (Doherty et al. 2009).....	126
Fig. 5.2. A typical ASPEN Plus flow sheet for biomass gasification in a CFB gasifier (Doherty et al. 2009). ....	127
Fig. 5.3. The schematic geometry and dimensions of the CFB riser used for the simulation of the reactive system .....	134
Fig. 5.4. The composition of the final gas product estimated for each component individually by adding all the generated products in dry basis.....	142
Fig. 5.5. Volume fractions of biomass and sand in the CFB riser for the base case simulation. The detailed operating conditions are given in Table 5.17. ....	148

Fig. 5.6. Sand velocity vectors at inlet to the CFB riser. Detailed operating conditions are given in Table 5.17. ....	149
Fig. 5.7. Vertical velocity of gas, biomass and sand in the CFB riser. Detailed operating conditions are given in Table 5.17. ....	150
Fig. 5.8. Temperature distribution of the gas, biomass and sand phases along the CFB riser for the base case. The detailed operating conditions are given in Table 5.17. ....	152
Fig. 5.9. Contours of the heterogeneous reactions rates (kmol/m <sup>3</sup> s) in the CFB riser. The detailed operating conditions are given in Table 5.17. ....	154
Fig. 5.10. Contours of the homogenous reactions rates (kmol/m <sup>3</sup> s) in the CFB riser. The detailed operating conditions are given in Table 5.17. ....	156
Fig. 5.11. Product gas mole fractions versus time at the outlet of the CFB riser. The detailed operating conditions are given in Table 5.17. ....	157
Fig. 5.12 Gas phase temperature data versus time at the outlet of the reactor. ....	158
Fig. 5.13. Concentrations of some components in the product gas for the base case in dry basis. ....	158
Fig. 6.1. Product gas composition and tar content for two different secondary pyrolysis models used. (Gerber et al., 2010). ....	162
Fig. 6.2. Gas species and bed temperature along the CFB height (Miao et al., 2013). ....	163
Fig. 6.3. Temperature, absorption coefficients of gas and particles distribution estimated in a CFB coal gasifier (Gräbner et al., 2007). ....	166
Fig. 6.4. Comparison of predicted and measured axial temperature of the gasifier ((Gao et al., 2012). ....	167
Fig. 6.5 . Comparison between the model predictions for the case of full combustion reactions (C, CO, H <sub>2</sub> and CH <sub>4</sub> ) and the case of CO and C combustions only (ignoring H <sub>2</sub> and CH <sub>4</sub> combustion) using steam/air as fluidizing agent (a) HHV of the product gas in (b) outlet temperature of char (c) outlet gas flow (d) tar yield (e) gas species molar concentrations (f) species mass fractions in the outlet. The operating conditions used in the simulation are given in Table 6.2. ....	170
Fig. 6.6 . Comparison between the model predictions for the case of full combustion reactions (CO, CO <sub>2</sub> , H <sub>2</sub> and CH <sub>4</sub> ) and the case of CO and H <sub>2</sub> combustions only using pure air as fluidizing agent. (a) The HHV of the product gas in (MJ/Nm <sup>3</sup> ). (b) The outlet temperature of biomass (K). (c) Tar yield (g/Nm <sup>3</sup> ) (e) Gas species molar concentrations. (f) Char species mass fractions in the outlet. The operating conditions used in the simulation are given in Table 6.4. ....	172
Fig. 6.7. Simulation results with and without inclusion of radiation term in the model (a) sand temperature (b) wood temperature (c) gas temperature (d) absorption coefficient contours (1/m) ....	174
Fig. 6.8 . Comparison between the model predictions for the cases with and without taken consideration of radiation through PI radiation model (a) The HHV of the product gas in (MJ/Nm <sup>3</sup> ). (b) The outlet temperature of biomass (the char) (K). (c) Tar yield (g/Nm <sup>3</sup> ) (e) Gas species molar concentrations. (f) Char species mass fractions in the outlet. ....	175
Fig. 6.9. Comparisons between the results of this study and studies by Gerber et al. (2010), Bingyan et al. (1994) and Li et al. (2004) using pure air as a fluidizing agent. ....	177
Fig. 6.10. Comparison of the model prediction of product gas composition for the case of pure steam gasification. The external data was obtained from (Ngo et al., 2011). ....	178
Fig. 7.1. Predicted effects of equivalence ratio on (a) main gas composition, (b) NO, NH <sub>3</sub> and HCN emissions, (c) gas yield and high heating value of the product gas, (d) tar emission and carbon conversion (Liu and Gibbs, 2003). ....	181
Fig. 7.2. Effects of equivalence ratio on syngas composition at gasifier output (a) hydrogen composition, (b) carbon monoxide composition, (c) carbon dioxide composition, and (d)	

methane composition. (Model simulation results are compared with Li et al. (2004) experimental data) (Gungor and Yildirim, 2013) .....	182
Fig. 7.3. Effect of steam to fuel ratio on final gas composition obtained from modelling in comparison with experiment data taken from the literature (Ngo et al., 2011).....	183
Fig. 7.4. Effect of biomass gasifier operating temperature on dry gas heating value for the equivalence ratio in a range ( $a=0.22-0.47$ ) (Li et al., 2004).....	186
Fig. 7.5. Effect of gasification temperature on the final gas composition obtained from a model in comparison with experiment data (Ngo et al., 2011). .....	187
Fig. 7.6. Effects of biomass particle size on $H_2$ composition (Gungor 2011). Validating data from (de Souza-Santos 1989). .....	188
Fig. 7.7 . The effect of varying the air ratio (0.1-0.4) for the case of wood gasification using sand as bed material ( $d_{wood}= 500 \mu m$ , $d_{sand}= 200 \mu m$ ) with mass flow rate 2g/s and 20g/s respectively. Operating conditions were summarised in Table 7.2. The figures showing the effect of different air ratio in the following parameters: (a) The HHV of the product gas in ( $MJ/Nm^3$ ). (b) The outlet temperature (K). (c) Tar yield ( $g/Nm^3$ ) (e) Gas species molar concentrations. (f) Char species mass fractions in the outlet. ....	196
Fig. 7.8 . The effect of using different biomass mass flow rates (2-10g/s) for the case of wood gasification using sand as bed material ( $d_{wood}= 500 \mu m$ , $d_{sand}= 200 \mu m$ ) with sand mass 20g/s respectively. Operating conditions were summarised in Table 7.3. The figures showing the effect of different biomass mass flow rates in the following parameters: (a) The HHV of the product gas in ( $MJ/Nm^3$ ). (b) The outlet temperature of biomass (c) Tar yield (e) Gas species molar concentrations (f) species mass fractions in the biomass at outlet. ....	198
Fig. 7.9. Variation of the inlet sand temperature or the gasifier temperature between 700 and 1200°C for the case of wood gasification ( $d_{wood}= 500 \mu m$ , $d_{sand}= 200 \mu m$ ) at biomass flow rate of 5 g/s (20°C) and sand flow of 30 g/s. Detailed operating conditions are summarised in Table 7.4. (a) HHV of the product gas (b) outlet temperature of gas (c) Tar yield (e) gas species molar concentrations. (f) biomass species mass fractions at the outlet.....	201
Fig. 7.10 The product gases molar contents against the biomass residence time for the operating conditions given in Table 7.4 and the data presented in Fig. 7.9.....	203
Fig. 7.11 . Variation of the sand (heat carrier) mass flow rate (20-40g/s) for the case of wood gasification ( $d_{wood}= 500 \mu m$ , $d_{sand}= 200 \mu m$ ) with biomass mass flow rate 5g/s (20°C). Operating conditions were summarised in Table 7.5. The figures showing the effect of different sand mass flow rate in the following parameters: (a) HHV of the product gas (b) outlet temperature of gas (c) Tar yield (e) Gas species molar concentrations (f) Char species mass fractions in the outlet.....	204
Fig. 7.12 . Variation of the sand (heat carrier) size (150 to 300 $\mu m$ ) for the case of wood gasification ( $d_{wood}= 500 \mu m$ ) with biomass mass flow rate of 5 g/s (20°C) and sand flow rate of 30 g/s (900°C). The operating conditions for this case are summarised in Table 7.6. (a) HHV of the product gas (b) The outlet temperature of gas (c) Tar yield (e) product gas species molar concentrations (f) biomass species mass fractions at the outlet.....	206
Fig. 7.13 . Variation of the biomass particle size (250-1000 $\mu m$ ) for the case of wood gasification ( $d_{sand}= 200 \mu m$ ) with biomass mass flow rate of 5 g/s (20°C) and sand flow rate of 30 g/s (900 °C). The operating conditions used for these results are summarised in Table 7.7. (a) HHV of the product gas (b) outlet temperature of gas (c) Tar yield (e) Gas species molar concentrations at outlet (f) biomass species mass fractions in the outlet. ....	208
Fig. 7.14 . Comparison between using pure air and air/steam mixture (ratio of 0.16) as a gasifying agent for the case of wood gasification ( $d_{wood}= 500 \mu m$ , $d_{sand}= 200 \mu m$ ) with mass flow rate 5 g/s (20°C) and sand flow of 30 g/s (900°C). The operating conditions used are summarised in Table 7.8. (a) HHV of the product gas (b) outlet temperature of gas (c) Tar yield (e) gas species molar concentrations (f) char species mass fractions in the outlet. ....	210

Fig. 7.15. Comparison between two different pure steam gasification at different gasification temperatures using with sand as bed material ( $d_{wood}= 500 \mu\text{m}$ ,  $d_{sand}= 200 \mu\text{m}$ ) with biomass mass flow rate of 5 g/s and sand of 30 g/s. The operating conditions are summarised in Table 7.9. (a) HHV of the product gas (b) Outlet temperature of gas (c) Tar yield (e) gas species molar concentrations (f) char species mass fractions in the outlet. ....212

Fig. 7.16. Variation of steam to biomass ratio (0.1-0.8) for the case of wood gasification using sand as bed material ( $d_{wood}= 500 \mu\text{m}$ ,  $d_{sand}= 200 \mu\text{m}$ ) with biomass flow rate of 5 g/s and sand of 30 g/s. The operating conditions are summarised in Table 7.10 for 900°C sand temperature. T (a) HHV of the product gas (b) outlet gas temperature (c) Tar yield (e) gas species molar concentrations. (f) char species mass fractions in the outlet. ....214

Fig. 7.17. The effect of different sand temperatures (900°C -1200°C) using steam to biomass ratio 0.8 for the case of wood gasification using sand as bed material ( $d_{wood}= 500 \mu\text{m}$ ,  $d_{sand}= 200 \mu\text{m}$ ) with mass flow rate 5g/s and 30g/s respectively. Operating conditions were summarised in Table 7.11. The figures showing the effect of steam to biomass ratio in the following parameters: (a) The HHV of the product gas in (MJ/Nm<sup>3</sup>). (b) The outlet temperature of gas (K). (c) Tar yield (g/Nm<sup>3</sup>) (e) Gas species molar concentrations. (f) Char species mass fractions in the outlet. ....216

## Nomenclature

$A_r$	Arrhenius low pre-exponential factor ( $s^{-1}$ )
$B_r$	Arrhenius low temperature exponent (-)
$C_{fr,ls}$	the coefficient of friction between the $l^{\text{th}}$ and $s^{\text{th}}$ solid-phase particles (-)
$C_{j,r}$	molar concentration of species $j$ in reaction $r$ ( $\text{kgmol}/\text{m}^3$ ),
$d_p$	Particle diameter (m)
$E_r$	Arrhenius low activation energy for the reaction ( $\text{J}/\text{kgmol}$ )
$e_{is}$	the coefficient of restitution (-)
$g$	Acceleration gravity constant ( $\text{m}/\text{s}^2$ )
$g_{0,ls}$	radial distribution coefficient (-)
$h_i^0$	standard-state enthalpy ( $\text{J}/\text{kgmol}$ )
$H(T)$	Heaviside function
$\bar{I}$	unit tensor
$J_j$	diffusion flux of species $j$
$k$	diffusion coefficient
$k_t$	turbulent thermal conductivity ( $\text{kg}/\text{ms}$ )
$k_{\text{eff}}$	effective conductivity ( $\text{kg}/\text{ms}$ )
$k_{f,r}$	forward rate constant for reaction $r$
$k_{b,r}$	backward rate constant for reaction $r$
$K_r$	the equilibrium constant
$M_{w,i}$	the molecular weight of the species $i$ ( $\text{kg}/\text{kgmol}$ )
$m_{l \rightarrow v}$	the mass transfer rate from the liquid phase to the vapour phase is in ( $\text{kg}/\text{s}/\text{m}^3$ )
$Nu$	Nusselt number (-)
$N$	number of chemical species in the system (-)
$N_R$	reactions that the species participate in (-)

$P$	Pressure (Pascal)
$P_m$	partial pressure of the gas species $m$ (Pascal)
$Pr$	Prantl number (-)
$Re$	Reynolds number (-)
$R$	universal gas constant (J/kgmol-K)
$R_i$	chemical source term
$\hat{R}_{i,r}$	the rate of reaction (kgmol/m <sup>3</sup> s)
$S_i^0$	standard-state entropy (J/kgmol K)
$S_h$	heat of chemical reaction, and any other volumetric heat sources
$t$	Time (s)
$T_{ref}$	Reference temperature (K)
$u$	Velocity (m/s)
$v_{i,r}^{\sim}$	stoichiometric coefficient for reactant $i$ in reaction $r$ (-)
$v_{i,r}^{\approx}$	stoichiometric coefficient for product $i$ in reaction $r$ (-)
$X_m$	the mass fraction of the solids species $m$ (-)
$Y_j$	mass fraction of species $j$ (-)

*Greek symbols*

$\rho_s$	Solid density (kg/m <sup>3</sup> )
$\rho_g$	Gas density (kg/m <sup>3</sup> )
$\tau$	stress-strain tensor
$\beta$	drag force coefficient
$\varepsilon$	Volume fraction (-)
$\theta$	Granular temperature
$\gamma$	The collisional dissipation of energy
$\phi$	The energy exchange between two phases

$\mu$	Viscosity (kg/ms)
$\gamma_{j,r}$	rate exponent for reactant species j in reaction r
$\tilde{\gamma}_{j,r}$	rate exponent for product species j in reaction r

# **1. Chapter 1: Introduction and Background**

## **1.1. Background**

This introductory section gives general information about (i) biomass gasification process (ii) circulating Fluidized Bed (CFB) reactor, its applications and advantages in biomass gasification (iii) the latest trends in Computational Fluid Dynamic (CFD) modelling of multiphase flow and its use as a predictive tool.

### **1.1.1. Biomass**

Biomass is any organic matter that is renewable over time and it is equally apply to both animal and plants derived materials. The biomass is mainly compose of carbon and a mixture of organic molecules including hydrogen, oxygen, nitrogen and also small quantities of alkali, alkaline earth and heavy metals. The biomass can be used for energy purposes and it includes a wide range of materials. These materials can be categorised into five basic categories: virgin wood; energy crops; agricultural residues; food waste; and industrial waste and co-products. The virgin wood consists of wood and other products such as sawdust.

The biomass mainly consist of ligno-cellulose which consist of cellulose, hemicelluloses and lignin. Willow is an example of ligno-cellulosic material which consist of 50% cellulose, 25% hemicelluloses and 19% lignin. The most common method for the analysis of biomass composition are the ultimate and proximate analysis. The ultimate analysis gives the biomass composition of the hydrocarbon and is expressed in term of basic elements, which typically consist of C, H, O, N, S, ash and moisture. The proximate analysis gives the compositions in gross terms such as moisture, volatile matters, fixed carbon and ash. As an example, the ultimate analysis in dry basis for Redwood is 53.4% C, 6% H, 0.1% N, 0% S, 40.3% O, 0.2% and ash (Basu, 2010b).

### **1.1.2. Biomass gasification**

Biomass gasification is the thermo-chemical conversion of biomass material at a high temperature and a control oxygen amount into fuel gas (syngas). The typical gasification

temperature is between 700-900 °C and the product gas mainly consisting of H<sub>2</sub>, CO, CO<sub>2</sub>, CH<sub>4</sub> and N<sub>2</sub>. The gasifying medium can be oxygen, air or steam or any combination of three medium. The heating value of the product gas depends on the gasifying agent used. If air is used then the heating value will be 4-7 MJ/NM<sup>3</sup>, for steam 10-18 MJ/NM<sup>3</sup>, and oxygen 12-28 MJ/NM<sup>3</sup> (Basu, 2010b).

Gasification has become more and more important in biomass utilization. A number of types of gasifiers have been developed to meet the different needs. The development of the fluidized bed gasifier has made great progress for biomass gasification. The productivity of the fluidized bed gasifier has increased by five times that of the fixed bed gasifier and the heating value of gas increased by about 20% ((Klass et al., 1985); (Bingyan et al., 1994)).

There is general agreement that the main stages in high temperature thermo-chemical conversion of biomass are drying, devolatilization, combustion and gasification. These stages often overlap and in most cases there is no sharp boundary between them as described by (Basu, 2010b). The biomass is first heated then thermally degraded, the products from the thermal degradation are solid gas and oil. These products then react to generate the final product through the various combustion and gasification reactions.

### **1.1.3. Circulating fluidized bed (CFB)**

Kunii and Levenspiel (1991) reported that the need to maintain a stable and continuous processing of solids in a gas-solid system has led to the circulating fluidized beds technology. These processes are usually large scale operations especially in the petroleum industry. The first use of circulating fluidized systems was represented in the development of fluid catalytic cracking (FCC). The most important in the operation of a CFB is the proper design for continuous solid circulation at a fixed rate. The solids will settle down to a circulating rate at which the sum of the static head terms just balances the sum of all the frictional resistance terms, including solids acceleration losses, bends, constrictions, and the valve of the circulating materials. In terms of design, there are two main types of

circulating fluidized bed gasification systems: single loop or single riser system and two loop or dual fluidized bed system, as shown in Fig.1.1. Both types are characterized by their excellent mixing heat and mass transfer. The circulation of solids makes it possible to remove or add the vast quantities of heat produced or needed in large reactors. These properties make fluidized beds an attractive proposition for many industrial processes ((Kunii and Levenspiel, 1991), (Lim et al., 1995)). CFB technology is currently used in the separation, classification, drying, and mixing of particles, as well as thermo-chemical reactions and thermal regeneration processes, such as biomass gasification and catalyst regeneration.

Biomass gasification in a circulating fluidized bed reactor is widely carried out at a fast fluidization regime. Fast fluidization enhances the heat and mass transfer, thus speeding the gasification process. The formation of a fast fluidized bed depends on the following conditions: (1) small particle materials; (2) high operating gas velocity; (3) continuous solid circulation. Small particles provide huge gas-solid contact surface, minimizing the transfer resistance inside the particles. High gas velocity with solids circulation means that there is an absence of bubbles forming a dilute continuum of discrete particles with solids clusters in it. The continual forming and dispersing of the solid clusters promote the contact of gas and solid and enhance heat and mass transfer. Continuous solid circulation maintains the density of the bed and uniform solids profile along the radial cross section. Consequently, the fast fluidized bed provides a high reaction rate for gasification and enough residence time of solids to complete the reactions.



Fig.1.1. Main types of a circulating fluidized bed biomass gasifier (a) single loop system (Chan et al., 2009c) (b) Two loop system (Pfeifer and Hofbauer, 2008)

#### 1.1.4. Modelling of multiphase flow

Multiphase flow can be solid-liquid, gas-solid, gas-liquid and liquid-liquid flows or combination of any of these three phases. Experimental investigations, especially when there is heat and mass transfer, are usually long and expensive, which demand complex and expensive measuring techniques, therefore arises the need for modelling and simulation in order to understand and parametrically analyse such processes with minimum experimentation.

In this study we are looking at modelling of a reactive system of solids-gas flow for the conversion of biomass to gases in a CFB riser. Review of the literature indicate that there are two main modelling approaches that can be used to simulate the solid-gas flow in this case: (i) Two-Fluid Model (TFM) approach (also referred to as two-phase flow model) and the (ii) Discrete Phase Model (DPM) approach (also referred to as Distinct Element Model (DEM)). Under the first modelling approach fall three options (i) Volume of Fluid (VOF) model (ii)

Mixture model and (iii) Eulerian-Eulerian model. For the particular case of gas-solid flow, the DEM approach is usually referred to as Eulerian-Lagrangian model. The next section gives brief discussion about approached (i) and (ii).

#### **1.1.4.1. Two fluid model (Euler-Euler approach)**

In this approach the solid and gas phases are treated as penetrating continua. That means each phase has volume fraction and the summation of these volume fractions equal to one. These volume fractions assumed to be continuous functions of space and time and calculated through conservation equations for each phase. The conservation equations have set of constitutive equations, commonly obtained by applying the Kinetic Theory of Granular Flow (KTGF).

As mentioned above three approaches can be used in Euler-Euler models which are VOF, Mixture and Eulerian model. The VOF model is not applicable to our case, mainly due to the applications of this model since this model is used to model two fluids (gases, liquids); examples of its applications are prediction of jet breakup or the motion of large bubbles in a liquid. Mixture model is as same as the Eulerian model but is relatively less accurate because of the limited number of equations used in the solution. It is recommended to particle-laden flows with low loading, bubbly flows, sedimentation and cyclone separators. The Eulerian model is relatively the most complex of the multiphase models as momentum and continuity equations are solved for  $n$ -number of phases. This is applicable to multiphase flow cases such as bubble columns, risers, particle suspension, and fluidized beds.

#### **1.1.4.2. Discrete Phase model (Eulerian-Lagrangian approach)**

The hydrodynamics in solid/gas flow can be simulated using Discrete Phas Model (DPM). In this model the solid phase is simulated as individual particles dispersed in the gas phase which is commonly treated as continuum by solving the Navier-Stokes equations. It is generally more accurate than the TFM approach, as the solution is based on tracking individual particles, however the solution is slow and therefore unrealistic to handle real

cases. In DPM models the following physical parameters have to be identified; particle number, particle diameter, particle density. One of the major assumptions in this model is the dispersed solid phase occupies a low volume fraction (less than 10-12%) therefore more suitable for flows in which particle streams are injected into a continuous phase such as in the case of spray driers and some particle laden flows. In this study, the use of DEM for modelling and simulating the hydrodynamic and thermo-chemical conversion of biomass is not realistic due to the limitation in the computation being huge in calculating high number of particles. There are more limitations such as the pressure drop cannot be calculated and the mass flow rate cannot be specified.

#### **1.1.4.3. *Ansys Fluent Computational Fluid Dynamic (CFD) software***

Ansys Fluent as identified in its documentations is a high-tech computer program written in C language to model hydrodynamics, heat transfer and chemical reactions in complex geometries. Fluent can read and solve the meshes in 2D and 3D with wide types of structures. After the mesh has been read then all the other operations will be performed within Fluent including setting the boundary conditions, defining materials properties, executing the solution and post processing and viewing the results.

Fluent solver can do steady state and transient solutions; incompressible and compressible flows; Inviscid, laminar, and turbulent flows; Newtonian or non-Newtonian flows; Ideal or real gases; heat transfer, including forced, natural, and mixed convection, conjugate (solid/fluid), heat transfer, and radiation; Chemical species mixing and reaction, including homogeneous and heterogeneous combustion models and surface deposition/reaction models; Free surface and multiphase models for gas-liquid, gas-solid, and liquid-solid flows; lagrangian trajectory calculation for dispersed phase (particles/droplets/bubbles), including coupling with continuous phase and spray modelling.

## **1.2. Objectives**

The main objectives of this thesis are:

- i. Develop a three-dimensional predictive model of biomass gasification in a CFB riser using advanced Computational Fluid Dynamic (CFD).
- ii. Experimentally validate the developed hydrodynamic model using conventional and advanced measuring techniques.
- iii. Study the complex hydrodynamics, heat transfer and reaction kinetics through modelling and simulation.
- iv. Study the CFB gasifier performance through parametric analysis and to identify the optimum operating condition to maximize the product gas quality.

### **1.3. Summary of chapters**

This thesis consists of seven main chapters, in addition to this introduction chapter. The main seven chapters are summarised as follows:

#### **Chapter 2:**

This chapter presents the experimental settings and procedure of the CFB used for validations of the hydrodynamic predictions presented in chapters 3. The first section in this chapter was the description of the equipment used in the experiments. This is then followed by discussion of the experimental operating conditions. The final section presents the procedure used for collecting and analyzing the experimental data.

#### **Chapter3:**

This chapter discusses building the model hydrodynamic and model validations. The hydrodynamics are particularly focused on the particle dynamics (velocity), pressure distribution and phase distribution of the multi-component flow mixture. The pressure predictions were experimentally validated using the standard method of pressure measurement along the riser height, while the predicted solids velocities were validated using an advanced particle tracking method, namely Positron Emission Particle Tracking (PEPT). This section also includes extensive review of related literature.

**Chapter 4:**

This chapter presents a gasification model of biomass (reactive system) in a fluidized bed reactor. This will be incorporated in the hydrodynamic model presented in Chapters 3 to simulate the gasification of biomass. The chapter also includes extensive literature review on various chemical reactions and the corresponding reaction rates.

**Chapter 5:**

In this chapter, the simulation of a base case is introduced to give an overview of the hydrodynamics, heat transfer and product gas quality in the reactive system. The gas quality includes data on the gas heating value, composition and tar content. This chapter also includes preliminary mass and heat balances, related literature on CFB modeling and simulation of biomass gasification in fluidized bed reactors is also discussed to identify the state of art and knowledge gaps in this area.

**Chapter 6:**

In this chapter the gasification model developed and presented in Chapter 4 has been further refined with respect to its sensitivity to various combustion reactions and inclusion of thermal radiation in the model formulation. The model was then compared with different experimental data from the literature.

**Chapter 7:**

This chapter presents investigations on the effect of operational parameters on the gasifier performance in general and in the product gas quality in particular. The parameters investigated are: equivalence ratio, biomass feed rate, heat carrier temperature and flow rate, biomass and heat carrier particle size, and steam to biomass ratio. This chapter also includes a review of the relevant literature.

**Chapter 8:**

The conclusions and achievements of this study are summarised in this chapter, moreover recommendations for future extension are also discussed.

## **2. Chapter 2: Experimental settings and procedure**

### **2.1. Introduction**

This chapter presents the experimental settings and procedure of the CFB used for the validations of the hydrodynamic model presented in chapter 3.

The first section in this chapter provides the description of the equipment. This is then followed by discussion of the experimental procedure and its operating conditions. The final section presents the procedure of collecting and analyzing the raw data of experiments.

### **2.2. Cold flow Circulating Fluidized Bed (CFB)**

The CFB equipment used in the experiments has only been used for non-reactive flow for the purpose of validating the hydrodynamics and heat transfer models. The experimental rig, shown in Fig.2.1, comprises a 5.2 cm diameter riser of 1.63 m height, a downer equipped with a solid receiving tank, primary and secondary cyclones, eight pressure probes along the riser height and two rotameters. The probes were placed at 21, 33, 45, 76, 107 and 138 cm above the distributor plate. The tips of the probes were covered by a metal fine mesh and were designed to facilitate radial movement for pressure measurements at various radial positions. The column was fitted with a gas distributor of ~3% open area for gas flow passage. The cyclones were fitted with filter bags for the collection of very fine entrained particles. Two valves were used to control the fluidizing gas at the main and secondary supply points. The function of the secondary gas was mainly to assist and ensure uniform flow of the solids circulation through the system. Both rotameters when combined can provide up to a total of 1500 lit/min. The receiving tank at the downer side is used for collecting the solids leaving the cyclone before sending it back to the riser. The solid feed and outlet are 2 cm and 4 cm in diameter and located 10 cm above the distributor and 10 cm below the top of the riser respectively. The downer side is equipped with a solid diversion valve to allow withdrawal and collection of solids, hence allowing for measuring the solid flow rate. The riser section was made of QVF glass and the downer side was made of stainless steel. Further details on the various parts of the CFB rig are given below.

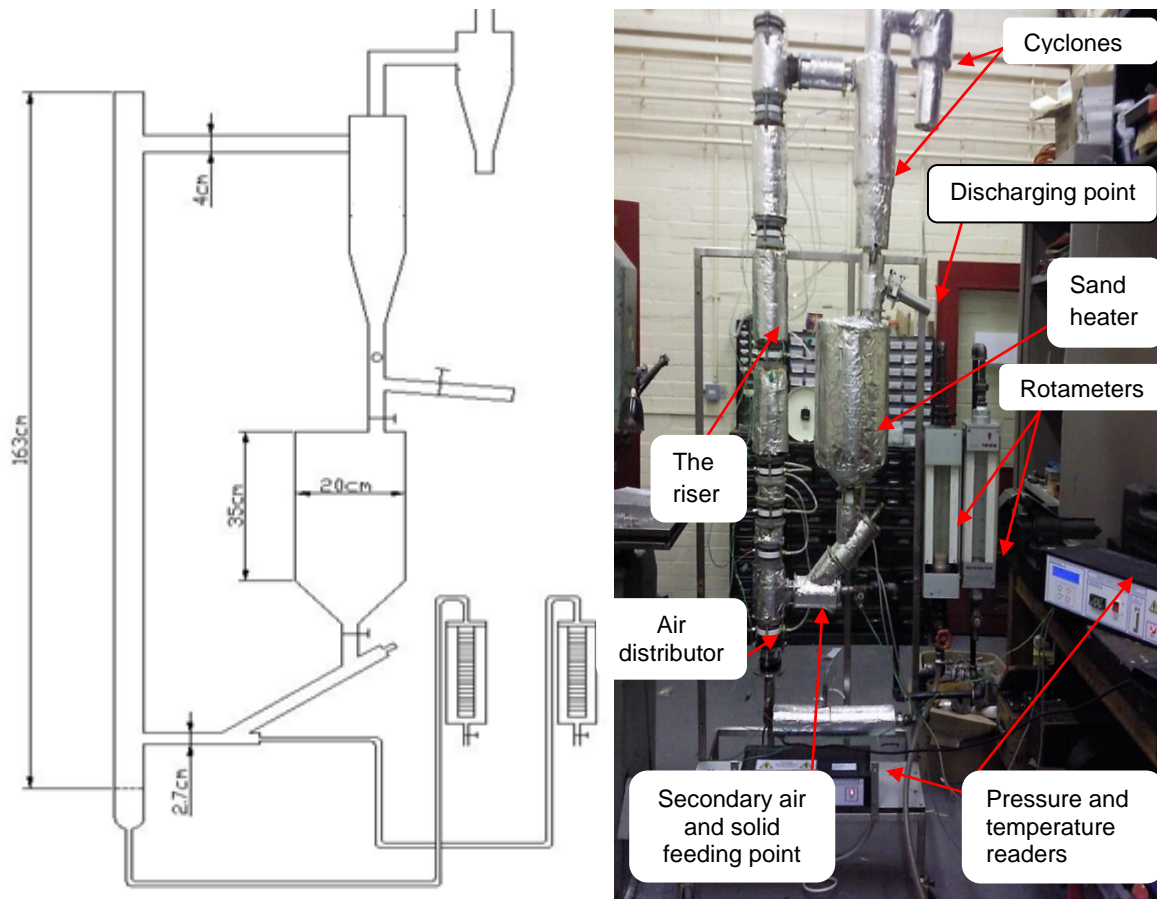


Fig. 2.1. Details of the circulating fluidized bed arrangement, dimensions and attached instrumentations

### 2.2.1. Riser

The riser was made of glass with approximately 5.2 cm internal diameter and 6.2 cm external diameter and about 0.5 cm wall thickness. The equipment including the riser is shown schematically in Fig. 2.2. The riser outlet was located 10 cm below the top and connected by a 4 cm stainless steel to a cyclone. The bottom of the riser is covered with an air distributor made of plastic with an air flow passage of around 3% of the total cross-sectional area. At around 10 cm above the air distributor a metal pipe was connected to allow for the circulating solids coming from the receiving tank to enter the riser.

As described earlier, the riser was equipped with probes for pressure measurement through pressure transducers. The distances between the probes points are shown in Fig. 2.2. As

shown the distance between the first three probes at the bottom are short in order to correctly collect steep pressure variations at this region.

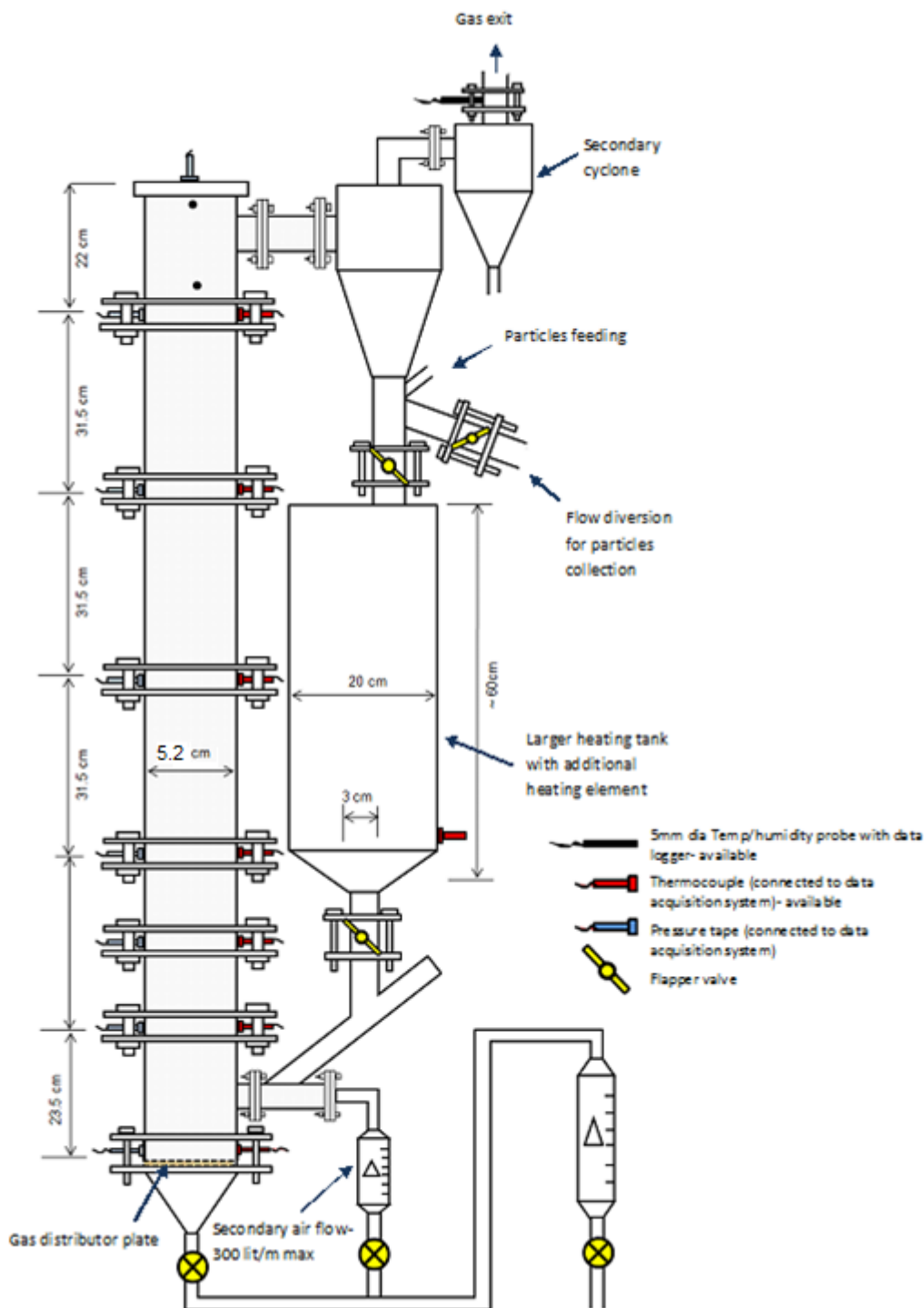


Fig. 2.2. The distance between the pressure taps in the riser of the CFB.

### 2.2.2. Return leg (downer)

The function of the return leg (downer) was to transfer the solids collected at the cyclone to the riser. All parts of the return leg were made of stainless steel. As described earlier the

return leg was connected to a receiving tank through a pipe. This pipe was designed with two small openings; one for solid feeding and other for discharge of solid from the system during operation. Two flopper valves were located before and after the receiving tank, allowing for control of solid circulation rate as well as diversion of solid for discharge out of the system. The details and dimensions of the return leg are shown in Fig. 2.3. The receiving tank is made of stainless steel with two parts, a conical shape part and a cylindrical shape part. The cylindrical part dimensions are about 20cm diameter and 35cm height. There are two valves above and under the receiving tank to control the solids going in and out.

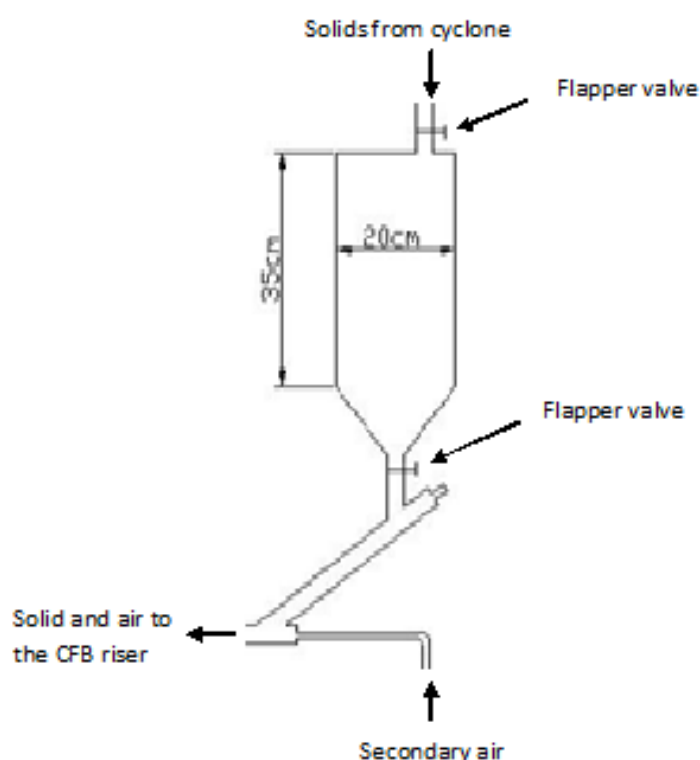


Fig. 2.3. Receiving tank for transferring solids between the downer and riser sides of the CFB

### 2.2.3. Rotameters

Two rotameters with different flow ranges were used in the experiments to measure the fluidizing air flow rate. The first rotameter, model TM 47 X FMK, works in a range between 150-1400 lit/min and is used as the source of main fluidization air. . The second one, model TM 35 FMA (Series 1000) works in a range between 30-500 lit/min, and is used as a secondary source of air to aid in smooth circulation of solids between the downer and riser

sections of the CFB system. The combined rotameters can give a flow up to 1900 lit/min. Full details of the rotameters used are given in Table 2.1.



Fig. 2.4 . The two rotameters supplying air to the CFB system.

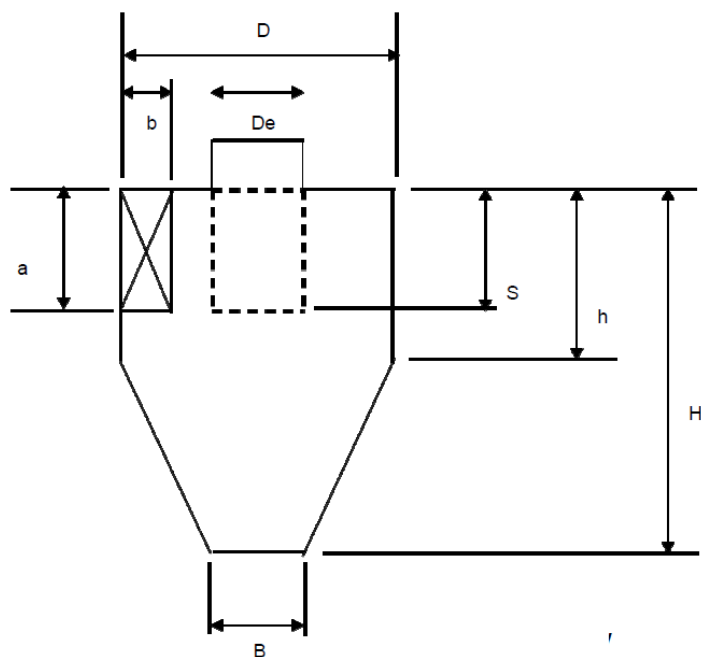
Table 2.1 Rotameters specifications

	For main air	Secondary air
Rotameter Type or Name	TM 47 X FMK	TM 35 FMA (Series 1000)
Range	150-1400 Litres/minute	30-500 litres/minute
Company Name	GEC-Elliot Instruments Ltd England	Process Rotameter MFG. Co Ltd Croydon England

#### 2.2.4. Cyclone

Cyclonic separation is a method of removing particulates from an air, gas or liquid stream, without the use of filters, through vortex separation. Two cyclones in series have been attached to the CFB system. Both cyclones were made of stainless steel and their dimensions are given in Fig 2.5. The purpose of the main cyclone was to collect most of solids coming from the riser. Particles entrained from the first cyclones were then collected by the secondary cyclone (usually very small fraction of very fine powder). Generally, in the CFBs the secondary cyclone is usually connected to the downer to allow recirculation within the system, however in this set-up, and due to the fact the amount of solid collected is

considerably small, the secondary cyclone was connected to a filter bag. Details of the main cyclone dimensions is given in Fig. 2.5.



		<b>Main Cyclone (cm)</b>
Dia	D	12
Inlet ht	a	6
Inlet width	b	2
Outlet length	S	6
Outlet dia	De	6
Cylinder ht	h	18
Overall ht	H	47
Dust outlet dia	B	4

Fig. 2.5. Dimensions of the main cyclone attached to the CFB system.

### 2.3. Operating procedure

All experiments were carried out using air as the fluidizing gas. Various types of particles were used as the bed material, including glass beads and sand-biomass mixture. A sample of properties of these particles are given in Table 2.2. The overall solid flow rate in the system was in the range of 10-60 g/s (5-28 kg/m<sup>2</sup>s). Summary of a sample of the experiment runs and operating conditions is given in Table 2.2. In the model validation, two measured parameters were used, namely the pressure drop and particle velocity. The method and procedure used for obtaining these two parameters is discussed in the next section. The

solid flow rate was obtained by collecting the solids in the outlet in specific time then the amount of the solids collected divided by the time measured to obtain the solid flow rate in kg/s. This procedure was repeated many times then the average calculated to give us more reasonable flow rates. The fluidization velocity were obtained from the measurements of the two rotameters in lit/min. Then the values changed to m<sup>3</sup>/s and divided by the cross sectional area of the riser to give us fluidization velocity. Regarding calculating the particle size, two methods were applied in the first one sieve analysis was conducted to measure particle size distribution then particle size average was calculated to obtain the size used. The second method is by narrowing the particle size ranges to get particles with almost similar sizes. For mixture of different sizes the particles was applied to the riser with definite percentages.

The terminal velocities of the particles were calculated before the experiments in order to identify the fluidization velocity required to attain circulation mode. To calculate the terminal velocity there are three equations used depends in the range of Reynolds number from (Kunii and Levenspiel, 1991) as follow:

Re<1

$$u = \frac{(\rho_s - \rho_g) g d_p^2}{18\mu} \quad (2.1)$$

1<Re<500

$$u = \frac{4(\rho_s - \rho_g) g d_p}{54\rho} \quad (2.2)$$

500<Re<2×10<sup>5</sup>

$$u = \left[ \frac{3(\rho_s - \rho_g) g d_p}{\rho} \right]^{1/2} \quad (2.3)$$

Reynolds number used in this study identified as:

$$Re = \frac{\rho u d}{\mu} \quad (2.4)$$

where

$\rho$  gas density (kg/m<sup>3</sup>)

$u$  velocity (m/s)

$d$  particle diameter (m)

$\mu$  gas viscosity (kg/m-s)

The solid diameter range used in the experiments was 0.00015 to 0.0008m (150-800 $\mu$ m). The velocity range which can be achieved in the system was in a range of 1.413m/s to 14.911m/s. The gas viscosity 1.7894e-05 kg/m-s and the gas density 1.225kg/m<sup>3</sup> so the range of Reynolds number will be between 14.51 to 816.63. therefore for these ranges of Reynolds numbers both Eq. 2.2 and 2.3 were used to calculate the terminal velocity.

#### **2.4. Pressure measurements and data logging**

The instrumentations used to obtain the pressure distribution along the riser height consisted of 8 pressure transducers connected to a data acquisition system. The transducers were connected by tubes to the probes distributed along the riser height at the locations given above. The transducers range between 1 to 7 bar absolute pressure, the supplier is Sensor Techniques, its series number is CTE7000/CTU7000. The data was recorded at the rate of 1 second and for the duration of 5-10 minutes for each one single run. Sample of the recorded pressure at different heights is shown in Fig. 2.8. Each data collected was then averaged over a given experiment duration time (usually around 10 minutes) to obtain the localized pressure at each height.

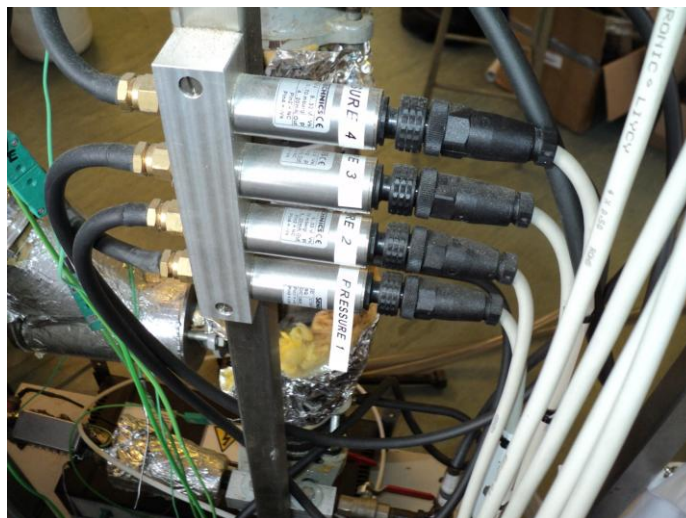


Fig. 2.6. The Pressure Transducers connected to the pressure taps in the CFB riser.

The Transducers mentioned above were connected to a data acquisition system which has multi functions i.e. reading pressure during CFB operation, logging and online displaying of data and transmit it to the computer. After the raw data was logged and transferred, a specially developed excel sheet was used to obtain the time averaged data Further information on the raw data treatment is given in Section 2.6 below.

## **2.5. Particle tracking**

In order to collect further information for the flow hydrodynamics in the CFB an advanced Positron Emission Particle Tracking (PEPT) system was used to track the movement of a single radioactive particle. This was achieved by activating the particle with Fluorine-18, which was absorbed into the particle surface. The activated particle was then tracked by Gamma photons detector as shown in Fig. 2.7. In these experiments activated particle was first placed inside the CFB particle receiving tank and then allowed to continuously circulate passing through the detector plates located around the lower part of the CFB riser. The solid circulation rate for each experiment was determined by using solid deflection/collection method described earlier prior to the introduction of the radioactive particle. Three fluidization experiments were carried out; one using a single solid phase of glass beads (755  $\mu\text{m}$ ) and a binary solid mixture of sand (700  $\mu\text{m}$ ) and wood (1000 $\mu\text{m}$ ) with the wood representing 2.5 wt% of the mixture. Air was the fluidizing gas in all experiments. In the trial tests sand produced the weakest signal, while the wood displayed the strongest activity. The activity was also found to be strong function of the particle size, such that the smaller the size the weaker the signal.

The average total duration of each particle tracking experiments was around 2 hours. This was a limiting factor as the life time of the particle activity was in the range of 3 hours. Because the active particle was circulating between the detection zone in the CFB riser side and the solid receiving tank in the downer side, there was about 5 minutes delay between each set of detections (further details on this is given in the result section). The record

transient data on the particle dynamics was analyzed using special software to obtain information on the particle velocity and location within the PEPT detection zone.

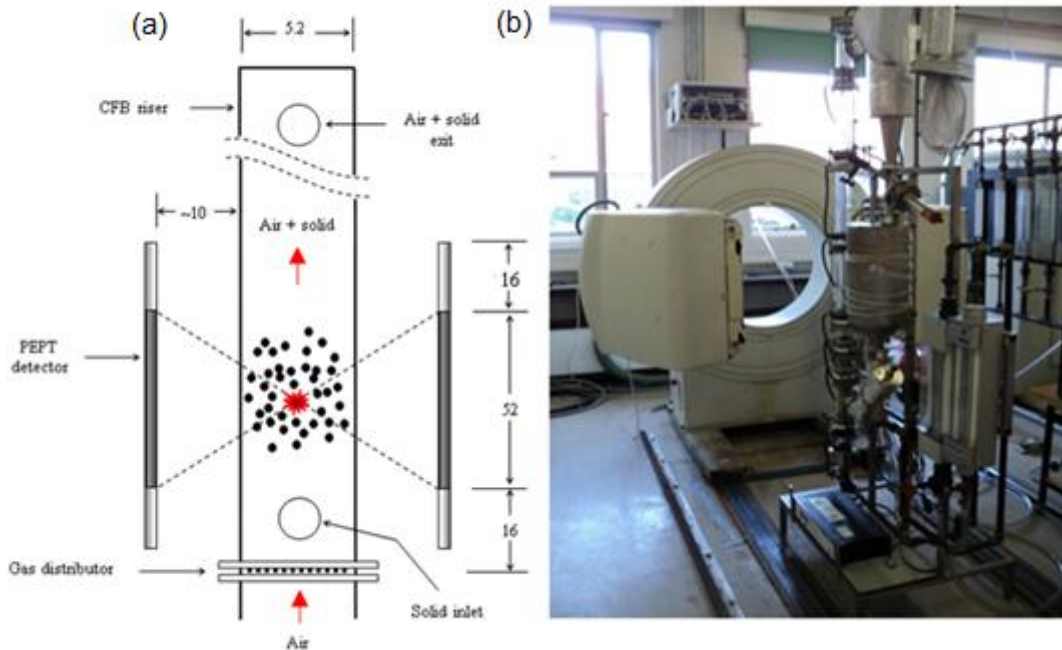


Fig. 2.7. (a) The schematic of the PEPT setup (All dimensions are in cm). (b) PEPT equipment in Birmingham university

Table 2.2 gives a summary of the three runs carried out for the particle tracking experiments. The glass beads size used is 755 microns and the wood is 1mm. Details on the raw data treatment to extract information on the particle dynamics and velocity is given in Section 2.6 below.

Table 2.2 The experiments operating conditions in the CFB riser used in the PEPT system experiment

Run #	Bed material	Air flow		Solid flow rate		Radioactive Particle
		Lit/min	m/s	g/s	kg/m <sup>2</sup> s	
1	Single phase: Glass beads, 755µm	600	4.71	36	14.61	Glass bead
2	Single phase: Glass beads, 755µm	550	4.32	35	14.20	Glass bead
3	Binary mixture: Wood, 1 mm (2.5%) Sand, 700 µm (97.5%)	550	4.32	33.54	13.61	Wood

## 2.6. Experimental raw data Analysis

As mentioned earlier, there are two types of raw experimental data produced during running the cold flow CFB. These are the time series data of pressure fluctuations at different locations along the riser height, and individual particle tracking data produced from the PEPT system. The data was collected for different types of particles (sand and glass beads with different sizes) and at different fluidization velocities. Fig. 2.8 demonstrate a typical pressure data recorded at different locations in the CFB riser at the frequency of 100 Hz

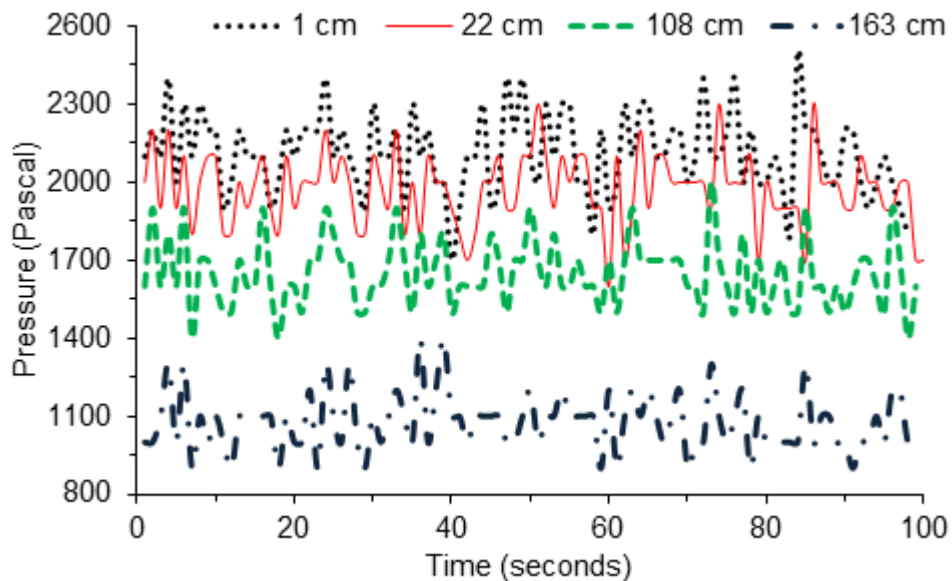


Fig. 2.8. Example of raw time-series pressure data produced at four different selected locations along the riser height. The operating conditions are for Run#1 given in Table 2.2.

Further treatment of this data is by time averaging to give one value for each point. Fig. 2.9 shows example of the time averaged pressure data as function of location in the CFB riser. The duration of experiment is usually within the range of 5-10 minutes. An excel spreadsheet was developed to produce the time-averaged data by direct transferred of the raw data from the acquisition system to a computer.

Figures 2.10 and 2.11 show a typical vertical velocity data recorded verses time. Further treatment of this data is by time averaging to give one value of the vertical velocity. This value was used to validate the hydrodynamic model. Validating the hydrodynamic model using pressure and PEPT data is discussed in chapter 3. A sample of raw data collected from PEPT experiments is available in appendix A.

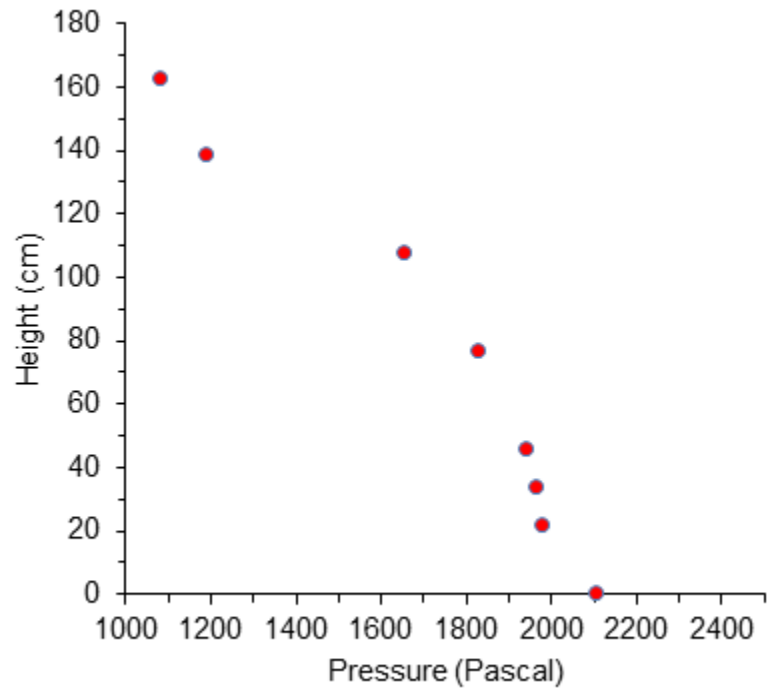


Fig.2.9. Time average pressure vs. height in the CFB riser. The operating conditions are for Run#1 given in Table 2.2.

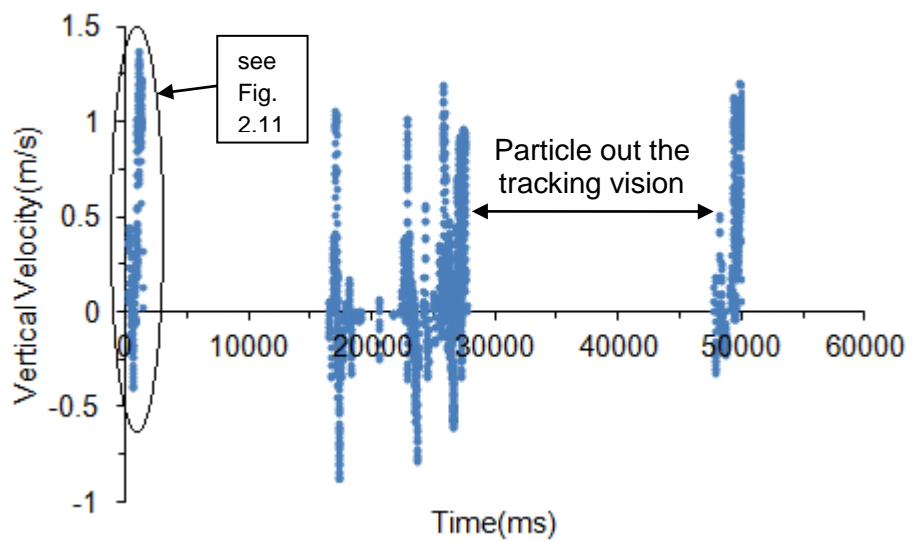


Fig. 2.10. PET data of particle vertical velocity (glass beads) recorded during 60 seconds of the CFB operation.

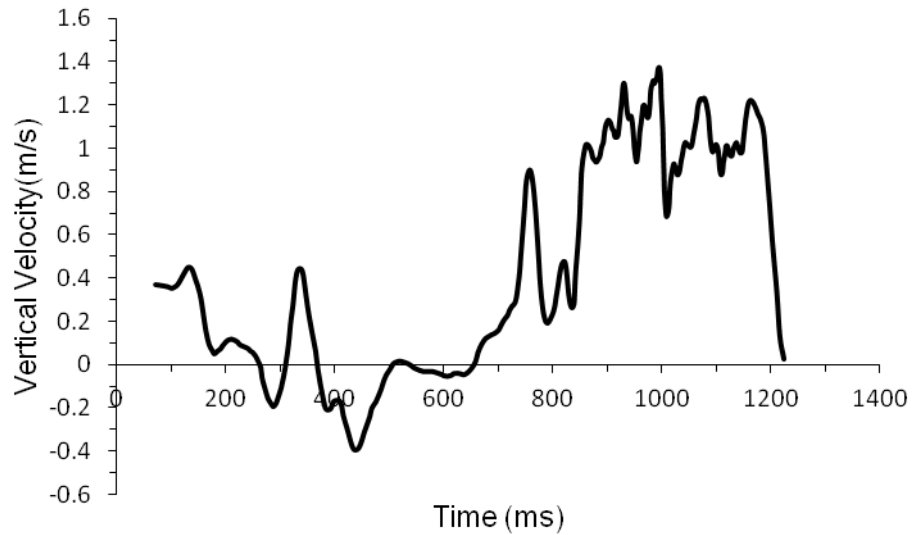


Fig. 2.11. PEPT data of particle vertical velocity (glass bead) recorded during 1.2s of the CFB operation.

## 2.7. Conclusion

This chapter presented a detailed description of the CFB used in validating the hydrodynamics and heat transfer models. The main parts of the CFB and the operating procedure of the system have been presented and discussed. Two different measurement techniques used in this study, namely, the pressure measurements and particle tracking have been described and discussed. Sample of the experimental data produced by these two different techniques and how the raw data is treated has also been presented.

### **3. Chapter 3: Hydrodynamics simulations and validations**

#### **3.1. Introduction**

Fluidized bed reactors have wide applications in the process industry due to their enhanced heat and mass transfer characteristics. Despite its simple operation, accurate prediction of its flow hydrodynamics is particularly challenging especially if the operation involve multiphase. In a circulating fluidized bed biomass gasifier, the biomass particles undergo rapid interaction with the product gas as well as with the inert solid phase (usually heat carrier sand). A valid hydrodynamic model is therefore essential for the correct prediction of such complex interactions before attempting to introduce the gasification reactions to the model.

In this chapter, a three dimensional hydrodynamic model based on the two-fluid approach is developed and validated. The model predictions are particularly focused on the particle dynamics (velocity), pressure distribution and phase distribution of the multi-component flow mixture. These predictions are experimentally validated using the standard method of pressure distribution measurements and the advanced particle tracking method for velocity validation, both experimental techniques have been described earlier in Chapter 2.

To avoid time consuming computation and to eliminate inaccurate options, some cases were started by looking at the simple case of monodispersed suspension first then compared and validated with experimental data obtained in a bidispersed suspension. This chapter also includes extensive review of related literature.

#### **3.2. Literature review**

The literature presented in this chapter is focused on (i) reported studies on the experimental validation of CFB hydrodynamics models using pressure measurements and particle tracking methods (ii) The various hydrodynamic models and the effect of simulation settings, options and parameters used on the model predictions.

### 3.2.1. Hydrodynamic experimental investigation in CFB

#### 3.2.1.1. *Studying Fluidized bed hydrodynamics using PEPT*

The PEPT measuring technique has been reported in various experimental studies of multiphase flow, including CFB systems. Chan et al. (2009a) used the PEPT to record real-time particle motion in L-valve in a CFB. This was presented as a function of the superficial injection air velocity. The results were compared with an earlier experimental work by the same group Chan et al. (2009b), carried out in a hopper connected to the top of a standpipe while the base is connected to a free-discharging L-valve. The authors reported that the PEPT results provided very useful data, and confirmed the existence of asymmetrical solids velocity profile along the vertical axis of the standpipe at any given height.

Van de Velden et al. (2008) used PEPT to study the movement and population density of particles in a CFB riser. The authors reported that the PEPT results can be successfully used to obtain (i) the vertical particle movement and population density in a cross sectional area of the riser, (ii) the transport gas velocity ( $U_{tr}$ ) required in order to operate in a fully established circulation mode, (iii) the overall particle movement mode (core flow versus core/annulus flow), and (iv) the particle slip velocity ( $U_s$ ). The authors concluded their work by reporting that only in a core flow mode can the particle slip velocity be estimated from the difference between the superficial gas velocity ( $U$ ) and the particle terminal velocity ( $U_t$ ). The slip velocity is lower than  $U-U_t$  outside the core flow mode.

#### 3.2.1.2. *Studying Fluidized bed hydrodynamics using pressure measurement*

Pressure measurement is a very common measurement method in various multiphase flow analysis, including CFB systems. For example, pressure measurement in a CFB has been reported by Zhou et al. (2011), van Ommen et al. (2011) and Sánchez-Delgado et al. (2011).

Zhou et al. (2011) simulated coal combustion in a CFB combustor using two dimensional computational fluid dynamics. The authors validated their hydrodynamic model using experimental data taken in a CFB riser of a total height of 4 m and equipped with six

pressure taps located at different heights along the riser ( $H= 0.15, 0.70, 1.50, 2.90, 3.70, 4.0$  m). The pressure data was used to estimate the voidage distribution. The authors reported that such a simple measurement can be used successfully for hydrodynamic validations as shown in Fig. 3.1.



Fig. 3.1. Comparison of time-averaged voidage distributions for CFB based on different drag models (Zhou et al., 2011).

Van Ommen et al. (2011) reviewed methods for time-series analysis for characterization of the dynamics of gas–solid fluidized beds from in-bed pressure measurements for different fluidization regimes. The paper covered analysis in time domain, frequency domain, and in state space. It is a follow-up and an update of a similar review paper written by Johnsson et al. (2000) a decade ago . The authors concluded, over the past decade, progress has been made in understanding fluidized-bed dynamics by extracting the relevant information from pressure fluctuation data.

### **3.2.2. Simulating Fluidized Bed Hydrodynamics**

In the following sections, the literature is reviewed to look into the latest two-fluid modelling trends and results with respect to the appropriate constitutive relations and sensitivity analysis.

### 3.2.2.1. Gas-solid drag models

Due to its great importance, gas-solid drag is the most widely researched constitutive relation in two fluid models. This literature considered both cases of dense flow, such as in bubbling bed, and dilute flow, such as in circulating beds.

#### Drag models for dilute system- CFB models

Almuttahir and Taghipour (2008) carried out a study in the fluid dynamics of a circulating fluidized bed under various fluidization conditions by a two-dimensional Eulerian–Eulerian model using Fluent CFD code (Version 6.2). The authors reported that there are several drag models applicable to the gas–solid flow in CFB risers in the literature, such as the Gidaspow et al. (1992), Arastoopour et al. (1990), and Syamlal and O’Brien (1987) drag models. These various drag models are given in Table 3.1.

In using the drag force of Syamlal and O’Brien (1987), Almuttahir and Taghipour (2008) did modification to the minimum fluidization condition. They used the same calculations of Zimmermann and Taghipour (2005) to modify the constants in the terminal velocity to match the minimum fluidization velocity. Zimmermann and Taghipour (2005) reported that this method gives good description of the hydrodynamics of fluidized beds with similar particles. Almuttahir and Taghipour (2008) also reported that in fluidized bed systems, the main forces for majority of the flows are the gravity and the drag forces apart from the very dense flow where the frictional stresses play an important role. Moreover, lift and virtual mass forces are less important than the drag force when the particles are relatively small and their density much larger than the continuous phase density. Thus the authors assumed that the gas–solid momentum exchange coefficient have only the drag contribution.

Behjat et al. (2011) developed a three dimensional CFD model of the riser section of a CFB considering three phase flow hydrodynamic, heat transfer and evaporation of the feed droplets. For modelling the gas and solid phases Eulerian approach was used for feed droplet flow, heat absorption, vaporization and their interactions with the gaseous phase

were developed applying Lagrangian approach. The drag force model used in this study was Syamlal and O'Brien (1987). Several experiments were performed in order to obtain the data needed to evaluate the model using a pilot scale CFB unit. The comparison between model predictions of catalyst particle velocity and volume fraction with the experimental data indicated that they were in good agreements. The authors did not discuss the effect of the drag force in their study but they reported that the drag force model used gave good agreement with experimental data.

Chalermssinsuwan et al. (2010) did a two dimensional transient Eulerian CFD modelling of tapered CFB reactor riser using Fluent (6.2.16) commercial software. The authors reported that the drag force model of Gidaspow et al. (1992) model, which is a combination of Wen & Yu and Ergun correlations to describe the interphase interaction between gas and solids, has shown good predictions with a low solid mass flux or a dilute system.

Challenge problem of a CFB was studied by Li et al. (2012) using MFIX open source simulation code. The authors reported that they used the drag force by Gidaspow et al. (1992). Similarly Seo et al. (2011) reported CFD simulation of a dual gas-solid CFB (using the same drag force model of Gidaspow et al. (1992)

#### *Drag models for dense system- BFB models*

One of the very few studies on wood gasification was reported by Gerber et al. (2010). The gas–solid drag coefficient used was that of Syamlal and O'Brien (1989), given by Eq. 3.1 in Table 3.1. The dispersed solid phase within the reactor was modelled as three continuous phases: one phase representing wood and two char phases with different diameters. For the model validation, a two-dimensional lab-scale bubbling fluidized bed reactor was used to compare the model predictions with the experimental data for product gas and tar concentrations and temperature. No discussion was given related to the validity of the drag force model used.

Table 3.1 Drag force models

Equation	Reference
$\beta_{sl} = \frac{3\varepsilon_s \varepsilon_l \rho_l}{4u_{r,s}^2 d_s} C_D \left( \frac{Re_s}{u_{r,s}} \right)  u_s - u_l $	(3.1) (Syamlal and O'Brien, 1989)
$C_D = \left( 0.63 + \frac{4.8}{\sqrt{Re_s/u_{r,s}}} \right)$	(Dalla Valle, 1948)
$u_{r,s} = 0.5 \left( \alpha_l^{4.14} - 0.06 Re_s + \sqrt{(0.06 Re_s)^2 + 0.12 Re_s (1.6 \alpha_l^{1.28} - \alpha_l^{4.14}) + \alpha_l^{8.18}} \right)$	(Garside and Al-Dibouni, 1977)
<p>Note: This model is applicable when <math>\varepsilon_l \leq 0.85</math> but if <math>\varepsilon_l &gt; 0.85</math> the term <math>1.6\varepsilon_l^{1.28}</math> will be <math>2\varepsilon_l^{2.65}</math>. This model is appropriate when the solids shear stresses are defined according to Syamlal et al. (1993)</p>	

$$\beta_{sl} = \frac{3}{4} C_D \frac{\varepsilon_s \varepsilon_l \rho_l |u_s - u_l|}{d_s} \varepsilon_l^{-2.65}$$

$$C_D = \frac{24}{\varepsilon_l Re_s} \left[ 1 + 0.15 (\alpha_l Re_s)^{0.687} \right]$$

(3.2) (Wen and Yu, 1966)

Note: This is appropriate for dilute systems when  $\varepsilon_l < 0.2$

$$\beta_{sl} = \frac{3}{4} C_D \frac{\varepsilon_s \varepsilon_l \rho_l |u_s - u_l|}{d_s} \varepsilon_l^{-2.65} \quad \text{when } \varepsilon_l > 0.8$$

$$C_D = \frac{24}{\varepsilon_l Re_s} \left[ 1 + 0.15 (\varepsilon_l Re_s)^{0.687} \right]$$

$$\beta_{sl} = 150 \frac{\varepsilon_s (1 - \alpha_l) \mu_l}{\varepsilon_l d_s^2} + 1.75 \frac{\varepsilon_s \rho_l |u_s - u_l|}{d_s} \quad \text{when } \varepsilon_l \leq 0.8$$

(3.3) (Gidaspow et al., 1992)

Note: This is appropriate for dilute and dense systems

A recent study by Wang et al. (2013) investigated the gas solid flow in a bubbling fluidized bed coal gasifier. The authors used Eulerian two dimensional transient model on the platform of Fluent (6.3). The authors reported that Syamlal and O'Brien (1987) drag model predicted better results in bed characteristics. They did a comparison between Syamlal and O'Brien (1987) drag model and the Gidaspow et al. (1992) drag models.



Fig. 3.2. Distributions of simulated and measured bed density in a bubbling fluidized bed (Wang et al., 2013).

Fig. 3.2 shows the results reported by Wang et al. (2013). It is clear that the drag model of Syamlal and O'Brien (1987) gives the best match with the experimental data. The authors concluded that the gas–solid drag model is the most important factor to predict the flow pattern in BFB correctly and they also concluded that the Syamlal and O'Brien (1987) drag model gives better results than the Gidaspow et al. (1992) model, as more realistic bed density distributions can be obtained.

One of the very few studies on binary mixtures was recently reported by Zhong et al. (2012). The hydrodynamics of binary solid mixtures in bubbling fluidized beds was modelled using CFD (Fluent 6.3.26) with more attention to the effect of wall boundary condition. The gas–solid drag force used in this study was that of Gidaspow et al. (1992) and the solid–solid drag force used was that of Syamlal (1987) which is shown in Eq. 3.12. The authors recommended in their study to use a new relation by Beetstra et al. (2007) for polydisperse systems. The authors concluded that, the successful simulation of gas–solid flows depends on the proper description of all possible inter-phase interactions, such as gas–solid interactions and interactions between wall and particles.

### 3.2.2.2. Turbulence models

#### Turbulence models for dilute system- CFB models

Hartge et al. (2009) looked into the various formulations for turbulence for gas-solid flow in a CFB. The formulations were tested in combination with two different approaches to solid phase turbulence as shown in Table 3.2. The authors used  $k$ - $\epsilon$  model (Launder and Spalding 1972) with different options; they used RNG model (Yakhot and Orszag, 1986) and Realizable model (Shih et al., 1995). The RNG model is different from the standard  $k$ - $\epsilon$  model. As reported in Fluent documentation RNG model is modified from the standard model to give more accuracy in rapidly strained flows and the swirl effect. The swirl effect can be used with the RNG model and it cannot be used with the standard model. The realizable model developed by Shih et al. (1995) so it can be described as a relatively recent developed model. Realizable model is different than the standard turbulence model in the turbulence viscosity formulation and the transport equation of the dissipation rate. As described in Fluent documentation the realizable model is more accurate in predicting the spreading rate of both planer and round jet as well as providing superior performance for flows involving rotation, boundary layers, separation, and recirculation. The options of turbulence models described above is for single phase and multiphase, then for multiphase there is special arrangements for describing the turbulence. To describe the turbulence of multiphase there are three more options in cooperated with the above mentioned options; mixture turbulence model, dispersed turbulence model, and turbulence for each phase or per phase turbulence model. The mixture model is used when the density ratio between the phases close to 1. The dispersed model is suitable when the concentrations for the secondary phases are dilute. Turbulence model for each phase or per phase model solves the turbulence equations for each phase and as it reported in Fluent documentation this model is suitable when the turbulence transfer among the phases plays a dominant role. However, this model is computationally expensive in contrast with the other models because two extra equations will be solved for each extra phase. The transport equations for standard  $k$ - $\epsilon$  model in one-dimensional formulation are shown in Eq. 3.4 and 3.5 (Launder and Spalding 1972):

$$\frac{\partial}{\partial t}(\rho k) + \frac{\partial}{\partial x_i}(\rho u_i k) = \frac{\partial}{\partial x_j} \left( \left( \mu + \frac{\mu_t}{\sigma_k} \right) \frac{\partial k}{\partial x_j} \right) + G_k + G_b - \rho \varepsilon - Y_M + S_k \quad (3.4)$$

$$\frac{\partial}{\partial t}(\rho \varepsilon) + \frac{\partial}{\partial x_i}(\rho u_i \varepsilon) = \frac{\partial}{\partial x_j} \left( \left( \mu + \frac{\mu_t}{\sigma_\varepsilon} \right) \frac{\partial \varepsilon}{\partial x_j} \right) + C_{1\varepsilon} \frac{\varepsilon}{k} (G_k + C_{3\varepsilon} G_b) - C_{2\varepsilon} \rho \frac{\varepsilon^2}{k} + S_\varepsilon \quad (3.5)$$

Where:

- $K$  the turbulence kinetic energy
- $\varepsilon$  the turbulence kinetic energy's dissipation rate
- $G_k$  represents the generation of turbulence kinetic energy due to the mean velocity gradients
- $G_b$  is the generation of turbulence kinetic energy due to buoyancy
- $Y_M$  represents the contribution of the fluctuating dilatation in compressible turbulence to the overall dissipation rate
- $C_{1\varepsilon}$ ,  $C_{2\varepsilon}$ , and  $C_{3\varepsilon}$  are constants
- $\sigma_k$  and  $\sigma_\varepsilon$  are the turbulent Prandtl numbers for  $k$  and  $\varepsilon$
- $S_k$  and  $S_\varepsilon$  are user-defined source terms.

More information about the equations of these variables and the correlation of the other turbulence correlations are available in fluent documentations.

Table 3.2 Turbulence formulations which have been tested (Hartge et al., 2009).



Hartge et al. (2009) used three dimensional CFD (Fluent 6.3) to simulate the hydrodynamics in the CFB. The model was validated using experimental data. In Fig. 3.3 Hartge et al. (2009) compared between the results of solid distribution obtained with the different turbulence models mentioned in Table 3.2. The authors reported that the results obtained with the realizable per phase setting show low concentrations near the gas distributor, which is not in agreement with what they observed in the experiments. Accordingly, the authors

concluded that the swirl modified RNG model and the dispersed multiphase approach gives the best agreement with the measurements.



Fig. 3.3. Comparison of time averaged distribution of solids inside a CFB riser using different turbulence models (Hartge et al., 2009).

Behjat et al. (2011) incorporated the turbulence effect in a CFB riser by using the modified  $k$ - $\epsilon$  model. The authors reported that the standard  $k$ - $\epsilon$  model is popular in modelling turbulence in industry because its strength, economy and rational accuracy. The authors concluded that the correlations used to model the hydrodynamics with the dispersed turbulence model lead to accurate prediction for the riser's hydrodynamics.

#### *Turbulence models for dense system- BFB models*

In a recent study, Wang et al. (2013) compared two different turbulence models against each other, namely the mixture and dispersed  $k$ - $\epsilon$  turbulence models. Fig. 3.4 shows the comparisons between these two models. The authors reported that the disperse turbulence model gives better prediction when compared to the mixture model because the bubbles formed were qualitatively very close to what was observed in their experiments. The authors

concluded that, the turbulence models have significant influence in modelling the hydrodynamics in fluidized beds and the dispersed k- $\epsilon$  turbulence model can be used effectively to predict the turbulence behaviour in the relatively dense fluidized beds.



Fig. 3.4. Distributions of instantaneous particle volume fraction in a bubbling fluidized bed (a) mixture turbulence model (b) disperse turbulence model (Wang et al., 2013).

### 3.2.2.3. Solid-solid friction models

#### Friction models in dilute system- CFB models

Almuttahir and Taghipour (2008) reported that in fluidized bed systems, gravity and drag are the main forces for the majority of flow regimes, except for very dense flow where the frictional stresses became more important. In most of the reported studies on CFB models the friction effect on the hydrodynamics was assumed negligible; mainly because the flow is dilute. However, in CFB, there is a chance of having dense regions, for example at the bottom region of a riser. It is therefore worth considering review of the related literature for the dense case flow.

#### Friction models for dense system- BFB models

Review of the literature on BFB models indicates conflicting conclusions on the importance of solid-solid friction. Gerber et al. (2010), used two different solid-solid friction models in modelling a BFB wood gasifier. The first model was that of (Schaeffer 1987), which is assumed applicable only if the void fraction was greater than 0.35, for void fraction less than that the model uses a second model proposed by Srivastava and Sundaresan (2003). Schaeffer (1987) frictional viscosity model is given mathematically as follows:

$$\mu_{s,fr} = \frac{p_s \sin \phi}{2\sqrt{I_{2D}}} \quad (3.6)$$

where  $p_s$  is the solids pressure,  $\phi$  is the angle of internal friction, and  $I_{2D}$  is the second invariant of the deviatoric stress tensor.

Wang et al. (2013) reported that in the dense gas–solid suspensions, such as coal gasification in fluidized bed, particles have contact with several neighbouring particles continuously. They added the particle interactions will be better described as frictional as opposed to collisional. Thus, the frictional viscosity should not be neglected in this dense suspension. For this purpose, the authors used Schaeffer (1987) frictional viscosity to incorporate the frictional effects.

#### 3.2.2.4. Two-dimensional vs. three -dimensional simulation

Benyahia et al. (2000) simulated gas/particle flow behaviour in the riser section of a circulating fluidized bed (CFB) using the CFD code Fluent. Fluid catalytic cracking (FCC) particles and air were used as the solid and gas phases, respectively. A two-dimensional, transient and isothermal flow was simulated for the continuous phase (air) and the dispersed phase (solid) particles. The simulation geometry and boundary conditions are shown in Fig. 3.5.



Fig. 3.5. Schematic drawing of 2-D riser with inlet and initial conditions (Benyahia et al., 2000).

The authors concluded real inlet and outlet conditions can be implemented only when using a 3-D simulation with complex geometry. However, computational time is still the major limiting factor to simulate gas-solid flow in complex 3-D geometry.

Almuttahir and Taghipour (2008) reported that, in two-dimensional simulation of a CFB riser the model showed some discrepancy in predicting the gas–solid flow behaviour in the riser operating in dense suspension up-flow and low density fast fluidization regimes. The authors attributed this to possible influence of the turbulence effects which may not have been accurately incorporated in the model. I think the discrepancy reported by Almuttahir and Taghipour (2008) is mainly arises from using 2-D instead of 3-D simulation and the turbulence effect may only play a very limited role on this. According to my own results and observation (discussed in later sections) accurate predictions of the flow hydrodynamics requires 3-D simulation, which in turn result in good results for the dense suspension up-flow and low density fast fluidization regimes. This is related to the observation reported by Benyahia et al. (2000) noted above, where it is concluded that the correct setting of inlet and exit boundaries in a CFB (e.g. solid and gas flux) indeed requires specifying dimensions typical to that existing in the actual three-dimensional experiments.

### **3.2.3. Exit and entrance effect**

Yan et al. (2003) carried out a three-dimensional study on the flow properties in the entrance and exit regions in a CFB riser by measuring particle velocity and solids concentration profiles experimentally, with solids circulation rate ranged up to 550 kg/m<sup>2</sup>s and the superficial gas velocities ranged up to 10.0 m/s, mimicking the industrial high-flux riser reactors. The authors observed asymmetry of the radial profiles of solids concentration and particle velocity at both entrance and exit regions under high-flux conditions. The authors concluded their work by; both the axial and radial profiles of solids concentration and particle velocity are non-uniform, the radial profiles of solids concentration and particle velocity at both entrance and exit regions are asymmetrical, as a result of the influence by the entrance and exit structures. A smooth exit structure, which causes no obvious changes in radial

solids distribution under low flux conditions, can become very “abrupt” under high flux conditions, which results in significant end effects to the flow structure. Such observations are important for comparison and validation of simulation models.

#### **3.2.4. Acceleration, fully developed and deceleration zones in the riser**

Another important characteristic behaviour of a circulating fluidized bed (CFB) riser is the existence of three different distinct flow regions usually classified as acceleration, fully developed and deceleration zones. Sabbaghan et al. (2004) developed a steady state predictive model in order to define the hydrodynamics of the acceleration zone in the riser of a CFB. The predictive model used in this study is the cluster-based approach (CBA) which assumes that all solids in the riser move as clusters and these clusters are treated as rigid spheres. Sabbaghan et al. (2004) described these three distinct zones, i.e., acceleration, fully developed and deceleration zones, as shown in Fig. 3.6. The acceleration zone is the region between the top of the dense bed and the fully developed zone. The authors reported that there is a good agreement between the model predictions and the experimental data. Sabbaghan et al. (2004) also reported that the height of each region depends on the superficial gas velocity, solids mass flux and properties of solids and fluid. Then they concluded the upper region of the riser is assumed to be axially composed of three zones, the acceleration zone is at the bottom part of the upper region where the solids are accelerated to a constant upward velocity, the fully developed zone is located above the acceleration zone, where the flow characteristics are invariant with height, the deceleration zone is located above the fully developed zone, where the solids are decelerated depending on the exit geometry of the riser. With respect to reactions, heat transfer and solid handling in the CFB, the acceleration zone is of particular importance because understanding the solid mixing and flow structure in the acceleration zone is very critical for highly exothermic reactions taking place in the CFB.



Fig. 3.6. Schematic diagram of a circulating fluidized bed reactor (Sabbaghan et al., 2004).

Chan et al. (2009c) experimentally defined the extent of the acceleration zone, including acceleration length and acceleration time; the establishment of a fully developed flow immediately after the acceleration zone; the occurrence of core-annulus flow under specific combinations of  $U$  and  $G$ ; and the disappearance of the intermediate core-annulus region at high values of  $U$  and  $G$ . When the solids circulation flux increases, the dilute transport mode no longer exist. These experimental observations are particularly helpful in qualitative validation of model predictions.

### **3.3. Developing CFB hydrodynamic model**

#### **3.3.1. Simulation Geometry**

The simulation geometries considered in this study are shown in Fig. 3.7a,b. Fig 3.7-a is typical in shape and size of the cold flow experimental riser shown earlier in Fig. 2.1, while Fig. 3.7-b represent a gasifying riser with an additional biomass feed inlet and steam as a

major gasifying agent. In all cases, the solid inlets and outlet were taken as 10cm length extending from the riser wall.

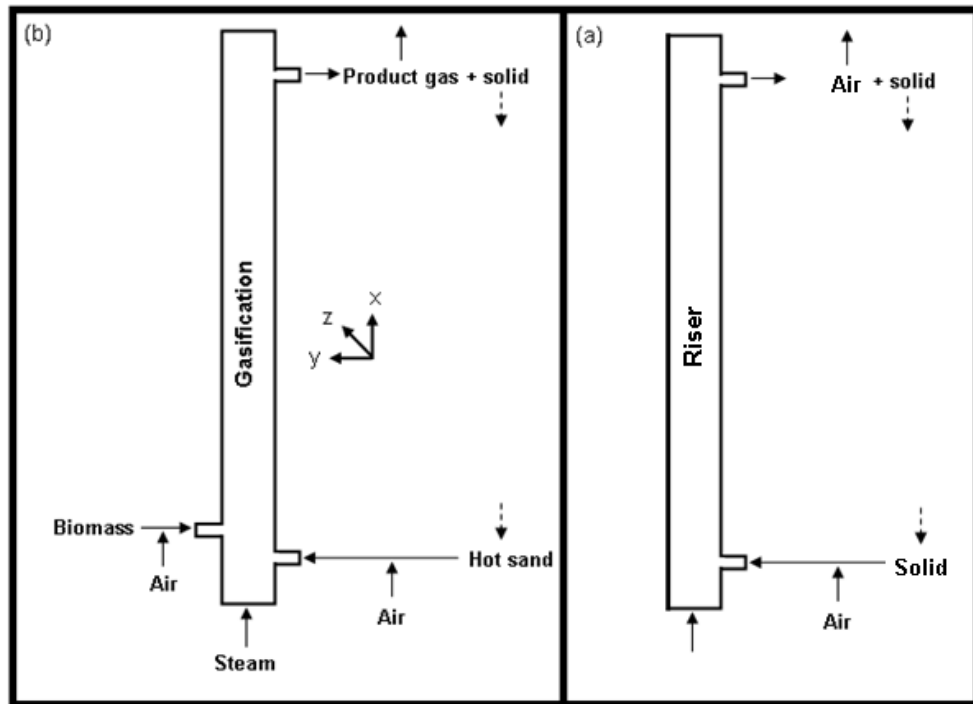


Fig. 3.7. simulation geometry

### 3.3.2. Mesh, grid and time step setting

Advanced Size Function with option of curvature was used in generating the meshes. This option examines curvature on edges and faces and computes element sizes according to the specified maximum angle that one element edge is allowed to span and the minimum and maximum size that the function will return to the surface mesher. This method generates different element sizes and shapes depending on the element position.

In setting the computational cell size for a monodispersed solid mixture, the rule of thumb suggests a minimum grid size of around 10 times the particle diameter. In this analysis, however, we are considering a polydispersed binary mixture of sand and wood spherical particles. In this case we are required to satisfy the rule of thumb for the larger particle size, while keeping the cell face size small enough to avoid losing relevant flow structures for the smaller particle. Unless otherwise specified, the minimum and maximum face sizes used in

this study are 0.08 cm and 0.1 cm respectively. Other parameters used in setting the cell size are given in Table 3.3.

Table. 3.3. The setting of the mesh

Relevance centre	Coarse
Smoothing	Medium
Transition	Slow
Span Angle center	Fine
Curvature Normal Angle	18°
Max Tet size	16.4630 cm

In terms of solution time step, the simple rule of thumb requires that ,  $\Delta t < \Delta x / (u_g + u_s)$  where  $\Delta x$ ,  $u_s$ , and  $u_g$  are grid size, solid velocity and gas velocity respectively. Assuming a grid size of 1 cm and  $(u_g + u_s)$  in the range of 4 m/s, then the time step would be <0.0025 seconds. In order to ensure accurate solution, and in the same time maintaining reasonable computational time, the time step has been set at 0.001, unless otherwise specified.

### 3.3.3. Model equations

The hydrodynamic model equations for the transient multiphase flow in the circulating fluidized bed riser have been solved using Fluent code (Ver 12.1). The model is solved for a primary phase of a gas and two secondary solid phases. The following continue equations for the s<sup>th</sup> sold and the g<sup>th</sup> gas phases have been used:

$$\text{Solid: } \frac{\partial}{\partial t} (\varepsilon_s \rho_s) + \nabla \cdot (\varepsilon_s \rho_s u_s) = 0 \quad (3.7)$$

$$\text{Gas: } \frac{\partial}{\partial t} (\varepsilon_g \rho_g) + \nabla \cdot (\varepsilon_g \rho_g u_g) = 0 \quad (3.8)$$

The volume fraction of each phase is obtained by satisfying the condition that their summation equals one. Note that in solving the solid continue equation for the inert phase, which is sand, the mass transfer term appearing in the right side is zero. Similarly, in the cold flow case (non-reactive system) the right side of the momentum equation for both solid and gas phases is zero.

The momentum equation for the  $s^{\text{th}}$  solid phase is given by:

$$\frac{\partial}{\partial t}(\varepsilon_s \rho_s u_s) + \nabla \cdot (\varepsilon_s \rho_s u_s u_s) = \nabla \cdot \bar{\tau}_s + \varepsilon_s \rho_s g - \varepsilon_s \nabla P - \nabla P_s + \sum_{l=1}^N k_{ls} (u_l - u_s) \quad (3.9)$$

Gas momentum:

$$\frac{\partial}{\partial t}(\varepsilon_g \rho_g u_g) + \nabla \cdot (\varepsilon_g \rho_g u_g u_g) = \nabla \cdot \bar{\tau}_g + \varepsilon_g \rho_g g - \varepsilon_g \nabla P + \sum_{s=1}^{n_s} k_{sg} (u_s - u_g) \quad (3.10)$$

where  $t, \rho, \varepsilon, u, P, g$  represent the time, density, volume fraction, velocity, pressure and gravity constant respectively. The stress-strain tensor and drag force coefficient (also referred to as interphase momentum exchange coefficient) are defined as  $\tau$  and  $\beta$  respectively, and these will be detailed in the model constitutive relations given below. The subscripts  $l$  appearing in Eq. 3.9 and 3.10 stands for solid or gas phases,  $s$  and  $g$  refers to solid and gas respectively.

The principles of the Kinetic Theory of Granular Flow (KTGF) (Ding and Gidaspow, 1990) have been applied to compliment the above hydrodynamic model and the following energy equation for each solid phase has been solved:

$$\frac{3}{2} \left[ \frac{\partial}{\partial t} (\alpha_s \rho_s \theta_s) + \nabla \cdot (\alpha_s \rho_s u_s \theta_s) \right] = \left( -p_s \bar{I} + \bar{\tau}_s \right) : \nabla u_s + \nabla \cdot (k_{\theta_s} \nabla \theta_s) - \gamma_{\theta_s} + \sum \phi_{ls} \quad (3.11)$$

where  $\theta, \bar{I}, k, \gamma, \phi$  represent granular temperature, unit tensor, diffusion coefficient, the collisional dissipation of energy and the energy exchange between the  $l^{\text{th}}$  fluid or solid phase and the  $s^{\text{th}}$  solid phase.

### 3.3.4. Model constitutive equations

In order to solve the above described model a number of constitutive equations are required. Constitutive equations for the case of monodispersed solid mixture in bubbling and circulating fluidized beds have been widely discussed, reviewed and validated in the literature. However very limited number of studies have been focused on the counter part version of these equations for the case of a polydispersed solid flow. Therefore, in this section

various constitutive equation options for a polydispersed solid mixture was presented and discussed, and latter discuss their validity in the simulation of our CFB consisting of a mixture of sand and wood particles. Namely, these are constitutive equations for the solid-fluid momentum exchange, solid-solid momentum exchange, solid pressure and radial distribution function. These equations are applicable to the case of mono-dispersed or poly-dispersed solid mixture, as they simply reduce to the former case by simply setting the number of solid phases to one in the simulation model. The remaining default constitutive equations used in our model are given in Table 3.4. Also various options for the solution of the granular energy equation was discussed in this study.

Table 3.4 Constitutive equations

Constitutive equation	Reference
gas and solid phases stress-strain tensor	
$\bar{\tau}_g = \alpha_g \mu_g (\nabla \cdot \mathbf{u}_g + \nabla \mathbf{u}_g^T) + \alpha_g (\lambda_g - \frac{2}{3} \mu_g) \nabla \cdot \mathbf{u}_g \bar{\mathbf{I}}$	(ANSYS Fluent 12, 2009)
$\bar{\tau}_s = \alpha_s \mu_s (\nabla \cdot \mathbf{u}_s + \nabla \mathbf{u}_s^T) + \alpha_s (\lambda_s - \frac{2}{3} \mu_s) \nabla \cdot \mathbf{u}_s \bar{\mathbf{I}}$	(ANSYS Fluent 12, 2009)
where:	
$\mu_s = \mu_{s,col} + \mu_{s,kin}$	
$\mu_{s,col} = \frac{4}{5} \varepsilon_s d_s \rho_s g_{0,ss} (1 + e_{ss}) \left( \frac{\theta_s}{\pi} \right)^{1/2} \varepsilon_s$	(Syamlal et al., 1993)
$\mu_{s,kin} = \frac{\alpha_s d_s \rho_s \sqrt{\Theta_s \pi}}{6(3 - e_{ss})} \left[ 1 + \frac{2}{5} (1 + e_{ss}) (3e_{ss} - 1) \alpha_s g_{0,ss} \right]$	(Syamlal et al., 1993)
<hr/>	
Energy dissipation and exchange between particles	
$\gamma_{\theta_s} = \frac{12(1 - e_{ss}^2) g_{0,ss}}{d_s \sqrt{\pi}} \rho_s \varepsilon_s^2 \theta_s^{3/2}$	(Lun et al., 1984)
$\phi_{ls} = -3\beta_{ls} \theta_s$	(Gidaspow et al., 1992)

### 3.3.5. Gas-Solid momentum exchange

For a polydispersed solid mixture in suspension, the solids momentum exchange must include, in addition to the drag force resulting from the gas momentum, an additional solid momentum force due to the velocity difference between the interacting solids. The latter is

less understood and often neglected in the formulation of solid momentum equation. It is particularly important when the size or density ratios of different solid is significant.

In this study we investigated three different formulas for the gas-solid momentum exchange coefficient,  $\beta$ , as shown in Table 3.1. The solid-solid momentum exchange was incorporated in the model by using the following equation of Syamlal (1987):

$$K_{sl} = \frac{3(1 + e_{ls}) \left( \frac{\pi}{2} + C_{fr,ls} \frac{\pi^2}{8} \right) \alpha_s \rho_l \alpha_l \rho_l (d_l + d_s)^2 g_{0,ls}}{2\pi(\rho_l d_l^3 + \rho_s d_s^3)} |u_s - u_l| \quad (3.12)$$

where  $C_{fr,ls}$  is the coefficient of friction between the  $l^{\text{th}}$  and  $s^{\text{th}}$  solid-phase particles,  $e_{ls}$  = the coefficient of restitution,  $d_l$  is the diameter of the particles of solid  $l$ ,  $g_{0,ls}$  is the radial distribution coefficient.

### 3.3.6. Solid pressure model and radial distribution function

The solid pressure is a measure of the momentum transfer due to the streaming motion of the particles. It is an important parameter required for the calculation of solid momentum and energy equations. The widely used solid pressure constitutive equation was derived from the principle of kinetic theory of granular flow and is given by Lun et al. (1984) as follows:

$$p_s = \alpha_s \rho_s \theta_s + 2\rho_s (1 + e_{ss}) \alpha_s^2 g_{0,ss} \theta_s \quad (3.13)$$

In this equation, the first term in the right side represents the kinetic contribution arising from the momentum transfer due particle movement across a shear layer and the second term represents the collision contribution arising from the direct particle-particle contacts. It is worth noting that, for a relatively dense system, Syamlal et al. (1993) proposed neglecting the kinetic contribution to the total solid pressure and only retaining the second term, such that Eq. 3.13 becomes:

$$p_s = 2\rho_s (1 + e_{ss}) \alpha_s^2 g_{0,ss} \theta_s \quad (3.14)$$

The sensitivity analysis carried out in this study has shown negligible difference between the hydrodynamic predictions obtained with Eq. 3.13 and those obtained with Eq.3.14.

For the case of a bidispersed suspension, the effect of the contacts between different particles on the overall solid pressure on solid  $s$  is considered through the summation of all collision with  $N=2$  solids, such that Eq. 3.13 becomes (Fluent documentations):

$$p_s = \alpha_s \rho_s \theta_s + \sum_{n=1}^N 2 \frac{d_{ns}^3}{d_s^3} \rho_s (1 + e_{ns}) \alpha_n \alpha_s g_{0,ns} \theta_s \quad (3.15)$$

### 3.3.7. Radial distribution function

The radial distribution function,  $g_0$ , is an important parameter introduced to take into consideration the probability of collisions when the solid phase becomes dense. It appears in the collisional part of the solid pressure equation (Eq. 3.15) and the solid-solid momentum exchange coefficient (Eq. 3.12). The various forms of the radial distribution function investigated in this study are given in Table 3.5.

Table 3.5 Various forms of the radial distribution function

Equation	Reference
$g_{o,ks} = \left[ 1 - \left( \frac{\alpha_s}{\alpha_{s,\max}} \right)^{1/2} \right]^{-1} + \frac{1}{2} d_k \sum_{k=1}^N \frac{\alpha_k}{d_k}$	(Lun et al., 1984)
Note: This is the default RDF, unless otherwise specified	
$g_{o,ks} = \frac{1}{(1 - \alpha_s)} + \frac{3 \sum_{k=1}^N \frac{\alpha_k}{d_k}}{(1 - \alpha_s)^2 (d_k + d_s)} d_k d_s$	(Syamlal et al., 1993)
where: $\alpha_s = \sum_{k=1}^N \alpha_k$	
$g_{o,ks} = \left[ 1 - \left( \frac{\alpha_s}{\alpha_{s,\max}} \right) \right] + \frac{3}{2} d_k \sum_{k=1}^N \frac{\alpha_k}{d_k}$	(Iddir and Arastoopour, 2005)

In Eqs. In Table 3.5,  $\alpha_{s,\max}$  is the maximum allowable solid volume fraction,  $\alpha_s$  and  $\alpha_k$  are the volume fractions of solids  $s$  and  $k$  respectively,  $d_k$  and  $d_s$  are the particle diameters. Note that all

the radial distribution functions given in Table 3.5 reduces to the standard single solid phase expressions when  $N = 1$  and  $k = s$ .

### 3.3.8. Boundary conditions

In the simulation geometry of the experimental riser shown in Fig. 3.7, there are four boundaries: gasifying agent inlet, solid/gas inlet, solid/gas outlet and wall. An additional biomass inlet boundary is shown for the gasifier.

At all the solids feeding points a specified flow rate have been used as a boundary condition, while at the fluidizing agent inlet a velocity boundary condition is specified. At the riser exit the boundary condition is a specified pressure. For the gas phase, the tangential velocity at the wall is assumed as zero (no slip condition). For each solid phase, the widely used boundary conditions of Johnson and Jackson (1987) are used as follows:

$$n_s \tau_s \frac{u_s}{|u_s|} + \frac{\sqrt{3}\pi\phi' g_o \rho_s \varepsilon_s |u_s| \sqrt{\theta}}{6\varepsilon_{s-\max}} = 0 \quad (3.16)$$

$$k_s \frac{\partial \theta}{\partial y} = \frac{\sqrt{3}\pi\rho_s g_o \varepsilon_s \sqrt{\theta}}{6\varepsilon_{s-\max} \mu_s} \left[ \phi' |u_s|^2 - \frac{3T}{2} (1 - e_w^2) \right] \quad (3.17)$$

Where  $\varepsilon_s$  and  $\phi'$  are the specified maximum solid volume fraction and the specularity coefficient, and the values used are 0.63 and 0.5 respectively.

## 3.4. Validation and verification of the hydrodynamic model for one solid phase

This section presents simulation results of the hydrodynamic behaviour using Fluent. In order to build a valid CFD hydrodynamics model of CFB, a number of constitutive relations and correlations have been implemented and compared using simulation code, this was followed by a sensitivity analysis for time steps and grid size were carried out to optimize the computational time with solution accuracy. To validate the simulation two types of experiments were carried out, namely pressure measurement and PEPT. The validated

model is then used to gain further detailed hydrodynamic predictions of particular relevance to gasification process.

### 3.4.1. Validation using pressure measurements

#### 3.4.1.1. Particle size effect

Particle size affects the hydrodynamics in CFBs; different particle shapes and sizes cause different flow behaviour. To investigate this issue, four different glass beads particle sizes were used in experiments to compare the pressure results with simulation pressure data.

Glass beads sizes are: 755 $\mu\text{m}$ , 550 $\mu\text{m}$ , and 409 $\mu\text{m}$  and 150  $\mu\text{m}$ .

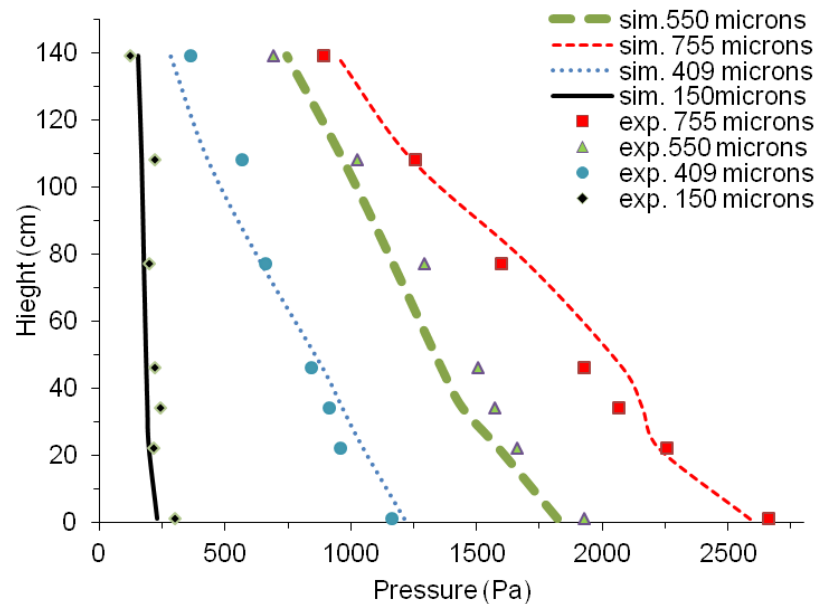


Fig. 3.8. Experimental and simulation pressure verses height for four different glass beads sizes

Fig. 3.8 shows pressure variations along the riser height as a function of particle size. It is clear that within the particle size range of 800-150 $\mu\text{m}$  there is a good match between the experiments and modelling.

#### 3.4.1.2. Turbulence model

Different combinations of turbulence models were set and compared with laminar option and experimental data. The combinations are Turbulence Standard Dispersed (T.S.D.),

Turbulence Standard Mixture (T.S.M.), Turbulence Standard Per Phase (T.S.P.P.) and RNG dispersed.

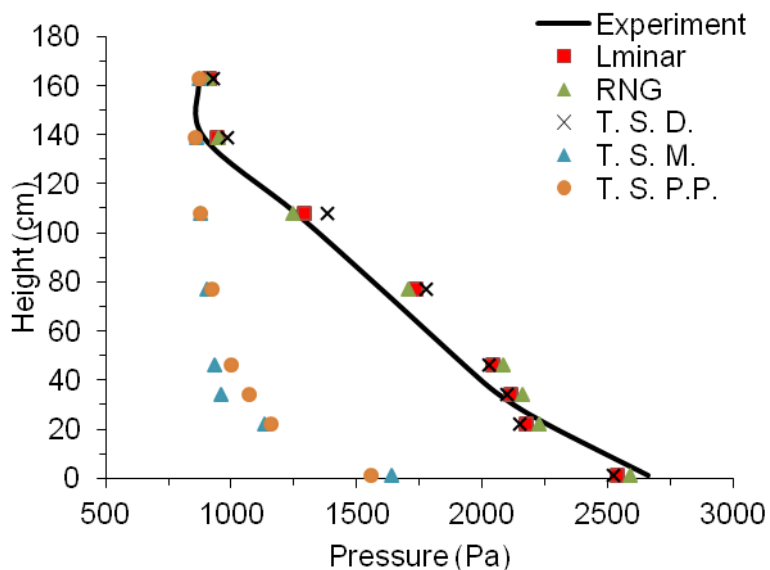


Fig. 3.9. Laminar and different turbulence models against experimental data. Using 755 $\mu$ m glass beads, 600 lit/min gas flow and 36.42g/s solid mass flow

Fig. 3.9 shows the pressure versus height using these different combinations. T.S.M. and T.S.P.P. show significant difference from the experiment data. RNG, Laminar and T.S.D. all appear to show good agreement with the experimental data.

#### 3.4.1.3. Gas-solid and solid-solid momentum exchange coefficient (drag coefficient)

In validating the gas-solid drag momentum exchange coefficient (drag coefficient) an investigation was first considered for the monodispersed phase. Different drag force models were used and compared, namely the models of Wen and Yu (1966), Syamlal and O'Brien (1989) and Gidaspow et al. (1992) as these are the optionally available coefficient in Fluent simulation code. These coefficients were validated by comparing with the predicted pressure distribution with the experimental data obtained for two different particle sizes and flow conditions as shown in Fig. 3.10. For case considered here, it is clear that the drag coefficient of Syamlal and O'Brien (1989) produces the best agreement with the experimental data. The poor predictions by the other two equations may be attributed to their limitation to a range of solid concentration, therefore fail to predict the flow in wide range of solid

concentration variations existing in this CFB riser. Wen and Yu (1966) correlation is understood to be only accurate for dilute suspension within the void fraction limit of  $>0.8$ . Gidaspow et al. (1992) correlation, on the other hand, suffers from discontinuity at the void fraction value of 0.8, which is assumed to be the switching point between dilute and dense flow. This problem appears to be eliminated in Syamlal and O'Brien (1989) equation as a result of smooth regime transition incorporated through the terminal velocity term appearing in the drag coefficient term.

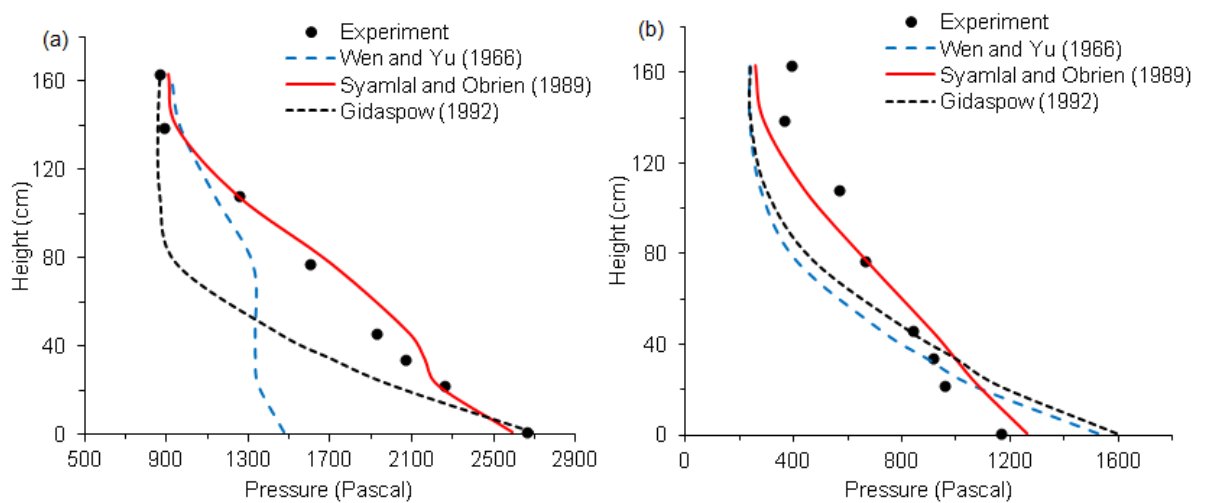


Fig. 3.10. Comparison of the different gas-solid drag models (momentum exchange) tested in the simulation of a monodispersed solid mixture. (a) particle size of  $755\mu\text{m}$  glass beads, 600 lit/min gas flow (velocity of 4.71 m/s) and 36.42 g/s solid mass flow (b) particle used of  $409\mu\text{m}$  glass beads, 405 lit/min gas flow (velocity of 3.18 m/s) and 23.0 g/s solid mass flow.

With the accurate and satisfactory results obtained by Syamlal and O'Brien (1989) gas-solid exchange momentum, this was then incorporated in the simulation of a polydispersed mixture. In doing this investigation the effect of solid-solid momentum exchange through the incorporation of Eq. 3.12 has been considered. The results shown in Fig. 3.11 clearly confirm the validity of the use for gas-solid exchange coefficients Syamlal and O'Brien (1989) for a bidispersed solid mixture. It is also shown that the effect of the solid-solid hydrodynamic drag is clearly very significant and appear to be modeled correctly by the introduction of the solid-solid momentum exchange coefficient of Syamlal (1987). The results is in good agreement with the study of Yin and Sundaresan (2009) where it the importance of solid-solid hydrodynamic drag in multi-solid suspension has been confirmed, the reader can also refer

to the reference for more detailed information on the derivation of alternative equations for the solid-solid momentum exchange coefficient.

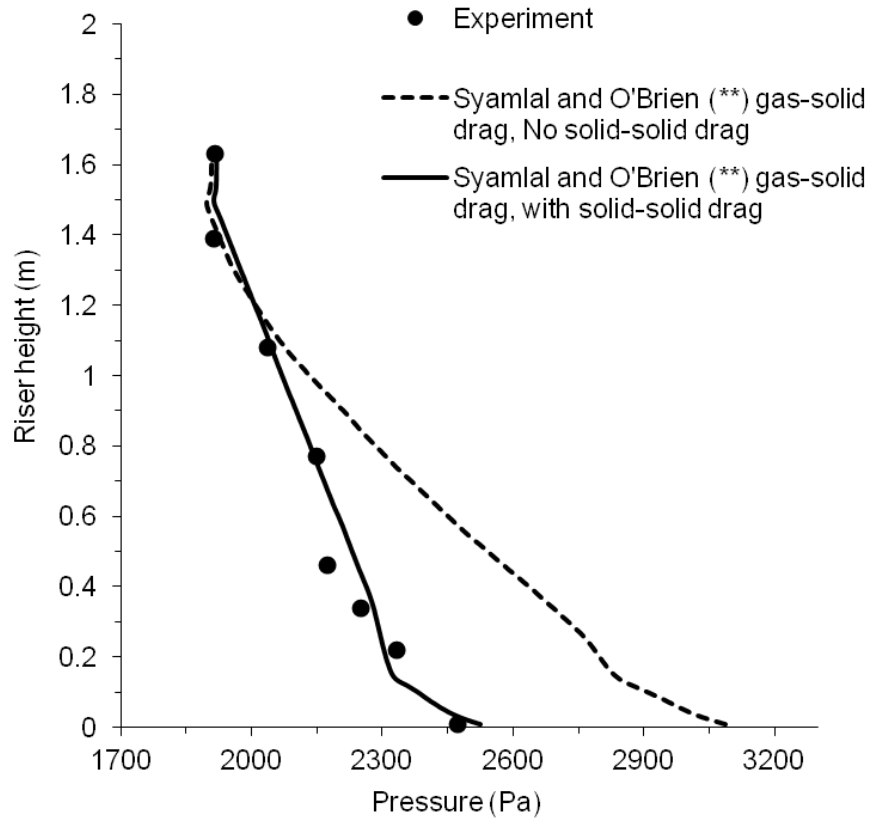


Fig. 3.11. Validation and sensitivity analysis of the model to the gas-solid and solid-solid momentum exchange coefficient for the case of a polydispersed binary mixture of glass beads. Phase 1 of  $d_s = 755 \mu\text{m}$ ,  $\rho_s = 2500 \text{ kg/m}^3$ ) and Phase 2 of  $d_s = 376 \mu\text{m}$ ,  $\rho_s = 2500 \text{ kg/m}^3$  with the mixing ratio of 83 wt% to 17 wt% respectively. The CFB riser was operating at a fluidization velocity of 3.6 m/s and a total solid feeding rate of 35 g/s.

#### 3.4.1.4. Granular temperature model and solution of the energy equation

Granular Temperature is a measure of the kinetic energy of the random motion of the particles. The energy equation is introduced into the two-fluid model formulations to determine the granular temperature, which is an important parameter required for the description of the solid phase stresses. The granular temperature is obtained by solving the partial differential equation (PDE) given in Eq. 3.11. Alternatively, a simplified energy equation can be obtained after neglecting the convection and diffusion terms in Eq. 3.11 to give the following equation:

$$0 = \left( -p_s \bar{I} + \bar{\tau}_s \right) : \nabla u_s - \gamma_{\theta_s} + \phi_{\theta_s} \quad (3.18)$$

In solving the partial differential equation option it is possible to choose different options for its properties. These options include the solids granular conductivity term,  $k_{\theta_s}$  in Eq. 1.8 , which can optionally be calculated using (Syamlal et al. (1993) or Gidaspow et al. (1992)) conductivity models. In order to investigate the accuracy of each of these model options, Fig. 3.12 shows the experimental pressure compared to the results obtained using the various model options discussed above

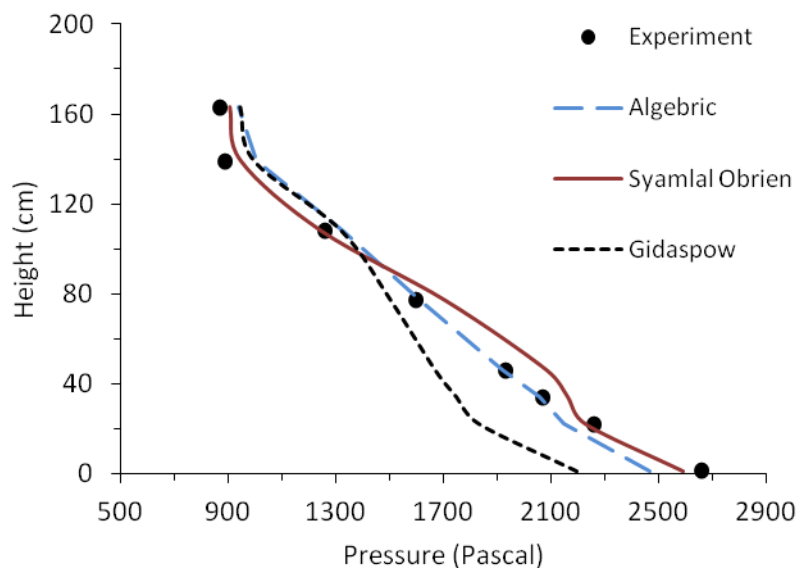


Fig. 3.12. Pressures versus height for different granular temperature models. Using 755 $\mu\text{m}$  glass beads, 600 lit/min gas flow and 36.42g/s solid mass flow

Generally, both of Syamlal et al. (1993) partial differential equation option and the simple algebraic equation show good match with the experimental data, The partial differential equation of option with Gidaspow et al. (1992) conductivity clearly deviate from the experimental data in the bottom zone of the riser, which may suggest inaccuracy of this model for a relatively dense suspension.

The solution of the PDE requires setting the solution to a relatively small time step to avoid complicated convergence problem, thus longer computational time. It is therefore, particularly important to verify the appropriate solution options for the energy equation, especially when treating complicated and time consuming computation for a polydispersed solid mixture.

However, the attempt to running the computer model for the case of polydispersed mixture was unsuccessful due to numerical difficulties, which causes solution divergence even at unrealistic small time step of  $10^{-6}$  s. On the hand, with the algebraic equation option, the solution was successful and fast, mainly because the granular temperature is directly obtained from a simple algebraic expression. Therefore, a decision has been made here to consider verifying the algebraic solution option by comparing it with the solution of the PDE for the simple case of monodispersed mixture.

Fig. 3.19 shows the comparison of the computed granular temperature using the PDE and the simplified algebraic equation options. It is interesting to see that both solution options provide comparable results. This is despite the recognized fact that the simple algebraic equation neglects the contributions of convection and diffusion terms. Nevertheless, taking into consideration the numerical difficulties associated with the solution of the PDE and considering the satisfactory results shown in Fig. 3.19 for the simplified algebraic equation, a decision has been made to use this simplified option in the final developed model.

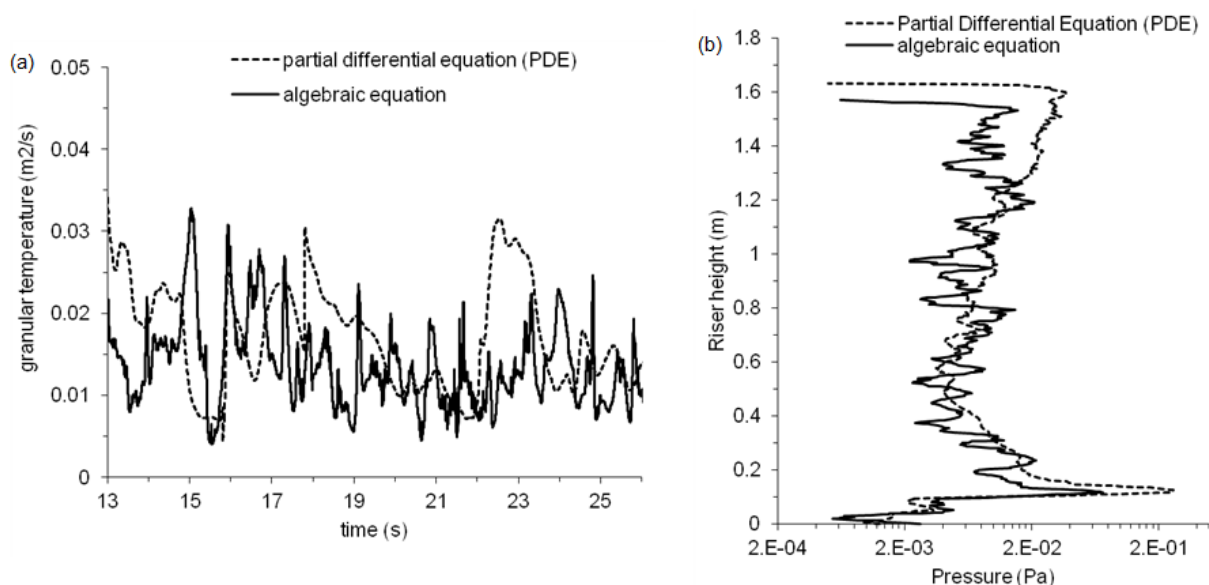


Fig. 3.19. Granular temperature predicted by two different solutions methods of the energy equation. (a) time series data represent the cross sectional average granular temperature obtained at 100 cm height (b) axial profile representing cross-sectional average granular temperature. Data produced with a monodispersed mixture of particle size of 755  $\mu\text{m}$  fluidized by air at 4.7 m/s at the solid circulation rate of 36.4 g/s.

#### 3.4.1.5. Solid-solid friction model

Frictional stresses play an important role in dense particle systems. As noted in the literature section, it is generally believed that CFB operate in a dilute regime, however it is of interest to confirm its effect within the operating conditions in this study, especially that the bottom region of the riser may relatively be dense.

There are two main correlations for friction effect, Johnson and Jackson (1987) and Schaeffer (1987) in addition to the option of ignoring the friction effect. These three options were used and compared with experimental data to find which one is the best in modelling the friction in CFBs. Friction limit used in fluent is between 0.61 packing limit minimum to 0.63 packing limit maximum. The volume fraction of solids does not exceed 30 percent in most the riser except in the entrance it may go over if the solid flow rate are very high. So, the friction do not have big influence in the hydrodynamics in CFBs. Fig. 3.13 emphasize this fact because this figure shows there is no significant variations simulation and experimental results. As it mentioned above there are three options which were used to simulate the friction effect, the first one is Johnson and Jackson (1987) which is shown in the figure as Johnson, None in the figure means ignoring the friction effect which is means no correlation was used to simulate the friction and finely Schaeffer (1987) which shows small divergence in the bottom.

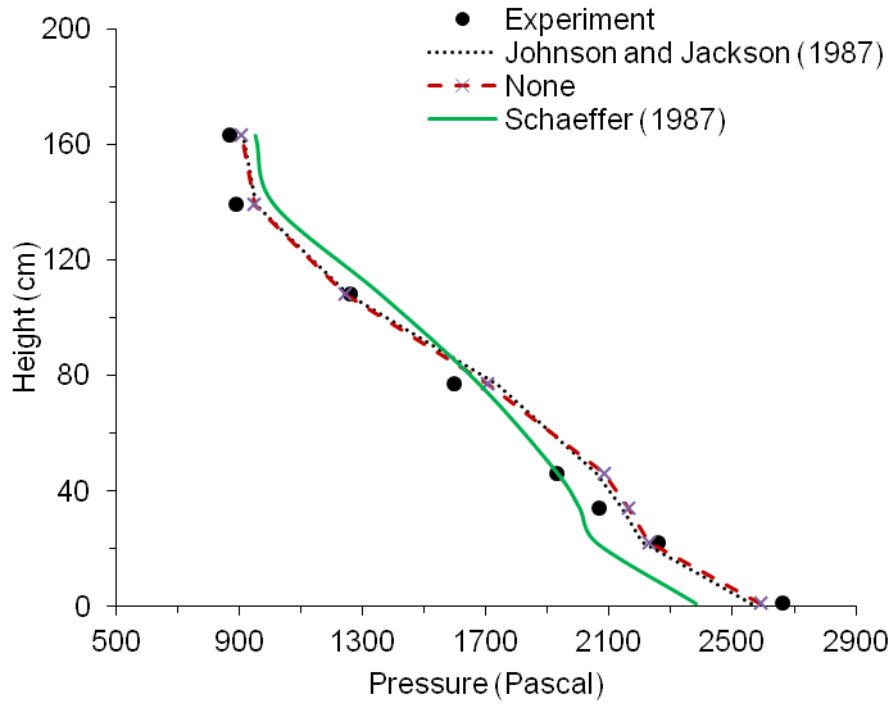


Fig. 3.13. Different friction correlations with experiment pressure data along the riser. Using 755 $\mu$ m glass beads, 600 lit/min gas flow and 36.42g/s solid mass flow

#### 3.4.1.6. Radial distribution function (RDF)

The radial distribution function (RDF),  $g_0$ , is a correction factor that modifies the probability of collisions between grains when the solid granular phase becomes dense. Three different models were applied and compared against each other. These models were illustrated in Table 3.5. From the definition of the  $g_0$ , this function works in dense conditions to modify the probability of collisions between grains but in CFBs the media is dilute so the effect of radial distribution function is weak as shown in Fig. 3.14. With the exception of Arastoooper RDF (Iddir and Arastoopour, 2005), the other two correlations appear to show good match with the experimental data.

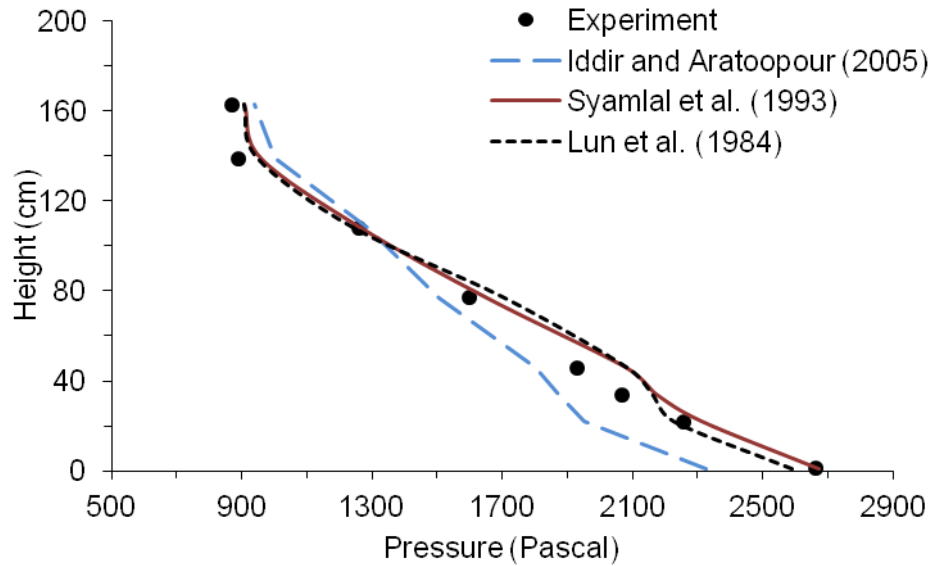


Fig. 3.14. Pressures verses height for different radial distribution correlations. Using 755 $\mu$ m glass beads, 600 lit/min gas flow and 36.42g/s solid mass flow

With the result for a monodispersed mixture validated, it was then important to further investigate and confirm the validity of the RDF for a polydispersed mixture. Fig. 3.15 shows the plot of the three radial distribution functions, shown in Table 3.5, for a polydispersed solid mixture as function of the total solid volume fraction ( $\alpha_s = \alpha_{s,1} + \alpha_{s,2}$ ). Lun et al. (1984) and Iddir and Arastoopour (2005) functions show exponential increase as the solid packing approach the maximum limit. The values obtained with the radial distribution function of Syamlal et al. (1993) are consistently low, with deviation of more than 80% when compared to the other two functions at high solid concentration. However, within the low solid concentration range of  $< 0.1$ , which is relevant to the case of CFB riser, this deviation is limited to  $< 25\%$ .

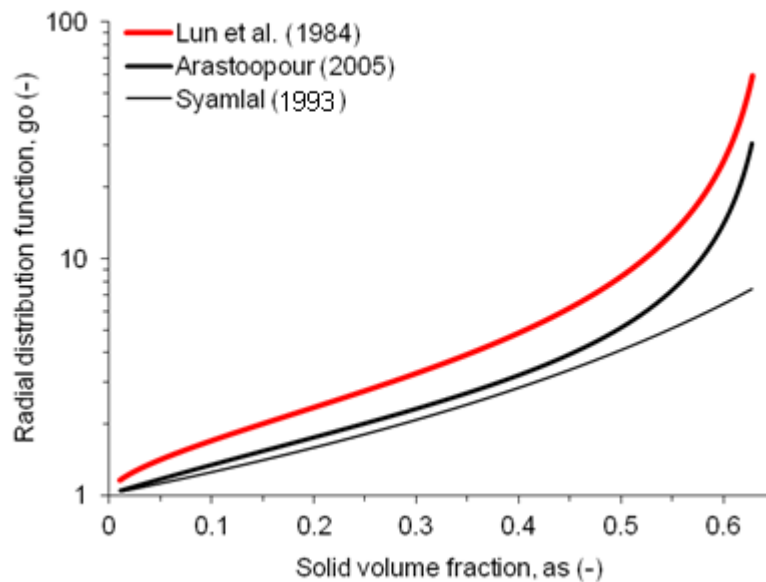


Fig. 3.15. Comparison of different radial distribution functions for a polydispersed solid mixture as function of the total mixture solid concentration. Calculation carried out with respect to the larger size for a mixture of particles size ratio of  $d_1 : d_2 = 755 : 400$  .

Further investigation of the model sensitivity to two of the RDFs are shown in Fig. 3.16 by comparing the predicted radial profiles of solid velocity and concentration as shown in Fig. 3.16. It is clear that there are no significant differences between the tested RDFs . This is not surprising since both functions produce very close values for the range of solid concentration given in Fig. 3.15. Even at a higher solid concentration close to 0.2, which is at the extreme end in CFB operation, the analysis confirms no significant differences in the hydrodynamic predictions. However, caution must be exercised when considering denser suspension.

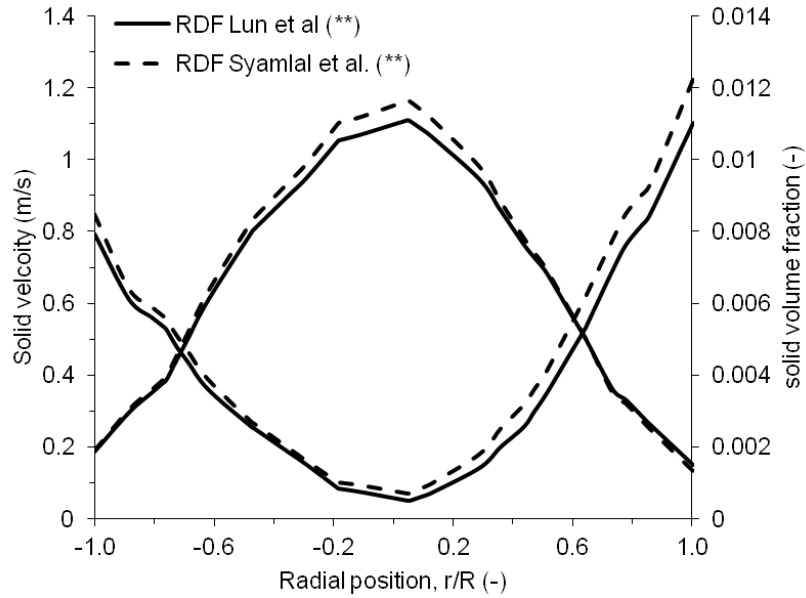


Fig. 3.16. Sensitivity analysis of the model to the radial distribution function the case of a polydispersed binary mixture of glass beads. Phase 1 of  $d_s = 755 \mu\text{m}$ ,  $\rho_s = 2500 \text{ kg/m}^3$ ) and Phase 2 of  $d_s = 376 \mu\text{m}$ ,  $\rho_s = 2500 \text{ kg/m}^3$  with the mixing ratio of 83 wt% to 17 wt% respectively. The CFB riser was operating at a fluidization velocity of 3.6 m/s and a total solid feeding rate of 35 g/s.

#### 3.4.1.7. Solids pressure

Two models were used to simulate solids pressure and compared with experimental data. These two options were plotted in Fig. 3.17. The two correlations used were Lun et al. (1984) and Syamlal et al. (1993). Lun et al. (1984) and Syamlal et al. (1993) has the good agreement with the experimental data but Syamlal et al. (1993) diverted from the experimental data when the radial distribution function is incorporated with Lun et al. (1984). It is therefore very critical to have the correct pairing of the solid pressure term with the corresponding radial distribution function

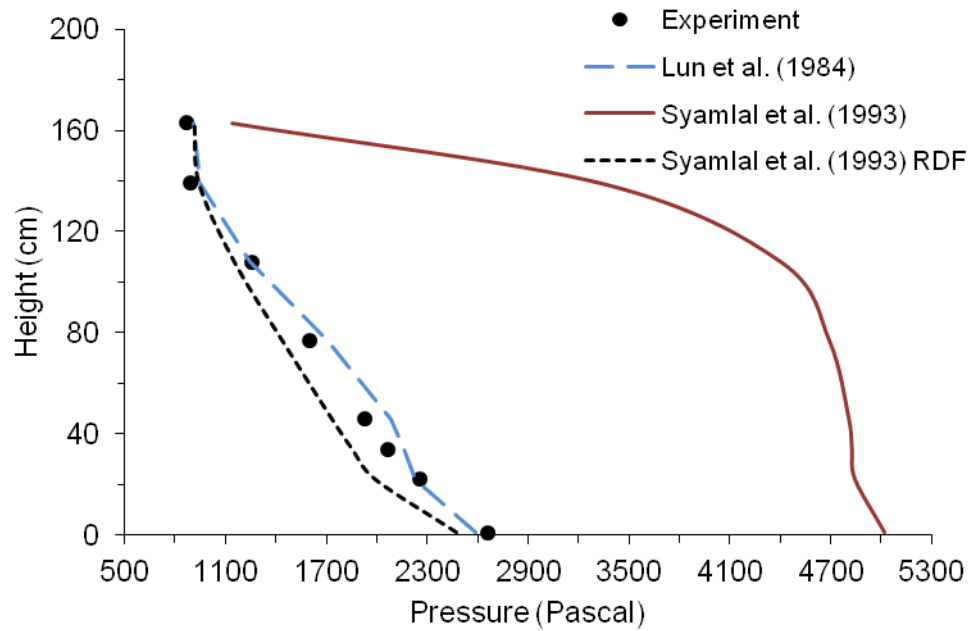


Fig. 3.17. Pressures versus height for different solids pressure correlations. Using 755 $\mu\text{m}$  glass beads, 600 lit/min gas flow and 36.42 g/s solid mass flow

### 3.4.2. Meshing (cell size) and solution time step

In terms of solution time step, the simple rule of thumb requires that  $\Delta t < \Delta x / (u_g + u_s)$ , where  $\Delta x$ ,  $u_s$ , and  $u_g$  are grid size, solid velocity and gas velocity respectively. Assuming a grid size of 1 cm and  $(u_g + u_s)$  in the range of 4 m/s, then the time step would be  $< 0.0025$  seconds. In order to confirm this five different time steps (0.001, 0.01, 0.05, 0.1 and 0.5 seconds) have been tested in the simulation of a mono-dispersed solid phase. The results shown in Fig. 3.18 indicate that there are no significant differences between all of the time steps investigated, except for a time step beyond 0.1, which may result in shifting away from the experimental data as confirmed shown in Fig. 3.18. In fact, the simulation completely diverged and no solution was obtained when attempting a time step of 0.5 seconds.

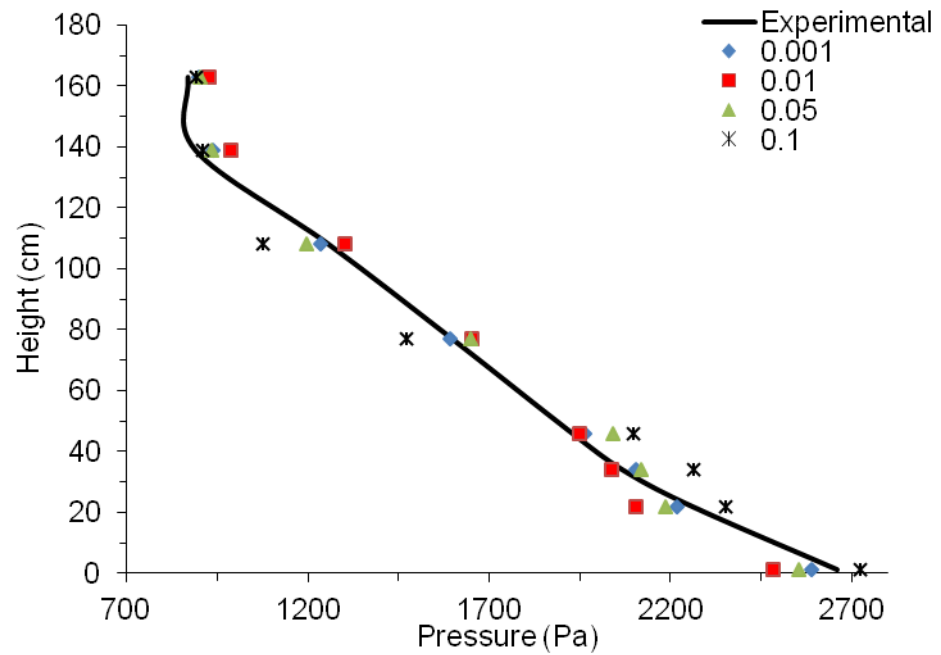


Fig.3.18. Time step sensitivity analysis for the same operating conditions. Using 755 $\mu$ m glass beads, 600 lit/min gas flow and 36.42g/s solid mass flow.

For the geometry under consideration a total number of computational cells in the range of 57006 to 69433 were tested to investigate the model sensitivity and accuracy with respect to the computational grid size. Three different Maximum face sizes of 0.8, 1.0 and 1.5 cm were considered in the analysis. The general rule of thumb for meshing is that the mesh face size has to be at least ten times the particle size, i.e. if the particle diameter is 100  $\mu$ m the grid diameter has to be 1000  $\mu$ m or more. Fig. 3.19 shows the comparisons between these three grid sizes for the case of a single solid phase of 755  $\mu$ m diameter. Clearly, great similarity between the results obtained with these three grid sizes can be observed, thus indicate accurate solution of the model equations for the grid size range considered here.

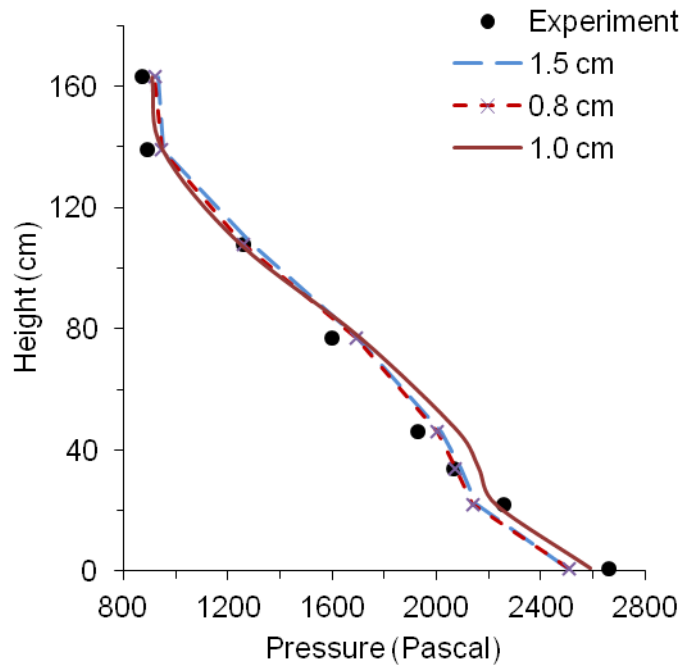


Fig. 3.19. Grid sensitivity analysis using three different grid sizes. Using 755 $\mu$ m glass beads, 600 lit/min gas flow and 36.42g/s solid mass flow

In the figures 3.18 and 3.19, the analysis was limited to monodispersed solid case. For the case of polydispersed solid mixture it is required to satisfy the rule of thumb for the larger particle size, while keeping the cell face size small enough to avoid losing relevant flow structures for the smaller particle. In order to confirm this for the case of polydispersed solid mixture it was critically important to (i) ensure cell-size independency solution that accurately captures both the meso and macro scale flow structures and (ii) limit the computational time to a reasonable level given the vast number of calculations required to predict multi-solid interactions. It is worth noting that sensitivity of the two-fluid model to the computational grid size and solution time step have been discussed in numerous studies in the past, however, most of these were focused on two-dimensional simulation of a single solid phase flow.

### 3.4.3. Hydrodynamic model validation using PEPT technique

#### 3.4.3.1. Observations from PEPT experiments

Very interesting observations were observed during PEPT experiments as shown in Fig. 3.20 the velocity and the vertical positions of the radioactive solid particle were plotted against the time. Both figures show that the particle goes out the vision of the PEPT zone then return to the PEPT zone again. In Fig. 3.20-a the velocity decreased then increased again and in Fig.

3.20-b the particle was falling then rising again. The falling of the particle was associated with the decreasing of the velocity and the rising of the particle associated with the increasing of the velocity. That means the particle does not go up all the time but it goes up and down or in another words it goes in swirling motion. This kind of motion will affect the gasification process specially in the bottom zone of the riser.

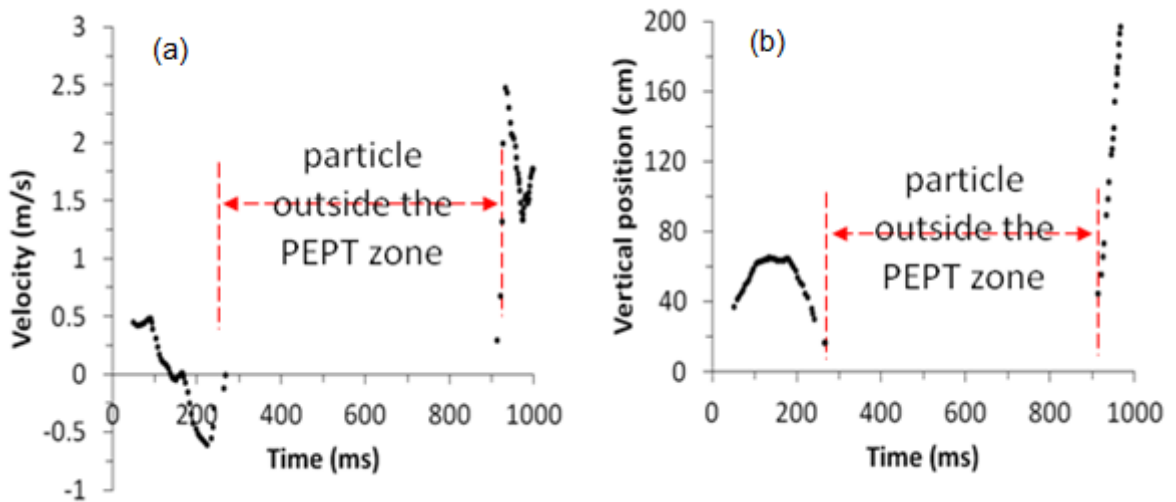


Fig. 3.20. PEPT experiment result using glass beads ( $d_s = 755 \mu\text{m}$ ,  $\rho_s = 2500 \text{ kg/m}^3$ ) with total air flow of 600 lit/min. (a) Vertical velocity of the radioactive particle (m/s) verses time ms. (b) Vertical position of the radioactive particle (cm) verses time (ms)

#### 3.4.3.2. Particle velocity

Fig. 3.22 compares the PEPT measurements and the model prediction of the solid velocity for the case of a polydispersed mixture of wood and glass beads in the CFB riser. Due to restrictions of the experiment set up and the PEPT sensor arrangement, the measurements were only taking at the lower part of the riser. The Measurements represent the volume average velocity within a height of 60 cm at the bottom region of the CFB riser as shown earlier in Fig.2.7. This comparison indicates a reasonable good match with the experimental data, thus giving more evidence on the validity of the proposed model and constitutive relations for the simulation of a polydispersed flow hydrodynamics in a CFB riser. Further interesting information extracted from the PEPT measurements are given in the next section.

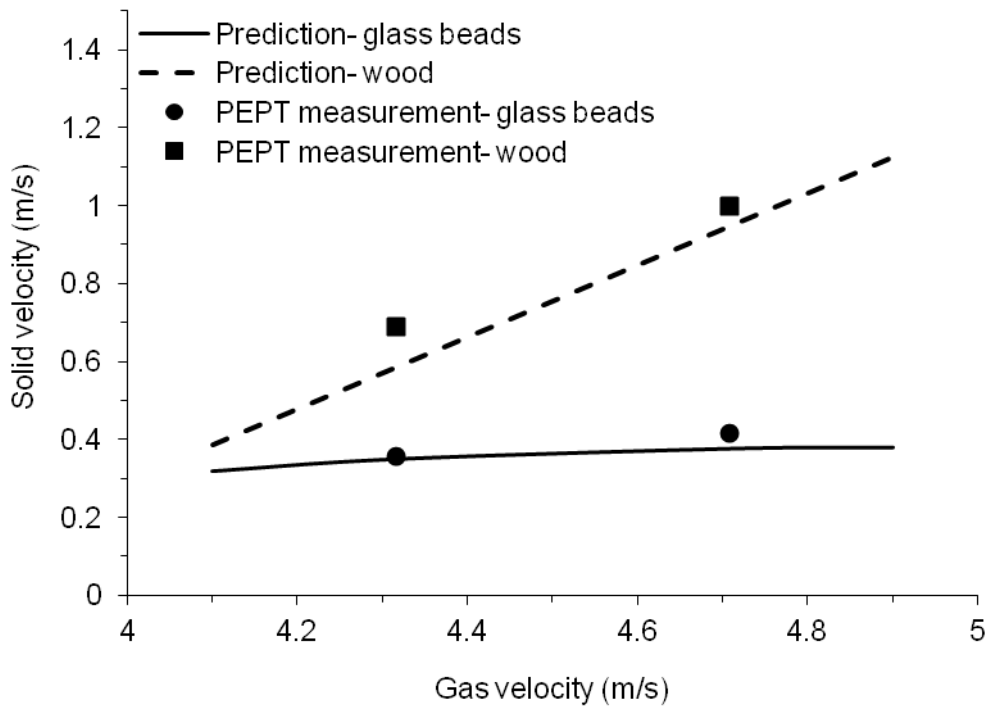


Fig. 3.21. Comparison of predicted and measured solid velocity for the case of a polydispersed binary mixture of glass beads ( $d_s = 755 \mu\text{m}$ ,  $\rho_s = 2500 \text{ kg/m}^3$ ) and wood ( $d_s = 1000 \mu\text{m}$ ,  $\rho_s = 585 \text{ kg/m}^3$ ).

#### 3.4.4. Interesting hydrodynamic features of the CFB gasifier

##### 3.4.4.1. Phase distribution and velocities (sand and biomass)

In a CFB biomass gasifier it is important to control the solid and gas residence time to ensure completion of the various homogenous and heterogeneous reactions. This is directly related to the flow velocities and phase distribution. The flow structure in a CFB riser is generally characterized by a dilute core and dense annulus with downwards flow of solids at the wall region. In this study the flow is complex due to the existence of multi-solid phases and the fact that the solids are introduced from the side walls (see Fig. 3.7).

Fig. 3.23 shows the axial profile of the wood and sand concentration and the corresponding contour of the sand velocity. It is clear that the cross sectional average concentration of both phases is constant after a short entrance length. It is interesting that the sand concentration is 10 times higher than the wood, which is the typical actual ratio of the mass flow of both phases. This indicates very limited segregation effects. The velocity contours indicate three distinctive zones. These are characterized by increasing solid velocity above the feeding

point (acceleration zone) followed by a constant velocity at region (fully developed zone) at an increasing velocity zone extending all the way to the solids exit (deceleration zone). Similar observation have been previously reported by Sabbaghan et al. (2004).

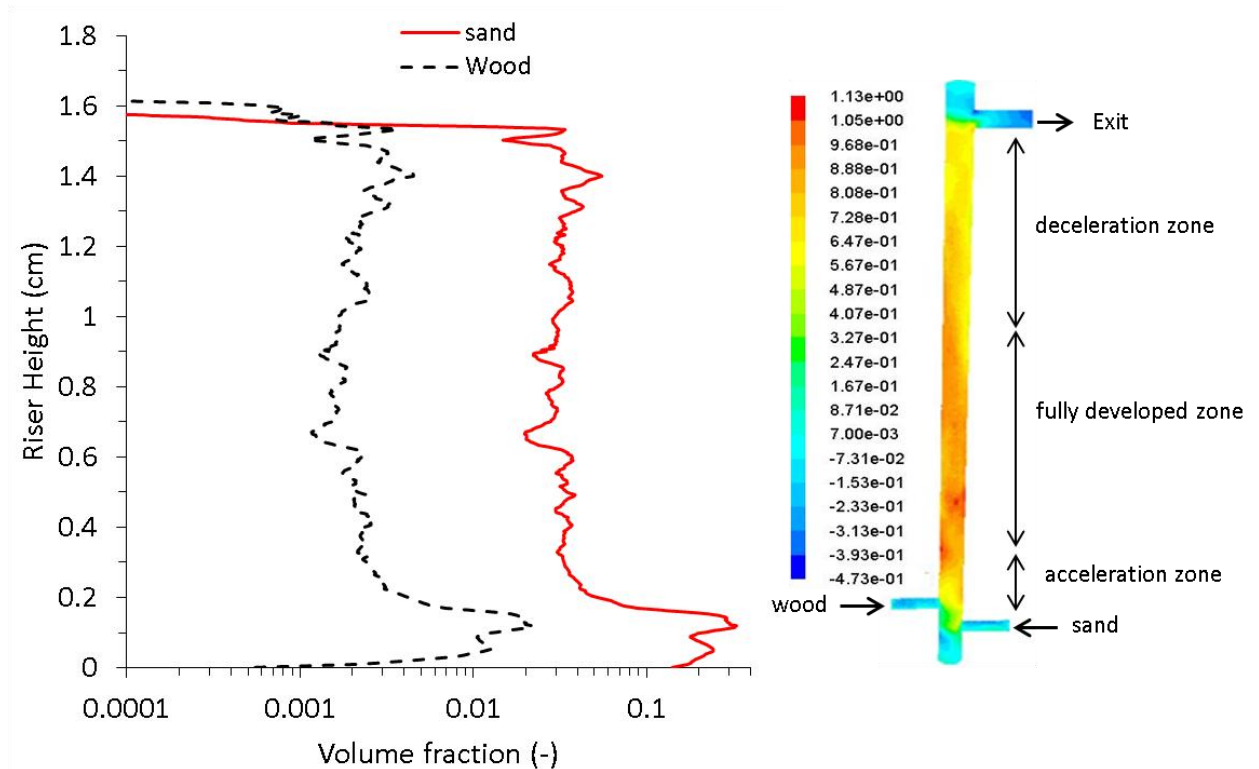


Fig. 3.22. Acceleration, developed and deceleration zones for two solids.

Fig. 3.24 show the radial profiles of solid distribution and velocity for a binary mixture (wood and sand) at two different heights in the CFB riser. In Fig. 3.24, both solid phases show a typical core and annular flow pattern, however with considerable differences in concentrations, which is obvious due to the fact the wood concentration in the feed is only 10 wt%. These profiles suggest negligible entrance and exit effects on the phase distribution despite the riser being of a relatively short one. The solid velocity profile on the other hand depicts a completely different behaviour, where it is clear that entrance and exit effects causes significant asymmetry due to the downfall of solids at the wall opposite to the solid feeding and exit. In the central region of the riser, the flow appears to be fully developed.

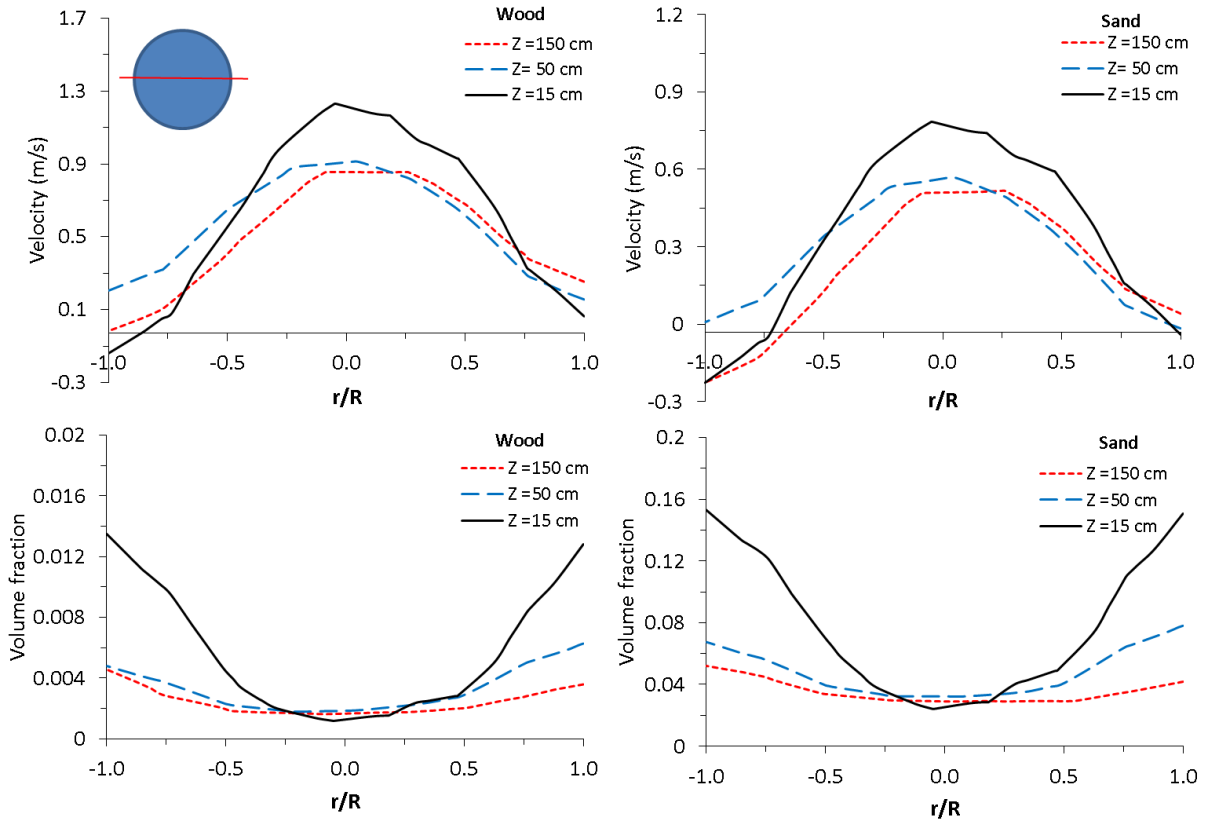


Fig. 3.23. Radial profiles of solid distribution and velocity for a binary mixture (wood and sand) at two different heights in the CFB riser

### 3.4.5. Final Hydrodynamic model

According to the above extensive model validation, the proposed final hydrodynamic model, which will be used in modelling the CFB riser gasification is summarised in Table 3.6. This table includes all the constitutive equations, boundary condition solution procedure (cell size, time step and energy equation) recommended for the simulation of a CFB gasifier using two-fluid model approach.

Table 3.6 The final proposed hydrodynamic model for the CFB riser

Model constitutive correlation	Model used
Turbulence model $\frac{\partial}{\partial t}(\rho k) + \frac{\partial}{\partial x_i}(\rho u_i k) = \frac{\partial}{\partial x_j} \left( \left( \mu + \frac{\mu_t}{\sigma_k} \right) \frac{\partial k}{\partial x_j} \right) + G_k + G_b - \rho \varepsilon - Y_M + S_k$	Dispersed standard k-ε model
$\frac{\partial}{\partial t}(\rho \varepsilon) + \frac{\partial}{\partial x_i}(\rho u_i \varepsilon) = \frac{\partial}{\partial x_j} \left( \left( \mu + \frac{\mu_t}{\sigma_\varepsilon} \right) \frac{\partial \varepsilon}{\partial x_j} \right) + C_{1\varepsilon} \frac{\varepsilon}{k} (G_k + C_{3\varepsilon} G_b) - C_{2\varepsilon} \rho \frac{\varepsilon^2}{k} + S_\varepsilon$	(Launder and Spalding, 1972)
Drag force model	
Gas-solid drag force model	

$\beta_{sl} = \frac{3\varepsilon_s \varepsilon_l \rho_l}{4u_{r,s}^2 d_s} C_D \left( \frac{Re_s}{u_{r,s}} \right)  u_s - u_l $	(Syamlal and O'Brien, 1989)
Solid-solid drag force model	
$K_{sl} = \frac{3(1+e_{ls}) \left( \frac{\pi}{2} + C_{fr,ls} \frac{\pi^2}{8} \right) \alpha_s \rho_l \alpha_l \rho_l (d_l + d_s)^2 g_{0,ls}}{2\pi(\rho_l d_l^3 + \rho_s d_s^3)}  u_s - u_l $	(Syamlal, 1987)
Granular Viscosity(kg/m s)	
$\mu_s = \mu_{s,col} + \mu_{s,kin}$	(Syamlal et al., 1993)
$\mu_{s,col} = \frac{4}{5} \varepsilon_s d_s \rho_s g_{0,ss} (1+e_{ss}) \left( \frac{\theta_s}{\pi} \right)^{1/2} \varepsilon_s$	
$\mu_{s,kin} = \frac{\alpha_s d_s \rho_s \sqrt{\Theta_s \pi}}{6(3-e_{ss})} \left[ 1 + \frac{2}{5} (1+e_{ss})(3e_{ss}-1) \alpha_s g_{0,ss} \right]$	
Granular Bulk Viscosity(kg/m s)	
$\lambda_s = \frac{4}{3} \alpha_s \rho_s d_s g_{0,ss} (1+e_{ss}) \left( \frac{\Theta_s}{\pi} \right)^{1/2}$	(Lun et al., 1984)
Solid-solid friction	
	None
Radial distribution	
	(Lun et al., 1984)
$g_{o,ks} = \left[ 1 - \left( \frac{\alpha_s}{\alpha_{s,max}} \right)^{1/2} \right]^{-1} + \frac{1}{2} d_k \sum_{k=1}^N \frac{\alpha_k}{d_k}$	
Solids pressure (Pascal)	
$p_s = \alpha_s \rho_s \theta_s + \sum_{n=1}^N 2 \frac{d_{ns}^3}{d_s^3} \rho_s (1+e_{ns}) \alpha_n \alpha_s g_{0,ns} \theta_s$	(Lun et al., 1984)
Energy equation	
$0 = \left( -p_s \bar{I} + \bar{\tau}_s \right) : \nabla u_s - \gamma_{\theta_s} + \phi_{ls}$	Simple algebraic equation
Energy dissipation and exchange between particles	
$\gamma_{\theta_s} = \frac{12(1-e_{ss}^2) g_{0,ss}}{d_s \sqrt{\pi}} \rho_s \varepsilon_s^2 \theta_s^{3/2}$	(Lun et al., 1984)
$\phi_{ls} = -3\beta_{ls} \theta_s$	(Gidaspow et al., 1992)

### 3.5. Conclusion

In this chapter the literature was reviewed to find the hydrodynamic models reported. Enough information was found in building hydrodynamic model for one solid phase but for more than one solid phase there was shortage in the literature. So the hydrodynamic model was discussed with more focus in binary solid mixtures. This study was started with a simple

poly-dispersed single solid phase then moved to binary solid phases. The single solid phase was used for primary validations and eliminating unnecessary options and steps in building the hydrodynamic model. Then the outcomes from the primary validations were applied to the secondary validations of the binary mixture to avoid time consuming in using two solid phases. The data used for validations was obtained from the experiments which were discussed in Chapter 2.

To develop the hydrodynamic model, firstly the geometry was generated using the same dimensions of the rig used in the experiments. Then the mesh was generated using advanced sizes function. A sensitivity analysis was conducted at this stage for the mesh maximum face size and the time step. The results of the sensitivity analysis for the mesh shows similarity in the range examined (0.8-1.5cm) and for the time step the sensitivity analysis confirmed the rule of thumb of the time step which in this case less than 0.0025s. Then after the mesh and the time step were considered, most of the hydrodynamic formulation options applicable to this case were used in different simulations and compared against experimental data for validations. The reliable models were then chosen and summarized in Table 3.6.

## **4. Chapter 4: Modeling of biomass Gasification (reactive system)**

### **4.1. Introduction**

This chapter presents a gasification model of biomass (reactive system) in a fluidized bed reactor. This will be incorporated in the hydrodynamic model presented in Chapter 3 to simulate the gasification of biomass in a CFB riser.

The first section in this chapter discusses the fundamentals of gasification process including the various homogeneous and heterogeneous reactions. This is then followed by review of the most important literature on the models used. The final section presents detailed formulation of the complete gasification model used in this study with full set of reactions and kinetics.

### **4.2. Literature review**

CFD studies and simulations of biomass gasification in a CFB riser are rare in the literature, particularly when considering transient three-dimensional simulations. Most of the available literature is on bubbling bed reactor, and in most case, the models used are either one or two-dimensional and the hydrodynamics considered are for one single solid phase in the reactor. Even good experimental data on CFB biomass gasification is limited to a handful number of studies (e.g. (Li et al., 2004).

#### **4.2.1. Fundamentals of biomass gasification**

In this literature review, we first present the principle of gasification process and related reaction kinetics as reported in the literature. There is general agreement that the main stages in high temperature thermochemical conversion of biomass are drying, devolatilization, combustion and gasification. These stages as illustrated in Fig. 4.1, often overlap and there is no sharp boundary between them as described by (Basu, 2010b).



Fig. 4.1. Potential paths for gasification (Basu, 2010b).

According to Fig. 4.1, the biomass is firstly heated then thermally degraded. The products from the thermal degradation step are solid gas and oil. These products then react to generate the final product through the various combustion and gasification reactions. Schematic representation of these stages in various types of gasification reactors are shown in Fig. 4.2.



Fig. 4.2. Stages of gasification and temperature distribution in various types of biomass thermochemical conversion reactors (a) downdraft gasifier (b) throated-type downdraft gasifier (d) bubbling fluidized-bed gasifier (d) circulating fluidized bed reactor. Figs (a)–(c) are reported by (Basu, 2010b) and (d) is reported by (Makkawi, 2013).

Moving bed reactors include the updraft and downdraft reactors as shown in Fig. 4.2 (a) and (b) respectively. In the updraft reactor the gasifying agent is fed from the bottom of the gasifier and the biomass is fed from the top to undergo drying, pyrolysis, gasification and finally combustion. The product gases evolve throughout these stage before finally exiting from the top of the gasifier. In the downdraft throated type gasifier the biomass enters from the top and the gasifying agent enters from somewhere under the biomass entrance. The product gases exit from the bottom of the gasifier. The combustion zone in downdraft gasifiers comes before the gasification zone in contrast with the updraft gasifier.

In fluidized bed reactors the boundaries of the various gasification zones are less distinct when compared to the moving bed gasifiers. Basu (2010b) identified two zones in bubbling

fluidized beds (BFBs); combustion, which comes first, and gasification, which comes afterwards. In Circulating Fluidized beds (CFBs), all zones are mixed up, mainly due to the high mixing of the various bed components. However, if we assume that a CFB holds some characteristics of fixed bed at the lower part and fluidized bed at the upper part then the schematic shown in Fig. 4.2-d may be the closest correct description of gasification zones in a CFB biomass gasifier. Accordingly, the sequence of the gasification in the CFBs gasification riser can be assumed to occur in the following sequence: drying, combustion, pyrolysis and finally gasification.

#### 4.2.1.1. Drying

The biomass freshly cut has high moisture content, close to 70-80%, so it must be dried to a certain limit before it goes into the gasifiers. The biomass typically goes to the gasifier in 10-20% moisture content and this requires 2260 kJ/kg to vaporize; this energy is not recoverable (Basu, 2010b). This heat is usually met by introducing hot gasifying agent, through external reactor heating, by circulating heat carrier solid or by combination of these methods. Noting that, the biomass only starts drying when its temperature reaches 100 °C.

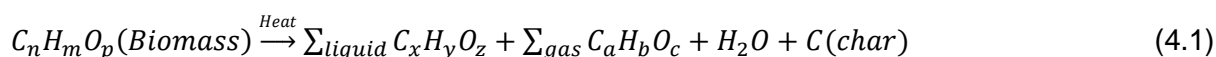
#### 4.2.1.2. Devolatilization

Devolatilization (sometimes referred to as pyrolysis) is the most important step in the gasification process because it generates the gases needed for the gasification steps. Most of the product gases mainly come from the devolatilization step. The devolatilization or pyrolysis can be described as shown in Fig. 4.3. Devolatilization mainly take place in the presence of heat and absence or limited oxygen to generate smaller gas molecular ( $\text{CO}$ ,  $\text{CO}_2$ ,  $\text{H}_2$  and  $\text{CH}_4$ ) and char and primary tar. The tar then can undergo cracking depending on temperature and residence time to produce more gases and condensable liquid as shown in Fig. 4.3.



Fig. 4.3. Schematic description of devolatilization (pyrolysis) in a biomass particle (Basu, 2010b).

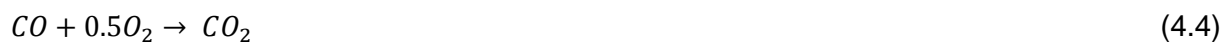
The devolatilization can be represented by a generic reaction (Basu, 2010b):



Corella and Sanz (2005) reported the values of  $n$ ,  $m$  and  $p$  as 4.2, 5.8 and 2.8 respectively for pine wood chips as an example.

#### 4.2.1.3. Combustion

The importance of the combustion during biomass gasification is in the heat generated to derive the highly endothermic pyrolysis step. The reactions involved in this stage include a range of homogenous and heterogeneous reactions. These are the main ones:



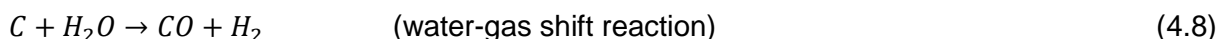
These reactions are related to the availability of the oxygen and the biomass species itself. Basu (2010b) reported that carbon and CO combustion reactions are faster than char gasification reactions as shown in Eq. 4.12, it is so fast that it quickly consumes the oxygen

leaving hardly any free oxygen for any other reactions. So carbon and CO oxidation reactions are the most important reactions during the combustion stage.

#### 4.2.1.4. Gasification

Biomass gasification is commonly carried out using different gasification mediums, namely oxygen, steam, air or air/steam mixture. The type of the gasifying medium has a direct impact on the quality and nature of the product gas. The heating values can be classified as high heating in the range of 12-28 MJ/Nm<sup>3</sup> produced with pure oxygen, medium heating in the range of 10-18 MJ/Nm<sup>3</sup> produced with steam mixture, and low heating in the range of 4-7 MJ/Nm<sup>3</sup> produced when using air. The mechanisms and kinetics of the reactions involved during the gasification step are discussed later in this chapter. While pure oxygen clearly increases the heating value of the product gas, steam and steam/air mixture are frequently used as a gasifying agent to increase hydrogen content in the product gas.

There are different gasification reactions reported in the literature but the most important ones are the carbon reactions (Boudouard, water-gas or steam, and hydrogasification), shift reaction and steam reforming reaction. These reactions are as follow:



Other gasification reactions, which are commonly ignored in biomass gasification modeling, can be found in the literature (e.g. (Basu, 2010b)). With reference to the carbon combustion reaction, which is the fastest reaction in the whole process, the other carbon gasification reactions can be classified according to their rate of reaction as follows:



#### 4.2.2. Modelling of the biomass drying

Review of the recent literature on biomass drying models reveals at least three different approaches (i) representing the drying rate as a chemical reaction with kinetic rate constants (ii) representing the drying as an evaporation/condensation process (iii) assuming instantaneous drying and add the biomass moisture to the surrounding gas. Example of studies adopting these methods and details of the model formulations used are given below.

In a mathematical model developed by Syamlal and Bisset (1991) for a moving bed, the drying step was introduced as a chemical reaction with kinetics constants using Arrhenius law. This is given by:



$$r = A \exp\left(\frac{E}{RT}\right) (1 - \varepsilon) \rho X \quad (4.14)$$

In this equation, the Arrhenius law constants, obtained from Wen et al. (1982), were  $E = 88.7$  kJ/mol and  $A = 1.1 \times 10^5 \text{s}^{-1}$ ,  $\varepsilon$  is the void fraction,  $\rho$  is the solids density, and  $X$  is the mass fraction of solid species. It is worth noting that the authors used the same rate constants for modelling the devolatilization step. Later on, Tinaut et al. (2008) applied a similar drying model in a one dimensional mathematical model of biomass gasification in a fixed bed downdraft gasifier. The drying “reaction” was given by:



$$r = k C_{(H_2O)_l} \quad (4.16)$$

with the Arrhenius law constants given as:  $E = 88$  kJ/mol and  $A = 5.13 \times 10^{10} \text{s}^{-1}$ .

On the principles of heat and mass transfer, Agarwal et al. (1986) developed a mathematical model to describe drying of wet coal in a fluidized bed combustor. The authors assumed that drying takes place at a boundary moving from the outer surface to the centre of the particle, an unsteady-state heat conduction equation in spherical coordinates with a convective boundary condition was solved analytically.

Lee (1979) defined the evaporation-condensation model as a mechanistic model with physical basis. Following this approach, Di Blasi (2004) presented a one-dimensional, unsteady mathematical model of a fixed-bed counter current wood gasifier, which couples heat and mass transport with wood drying and devolatilization, char gasification, and combustion of both char and gas-phase species. The drying model included moisture evaporation/condensation. The author mentioned that moisture evaporation is diffusion controlled and the equation for calculating the moisture transfer is:

$$m_M = v_p A_p k_m (\rho_v - \rho_{H_2O}) \quad (4.17)$$

$$\frac{\rho_v R T^*}{M_v} = \exp\left(a_1 - \frac{a_2}{T^*}\right) \quad (4.18)$$

where

$m_M$	=	moisture evaporation rate, $\text{kg m}^{-3} \text{s}^{-1}$
$v_p$	=	particle density number, 1/m
$A_p$	=	particle surface area, $\text{m}^2$
$k_m$	=	mass transfer coefficient, m/s
$\rho_v$	=	vapour mass concentration (mass/gas volume), $\text{kg/m}^3$
$\rho_{H_2O}$	=	steam mass concentration (mass/gas volume), $\text{kg/m}^3$
$T^*$	=	is average temperature between gas and solid, K
$a_1, a_2$	=	are constants
$R$	=	universal gas constant, J/kgmol-K
$M_v$	=	molecular weight, kg/kgmol

A different and a simpler method to incorporate the drying step in a gasification model was recently reported by Gerber et al. (2010). Using an Eulerian-Eulerian model for wood gasification in a bubbling fluidized bed reactor, the authors assume that the wood entering the reactor contains no water and then added moisture of 10 wt% to the fuel inlet in the form of gaseous water.

Most recently, Kaushal et al. (2011) developed a one-dimensional steady state mathematical model for biomass steam gasification in a dual fluidized bed reactor using wood chips as a fuel. The authors described the drying of the biomass as an irreversible mass transfer

process with changing phase of the moisture from liquid to gas at a temperature above 100 °C. The drying equation used in the model is:

$$w_m m_{B_{l0}} |_{Liquid} = w_m m_{B_{l0}} |_{Gas} \quad (4.19)$$

where  $m_{B_{l0}}$  is the mass flow rate of the biomass [ $\text{kg s}^{-1}$ ] and  $w_m$  is the mass fraction of the moisture in the wood. This is the modelling approach that will be used in this study as described later in Section 4.3.2.

#### 4.2.3. Modelling of the biomass devolatilization

As discussed in Section 4.3, in a FB reactor the devolatilization is one of the main reactions that take place after the drying and combustion steps and before the gasification step.

One of the earliest models on biomass wood pyrolysis was proposed by Shafizadeh and Chin (1977). The authors proposed that in high temperature conditions (Over the temperature range of 259-341°C) a single or three parallel reactions will occur to form the main products from the fuel, these are char, tar and gas. The mechanism of this model is shown in Fig. 4.4 below.



Fig. 4.4 . One-component mechanism of primary wood pyrolysis proposed by Shafizadeh and Chin (1977).

Fletcher et al. (2000) used CFX commercial CFD code to model the biomass gasification in entrained flow gasifier using Lagrangian approach. The authors noted that the devolatilization reactions take place at a very fast rate to produce  $\text{CH}_4$ ,  $\text{H}_2$ ,  $\text{CO}$ ,  $\text{CO}_2$ ,  $\text{H}_2\text{O}$  and tar. After the gases are generated, a mixture of char and ash remains. Depending on its quality and composition the product gas can then be condensed and used as liquid fuel for heat and power generation or further treated/upgraded to produce specialized chemicals.

The authors assumed the volatile components released via flash pyrolysis according to the following rate:

$$\dot{M}_{vol} = -H(T - T_{ref})M_{vol}/\tau \quad (4.20)$$

where  $H(T)$  is the Heaviside function,  $\tau$  a time constant (set to 0.1 s) and  $T_{ref}$  is a critical temperature for pyrolysis to commence (set to 227 °C). In this model the volatile release rate is proportional to the mass of volatiles remaining in the particle. The model was described as a powerful tool for predicting the performance of the gasifier however the authors suggested further experimental validations.

Grønli and Melaaen (2000) reported a simple experimental study on wood devolatilization. The experiment was carried out to extract pyrolysis kinetic data. This included pyrolysis of a single particle wood in a bell shaped Pyrex reactor with 20 cm diameter and 30 cm length using Xenon-arc lamp as heating supply to produce char tar and gas. In modelling the process, the authors assumed three parallel reactions to account for gas, tar and char yields from the primary pyrolysis reactions then followed by a fourth reaction for the tar cracking. This is described in Fig. 4.5. In calculating the rate of reaction reactions, the authors used Arrhenius. Table 4.1 gives the Arrhenius law constants for the production of gas, tar, char and tar cracking with these reaction denoted by 1, 2,3 and 4 respectively.

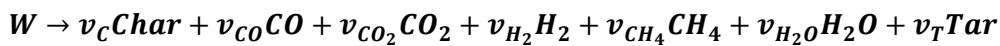


Fig. 4.5. Kinetic scheme used in the devolatilization model of (Grønli and Melaaen, 2000).

Table 4.1 Arrhenius law constants for calculating the rate of wood devolatilization (Grønli and Melaaen, 2000)



Di Blasi (2004) considered a one-step global reaction for wood devolatilization as follows:



(4.21)

The tar, gas and char fractions were obtained from the data reported by Di Blasi (1993).

Table 4.2 shows these fractions along with other fractions reported in the literature.

The reaction rate for Eq. 4.21 was given by:

$$r = A \exp\left(\frac{E}{RT}\right) \rho \quad (4.22)$$

where  $\rho$  is the apparent solid density (mass/total volume),  $\text{kg/m}^3$  and T is the solids temperature. The Arrhenius law constants were obtained from Roberts and Clough (1963) as  $A = 1.516 \times 10^3 \text{ s}^{-1}$  and  $E = 628.114 \text{ kJ/mol}$ .

Table 4.2 Pyrolysis gases fractions as reported in the literature

Sources	Pyrolysis fractions						
(Di Blasi et al., 1999)	CO	CO <sub>2</sub>	CH <sub>4</sub>	H <sub>2</sub>	H <sub>2</sub> O	Tar	Char
	0.045	0.1	0.003	0.002	0.115	0.35	0.385
	Tar cracking						
(Boroson et al., 1989)	0.7	0.18	0.12				

In modelling the tar cracking the authors proposed the following reaction:



The reaction rate for Eq. 4.23 was given by:

$$r = \varepsilon A \exp\left(\frac{E}{RT}\right) \rho \quad (4.24)$$

where  $\rho$  is the gas phase mass concentration (mass/gas volume),  $\text{kg/m}^3$ ,  $\varepsilon$  porosity and  $T$  is the gas temperature. The kinetic constants for the rate of reaction were  $A = 4.26 \times 10^6 \text{ s}^{-1}$  and  $E = 107.409 \text{ kJ/mol}$  (Liden et al., 1988). In a later review paper by the same author Di Blasi (2008) it was reported that the activation energy ( $E$ ) in the Arrhenius law constant can be classified into three groups based on temperature. For temperatures From 527 up to 1127 °C  $E$  is in the range of 69-91 KJ/mol ; between 427-527 °C  $E$  is in the range of 56-106 KJ/mol; and for lower than 427 °C  $E$  is in the range of 125-174 KJ/mol.

Basu (2010a) reported that the kinetic models of the pyrolysis of ligno-cellulosic fuels like biomass may be broadly classified into three types of models; one-stage global reaction as discussed above, one stage of multiple reactions and two stage semi-global. More information about these models and their uses can be found in Di Blasi (1993), Basu (2010a) and Di Blasi (2008). The different kinetic constants for the one-stage global single reaction case are shown in Table 4.3 for various biomass materials.

Table 4.3 Kinetic constants for one-stage global pyrolysis reaction for different materials (Basu, 2010a)



Gerber et al. (2010) used a 2D Eulerian multiphase model to simulate the gasification of wood in a lab scale bubbling fluidized bed reactor and compare the model predictions with experimental data of product gas composition and tar. The authors implemented a primary pyrolysis to produce gases of  $\text{CO}$ ,  $\text{CO}_2$ ,  $\text{CH}_4$ ,  $\text{H}_2\text{O}$ ,  $\text{H}_2$  and tar with given fractions obtained from Seebauer (1999) as shown in Table 4.4. This is followed by a secondary reaction for tar cracking. Two different tar cracking models were used and compared against each other. In modelling the devolatilization step, three reactions were used to produce gas, char and tar.

The Arrhenius law constants used in the reaction rates are as follow: for gas production;  $A= 1.43 \times 10^4 \text{ s}^{-1}$  and  $E= 88.6 \text{ kJ/mole}$ ; for tar  $A= 4.13 \times 10^6 \text{ s}^{-1}$  and  $E= 112.7 \text{ kJ/mole}$ ; for char  $A= 7.38 \times 10^5 \text{ s}^{-1}$  and  $E= 106.5 \text{ kJ/mole}$ .

Table 4.4 Composition of wood gas from the primary pyrolysis step (Gerber et al., 2010)



The secondary pyrolysis reaction, which is for tar cracking was implemented by applying two models; the first one, obtained from Boroson et al. (1989), assumes that the tar from primary pyrolysis step is composed of reactive tar and inert tar. The latter is assumed to be un-reactive while the first is assumed to be thermally cracked to produce gases  $\text{CO}$ ,  $\text{CO}_2$ ,  $\text{CH}_4$ ,  $\text{H}_2\text{O}$ , and  $\text{H}_2$ . The fractional compositions of tar inert and gases produced were obtained from Boroson et al. (1989) and Rath and Staudinger (2001) as shown in Tables 4.5 . The rate of reaction calculated according to Arrhenius law using  $A= 2.3 \times 10^4 \text{ s}^{-1}$  and  $E= 80000 \text{ kJ/mole}$ . The second cracking model from Rath and Staudinger (2001) assuming that there is  $\text{H}_2\text{O}$  and there is no  $\text{H}_2$  in products from cracking reaction.

Table 4.5 Composition of intermediate and inert tar for secondary pyrolysis models 1 and 2 used by (Gerber et al., 2010).



Table 4.6 Wood gas composition from secondary pyrolysis for model 1 and model 2 used by (Gerber et al., 2010).



Gerber et al. (2010) identified as a critical sub-model which influences the composition of the product gas quite significantly. The authors added the available kinetic parameters in the literature for pyrolysis kinetics vary over many magnitudes and it has to be expected that they will lead to even bigger variations.

Syamlal and Bisset (1991) modelled the devolatilization using reactions suggested by Solomon et al. (1988) and Saxena (1990). The authors used two reactions; the first to produce gases or volatiles from the devolatilization step, with kinetic constants  $E = 88.7$  kJ/mol and  $A = 1.1 \times 10^5 \text{ s}^{-1}$ , and the second for tar cracking with  $E = 121.3349$  and  $A = 2.5 \times 10^7 \text{ s}^{-1}$ . The authors concluded that their one dimensional model can successfully simulate the addition and withdrawal of gas and solids in a fixed bed reactor.

Larfeldt et al. (2000) modelled the pyrolysis of large wood particles by modifying an earlier model by Melaaen (1996). The authors studied the changes in the structure, pyrolysis mechanism and heat transfer properties in large wood particles at 700 °C and compared their one dimensional predictions with four different pyrolysis models reported by Chan et al. (1985), Grønli (1996), Broido (1976) and Shafizadeh (1984). Larfeldt et al. (2000) reported that the comparisons of measurements and model simulations showed that the inclusion of a shrinking model reduces the time of pyrolysis substantially. The varying interior heating rate was found to influence the choice of pyrolysis mechanism. Out of the four pyrolysis

mechanisms found in literature, only one was found to be in agreement with the measurements.

Grønli (1996) defined the one step global devolatilization model as the dry solid material decomposes into volatiles and char as shown in Eq.4.25. The dry biomass (S) decomposes into volatile (V) and char (C) as shown in Eq. 4.25 below.



In this study, a similar approach will be implemented to simulate the devolatilization step. Grønli (1996) reported in his thesis that the one-step global model is the most practically applicable option. Different rate constants for different wood materials;  $E$  in a range of 23.6 to 138.8 KJ/mole and  $A$  in the range of 0.45 to  $5.3 \times 10^8 \text{ s}^{-1}$  have been studied. The author reported that the main disadvantage of this model is that the char density is assumed to be constant and is not dependent on operating conditions. However, this was not considered to be of serious limitation.

#### **4.2.4. Modelling of the biomass partial combustion and gasification**

##### **4.2.4.1. Combustion reactions**

Combustion occurs when highly exothermic reactions take place between the solid fuel and oxygen. In a biomass gasifier, the oxygen is usually introduced to the reactor through the gasifying agent; being air, oxygen or a mixture of any of these with steam. The combustion step is important to provide the heat required to derive the highly endothermic pyrolysis step. In the special case of pure steam gasification, no combustion takes place; therefore, an external source of heating must be supplied.

The combustion reactions involve homogenous and heterogeneous reactions as follows:





The combustion of Carbon is classified as heterogeneous reaction, while the combustion of CO, H<sub>2</sub> and CH<sub>4</sub> gases are classified as homogeneous reactions. The Arrhenius law constants used for calculating the rates of these reactions as reported in the various literature sources are given in Table 4.7. It is clear that there is a reasonable agreement on the values for energy unit (*E/R*) but the Arrhenius law pre-exponential factor (*A*) varies considerably.

Table 4.7 Kinetic constants for combustion reactions

Component	E/R	A (s <sup>-1</sup> )	References
C	13078	1.5 × 10 <sup>6</sup>	(Colomba Di Blasi et al., 1999); (Miao et al., 2013)
	11200	1.04 × 10 <sup>3</sup>	(Gerber et al., 2010)
	17977	8.71 × 10 <sup>3</sup>	(Mansaray et al., 1999); (Gungor and Yildirim, 2013)
CO	20119	3.980 × 10 <sup>14</sup>	(Dryer, 1972); (Gerber et al., 2010)
	20129	3.980 × 10 <sup>20</sup>	(Gungor and Yildirim, 2013)
	20119	3.98 × 10 <sup>11</sup>	(Miao et al., 2013)
H <sub>2</sub>	13127	2.196 × 10 <sup>12</sup>	(Mitani and Williams, 1980) and (Gerber et al., 2010)
	13127	2.196 × 10 <sup>18</sup>	(Gungor and Yildirim, 2013)
	13127	2.19 × 10 <sup>9</sup>	(Miao et al., 2013)
CH <sub>4</sub>	24157	1.585 × 10 <sup>7</sup>	(Gungor and Eskin, 2008) and (Miao et al., 2013)
	24343	1.58 × 10 <sup>13</sup>	(Dryer, 1972) and (Gerber et al., 2010)
	24343	1.58 × 10 <sup>19</sup>	(Gungor and Yildirim, 2013)

#### 4.2.4.2. Heterogeneous gasification reactions

In addition to heterogeneous combustion reactions, reaction of pyrolysis gases with carbon are also classified as heterogeneous gasification reactions. The main reactions commonly included in biomass gasification models are:



According to Gerber et al. (2010), the rate of these reactions can be given by:

$$\frac{d[c]}{dt} = -k[CO_2] \quad (4.34)$$

$$\frac{d[c]}{dt} = -k[H_2O] \quad (4.35)$$

$$\frac{d[c]}{dt} = -k[H_2] \quad (4.36)$$

where  $k$  is the rate constant given by Arrhenius law. Summary of the most widely used pre-exponential factor ( $A$ ) and energy unit ( $E/R$ ) for the rate constant in the above reactions are given in Table 4.8.

Table 4.8 Arrhenius law constants for heterogeneous gasification reactions

Reaction No.	E/R	A (s <sup>-1</sup> )	References
	15600	3.42	(Hobbs et al., 1992); (Gerber et al., 2010)
4.31	29844	4.364	(Miao et al., 2013)
	29844	4364	(Westbrook and Dryer, 1984); (Gungor and Yildirim, 2013)
	6000	200	(Miao et al., 2013)
4.32	15600	3.42	(Hobbs et al., 1992); (Gerber et al., 2010)
	18522	4.930	(Westbrook and Dryer, 1984); (Gungor and Yildirim, 2013)
4.33	15600	0.00342	(Hobbs et al., 1992); (Gerber et al., 2010)

#### 4.2.4.3. Homogeneous gasification reactions

The homogenous gas phase reactions taking place during biomass gasification involve all the gases produced after pyrolysis, namely, CO, CO<sub>2</sub>, CH<sub>4</sub>, H<sub>2</sub>O and H<sub>2</sub>. The most important reactions that are particularly relevant to steam gasification involve water gas shift reaction and methane reforming reaction. The water gas shift reaction is given by:



The rate of reaction is as follow from Gerber et al. (2010):

$$\frac{d[CO]}{dt} = -k[CO][H_2O] + \frac{[CO_2][H_2]}{K_P(T)} \quad (4.38)$$

Gungor and Yildirim (2013) and Miao et al. (2013) reported another form of rate of reaction as follow:

$$\frac{d[CO]}{dt} = \frac{[CO][H_2O] - [CO_2][H_2]}{K_P(T)} \quad (4.39)$$

The kinetic constants for water gas shift reaction (Eq. 4.37) are given in Table 4.9. This reaction is exothermic but it relatively gives lower heat than combustion reactions.

The steam reforming reaction is given by:



The rate of reaction is as follow from Miao et al. (2013):

$$r = kC_{H_4}C_{H_2O} \quad (4.41)$$

Gungor and Yildirim (2013) reported another form of rate of reaction as follow:

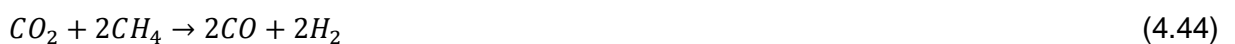
$$r = kC_{CH_4}^{1.7}C_{H_2}^{-0.8} \quad (4.42)$$

The steam reforming reaction (Eq. 4.40) is highly endothermic and is strengthened with increasing temperature, this leads to increase in H<sub>2</sub> concentration and decrease in CH<sub>4</sub> concentration. The kinetic constants of this reaction are given in Table 4.9. It is clear that the steam reforming and water gas shift reactions are particularly important for increasing hydrogen production during steam gasification of biomass. It is worth noting that Eqs. 4.37 and 4.40 can be expressed as one single reaction by adding together to give:



Review of the literature indicates that the use of this equation in gasification model is rare, mainly due to unavailability of reliable kinetic data.

Grammelis (2011) and Siedlecki et al. (2009) reported another homogeneous reaction that may occur in gasification system to generate CO and H<sub>2</sub> as follows:



This is sometimes referred to as dry reforming reaction and it is classified as an endothermic reaction, requires 247KJ/mol. This reaction is rarely used in the literature of biomass gasification.

Table 4.9 Kinetic constants for heterogeneous reactions from the literature

Reaction name	E/R	A (s <sup>-1</sup> )	References
water gas shift	1510	2.7 × 10 <sup>3</sup>	(Radmanesh et al., 2006)
Methane reforming	28865.4 15000	3.3×10 <sup>10</sup> 3.1005	(Morf et al., 2002) and (Gungor and Yildirim, 2013) (Corella and Sanz, 2005)

### 4.3. Proposed gasification reactions model

This section gives details of the chemical reactions, rate of reactions and kinetic constants used in this study for the simulation of the CFB biomass gasifier. The reaction model used is the laminar finite rate model for homogeneous reactions, a user defined function (UDF) for heterogeneous reactions and a mass transfer was developed and implemented in the gasification model.

#### 4.3.1. The Laminar finite rate model

The Laminar finite rate model calculates the chemical source term  $R_i$  in Eq. 4.45 using Arrhenius law as follows:

$$R_i = M_{w,i} \sum_{r=1}^{N_R} \hat{R}_{i,r} \quad (4.45)$$

where  $M_{w,i}$  is the molecular weight of the species  $i$ ,  $\hat{R}_{i,r}$  the rate of reaction,  $N_R$  reactions that the species participate in

$$\hat{R}_{i,r} = (v_{i,r}^{\sim} - v_{i,r}^{\approx}) \left( k_{f,r} \prod_{j=1}^N [C_{j,r}]^{\gamma_{j,r}^{\sim} + \gamma_{j,r}^{\approx}} \right) \quad (4.46)$$

where  $v_{i,r}^{\sim}$  stoichiometric coefficient for reactant  $i$  in reaction  $r$ ,  $v_{i,r}^{\approx}$  stoichiometric coefficient for product  $i$  in reaction  $r$ ,  $k_{f,r}$  forward rate constant for reaction  $r$ ,  $N$  number of chemical species in the system,  $C_{j,r}$  molar concentration of species  $j$  in reaction  $r$  (kgmol/m<sup>3</sup>),  $\gamma_{j,r}^{\sim}$  rate exponent for reactant species  $j$  in reaction  $r$ ,  $\gamma_{j,r}^{\approx}$  rate exponent for product species  $j$  in reaction  $r$ . The above equations are for forward reaction but for the reversible reactions the following relation will be applied:

$$\hat{R}_{i,r} = (v_{i,r}^{\sim} - v_{i,r}^{\approx}) \left( k_{f,r} \prod_{j=1}^N [C_{j,r}]^{\gamma_{j,r}^{\sim}} - k_{b,r} \prod_{j=1}^N [C_{j,r}]^{\gamma_{j,r}^{\approx}} \right) \quad (4.47)$$

where  $k_{b,r}$  is backward rate constant for reaction  $r$ . The forward rate constant for reaction  $r$  is computed using the Arrhenius expression as follows:

$$k_{f,r} = A_r T^{B_r} e^{-E_r/RT} \quad (4.48)$$

where  $A_r$  pre-exponential factor (consistent units),  $B_r$  temperature exponent (dimensionless),  $E_r$  activation energy for the reaction (J/kgmol) and  $R$  universal gas constant (J/kgmol-K). The temperature exponent was taken in all the reactions as zero according to the most literature reviewed so the term of  $T^{B_r}$  will be equal to one.

For the backward reactions, the backward constant is calculated using the following equations:

$$k_{b,r} = \frac{k_{f,r}}{K_r} \quad (4.49)$$

where  $K_r$  is the equilibrium constant:

$$K_r = \exp\left(\frac{\Delta S_r^0}{R} - \frac{\Delta H_r^0}{RT}\right) \left(\frac{p_{atm}}{RT}\right)^{\sum_{i=1}^N (v_{i,r}^{\approx} - v_{i,r}^{\sim})} \quad (4.50)$$

where  $p_{atm}$  atmospheric pressure. Changing in the Gibbs free energy is calculated from the term within exponential and can be computed from the following expressions:

$$\frac{\Delta S_r^0}{R} = \sum_{i=1}^N (v_{i,r}^{\approx} - v_{i,r}^{\sim}) \frac{S_i^0}{R} \quad (4.51)$$

$$\frac{\Delta H_r^0}{RT} = \sum_{i=1}^N (v_{i,r}^{\approx} - v_{i,r}^{\sim}) \frac{h_i^0}{R} \quad (4.52)$$

where  $S_i^0$  is the standard-state entropy and  $h_i^0$  standard-state enthalpy (heat of formation).

#### 4.3.2. Drying model

The biomass drying models discussed in the literature section suggest three modelling options. The first option is by treating the drying as a chemical reaction, the second option is assuming the drying model as evaporation/condensation based on mass transfer principles, and the third option is by assuming the moisture coming with the biomass as gas phase entering the reactor with a given mass flow and velocity.

In this study, the biomass drying rate implemented in the model is based on the second option, i.e. mass transfer from liquid moisture associated to the biomass to gas phase. This option was chosen for two reasons (i) if we assumed the moisture is coming with the biomass as gas in the feeding point then the heat transfer and the mass transfer associated to the drying process will be lost and the gasification process will be affected (ii) if we decided to choose the first option then more reaction will be added and therefore, the numerical solver will be slower and the solution convergence may be more difficult.

The mass transfer depends on the saturation temperature so; the temperature of the media must be higher than the saturation temperature to let the evaporation carry out. In our model the drying of the biomass is modelled as evaporation model and the mass of the moisture will transfer from the biomass to gases according to the following mass transfer relation:

$$m_{l \rightarrow v} = \epsilon_l \rho_l \frac{T - T_{sat}}{T_{sat}} \quad (4.53)$$

where  $m_{l \rightarrow v}$  is the mass transfer rate from the liquid phase to the vapour phase is in (kg/s/m<sup>3</sup>).  $\epsilon_l$ ,  $\rho_l$  represent the moisture volume fraction and density, respectively. In energy Eq. 4.78 the source term  $S_h$  can be calculated by multiplying the rate of mass transfer by the latent heat of evaporation.

#### 4.3.3. Devolatilization and tar cracking model

Devolatilization is the most important process in biomass gasification because it releases vapours and gases, which then go into gasification reaction afterwards. In a CFB riser heated by circulating solids, such is in the case under consideration; the biomass devolatilization step may take place simultaneously with the drying and combustion. Tar cracking is another complex process following the devolatilization. It is mainly breaking down the heavy hydrocarbons produces from the devolatilization into small molecules at a relatively higher temperature.

In the model developed in this study, it is assumed that the biomass devolatilization step produces volatiles, fixed carbon, and char with fixed percentages. The volatiles are assumed to consist of CO, CO<sub>2</sub>, CH<sub>4</sub>, H<sub>2</sub>, H<sub>2</sub>O and tar. In reality this step is very complex and these gases do not generate directly from one step devolatilization but after very complex reactions. However, reported studies have shown that such a simplification is reasonable and produces, to a great extent, accurate results when applied in modelling of biomass thermal conversion (Gerber et al., 2010).

The char produced from the pyrolysis reaction is assumed to be mainly consisting of carbon, the remaining part of the volatiles and ash. The ash was modelled in this study as an inert so the amount of the ash going in equals the amount out, but of course the percentage of the ash in the char will vary depending on the quantities of the fixed carbon and volatiles remaining.



Fig. 4.6. The bath of the biomass in the first step of devolatilization (Makkawi, 2013).

The devolatilization reaction is modelled as a heterogeneous reaction and the rate of reaction is calculated through a User Define Function (UDF). The UDF was based on the model originally developed by Syamlal and Bisset (1991) for coal gasification, then modified and used in Fluent documentation for modelling heterogeneous reactions, then modified in this study to include new materials specification, devolatilization reaction and more heterogeneous reactions for biomass gasification. The UDF is available in Appendix B.

The rate of devolatilization reaction added to the UDF was given according to the following equation:

$$\hat{R}_i = -k * C_{volatiles} \quad (4.54)$$

where rate constant  $k$  is calculated from Arrhenius law:

$$k = A \exp(-E/RT) \quad (4.55)$$

with frequency factor  $A=1.1 \times 10^3 \text{s}^{-1}$  and activation energy  $E = 8.86 \times 10^7 \text{J/kmol}$  (Syamlal and Bisset, 1991) and  $C_{volatiles}$  is the concentration of the volatiles in  $\text{kmol/m}^3$ . In calculating the rate of reaction, and to avoid convergence problem a condition was set to ensure the availability of the biomass by limiting the gas phase volume fraction to lower than  $0.9 \times 10^{-6}$ . The product volatiles are assumed to consist of  $\text{CO}$ ,  $\text{CO}_2$ ,  $\text{CH}_4$ ,  $\text{H}_2\text{O}$ ,  $\text{H}_2$  and Tar with specified fixed mass fractions as given in Table 4.10.

Table 4.10 The composition of the gas (Ragland et al., 1991)



In a second step, it is assumed that the tar will be cracked into volatile species ( $\text{CO}$ ,  $\text{CO}_2$ ,  $\text{CH}_4$ ,  $\text{H}_2$ ) and inert tar, each with a specified mass fraction as given Table 4.11.

Table 4.11 Composition of the gases released during tar cracking (Gerber et al., 2010).



This reaction is classified as homogeneous reaction with the following rate equation:

$$\hat{R}_i = -k_f * C_{tar} \quad (4.56)$$

where  $C_{tar}$  is the tar concentration and  $k_f$  is the reaction rate constant calculated from Arrhenius law with frequency factor  $A=2.3 \times 10^4 \text{ s}^{-1}$  and activation energy  $E= 665169.7 \text{ J/ kmol}$  (Gerber et al., 2010).

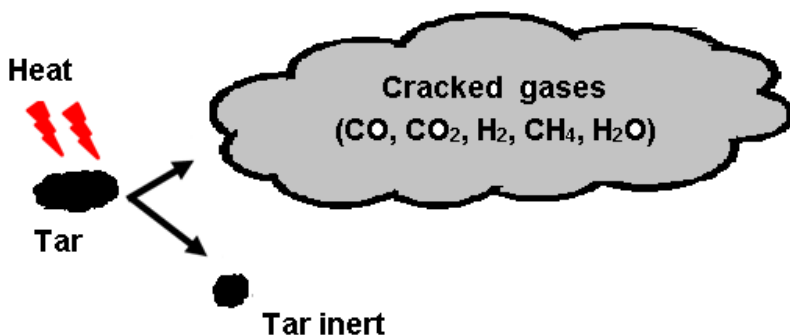


Fig. 4.7. The bath of the biomass in the secondary step of devolatilization (tar cracking)

#### 4.3.4. Partial combustion and gasification model

Partial combustion takes place when the oxygen supply is insufficient to cause complete combustion of carbon and hydrogen in the solid fuel. oxygen is the combustion of combusted materials which is C, H<sub>2</sub>,CO and CH<sub>4</sub> and it is called partial combustion because the amount of the oxygen added to the reactor is part from the whole oxygen needed for combustion. In our case most of the simulations carried out using mixture of steam and air. In most of the literature the gasifying agent used is pure air or pure steam few used mixture of air and steam so, in the following sections we are going to discuss the reactions used and reactions eliminated and also we are going to discuss why they were eliminated. The most important reactions used in most of the literature is the combustion reactions of CO and C and the water gas shift reaction, the Boudouard reaction, Methane reforming reaction. These reactions are classified as heterogeneous reactions and homogenous reactions. The homogenous reactions are the gas phase reactions and the heterogeneous reactions are the solid and gas phase reactions. In the next section firstly we discuss the combustion reactions which are including some of the homogenous reactions and combustion of the Carbone as

heterogeneous reaction. All the heterogeneous reactions were modelled using a User Defined Function (UDF) implemented in Fluent code. The UDF is shown in appendix B.

#### 4.3.4.1. Combustion reaction model

The combustion reactions considered in the gasification model are given by:



The heterogenous reaction rate for the carbon combustion reaction (Eq. 4.57) is given by Syamlal and Bisset (1991):

$$r = \frac{fP_{O_2}}{1/k_1 + 1/k_2} \quad (4.61)$$

where

$$k_1 = \frac{0.292(1-\varepsilon)D}{2d_p^2 T_g} \quad (4.62)$$

$$D = 4.26 \left( \frac{T_g}{1800} \right)^{1.75} \quad (4.63)$$

$$k_2 = k_1 \varepsilon^{2.5} \frac{d_c}{1-d_c} \quad (4.64)$$

$$d_c = \left( \frac{X_{Fc} X_{A0}}{(1-X_{Fc}) X_{Fc0}} \right)^{1/3} \quad (4.65)$$

$$f_1 = \frac{X_{Fc}}{X_{Fc0} + 10^{-6}} \quad (4.66)$$

In the above equations,  $T_g$  is the gas temperature,  $P_m$  is the partial pressure of the gas species  $m$ ,  $X_m$  is the mass fraction of the solids species  $m$ , and  $\varepsilon$  void fraction. The abbreviations  $Fc$ , and  $A$  stands for fixed carbon and ash respectively.

The CO combustion is modelled as a homogeneous reaction. The rate of reaction is calculated as follow:

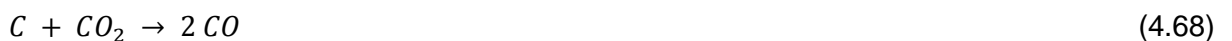
$$R = k * C_{CO} C_{O_2}^{0.25} C_{H_2O}^{0.5} \quad (4.67)$$

where  $k$  is given by the Arrhenius law with  $A=3.98 \times 10^{11}$  and  $E=1.6728 \times 10^8$  (j/kgmol). (Miao et al., 2013)

It should be noted that, following the sensitivity analysis carried out in Chapter 6, some of the above gasification reactions were eliminated from the model after being found to be of no significant effect on the overall gasifier performance or final product gas quality.

#### 4.3.4.2. Heterogeneous reactions model

The heterogeneous reactions considered in the gasification model are:



All of the above three reactions are assumed to be of a first order and their rates are given by

$$r = -k_{CO_2} * C_{CO_2} \quad (4.71)$$

$$r = -k_{H_2O} * C_{H_2O} \quad (4.72)$$

$$r = -k_{H_2} * C_{H_2} \quad (4.73)$$

where  $k$  is the reaction rate constants, calculated according to Arrhenius law, and  $C$  is the concentration. The kinetics rate constants of these reactions are given in Table 4.14.

These three reactions were implemented in the fluent simulation model using a UDF function as given in appendix B. Please note this UDF also included other heterogeneous reactions representing the devolatilization and the carbon combustion reactions as discussed earlier.

#### 4.3.4.3. Homogeneous reactions model

The homogenous reactions or gas phase reactions considered in this model are the water gas shift reactions and methane reforming. These are particularly important in pyrolytic gasification and play a major role in enhancing  $H_2$  production. Note that this does not include the tar cracking and CO combustion, as these already have been discussed separately in section 4.3.3. and 4.3.4.1. respectively.

The water gas shift reaction is given by:



The steam reforming reaction is given by:



The water gas shift reaction is modelled as reversible reaction so the rate of reaction is calculated using the equation below:

$$R = k_f C_{CO} C_{H_2O} - k_b \quad (4.76)$$

where  $k_f$  is the forward constant and can be calculated according to Eq.4.48 and  $k_b$  is the backward reaction and can be calculated according to Eq.s 4.49 to 4.52. The constants E and A were used from the above mentioned literature.

The methane reforming reaction is calculated according to the following equation:

$$R = k_f C_{CH_4} C_{H_2O} \quad (4.77)$$

The reaction rate constants used in Eqs 4.76 and 4.77 are calculated using Arrhenius law, and the constants used are given in Table 4.12.

Table 4.12 The kinetic constants gas shift and methane reforming reactions

Reaction (Eq. No.)	E/R	A(s <sup>-1</sup> )	References
(4.74)	1510	$2.78 \times 10^3$	(Miao et al., 2013)
(4.75)	15000	$3.0 \times 10^5$	(Liu and Gibbs, 2003)

#### 4.3.5. Heat transfer model

The following heat transfer balance equation was used to account for the heat exchange between the solids and the gas phase:

$$\frac{\partial}{\partial t} (\rho E) + \nabla \cdot [\bar{u}(\rho E + p)] = \nabla \cdot \left[ (k_{eff} + \nabla T) - \sum h_j \bar{J}_j + (\bar{\tau}_{eff} \cdot \bar{u})_{eff} \right] + S_h \quad (4.78)$$

where:

E is the total energy:

$$E = h - \frac{p}{\rho} + \frac{u^2}{2} \quad (4.79)$$

$h$  is the sensible enthalpy and it has two definitions; for ideal gases and incompressible flows:

for ideal gases:

$$h = \sum_j Y_j h_j \quad (4.80)$$

Incompressible flows:

$$h = \sum_j Y_j h + \frac{p}{\rho_j} \quad (4.81)$$

$$h_j = \int_{T_{ref}}^T c_{pj} dT \quad (4.82)$$

where  $Y_j$  is the mass fraction of species  $j$  and  $T_{ref}$  is 298.15 K.

In Eq. 4.78  $k_{eff}$  is the effective conductivity ( $k+k_t$ ) where  $k_t$  is the turbulent thermal conductivity, defined according to the turbulence model being used).  $J_j$  is the diffusion flux of species  $j$ . The first three terms on the right-hand side of Eq. 4.78 represent energy transfer due to conduction, species diffusion, and viscous dissipation, respectively.  $S_h$  includes the heat of chemical reaction, and any other volumetric heat sources.

#### 4.3.5.1. Heat transfer between different phases

The equation of the heat transfer between phases was given by:

$$Q_{sl} = h_{sl}(T_s - T_l) \quad (4.83)$$

where the heat transfer coefficient is calculated by:

$$h_{sl} = \frac{6k_s \alpha_s \alpha_l Nu_s}{d_s^2} \quad (4.84)$$

The Nusselt correlations used was obtained from Gunn (1978) as follows:

$$Nu_s = (7 - 10\alpha_l + 5\alpha_l^2) \left( 1 + 0.7 Re_s^{0.2} Pr^{1/3} \right) + (1.33 - 2.4\alpha_l + 1.2\alpha_l^2) Re_s^{0.7} Pr^{1/3} \quad (4.85)$$

where

$$Re = \frac{\rho_g |v_g - v_s| d_s}{\mu_e} \quad (4.86)$$

#### 4.3.5.2. Radiation model equations

In order to account for the heat of radiation the simple P-1 radiation model was used. In this model the radiation flux  $q_r$  is given by:

$$q_r = -an^2 \frac{1}{3(a + \sigma_s) - C\sigma_s} \nabla G \quad (4.87)$$

where  $a$  is the absorption coefficient,  $\sigma_s$  is the scattering coefficient,  $G$  is the incident radiation, and  $C$  is the linear-anisotropic phase function coefficient. After introducing the parameter

$$\Gamma = \frac{1}{3(a + \sigma_s) - C\sigma_s} \quad (4.88)$$

Eq. 4.88 simplifies to:

$$q_r = -\Gamma \nabla G \quad (4.89)$$

The transport equation for  $G$  is

$$\nabla \cdot (\Gamma \nabla G) - aG + 4an^2 \sigma T^4 = S_G \quad (4.90)$$

where  $n$  is the refractive index of the medium,  $\sigma$  is the Stefan-Boltzmann constant and  $S_G$  is a user-defined radiation source. Combining Equations 4.89 and 4.90 yields the following equation:

$$-\nabla \cdot q_r = aG - 4an^2 \sigma T^4 \quad (4.91)$$

The expression for  $-\Delta \cdot q_r$  can be directly substituted into the energy equation (term  $S_h$ ) to account for heat sources (or sinks) due to radiation.

## 4.4. Conclusion

This chapter presented a background on gasification fundamentals, literature review on most recent and important studies on biomass gasification models. Based on the literature review, a gasification reactive model has been identified with full details of the reactions involved and their kinetics as given in Table 4.13 and 4.14. According to the defined general gasification steps the developed model has been separated into three main processes; drying, devolatilization and tar cracking, and partial combustion and gasification. The reactions have been classified into homogenous and heterogeneous reactions. The developed reactive

model will be implemented in a CFD code (Fluent Ver 12.1), along with the hydrodynamics and heat transfer models presented in Chapters 3 and 4, to predict the detailed performance of a CFB biomass gasifier.

The drying model was modelled as a mass transfer from solid phase to gas phase. The devolatilization and tar cracking model consisted of two steps; the devolatilization of the biomass, which is used as a single reaction, to generate the biomass gases from the volatile materials and tar cracking. The latter is also modelled as one reaction to generate gases with fixed mass fractions. The first reaction was classified as a heterogeneous reaction while the second reaction was classified as homogenous reaction. The partial combustion and gasification model consisted of carbon combustion reactions and carbon and gas phase reactions. The partial combustion is for C, CO, H<sub>2</sub> and CH<sub>4</sub>. The carbon gasification reactions used in this model are the Boudouard reaction with CO<sub>2</sub>, the reaction with H<sub>2</sub>O and Methanation (Methane forming reaction) reaction to generate methane. The other gas phase reactions considered in this study are the water gas shift reaction, which is modelled as a reversible reaction, and the methane steam reforming reaction.

Table 4.13 Summary of the mass transfer model for biomass drying

Name of the process	Mass transfer correlation	Reference
Drying	$m_{l \rightarrow v} = \epsilon_l \rho_l \frac{T - T_{sat}}{T_{sat}}$	Lee, 1979

Table 4.14 Summary of the reactions and the rate of reactions used in this study for the simulation of the CFB biomass gasification

Name of reaction	Chemical reaction	Kinetic	References
Heterogeneous reactions			
Devolatilization	$Wood \rightarrow 0.2CO + 0.1CO_2 + 0.1H_2 + 0.1CH_4 + 0.3H_2O + 0.2Tar$		Syamlal and Bisset, 1991
		$R = -k * C_{CO_2}$ $A = 1.1 \times 10^5 \text{ s}^{-1}$ $E = 8.86 \times 10^7$	
Char combustion	$C + 0.5O_2 \rightarrow CO$	$r = \frac{f^{PO_2}}{1/k_1 + 1/k_2}$ <p>where</p> $k_1 = \frac{0.292(1-\epsilon)D}{2d_p^2 T_g}$	Syamlal and Bisset, 1991

		$D = 4.26 \left( \frac{T_g}{1800} \right)^{1.75}$ $k_2 = k_1 \varepsilon^{2.5} \frac{d_c}{1-d_c}$ $d_c = \left( \frac{X_{Fc} X_{A0}}{(1-X_{Fc}) X_{FCO}} \right)^{1/3}$ $f_1 = \frac{X_{Fc}}{X_{FCO} + 10^{-6}}$	
Boudouard	$C + CO_2 \rightarrow 2 CO$	$R = -k * C_{CO_2}$ $A = 3.42 \text{ s}^{-1}$ $E/R = -15600$	Gerber et al., 2010
Water-gas shift	$C + H_2O \rightarrow CO + H_2$	$R = -k * C_{H_2O}$ $A = 3.42 \text{ s}^{-1}$ $E/R = -15600$	Gerber et al., 2010
Hydrogasification	$C + 2H_2 \rightarrow CH_4$	$R = -k * C_{H_2}$ $A = 3.42 \times 10^{-3} \text{ s}^{-1}$ $E/R = -15600$	Gerber et al., 2010
Homogeneous reactions			
Tar cracking	$Tar \rightarrow 0.4CO + 0.1CO_2 + 0.2H_2 + 0.1CH_4 + 0.2Tar_{inert}$		Gerber et al., 2010
		$R = -k * C_{Tar}$ $A = 2.3 \times 10^4 \text{ s}^{-1}$	

		$E=8 \times 10^{10}$	
Carbone monoxide combustion	$2CO + O_2 \rightarrow 2CO_2$	$R = k * C_{CO}C_{O_2}^{0.25}C_{H_2O}^{0.5}$ $A=3.98 \times 10^{11} \text{ s}^{-1}$ $E=1.6728 \times 10^8 \text{ (J/kgmol)}$	Miao et al., 2013
Hydrogen combustion reaction	$H_2 + 1/2O_2 \rightarrow H_2O$	$R = k * C_{H_2}C_{O_2}$ $A= 2.196 \times 10^9 \text{ s}^{-1}$ $E= 1.0914 \times 10^8 \text{ (J/kgmol)}$	Miao et al., 2013
Methane combustion reaction	$CH_4 + 2O_2 \rightarrow CO_2 + 2H_2O$	$R = k * C^{0.7}_{CH_4}C^{0.8}_{O_2}$ $A= 1.58 \times 10^9 \text{ s}^{-1}$ $E= 2.024 \times 10^8 \text{ (J/kgmol)}$	Liu and Gibbs, 2003
Shift reaction	$CO + H_2O \rightarrow H_2 + CO_2$	$R = k_f C_{CO}C_{H_2O} - k_b$ $A=2.78 \times 10^3 \text{ s}^{-1}$ $E=1.2554 \times 10^7 \text{ (J/kgmol)}$	Miao et al., 2013
Methane steam reforming	$CH_4 + H_2O \rightarrow 3H_2 + CO$	$R = k_f C_{CH_4}C_{H_2O}$ $A= 3.0 \times 10^5 \text{ s}^{-1}$ $E= 1.2552 \times 10^8 \text{ (J/kgmol)}$	Liu and Gibbs, 2003

## **5. Chapter 5: Simulation of a CFB biomass gasifier**

### **5.1. Introduction**

In this chapter, the simulation of a base case is introduced to give an overview of the hydrodynamics, heat transfer and product gas quality in the reactive system. The gas quality includes data on the gas heating value, composition and tar content. This chapter also includes preliminary mass and heat balance, The related literature on CFB modeling and simulation of biomass gasification in fluidized bed reactors is also discussed to identify the state of art and knowledge gaps in this area.

### **5.2. Literature review**

In this literature review, the reported studies on modelling biomass gasification on fluidized bed reactors with particular focus on the models used for CFB gasifiers were covered. Generally, theoretical models on gasification of solid fuels are widely available in the literature, especially for coal gasification. However, CFD models on biomass gasification in CFBs, and to some extent experiments, are rare. The following literature looks into the various reported models for biomass gasification in fluidized bed reactors with particular focus on CFB type. Notably, up to 2013, there are no reported studies on three dimensional CFD simulation of biomass gasification in CFBs. Perhaps, mainly due to the long computational time required for such case. The literature discussed in this section has been classified based on the simulation domain, i.e. one, two and three dimensional. Under each type of simulation domain the models for both types of fluidized bed gasifiers, i.e. bubbling and circulating fluidized bed types has been considered.

#### **5.2.1. One-dimensional CFD models**

Majority of the reported literature on modelling and simulation of biomass gasification are using one-dimensional model. Some of these studies were focused on devolving

the mathematical models and its formulations; while others were just focused on using available models from the literature for parametric sensitivity analysis.

#### 5.2.1.1. Bubbling Fluidized Bed (BFB) studies

Simple one-dimensional models of bubbling fluidized bed biomass gasification have been widely reported in the literature, such as the one reported by Gungor (2011), Radmanesh et al. (2006), Gungor (2011) and Radmanesh et al. (2006). Summary of some of the recent studies on one-dimensional gasification models and the parameters used in the analysis are given in Table 5.1

Radmanesh et al. (2006) modelled the gasification of beech wood particles in a BFB gasifier. The model included the hydrodynamics and reaction kinetics based on two phase model. The authors studied the effect of using two different pyrolysis models in the quality of the product gases. They then validated their model with experimental data from their own experiments and other published data. The authors reported that their model predictions were in good agreement with the experimental results. The authors made many assumptions in their model, the most important ones are: the pyrolysis considered taking place instantaneously in the feeding zone, char contains pure carbon, counter current back mixing (CCBM) model was used to describe char particles mixing and the volume fraction of solids in the bubble phase was taken to be 0.005. The authors concluded that the pyrolysis is an important step in the overall gasification model and that the model proposed by Nunn et al. (1985) produced the most accurate results.

Gungor (2011) developed a two-fluid isothermal steady state model to simulate biomass gasification in a bubbling fluidized bed gasifier. The authors compared their model results with experimental data available from the literature. It was found that  $H_2$  increased with increasing gasification temperature, small biomass particles enhance  $H_2$

composition, and the gas shift reaction has a significant effect in increasing the mole fraction of H<sub>2</sub> in the product gas when the steam flow increases. The authors also reported that their comparison with experimental data from the literature showed satisfactory agreement but further validation is still required.

Kaushal et al. (2010) and Nguyen et al. (2012) both reported a one dimensional steady state model of a dual fluidized bed system, where the gasification is assumed to take place in the bubbling bed part of the dual system. The authors discussed the effect of a range of operating conditions (see Table 5.1) on the gasifier performance and product gas quality. Kaushal et al. (2010) reported that during devolatilization step the gases release and mixing are sensitive and critical parameters. Their model prediction was in good agreement with the literature experimental data, but recommended further work to improve the model predictive capabilities. Nguyen et al. (2012) developed a model based on three stages gasification; (i) biomass pyrolysis (ii) char gas reactions and (iii) gas phase reactions. The authors assumed that the unconverted char and fuel were completely combusted at 950 °C in the combustor and the heat generated from this process is then carried in silica sand to the gasifier to provide the heat required for gasification. The authors reported that the model showed reasonable agreement with the experimental data at a wide range of operating conditions. It was also reported that the syngas is mainly generated from the pyrolysis step and only a small part of fixed carbon of biomass is converted to gaseous components.

#### Circulating Fluidized bed (CFB) studies

One-dimensional models have also been reported for the simulation of biomass gasification in CFBs (e.g. (Miao et al., 2013); (Corella and Sanz, 2005); and (Sanz and Corella, 2006). Miao et al. (2013) developed a one dimensional steady state model to simulate biomass gasification in the riser of a CFB system. The authors assumed the devolatilization as an instantaneous reaction and a mixture of char, tar and gas can be

assumed as soon as the biomass enters the gasifier. Uniform temperature was assumed in the same axial height, no heat transfer between the two phases, the effects of reactor inlet and outlet on the model are neglected and the effect of temperature on the bed hydrodynamics is neglected. The authors reported that the product gases from their model were close to the experimental data reported by Wu et al. (2009).

Corella and Sanz (2005) developed a one dimensional biomass CFB gasifier model under stationary state. The authors used both their own kinetic data and published equations for twelve different reactions. The hydrodynamics, mass and heat transfer formulation were considered in the model. The authors reported that the model has some empirical aspects therefore it can be considered as a semi rigorous. In a later study, the same authors Sanz and Corella (2006) used this model for parametric analysis. The authors analysed the effect of the equivalence ratio(ER), percentage of the secondary air flow, height (location) of the secondary air flow and biomass moisture and biomass flow rate. The authors indicate that the model results agreed with experimental data reported in the literature. It was concluded that the ER, percentage of the second air flow and the biomass moisture are the most important parameters affecting the product gas quality. Finally, the authors indicated that their model is particularly good for a quick estimation for the properties and quantities of the product gas, and to improve the design of the CFB gasifier.

### **5.2.2. Two-dimensional CFD models**

Two-dimensional models are more common in the simulation and modelling of biomass gasification in fluidized beds, however, when compared to one-dimensional models, they are relatively more computationally expensive, but believed to give more realistic results. Here below a review of the most recent reported two-dimensional models for biomass gasification

### Bubbling Fluidized Bed (BFB) studies

A detailed study by Gerber et al. (2010) presented a two-dimensional model for biomass gasification in BFB using a CFD simulation code (MFIx). The study discussed the effect of the initial bed height, wood feeding rate, thermal boundary conditions, pyrolysis kinetics in their model as mentioned in Table 5.1. The authors provided details of the hydrodynamics, heat transfer and reactions formulations used in their model. Compared to other literature, this study was found to give the most detailed information about the biomass gasification model used. Details on building the hydrodynamic model equations and how this was employed in simulating the gas and solid phase interactions was discussed in details. The study also presented detailed steps on building the reaction models, starting from the pyrolysis, homogeneous and heterogeneous reactions. The rate of reactions how is calculated and their constants were discussed in details. The authors then validated their model with experimental data and finally they carried out parametric analysis. This study was found to give very good guide in modelling biomass gasification. There is just one concern about this study which is that it was carried out in a two dimensional domain, which as we discussed in Chapter 3 may not be appropriate for a real three-dimensional system, therefore two-dimensional modelling should be handled carefully and the results obtained must be treated cautiously.

### Circulating Fluidized bed (CFB) studies

Gungor and Yildirim (2013) carried out a two-dimensional model to simulate biomass gasification in a CFB. The authors discussed the effect of the temperature and the equivalence ratio on the overall gasifier performance. The authors modelled the hydrodynamics following a previous study by Gungor and Eskin (2008). The author used a model called Particle Base Approach (PBA) model for the particulate phase. This model considers two-dimensional motion of single particles through the fluid. The

gasification model was validated using experimental data from the literature; the authors indicated that there is a range of error between 1-25% when comparing their results with the experimental results. They recommended modifications in their model to improve the simulation results.

### **5.2.3. Three-dimensional CFD models**

As mentioned earlier, three-dimensional CFD models for the simulation of fluidized bed biomass gasification are few in the literature. To my understanding there are no reported study on two-fluid model for CFB biomass gasifier, where the hydrodynamics, heat transfer and reactions are solved simultaneously in a three-dimensional domain. This section presents some of the very few reported studies on three-dimensional modelling and simulation, which are either for a gasifiers' type different than a CFB or using a modelling approach different than the two-fluid.

#### **5.2.3.1. Bubbling Fluidized Bed (BFB) studies**

Wang and Yan (2008) reported a three dimensional simulation of sewage sludge gasification in a bubbling fluidized bed using Computational fluid dynamic modelling (Fluent 6.1). The study used Eulerian–Lagrangian approach to model the hydrodynamics of the multiphase flow mixture. The model employed slandered k- $\epsilon$  for turbulence and non-premixed combustion model for gasification reactions. The authors compared their model results with experimental data from Manyà et al. (2005). The authors concluded that their study had some limitations due to using estimated parameters without enough practical data. It was also noted that more research is needed to understand the complex pyrolysis process and to improve the model predictive capabilities. Despite of using the computational time consuming Eulerian–Lagrangian modelling approach, the authors did not discuss how to address this problem in the future.

Wang et al. (2005) developed a three dimensional model for the gasification of biomass (Sorghum) in a bubbling fluidized bed. The inert bed material used in this model was sand. The authors developed their own code using C++ language and they included turbulence in their model. This study was mainly focused on developing the model rather than carrying analysis and discussion of the gasification process. The authors did not discuss the validity of their model or compare it with experimental data, but proposed to use the model in future investigation of the effect of different operating parameters in the production efficiency and product quality. This study has never materialized.

#### **5.2.4. Other non-CFD models**

Other non-CFD methods which have been reported in the literature for modeling and simulation of biomass gasification include Aspen models, non-stoichiometric equilibrium model and quasi-equilibrium three-stage gasification model. Examples of these studies are summarized in Table 5.1.

Li et al. (2004) developed a non-stoichiometric equilibrium model based on direct minimization of Gibbs free energy to predict the performance of a pilot biomass CFB gasifier. The authors reported that their model had a good agreement with the experimental data. This study has been further reviewed in chapter 6.

Loha et al. (2011) developed an equilibrium approach to model gasification of rice husk in a fluidized bed. This model was validated using experimental data and then further used to model gasification of other biomass feedstock such as sugarcane bagasse, rice straw and groundnut shell. Parametric analysis was carried out to investigate the effects of temperature and steam to biomass ratio in the product gas. It was found that increasing the temperature of the gasifier increase the CO and H<sub>2</sub> production and

decrease  $\text{CH}_4$  and  $\text{CO}_2$ . They also found that all of the above mentioned gases increase except CO decrease when the steam increases. The amount of  $\text{H}_2$  was noted to mostly depend on the biomass material, as rice husk has the lowest  $\text{H}_2$  content while straw had the highest.

Ngo et al. (2011) used quasi-equilibrium three stage model to investigate the effect of temperature and steam to fuel ratio in steam gasification of wood pine chips. The authors reported that this model is divided into three stages; biomass pyrolysis, char-gas reactions, and gas phase reactions. In the first stage they assumed that the volatiles and tar in the biomass are completely and spontaneously converted into five gaseous components ( $\text{CO}$ ,  $\text{CO}_2$ ,  $\text{CH}_4$ ,  $\text{H}_2$ , and  $\text{H}_2\text{O}$ ). Then in the second stage the steam participation ratio was used to determine the amount of steam involved in the char-gas reactions and in the third stage a non-equilibrium factor was employed to account the deviation from the thermodynamic equilibrium of the water gas shift reaction. The authors assumed that the steam reforming reaction not to take place in the third stage because it is not favourable at temperatures above  $800^\circ\text{C}$ , and they attributed that to the Gibbs free energy of formation as it has a positive value above this temperature. So, they considered just one reaction in this stage which is the gas shift reaction. The authors reported that their model was in a good agreement with experimental data but the prediction accuracy can be improved if the tar formation and cracking included in the model.

Studies on biomass gasification using Aspen simulation model have been reported by (Nikoo and Mahinpey, 2008), (Ardila et al., 2012), (Hannula and Kurkela, 2012) and (Doherty et al., 2009). In most of these studies, the authors studied the effect of different operating parameters on the product gas quality. Doherty et al. (2009) developed a computer model to model biomass gasification in a CFB using Aspen Plus. The authors reported that the model is based on Gibbs free energy minimisation.

They described Aspen Plus simulation package as steady state chemical process simulator, uses unit operation blocks, which are models of specific process operations such as reactors, heaters and pumps. The authors added these blocks can be placed in a flow sheet and connected with specified material and energy streams. There is an extensive built in physical properties database can be used for simulation calculations. The authors added the calculation approach uses in the program is the sequential modular (SM) approach, which is solve the process scheme module by module, calculating the outlet stream properties using the inlet stream properties for each block. They added this software has the capability to incorporate Fortran code written by the user into the model. Then the authors described how they build their own model to model the CFB biomass gasifier. They reported that the overall process has to be broken down into a number of sub-processes (drying, pyrolysis, partial oxidation and gasification) the details of sub-process are shown in Fig.5.1. The authors reported that this model include many assumptions; the main assumptions are it is steady state, zero dimensional, isothermal (uniform bed temperature), drying and pyrolysis are instantaneous. The flow sheet of the process is shown in Fig. 5.2. In my opinion the advantages of using Aspen Plus model are; it is easy to build, less expensive computationally, and it is accurate to some extent in calculating the mass and energy balance. On the other hand it has a lot of assumptions which makes it weak in conducting comprehensive study for design.



Fig. 5.1. Example of uncoupled CFB gasification process simulated using ASPEN Plus (Doherty et al. 2009).



Fig. 5.2. A typical ASPEN Plus flow sheet for biomass gasification in a CFB gasifier (Doherty et al. 2009).

Table 5.1 Summary of recent studies on modeling of biomass gasification in bubbling and circulating fluidized beds

<b>One-dimensional CFD models</b>			
Model/software used	Type of reactor	Parameters Studied	Source
Model: pseudo-rigorous, one-dimension under steady state model	- Circulating FB	- Mainly the model development	Corella and Sanz, 2005
Model: pseudo-rigorous, one-dimension under steady state model	- Circulating FB	- Equivalence ratio - Percentage of secondary air flow - Height of the secondary air flow - Biomass moisture and - Biomass flow rate	Sanz and Corella, 2006
Model: one-dimension mathematical model	- Bubbling FB	- Two different kinetic models for pyrolysis - Effect of temperature - Equivalence ratio - Steam-to-biomass ratio - Feed location	Radmanesh et al., 2006
mathematical model	- Circulating FB	- predicting the bed temperature distribution along the gasifier -the concentration and distribution of each species in the vertical direction of the bed -the composition and heating value of produced gas -the gasification efficiency, -the overall carbon conversion and the produced gas	Miao et al., 2013

		production rate	
Model: one-dimensional steady state model	- Dual FB	- Mixing of devolatilized gas - Average temperature of incoming bed material - Effect of moisture content - Effect of steam to biomass ratio	Kaushal et al. (2011)
Model: one-dimensional steady state model	- Dual FB	- Effect of temperature - Steam-to-biomass ratio - Effective operating conditions for electric power generation of syngas	Nguyen et al., 2012
steady state mathematical model based on two-phase theory of fluidization	- Bubbling FB	- Effect of temperature - Equivalence ratio - Steam-to-biomass ratio - Particle size - bed operational velocity	Gungor, 2011
steady state mathematical model based on two-phase and two-zone formulations	- Bubbling FB	- Mainly the model development and the validations. - The effect of temperature in tar yield and product gas	Kaushal et al., 2010
<b>TWO-DIMENSIONAL CDF MODELS</b>			
Eulerian- Eulerian Software: MFIX	- Bubbling FB	- initial bed height - wood feeding rate - thermal boundary conditions - pyrolysis kinetics	(Gerber et al. 2010)
FORTTRAN language, Particle	- Circulating FB	- Effect of temperature	Gungor and Yildirim 2013

Base Approach (PBA)		- Equivalence ratio	
<b>THREE-DIMENSIONAL CFD MODELS</b>			
Model: three-dimension, Software: An object-oriented computer program was developed in Visual C++	- Bubbling FB	- Mainly the model development	Wang et al., 2005
Eulerian–Lagrangian Software: Fluent 6.1	- Bubbling FB	- Effect of temperature - Equivalence ratio	Wang and Yan 2008
<b>OTHER MODELS</b>			
Model: An equilibrium modelling approach	- Bubbling FB	- Performance from different biomasses - Effect of temperature - Steam-to-biomass ratio	Loha et al., 2011
Model: a quasi-equilibrium three- stage gasification model	- Circulating FB	- Performance from different biomasses - Effect of temperature - Steam-to-biomass ratio	Ngo et al., 2011
Software: Aspen plus	- Bubbling FB	- Effect of temperature - Equivalence ratio - Steam-to-biomass ratio	Nikoo and Mahinpey, 2008
Software: Aspen plus	- Circulating FB	- Effect of temperature - Equivalence ratio - Steam injection	Ardila et al., 2012

---

Software: Aspen plus	- Bubbling FB	<ul style="list-style-type: none"> <li>- The influence of heat losses, gasification pressure and steam/oxygen ratios</li> <li>- The effects of filtration temperature and reformer conversion levels</li> <li>- The effect of reforming temperature</li> <li>- The effect of drying</li> </ul>	Hannula and Kurkela, 2012
Software: Aspen plus	- Circulating FB	<ul style="list-style-type: none"> <li>- Effect of temperature</li> <li>- Equivalence ratio</li> <li>- Steam injection</li> <li>- Air preheating</li> <li>- Biomass moisture</li> </ul>	Doherty et al., 2009
Model: non-stoichiometric equilibrium model based on direct minimization of Gibbs free energy	- Circulating FB	<ul style="list-style-type: none"> <li>- Effect of temperature</li> <li>- Equivalence ratio</li> <li>- Steam injection</li> <li>- Suspension density</li> <li>- Fly ash re-injection</li> </ul>	Li et al., 2004

---

### **5.2.5. Conclusion of the literature review**

The literature was reviewed in order to understand the state of the art in modelling biomass gasification, particularly in fluidized bed gasifiers. The literature review indicated that most of the literature is focused on one-dimensional models; fewer studies were found in using two-dimensional models and very few using three-dimensional models. Specifically, a two-fluid model on three-dimensional domain of a CFB gasifier is not available, as far as my knowledge.

Perhaps, the choice of one-dimensional approach is mainly to avoid complicated computations when adding simulations heat transfer and reactions. In addition, one-dimensional models are easier to develop and implement for biomass gasification because they are less expensive computationally. However one-dimensional modelling suffers from a number of limitations, since it only gives axial profiles of the particular parameter and ignores the other dimensions profiles. The effects of hydrodynamics in the gasifier calculations cannot be calculated locally. In most cases, important features, such as the entrance and exit effects, heat transfer between gas and solids are neglected. In general, it is too simple for such a complex multiphase flow interactions which considerably vary locally.

Review of the literature reveals that the most important study on CFD modelling of biomass gasification has been reported by Gerber et al. (2010). The study provided details derivation of the flow hydrodynamics and reaction kinetics, which appeared to satisfactory capture the gasifier performance. However, the study was on a bubbling fluidized bed type of reactor and was carried out in a two-dimensional domain. Recent comparative studies on two-dimensional against three-dimensional modelling have shown critically differences and therefore the former modelling approach should be treated with caution. Furthermore, the two-dimensional simulation domain, have been

found to result in critically wrong mass balance when applied in the CFB under consideration in this study.

Accordingly, three-dimensional simulation is the best option for the simulation of a cylindrical CFB gasifier, such that realistic boundary condition can be applied. In order to limit the computational time with three-dimensional setting, it is recommended to use CFD two-fluid modelling approach as opposed to discrete modelling. The later may provide accurate results but will be unrealistic in handling realistic cases due to the computational time constraint. The other modelling options, such as equilibrium modelling approach, Aspen plus, and quasi-equilibrium three-stage model, may be useful for preliminary analysis, but for sure not capable for providing accurate transient data at the microscopic level as produced by the CFD two-fluid option. As discussed later in this study very good results were obtained in a reasonable time because the work was carried out using a high performance work station machine with parallel processing.

### **5.3. The base case**

In Chapter 3 the hydrodynamics in a CFB riser was modeled and validated using experimental data. In this chapter, and based on the conclusions drawn from the above literature review, this model has been further extended to include the chemical reactions, reaction kinetics and heat transfer (detailed in Chapter 4) in order to predict the multiphase flow and the biomass thermo-chemical performance conversation in the CFB riser. A base case study is presented starting from the system geometry, properties of the solids and gasifying agents, and operating and boundary conditions. This is followed by description and discussion of the base case predictions. The predictions for this base case will then be used as a reference when considering different operating parameters as discussed later in chapters 6 and 7.

### 5.3.1. Reactor geometry, solids properties and operating conditions

The geometry used for the simulation of the reactive system is shown in Fig. 5.3. This geometry is in exact size and shape of the unit used in the hydrodynamics validation part reported in chapter 3, except that here the riser has one additional solid inlet point at the bottom to allow for biomass feeding. This makes the CFB riser consisting of three inlets and one outlet. The three inlets are for the main gasifying agent (steam, air or the mixture of the two) and the other two inlets are for the circulating heat carrier (sand) and the biomass (wood); both of these inlets include a small fraction of air to aid in forcing the solids into the reactor.

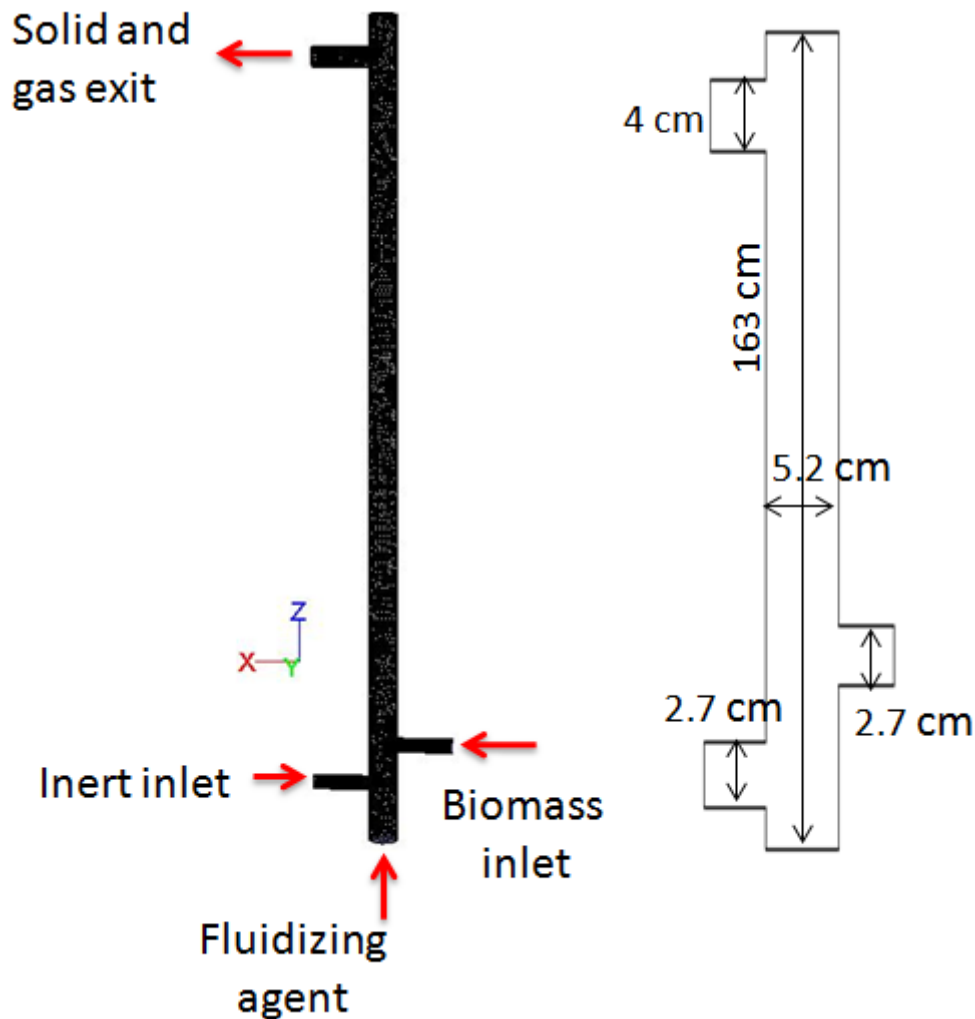


Fig. 5.3. The schematic geometry and dimensions of the CFB riser used for the simulation of the reactive system

The simulation was carried out using steam as the main gasifying agent and air as the secondary gasifying agent, which is in very small amounts to aid in forcing the sand and the biomass into the riser as mentioned earlier. Table 5.2 shows a summary of the operating conditions used in the base case simulation study.

Table 5.2 The properties of the biomass fuel and sand

	Fuel			Sand	
Thermal conductivity (w/m k)	1.5			0.25	
Material Size (diameter)	500 $\mu\text{m}$			700 $\mu\text{m}$	
Components	Carbone	Ash	Volatile	Moisture	
Density ( $\text{kg/m}^3$ )	1400*	700*	Calculated	998.2*	2500
Specific heat ( j/kg k)	2092*	2092*	Calculate	4182*	830
Molecular Weight	12.0*	-	Calculated	18.0*	-

\* from fluent documentation

### 5.3.2. Properties, initial and boundary conditions of the biomass and gases

As discussed earlier in Chapter 4, the wood and the gas were modelled as mixtures consisting of different species; the wood phase consists of C, volatiles, moisture and ash, and the gas phase consist of  $\text{CO}_2$ , CO,  $\text{H}_2\text{O}$ ,  $\text{CH}_4$ ,  $\text{O}_2$ ,  $\text{N}_2$ ,  $\text{H}_2$ , tar and tar-inert. The heat carrier (sand) was modelled as a separate granular solid phase.

At the initial conditions, the fluidized riser is assumed at ambient temperature and pressure. The secondary gas (air) is introduced to the riser with given volume fraction of 21% oxygen and 79% nitrogen. The main fluidizing gas is assumed to initially consist of zero CO,  $\text{CO}_2$ , tar, tar-inert,  $\text{CH}_4$  and  $\text{H}_2\text{O}$  and a given flow of pure  $\text{H}_2\text{O}$  (steam). In this base case, the wood is introduced as a mixture with the mass percentage of 73.89% volatiles, 9.09% moisture 15.64% carbon and 1.38% ash. This composition is taken from (Telmo et al. 2010) for wood. For the mixture wood, the

specific heat capacity and density are calculated using the volume weighted mixing law such that:

$$C_p = \sum_i Y_i C_{p_i} \quad (5.1)$$

$$\rho = \sum_i Y_i \rho_i \quad (5.2)$$

While for the gas phase, the density is calculated as incompressible ideal gas using Eq. 5.3 as follows:

$$\rho = \frac{p_{op}}{RT \sum_i \frac{Y_i}{M_{w,i}}} \quad (5.3)$$

- $R$  = the universal gas constant
- $Y_i$  = the mass fraction of species  $i$
- $M_{w,i}$  = the molecular weight of species  $i$
- $p_{op}$  = the operating pressure

The specific heat of the individual species in the gas phase is calculated according to Piecewise-Polynomial function of temperature as follows:

$$C_p(T) = a + bT + cT^2 + dT^3 + eT^4 \quad \text{for } 300 \text{ K} \leq T < 1000 \text{ K} \quad (5.4)$$

$$C_p(T) = aa + bbT + ccT^2 + ddT^3 + eeT^4 \quad \text{for } 1000 \text{ K} \leq T < 5000 \text{ K} \quad (5.5)$$

where  $a, b, \dots, e$  are the constants of the first range of temperature and  $aa, bb, \dots, ee$  are the constants of the second range. These constants were reported in Table 5.3 and 5.4.

Table 5.3: The constants used in calculating the specific heat capacities of the gas components for  $300 \leq T < 1000$

Components	a	b	c	d	e
O <sub>2</sub>	834.8265	0.292958	-0.0001496	3.4139e-07	-2.2784e-10
CO <sub>2</sub>	429.9289	1.874473	-0.0019665	1.29731e-06	-3.99996e-10
H <sub>2</sub> O	1563.077	1.603755	-0.0029328	3.21610e-06	-1.15683e-09
N <sub>2</sub>	979.043	0.4179639	-0.00117628	1.67439e-06	-7.25630e-10
CO	968.3898	0.4487877	-0.00115222	1.65688e-06	-7.34637e-10
H <sub>2</sub>	13602.45	3.402317	-0.00335842	-3.90795e-07	1.70535e-09
CH <sub>4</sub>	403.5847	9.057335	-0.01442509	1.58052e-05	-6.34305e-09

Table 5.4: The constants used in calculating the specific heat capacities of the gas components for  $1000 \leq T < 5000$

Components	aa	bb	cc	dd	ee
O <sub>2</sub>	960.7523	0.1594126	-3.27089e-05	4.61277e-09	-2.95283e-13
CO <sub>2</sub>	841.3765	0.5932393	-0.00024152	4.52273e-08	-3.15313e-12
H <sub>2</sub> O	1233.234	1.410523	-0.00040291	5.54277e-08	-2.94982e-12
N <sub>2</sub>	868.6229	0.4416295	-0.00016872	2.99679e-08	-2.00439e-12
CO	897.9305	0.4282316	-0.00016714	3.02344e-08	-2.05137e-12
H <sub>2</sub>	12337.53	2.887275	-0.00023236	-3.80738e-08	6.52774e-12
CH <sub>4</sub>	872.4671	5.305473	-0.00200830	3.51665e-07	-2.33391e-11

Table: 5.5 Composition of the biomass used in the simulation of the base case (Telmo et al., 2010)



The volatiles gas released during the pyrolysis stage is assumed to consist of a fixed composition. The fractions of the component are taken from the data reported by Ragland et al. (1991) as shown in Table 5.6. The tar produced in the pyrolysis stage will be further cracked into gases and tar inert as described in Tables 5.7 and 5.8.

Table: 5.6 The composition of the gas (Ragland et al., 1991)



Table 5.7 The tar from the primary de-volatilization step (Gerber et al., 2010).



Table 5.8 Composition of the gases released during tar cracking (Gerber et al., 2010).



#### **5.4. Preliminary mass and energy balance**

This section presents a preliminary mass and energy balance calculations for the base case. In the mass balance section the following parameters were calculated; initial conditions, volatile gases calculations, reactions mass balance and overall mass balance. Then the energy balance calculations included the heat of reactions and the overall heat balance.

The purpose of this was to obtain a rough estimate of the required range of initial and inlet operating conditions such as the temperature, flow rates of the various phases, as well as an indicate of the expected product gas composition. This information will then be used for setting the input parameters for the computer simulation model in Fluent.

#### **5.4.1. Mass Balance**

##### 5.4.1.1. Initial conditions

The biomass feedstock is assumed to consist of fixed carbon, volatile matter, ash and moisture, with the mass composition as given in Table 5. 9. The biomass flow rate is assumed to be 2 g/s.

Table 5.9. Mass flow rate calculations based on biomass composition given by Ragland et al. (1991) Assumed biomass federate of 2 g/s.



##### 5.4.1.2. Volatile gases calculation

It is assumed that the devolatilization step produces a gas mixture consisting of CO, CO<sub>2</sub>, H<sub>2</sub>, CH<sub>4</sub>, Tar and H<sub>2</sub>O. This gas is assumed to have a fixed mass fraction composition as given in Table 5. 10. This table also includes calculation of the molar flow rates, molecular weight of the mixture, and mass flow rates.

Table. 5.10. Mass balance calculation of the volatiles produced from biomass pyrolysis

	Mass fraction*	Mass (g/s)	Molecular Weight (g/mol)	Molar flow mol/s	Mole fraction	Mixture molecular weight
H <sub>2</sub> O	0.3125	0.462	18.0	0.026	0.377	6.786
CO	0.22875	0.338	28.0	0.012	0.174	4.872
CO <sub>2</sub>	0.14375	0.212	44.0	0.005	0.072	3.168
H <sub>2</sub>	0.00625	0.009	2.0	0.005	0.072	0.144
CH <sub>4</sub>	0.05875	0.087	16.0	0.005	0.072	1.152
TAR	0.25	0.370	22.7	0.016	0.232	5.266
TOTAL	1	1.478		0.069	1	21.388

\* taken from Ragland et al. (1991)

#### 5.4.1.3. Reactions mass balance

The main reactions involved in the biomass gasification are given in Table 5. 11. This table also contains the heat of reactions and the heat required for drying.

In order to estimate the reactions conversion for the mass balance a number of assumptions have been made. For the heterogeneous combustion reaction (R3) the Air ratio ( was assumed to be 10%. The equivalence ratio was calculated as follows:

The percentage reacted of the carbon in the other heterogeneous reactions (R1, R4 and R5) was assumed as follow: for water gas shift reaction (R1) 15%, 10% with CO<sub>2</sub> (R4) and 5% with H<sub>2</sub> (R5) and 50% of the carbon remains without conversion. Accordingly, the mass balance calculation of the gas produced from the homogenous reactions is given in the left column in Table 5.12.

Table 5.11 Proposed gasification reactions, heat of reactions, heat required for drying

Reaction	Heat of reaction (MJ/kmol)	Reaction name
(R1) $C+H_2O \rightarrow H_2+ CO$	131	water-gas shift reaction
(R2) $Volatile \rightarrow 0.2127Tar+0.1809CO+0.0724CO_2+0.3843H_2O+0.0811CH_4+0.0687H_2^*$	5.907	Devolatilization
(R3) $C + 0.5 O_2 \rightarrow CO$	-111	Carbon Combustion reaction
(R4) $C + CO_2 \rightarrow 2 CO$	172	Boudouard reaction
(R5) $C+2H_2 \rightarrow CH_4$	- 74.8	Methanation
(R6) $2CO+O_2 \rightarrow 2CO_2$	- 284	CO Combustion reaction
(R7) $CO+H_2O \rightarrow H_2+ CO_2$	- 41.2	Shift reaction
(R8) $2H_2+O_2 \rightarrow 2H_2O$	- 242	Hydrogen combustion reaction
(R9) $CH_4+2O_2 \rightarrow CO_2+H_2O$	- 803	Methane combustion reaction
(R10) $CH_4+H_2O \rightarrow CO+3H_2$	206	Steam methane reforming reaction
(R11) $Tar \rightarrow 0.4566CO+0.1251CO_2+0.0572CH_4+0.1949H_2+0.1661Tar_{inert}$	Included with (R2)	Tar cracking reaction
Drying	40.715	

\* *Ratha et al. (2003)*

The homogeneous reactions considered in these preliminary calculations include oxidation, methanation, steam reforming and the shift reaction. The main fluidizing agent was steam and the air is assumed to be a secondary fluidizing agent, therefore, the main homogeneous combustion (oxidation) reactions is assumed to take place in the conversion of CO to CO<sub>2</sub>. The shift reaction is an important gas-phase reaction as it increases hydrogen content and reduces carbon monoxide in the product gas. Another important homogeneous reaction is the methane steam reforming reaction. An assumption was made in this calculations assuming 10% of the methane was reacted. The last homogeneous reaction considered in the mass balance is for the tar cracking. It is assumed that all the tar produced from the primary pyrolysis is cracked to form volatile gases with different fractions (see Table 5.8 for example). The right column in Table 5.12 illustrate the calculation and results of the gases produced from the

homogenous reactions. Finally, Fig. 5.4 graphically shows the composition of the final gas product estimated for each component individually by adding all the generated products in dry basis. While this simple calculation gives useful information on the mass balance, it can further be used to estimate the heat supply required, hence helping in specifying the range for the heat carrier (sand) feed rate as input in the CFB gasifier simulation.

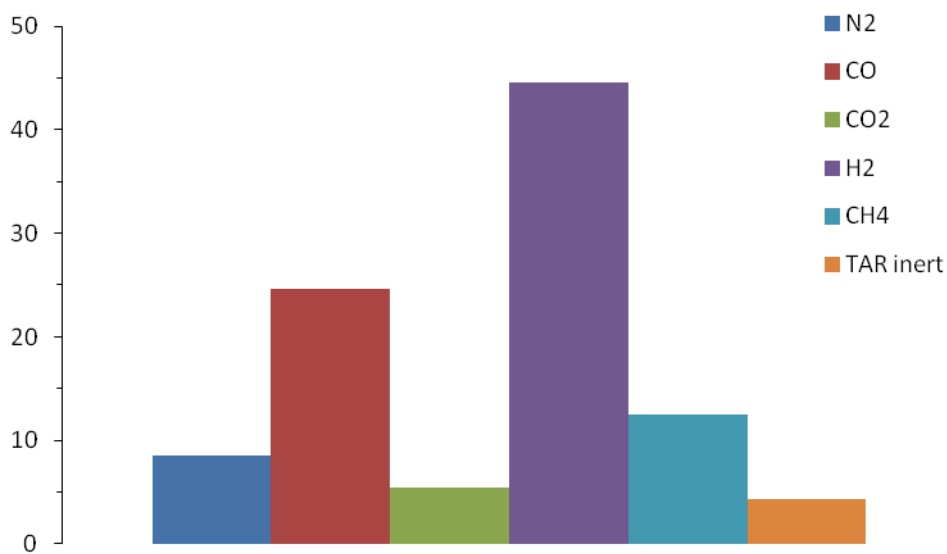


Fig. 5.4. The composition of the final gas product estimated for each component individually by adding all the generated products in dry basis.

Table.5.12. Material balance calculations for Heterogeneous and homogeneous reactions

Heterogeneous reaction	Homogenous reaction
<p>Oxidation reaction (R3):</p> $\text{C} + 0.5 \text{O}_2 \rightarrow \text{CO}$ <p>Carbon oxidized = 2.86774E-06 kmol/s  Oxygen needed = 1.43387E-06 kmol/s  CO produced = 2.86774E-06 kmol/s</p>	<p>CO combustion reaction (R6):</p> $2\text{CO} + \text{O}_2 \rightarrow 2\text{CO}_2$ <p>CO oxidized = 2.70149E-07 kmol/s  Oxygen needed = 1.35074E-07 kmol/s  CO<sub>2</sub> produced = 2.70149E-07 kmol/s</p>
<p>Water gas shift reaction (R1):</p> $\text{C} + \text{H}_2\text{O} \rightarrow \text{H}_2 + \text{CO}$ <p>Carbon reacted = 3.89638E-06 kmol/s  H<sub>2</sub>O needed = 3.89638E-06 kmol/s  H<sub>2</sub> produced = 3.89638E-06 kmol/s  CO produced = 3.89638E-06 kmol/s</p>	<p>CO shift reaction (R7):</p> $\text{CO} + \text{H}_2\text{O} \rightarrow \text{H}_2 + \text{CO}_2$ <p>CO reacted = 1.64785E-05 kmol/s  H<sub>2</sub>O needed = 1.64785E-05 kmol/s  H<sub>2</sub> produced = 1.64785E-05 kmol/s  CO<sub>2</sub> produced = 1.64785E-05 kmol/s</p>
<p>Boudouard reaction (R4):</p> $\text{C} + \text{CO}_2 \rightarrow 2 \text{CO}$ <p>Carbon reacted = 2.59759E-06 kmol/s  CO<sub>2</sub> needed = 2.59759E-06 kmol/s  CO produced = 5.19517E-06 kmol/s</p>	<p>Steam methane reforming reaction (R10):</p> $\text{CH}_4 + \text{H}_2\text{O} \rightarrow 3\text{H}_2 + \text{CO}$ <p>CH<sub>4</sub> reacted = 8.74728E-07 kmol/s  H<sub>2</sub>O needed = 8.74728E-07 kmol/s  H<sub>2</sub> produced = 2.62418E-06 kmol/s  CO produced = 8.74728E-07 kmol/s</p>
<p>Hydro-gasification (methanation)(R5):</p> $\text{C} + 2\text{H}_2 \rightarrow \text{CH}_4$ <p>Carbon reacted = 1.29879E-06 kmol/s  H<sub>2</sub> needed = 2.59759E-06 kmol/s  CH<sub>4</sub> produced = 1.29879E-06 kmol/s</p>	

#### 5.4.2. Energy Balance

The mass flow rates calculated in the previous section was employed to calculate the energy balance, specifically, the estimated heat content in the product gas and the

amount of heat required and supplied to the CFB gasifier. In order to estimate the higher heating value (HHV) of the product gas the following equation from Li et al. (2004) has been used:

$$\text{HHV} = (12.75 [\text{H}_2] + 12.63 [\text{CO}] + 39.82 [\text{CH}_4] + 63.43 [\text{C}_2\text{H}_4] + \dots) / 100 \quad (5.6)$$

Using the estimated molar flow rates of gases produced, the HHV of the product gas was found to be 13.77 MJ/m<sup>3</sup> as demonstrated in Table 5.13.

Table 5.13 Overall material balance and HHV calculations for the 2 g/s biomass gasification

Components	Kmol/s	mol% dry	Heat content (MJ/m <sup>3</sup> )
N <sub>2</sub>	5.39E-06	8.54	0
H <sub>2</sub> O	8.11E-05		0
CO	1.56E-05	24.68	3.12
CO <sub>2</sub>	3.43E-06	5.44	0
H <sub>2</sub>	2.82E-05	44.59	5.69
CH <sub>4</sub>	7.87E-06	12.47	4.96
TAR inert	2.70E-06	4.28	0
Total		100.00	13.77

#### 5.4.2.1. Calculation of heat of reactions

The heat of reactions was estimated using the mass balance by multiplying the number of moles of the product gas component with the corresponding heat of the reaction as demonstrated in Table 5.14. This gives an estimated total head demand of 0.814 KJ/s.

Table 5.14 Estimated heat of reactions and drying during the gasification of 2 g/s biomass feed

Reaction	Heat of reaction (MJ/kmol)	Heat of reaction (KJ/s)
(R1) $C + H_2O \rightarrow H_2 + CO$	131	0.510
(R2) Volatile $\rightarrow 0.2127\text{Tar} + 0.1809\text{CO} + 0.0724\text{H}_2 + 0.3843\text{H}_2\text{O} + 0.0811\text{CH}_4 + 0.0687\text{H}_2$	5.907	0.407
(R3) $C + 0.5\text{O}_2 \rightarrow CO$	-111	-0.288
(R4) $C + CO_2 \rightarrow 2\text{CO}$	172	0.447
(R5) $C + 2\text{H}_2 \rightarrow CH_4$	-74.8	-0.097
(R6) $2\text{CO} + \text{O}_2 \rightarrow 2\text{CO}_2$	-284	-0.077
(R9) $CH_4 + H_2O \rightarrow 3\text{H}_2 + CO$	206	0.180
(R7) $CO + H_2O \rightarrow H_2 + CO_2$	-41.2	-0.679
Drying	40.715	0.411
Total		0.814

#### 5.4.2.2. Overall heat balance

In calculating the overall heat balance for the gasification of 2 g/s biomass gasification in a CFB, it is important to estimate the heat required deriving pyrolysis stage, the heat released from the gasification reactions and the mass flow rate of the circulating heat carrier (sand) required to complete the gasification process. It is assumed that main gasifying agent (steam) enters the reactor at the temperature of 153 °C , while the secondary air and biomass both enter at the ambient temperature of 20 °C. With these assumed operating conditions and heat of reactions and drying calculated in the previous section, the overall heat balance around the CFB reactor for the case of 2 g/s biomass feed rate is demonstrated in Table 5.15 for the total heat in and Table 5.16 for the total heat out.

Table 5.15 Total heat in

Heat in fluidizing steam (KJ/s)	3.1
Heat in secondary air feed (KJ/s)	0
Heat in biomass feed (KJ/s)	0
Heat of sand	730.4 $\times m^*$

*\* m is the mass of the sand needed*

Table 5.16 Total heat out

Total heat of reaction (KJ/s)	0.403
Heat required for drying	0.411
Heat in fluidizing steam (KJ/s)	3.9636
Heat in secondary air (KJ/s)	1.594
Heat in biomass (KJ/s)	2.514
Heat of sand	481.4 $\times m$

Assuming the sand enters the reactor at the temperature of 900°C and leaves with the products (solids and product gas) at the temperature of 600°C, then using the total heat demand calculated in table 5.15 and 5.16, the estimated sand flow rate required to complete the gasification process will be around 0.02 kg/s. According to the above preliminary mass and energy balance table 5.17 shows a summary of the operating conditions used in the base case simulation.

Table 5.17 The CFB gasifier operating conditions considered in the base case

Secondary air for biomass inlet (g/s)	9.8361e-02
Secondary air for sand inlet (g/s)	9.8361e-02
Steam (g/s)	1.2
Sand flow (g/s)	20.0
Biomass flow (Kg/s)	2.0
Air inlet Temperature (K)	293
Steam inlet Temperature (K)	426
Sand inlet Temperature (K)	1173
Biomass inlet Temperature (K)	293

## 5.5. Simulation results for the base case

In this section the base case was simulated using the operating condition identified from the above preliminary mass and energy balance calculation. The flow conditions have been summarized in Table 5.17. The purpose of running this base case is to gain basic understanding of the overall features of the hydrodynamics, heat transfer and the product gases in the reactive system, which can then be used for further detailed parametric analysis, as discussed in Chapters 6 and 7.

### 5.5.1. Hot flow hydrodynamic predictions of the CFB riser

In order to understand the overall hydrodynamics in the gasifier the axial profiles and the contours of the volume fraction of solids as well as the vertical velocity of the solids and gases are presented and discussed. Fig. 5.5 shows the volume fractions for the biomass and sand. For the operating condition considered in this case, it is that the sand is highly concentrated in the regions below the sand entrance and above the exit, with highest volume fraction near the above corner of the exit. The accumulation of solids near the entrance and exit is generally classified in the literature as a result of boundary effect. As expected the biomass is less concentrated throughout the riser compared to the sand because it represents only 10% of the sand feed rate. The velocity vectors for the heat carrier sand shown in Fig. 5.6 indicate a very complex and

interesting hydrodynamic behaviour. It is shown that part of the sand entering the CFB riser is flowing downwards before recirculation towards the top parts of the riser. The importance of such phenomena lies in the fact that it plays an important role in the heat transfer mechanism as it is expected to cause rapid heat loss from the heat carrier sand to the fluidizing gas at the bottom part of the riser. Accordingly, the gases and solids are expected to reach thermal equilibrium at a very short distance above the solid feeding point. It must be noted that the solid recirculation at the bottom of the CFB riser strongly depend on the fluidizing gas velocity, such that it almost diminished at considerably high gas fluidization velocity.

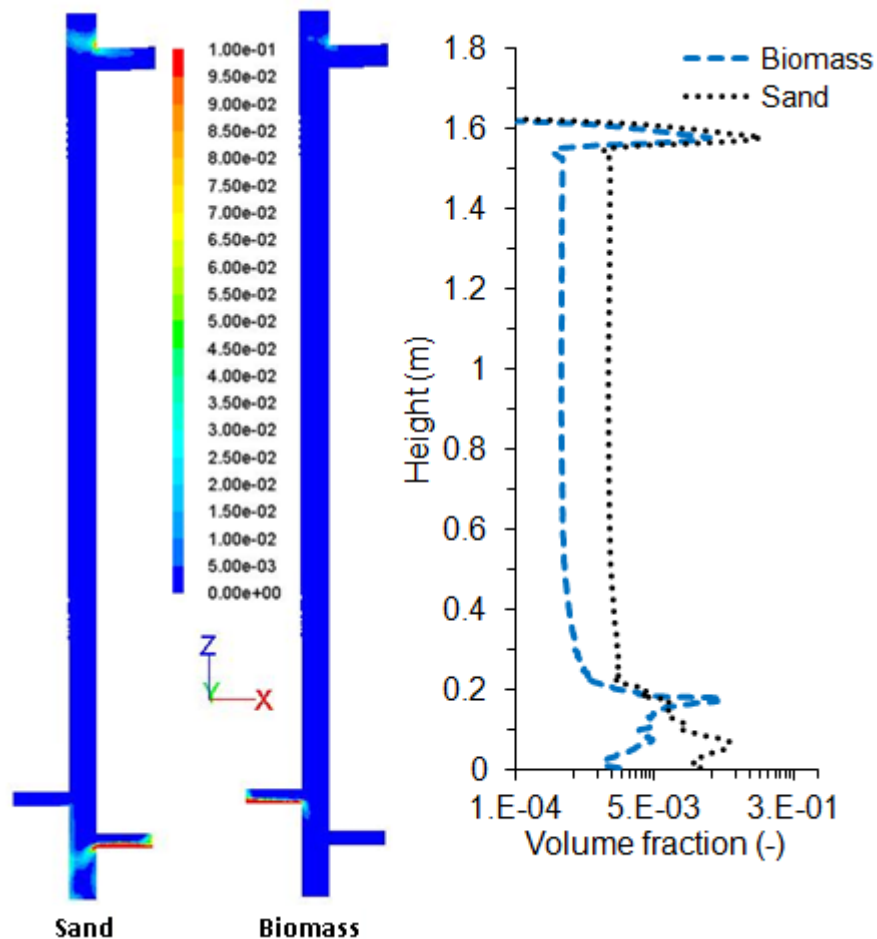


Fig. 5.5. Volume fractions of biomass and sand in the CFB riser for the base case simulation. The detailed operating conditions are given in Table 5.17.

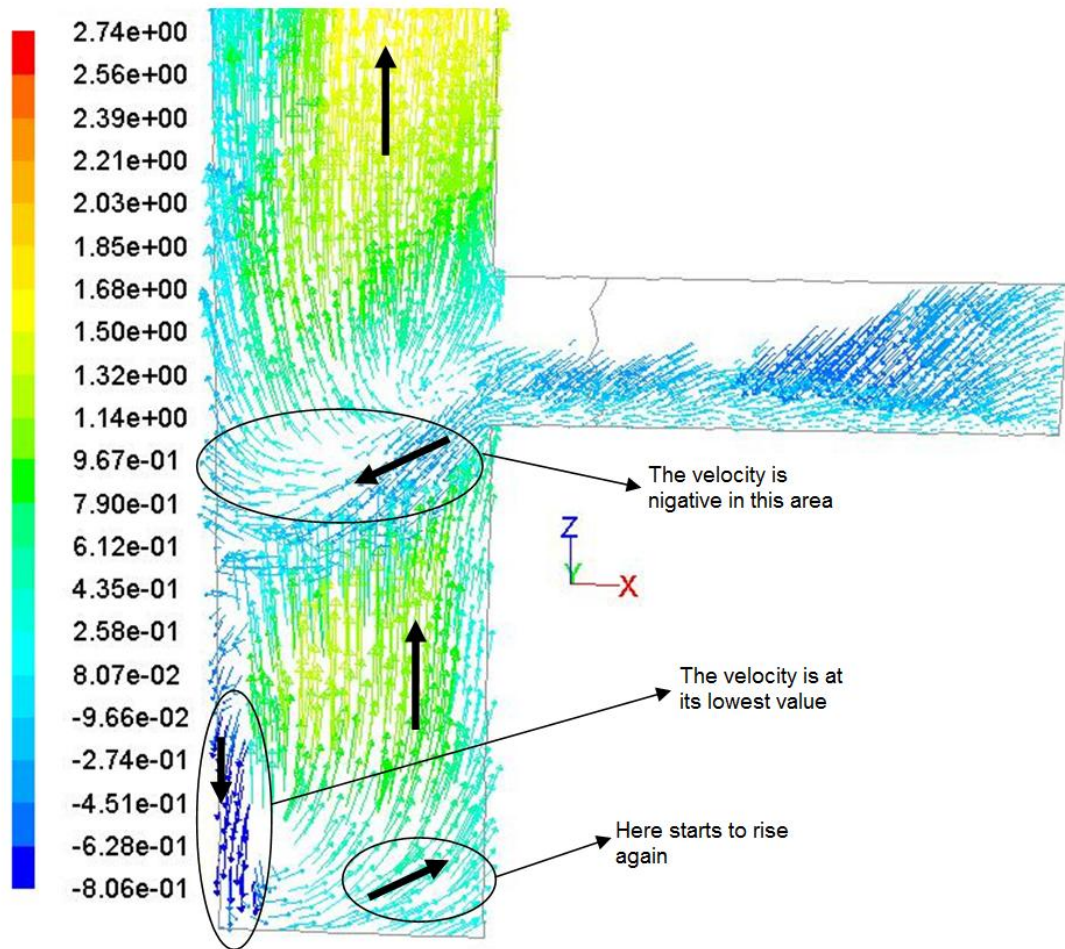


Fig. 5.6. Sand velocity vectors at inlet to the CFB riser. Detailed operating conditions are given in Table 5.17.

Fig. 5.7 shows the vertical velocities of the three phases involved in the CFB riser. A number of important observations include:

- i. Neglecting the entrance and exit effects, the three phases show almost constant velocity in the region between 0.6 m and 1.4 m heights.
- ii. Generally, all three phases (sand, biomass and gas) show increasing velocity with height and the similar axial profiles.
- iii. The two solid phases (biomass and sand) are very close in velocity throughout the riser height.
- iv. The gas phase mixture is more sensitive to the exit effect when compared to the solid phases.
- v. Generally, the gas velocity is around 1.6 higher than the solid phases.

- vi. Both the solids and gas phases shown negative velocities at the bottom and top of the riser as a result of entrance and exit effects.

The negative velocities noted in point (vi) above, which is more pronounced for solids, suggest solids circulation within the bottom and top regions. This is particularly important for increasing the multiphase flow residence time, which has direct effect of the rate of biomass conversion as discussed in Chapter 7.

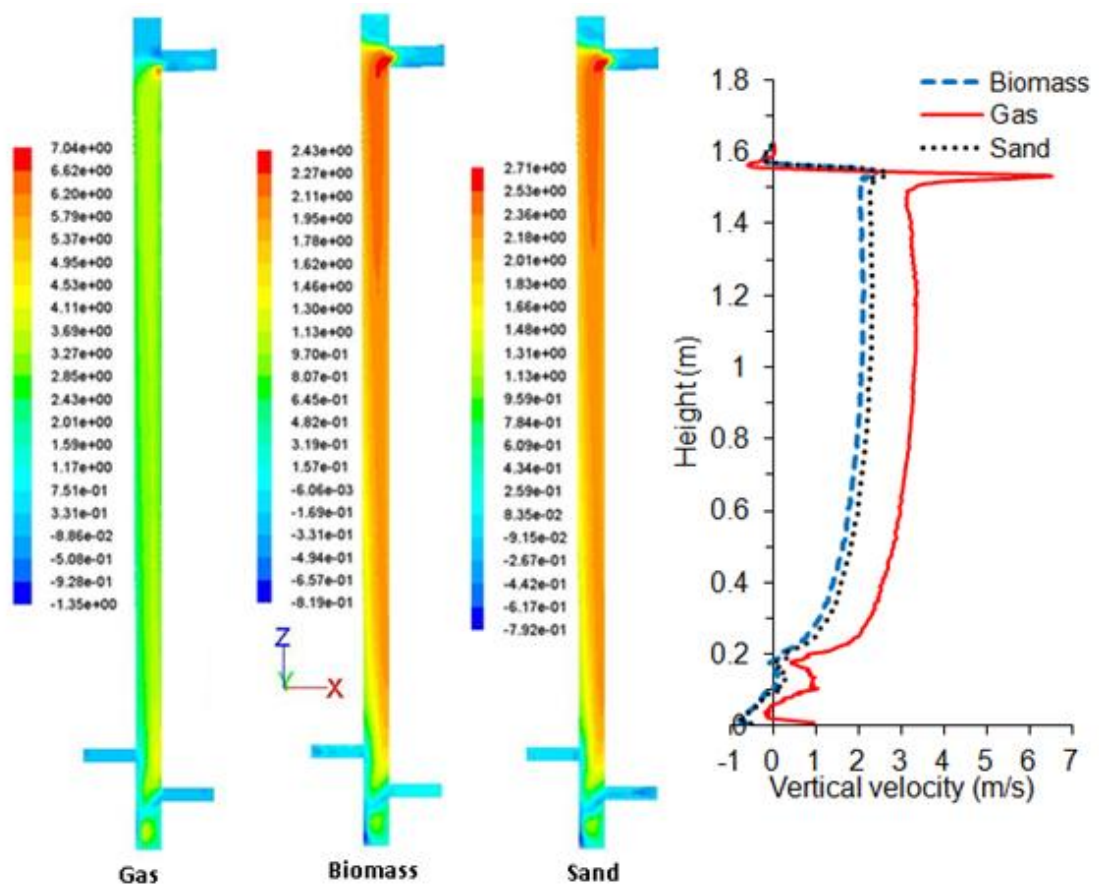


Fig. 5.7. Vertical velocity of gas, biomass and sand in the CFB riser. Detailed operating conditions are given in Table 5.17.

Quantitatively, the calculated overall biomass volume average vertical velocity is 1.47m/s, this corresponds to a residence time around 1.11s and for the gas phase the volume average vertical velocity was 2.52m/s, this corresponds to a residence time

around 0.65s. The effect of the biomass residence time was discussed in the Chapter 7 after manipulating this parameter by changing the simulation operating conditions.

### **5.5.2. Temperature distribution prediction in the CFB riser**

The heat transfer and temperature distribution during the biomass gasification is very important and plays a main role on the rate of biomass conversion and final product gas quality. It is absolutely important to maintain the riser temperature within the recommended temperature range which is between 750°C and 1000°C.

Fig. 5.8 shows the temperatures of the solids and the gas phases along the riser height. The sand, which is the main source of the heat supply to the gasifier, is introduced at the temperature of 900°C. This heat is then lost to the surrounding biomass and gas phases in order to release the volatiles from the biomass and further provide the heat required deriving other endothermic reactions. The main heat transfer mechanism modelled is the heat of convection between the solids and gas phase. Solid-solid conduction is neglected due to the system being relatively dilute as shown earlier in Fig. 5.5 and the heat of radiation was not included in this stage but it was discussed in sensitivity analysis section in the following chapter (chapter 6). The cross-sectional average temperature distribution along the riser height for the various phases is shown in Fig. 5.8. The most interesting features in this figure can be summarized as follows:

- i. Phases, the sand and gas, both reach thermal equilibrium in a very short distance above the sand entrance point, after which the temperature remains constant.
- ii. Unlike the sand and gas phases, the biomass temperature increase gradually to reach the maximum temperature and attain thermal equilibrium with the other two phases at a relatively high point almost at the middle point of the riser height.

- iii. The trends of the axial temperature profiles are very similar for the three phases (sand, biomass and gas).
- iv. There is clear evidence of strong entrance effects on the heat transfer and temperature, however, the exit effects are less pronounced.

It should be noted that, while the results shown in Fig. 5.8 are for the particular base case considered here, further analysis presented in the next chapters confirms the applicability of the above described thermal behaviour and trends in temperature distribution to most of the other cases considered in this study. Additional information related to the heat of reactions is discussed in the next section.

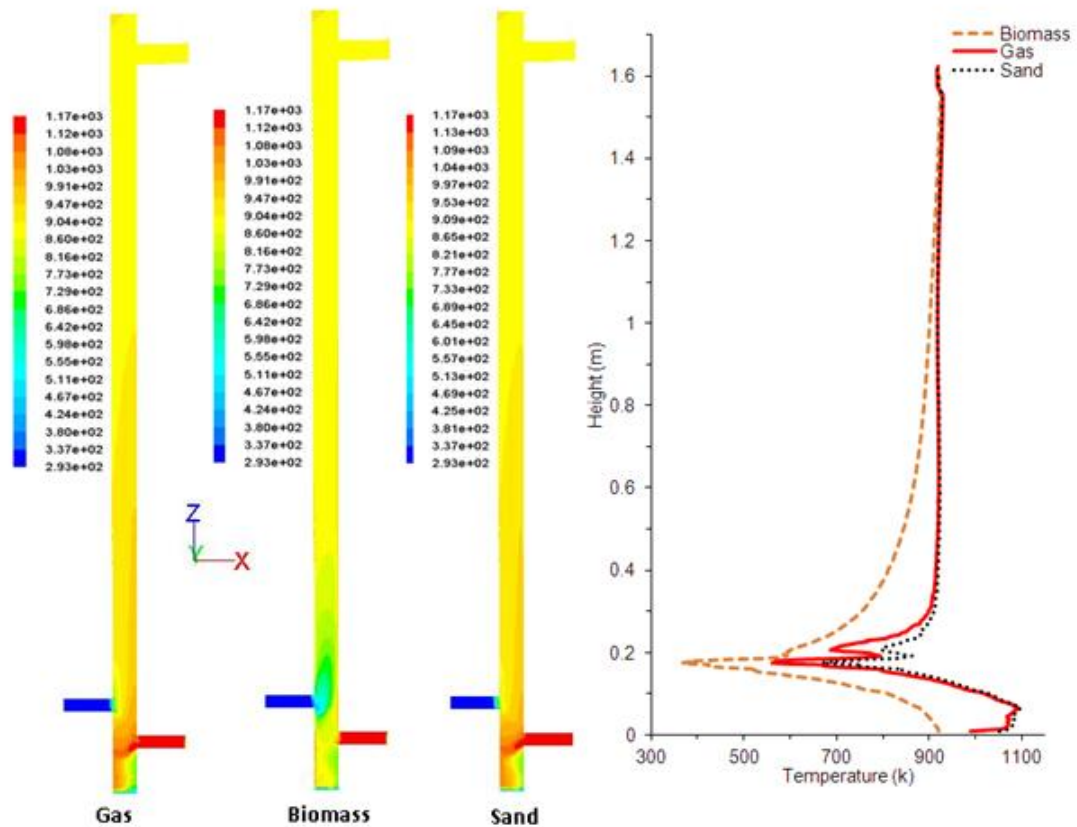


Fig. 5.8. Temperature distribution of the gas, biomass and sand phases along the CFB riser for the base case. The detailed operating conditions are given in Table 5.17.

### 5.5.3. Reactions and product gases in the CFB riser

This section presents results of the base case simulation of the gasification with the operating conditions given earlier in Table 5.17. The gasification reactions considered have been detailed earlier in Table 5.14. The results discussed in this section include the rate of reactions, heat of reactions and the contours of the product gas composition and distribution throughout the riser's height.

#### 5.5.3.1. Predicted rates of heterogeneous reactions

The rates of reactions of the heterogeneous reactions are illustrated in Fig. 5.9. As previously mentioned in Chapter 4, the number of heterogeneous reactions modelled in this study are five reactions; the boudouard reaction (R4), the water shift reaction (R1), the methanation reaction (R5), carbon combustion reaction (R3) and devolatilization reaction (R2). The main conclusions drawn from Fig. 5.9 are:

- i. The highest rate of reactions occurs at the top of the riser near the exit where the volume fractions of the biomass and sand are at their highest level (see Fig. 5.5 for solid concentration)
- ii. Compared to other reactions, the devolatilization occurs at the highest rate and takes place uniformly throughout the riser height, with the exception of the far top part, where the rate is at its highest.
- iii. The partially combustion reaction (R3) of the carbon to generate carbon monoxide comes second in the rate of reactions, this is followed by the boudouard reaction (R4), the water gas shift reaction (R1) and finally the methanation reaction (R5).

In steam gasification, it is most desirable to increase the hydrogen content in the product gas, so the most important reaction is the water gas shift reaction (R1), which generates the hydrogen from the reaction of the carbon with the steam. Unfortunately, the rate of this reaction is very low, therefore further investigation was considered, was

discussed in the Chapter 7, to identify the parameters which could enhance the hydrogen production during the biomass gasification process. It is also worth noting that another reaction, which is the methanation reaction (R5), may play a negative impact on the final hydrogen content in the product gas, as this reaction consumes the hydrogen through the reaction with carbon to produce methane. On the other hand, the reforming of the methane (R10) can limit the negative effect of the methanation reaction because the methane itself can be reacted with steam to generate hydrogen again.

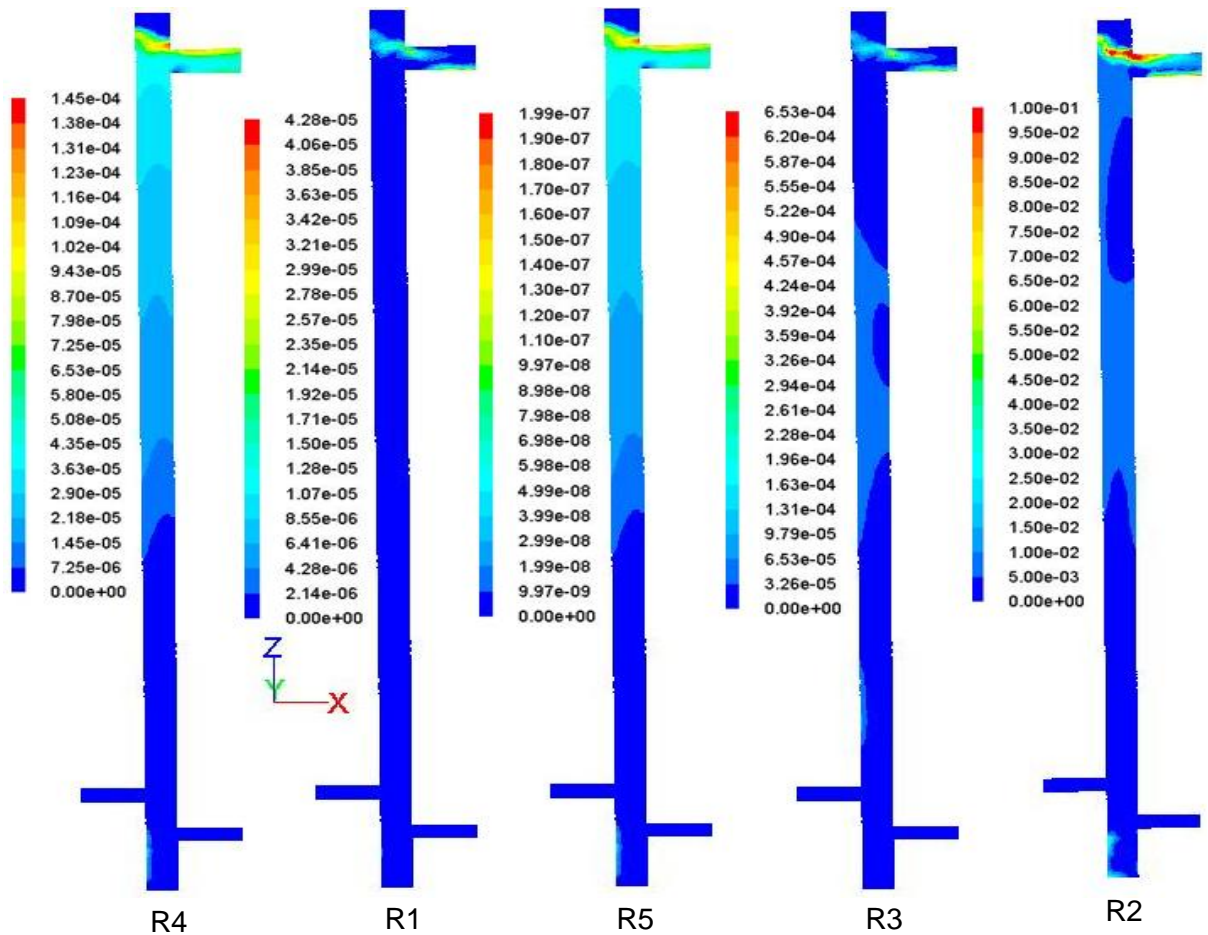


Fig. 5.9. Contours of the heterogeneous reactions rates (kmol/m<sup>3</sup>s) in the CFB riser. The detailed operating conditions are given in Table 5.17.

#### 5.5.3.2. Predicted rates of homogenous reactions

The homogeneous reactions considered in the gasification models are the combustion of carbon monoxide (R6), shift reaction of carbon monoxide with the steam (R7), the tar cracking reaction (R11) and the steam methane reforming reaction (R10). The rates of these reactions are shown in Fig. 5.10. The most important conclusions that can be drawn from Fig. 5.10 are:

- i. The highest rate of reaction is the tar cracking. It is interesting to note that this rate is very close to that of devolatilization (see Fig. 5.9).
- ii. The reactions of CO and CH<sub>4</sub> with steam (R7 and R10) both shown two distinct regions of high conversion rate at the bottom and far top of the riser, while the other two reactions (R6 and R11) appear to have only one region of enhanced conversion at the top of the riser.
- iii. The increased rate of tar cracking noticed in the bottom and far top parts of the riser is related to the increased devolatilization in these regions as shown in Fig. 5.9.

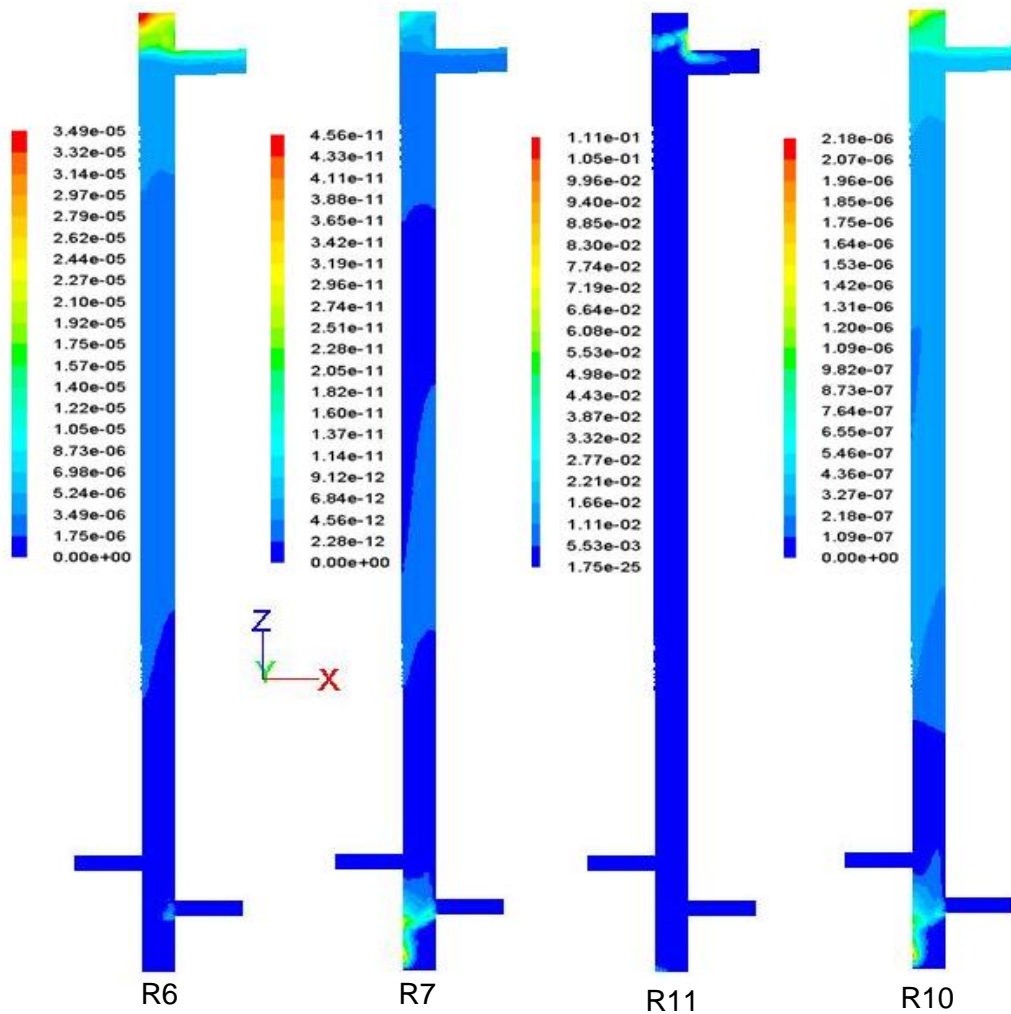


Fig. 5.10. Contours of the homogenous reactions rates (kmol/m<sup>3</sup>s) in the CFB riser. The detailed operating conditions are given in Table 5.17.

#### 5.5.4. Time series data of product gas composition

Product gas composition at the outlet of the reactor versus time is shown in fig. 5.16. It is interesting to observe the gradual increase in the various gas products, rapidly reaching steady state within the first second after introducing the biomass to the CFB riser. The mole fractions of the main gasification products H<sub>2</sub> and CO increase continuously until the simulation reaches a statistically steady state. The increase in these two gasification products goes along with a decrease in O<sub>2</sub>. The mean values at steady state for H<sub>2</sub> and CO in dry basis are 12.47% and 31.99%, respectively. The value of the CH<sub>4</sub> mole fractions is more or less constant at 11.94%. All mean values given before are averaged over the last 5s of the simulation. The time-averaged

temperature value in the outlet for the mixture gas in the outlet for the last 5s of the simulation is about 890.26 K.

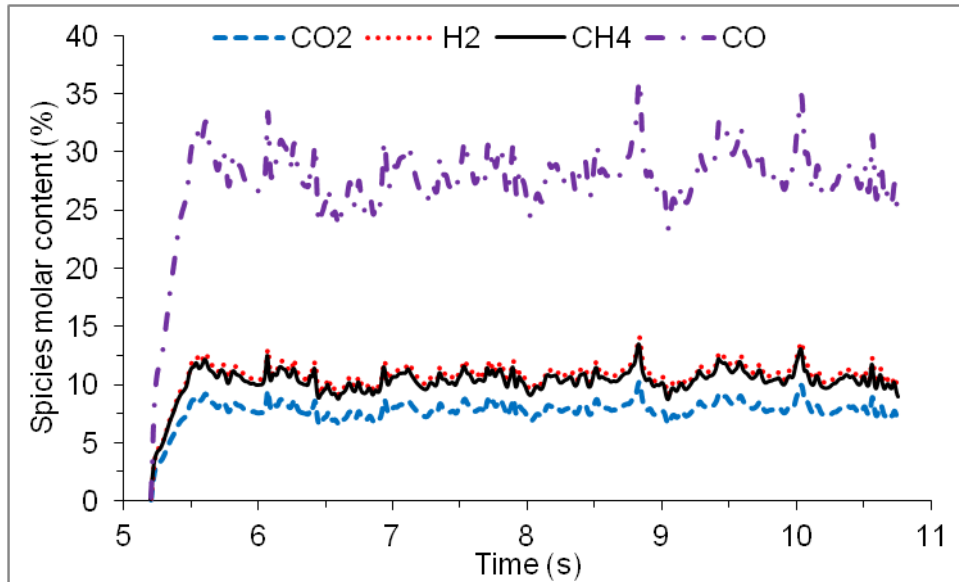


Fig. 5.11. Product gas mole fractions versus time at the outlet of the CFB riser. The detailed operating conditions are given in Table 5.17.

Fig. 5.16 shows the time series data of the average gas temperature. This data indicate that the reactor reaches steady state in a relatively short time within the range of 2 seconds. This indicates that there is no need for long real time simulations in order to get steady state results.

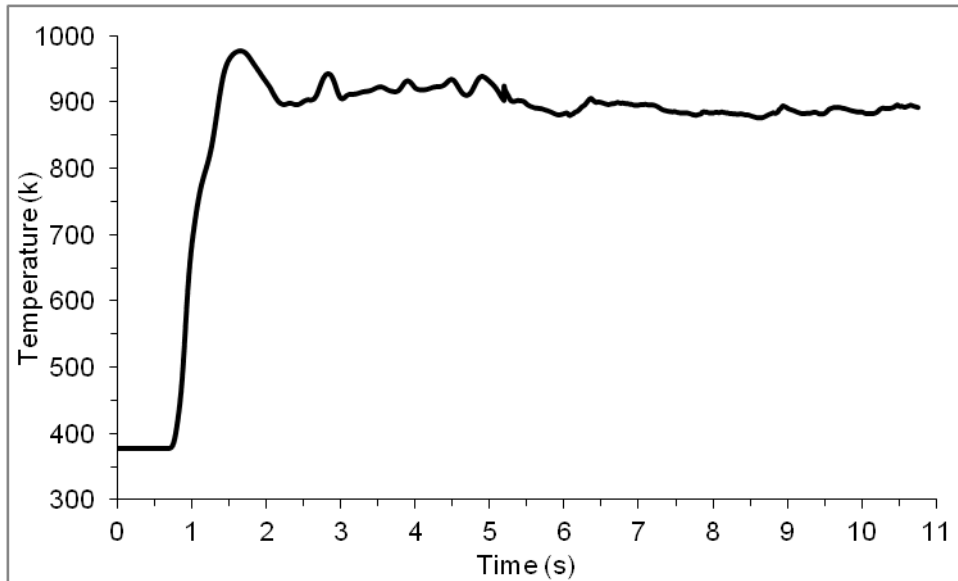


Fig. 5.12 Gas phase temperature data versus time at the outlet of the reactor.

Fig. 5.18 summarizes steady state molar content of concentrations of some components in the product gas for the base case in the dry basis.

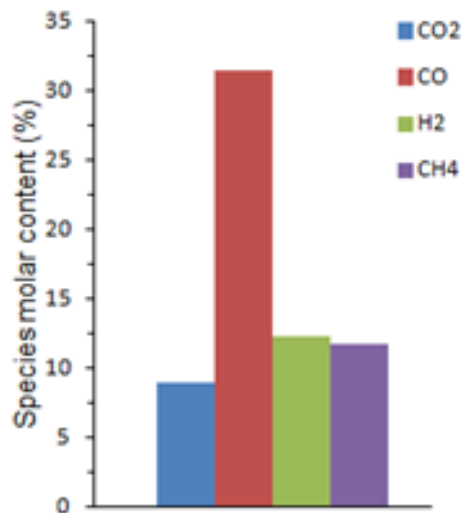


Fig. 5.13. Concentrations of some components in the product gas for the base case in dry basis.

## 5.6. Conclusions

In this chapter, a base case gasification simulation has been conducted and the results have been analysed to gain basic understanding of the hydrodynamics, temperature

distribution and product gas composition and quality. This was first preceded by review of the relevant literature to identify the state of art and knowledge gaps in modelling and simulation of such process. The literature indicated that there is scarcity in CFD biomass gasification models, especially for 3D CFBs with the reactions derived by circulating solid phase heat carrier. Moreover, there is no reported attempts and analysis of performance of a relatively short CFB gasifiers such as the one considered in this study.

The various homogenous and heterogeneous reactions considered in the base case have been introduced and incorporated in the simulation model. The base case model operating conditions were set based on a simple mass and energy balance.

The outcome of this chapter confirmed the feasibility and applicability of the proposed model for biomass gasification in a CFB. This was particularly important given that the reactor used in the simulation study was relatively short in height. The results included the product gas composition, riser temperature, the multiphase flow velocities/distribution, residence time and tar content. While no comparison with literature is considered in this chapter, these results all appeared to be reasonable, thus setting the scene for further parametric analysis and validation as will be discussed in the next chapters. Finally, the results on time series data on the product gas composition and temperature indicate that a simulation time within the range of 2 seconds is sufficiently enough to achieve steady state thermochemical conversion in a reactive CFB riser system.

## **6. Chapter 6: Model sensitivity analysis and comparisons**

### **6.1. Literature review**

#### **6.1.1. Studies on comparison of gasification models**

First, it must be noted that studies on pure pyrolytic biomass gasification (i.e. steam-only gasification) in CFB, either experimental or theoretical, are rare in the open literature. Air biomass gasification has received more attention and therefore more frequently reported in the literature. However, effort has been made to identify the most relevant published papers and make use of the results to compare with our general simulations trends and findings. In doing this, the fact that most of the literature investigations are either using a different reactor type, geometry or biomass material were taken into consideration. The papers reviewed and subsequently used for comparison with the model predictions are those of Bingyan et al. (1994), Li et al. (2004), Gerber et al. (2010), Miao et al. (2013) and Ngo et al. (2011). With the exception of the last paper of Ngo et al. (2011), which is on biomass steam gasification, all the other papers are on biomass air gasification as discussed in more details below.

Bingyan et al. (1994) carried out experiments in a CFB riser gasifier with 0.41 m diameter and 4 m height using wood powder (flow rate 250 kg/h) and air as the gasifying agent. Eight experiments were carried out in this study using different air to fuel ratio within the range of 0.171 and 0.283. The authors reported inconsistent and uncorrelated trends in terms of the product gases CO and CO<sub>2</sub> and the heating value with the increase in the equivalent ratio (ER). The ranges of the product gas composition were 13.1% to 20.4 % for CO<sub>2</sub>, 12.2% to 17.8% for CO and the heating value was between 6.9 to 7.4 MJ/m<sup>3</sup>. However, it was also reported that values of CH<sub>4</sub> decreased (from 5.34% to 9.43%) while the H<sub>2</sub> increased (from 5.34% to 16.57%) with the increase in ER. The temperature was also observed to increase from 630 °C to 1042 °C by increasing ER. The authors concluded their study by recommending the

ER between 0.2 to 0.28 and the reaction temperature between 800 to 1000°C in order to get higher performance efficiency. The authors added these recommended parameters will favour the fast pyrolysis and reduction, shift and secondary reactions.

Gerber et al. (2010) carried out theoretical and experimental on wood gasification in a bubbling fluidized bed reactor using char as a bed material and air as a gasifying agent. The model used was using Eulerian- Eulerian modelling approach. The air was assumed to enter the reactor with 0.25 m/s velocity and 673 k (400 °C) temperature. The authors used heating bands to heat the reactor from the outside with 24 m length and 3.6 kw heating power. They used nitrogen in the beginning of their experiments to heat up the system. The authors reported the temperature during the experiments to be in a range between 900 to around 1100 k (627-827 °C) between the top and the bottom of the reactor. The experimental data ranges used for comparison were as follow; 3-21% CO, 13-17% CO<sub>2</sub>, 7-11% H<sub>2</sub>, and 2-6% CH<sub>4</sub>. The authors considered a number of parametric analysis as given in the literature summary in Table 6.2. One of the interesting analyses they carried out was on applying different secondary pyrolysis model. The authors reported that the type of the secondary pyrolysis models used had significant effect on the product gases and that the amount of H<sub>2</sub>, may change considerably depending on the type of the secondary pyrolysis model used, as shown in Fig. 6.1.



Fig. 6.1. Product gas composition and tar content for two different secondary pyrolysis models used. (Gerber et al., 2010).

Miao et al. (2013) modelled biomass gasification in a CFB and validated their model using experimental data from Wu et al. (2009). In the experiment, the biomass used was rice husk and the gasifier dimensions were 1.4 m diameter and 1.2 m height for the bottom section and 2 m diameter and 8 m height for the top section. The biomass feed rate was 1435 kg/h and the gasifying agent was air at 20°C temperature and 0.26 equivalence ratio. The data extracted from Wu et al. (2009) for the product gas compared reasonably well with the predicted values is as shown in Table 6.1. Based on the axial profiles of the product gases as shown in Fig. 6.2, the authors reported that in the dense region (boundary shown as dashed line) the main reaction is dominated by combustion because the concentration of the oxygen is in its highest level. So, the temperature is high in these region then decreases towards the top especially in the dilute region because of the gas phase reactions which are mostly endothermic. The authors noted that most of the gases were created in the dense zone. The later observation is particularly important since it confirms that in a relatively short reactor, such as the one used in this study can be used for successful thermal conversion.

Table 6.1 Comparison of prediction and experimental product gas composition (Miao et al., 2013).



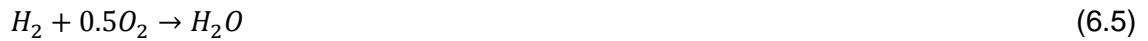
Fig. 6.2. Gas species and bed temperature along the CFB height (Miao et al., 2013).

### 6.1.2. Options on modeling the combustion reactions

In biomass gasification, the main combustion reactions involve C, H<sub>2</sub>, CO and CH<sub>4</sub>.

These are given by:





The importance of each of these reactions depends on number factors, mainly the concentrations, rate of reactions and availability of oxygen. In this study pure steam, pure air or steam-air mixture is used as the gasifying agent. In most of the simulation considered in this study, the air is introduced as a secondary agent through the feeding points for biomass and inert solid (sand). The purpose of this is to ensure sufficient drag force to push the particles into the riser section. Because some simulations considered in this study are with pure air or with a considerable fraction of air in steam mixture, literature have been reviewed to identify the most important combustion reactions required in the gasification model

Recently, Huynh and Kong (2013) carried out experimental study on biomass gasification in a BFB using oxygen-enriched air and steam. The authors reported that the combustion of the carbon is the fastest reaction in char gasification to produce CO and CO<sub>2</sub>; there was no mention of any other combustion reactions such as H<sub>2</sub> and CH<sub>4</sub> combustions. Lv et al. (2003) and Lv et al. (2004) reported experimental study on biomass gasification in a bubbling fluidized bed gasifier using pine wood saw dust as feedstock and air-steam as gasifying agents. It was reported that carbon combustion reactions result in the formation of CO<sub>2</sub> and CO, however, the combustion reaction favours the formation of CO due to the lack of sufficient oxygen. Similarly, the authors did not report or discuss other combustion reactions.

Other studies, such as the ones by Nikoo and Mahinpey (2008), Li et al. (2004), Ardila et al. (2012) and Doherty et al. (2009) all assumed dominant carbon combustion

reactions and ignored the other possible combustion reactions. This is despite the fact that most of these studies were conducted using air as the main fluidizing agent. Generally, combustion reactions are theoretically more complex and may involve various homogenous and heterogeneous reactions.

### **6.1.3. Studies on modeling the heat of radiation**

It is widely believed that heat of radiation in general becomes important only at high temperature  $>1000$  °C. Most of the reported studies on biomass gasification ignores the heat of radiation, assuming that it is negligible within the normal gasifier operating condition (usually  $<1000$  °C). However, in reality, localised instantaneous temperatures may well reach above this temperature, thus, heat of radiation becomes effective. This hypothesis is true when considering highly sensitive reaction rates such as carbon combustion reaction and tar decomposition during gasification. It is therefore of interest to investigate the various options to incorporate heat of radiation within a gasification model and then see how this affect the temperature distribution in the reactor and the final product gas composition.

Radiation models have been frequently reported in the literature for many high temperature operation processes such as combustions. This literature is particularly focused on the radiation models used in the simulation of gasification in CFBs reactors. Miao et al. (2013) reported a study on biomass gasification in a CFB. It was concluded that the inclusion of heat of radiation in the simulation model has negligible effect on the predicted gasifier temperature. In a simulation study of coal gasification, Jennen et al. (1999) reported the term used for the heat of radiation in the heat transfer equation without discussing the effect of such term on the model predictions.

A CFD model of a pressurised CFB gasifier using coal as feedstock was reported by Gräbner et al. (2007). The authors used the commercial code Fluent (Ver 6.2) with the

incorporation of radiative term. This term was applied in the model using P-1 radiation model, a Fluent built-in radiation model, which has been discussed in Chapter 4. Fig. 6.3 below shows the temperature and absorption coefficients of solids and gases reported by Gräbner et al. (2007). The authors noticed that the range of the absorption coefficient of particles is much higher than that of the gas. The model formulations assumed the gas radiation absorption coefficient to be only effective for the CO<sub>2</sub> and H<sub>2</sub>O by employing the WSGG-model, which only includes the CO<sub>2</sub> and H<sub>2</sub>O as radiation relevant species. No experimental validation was given for this model prediction.



Fig. 6.3. Temperature, absorption coefficients of gas and particles distribution estimated in a CFB coal gasifier (Gräbner et al., 2007).

Dupont et al. (2007) carried out a study on the kinetics of biomass steam gasification in a fluidized bed. The authors reported that the radiation effect in the overall heat transfer is negligible because the particle size used was relatively small, around 50 $\mu$ m. Under this condition the radiation is much less than the convection, however the radiation may be significant for larger particles. In another study, Gao et al. (2012) used the P-1 radiation model in Fluent code to simulate the gasification of sawdust in

an air cyclone gasifier. The particle phase was simulated using the Lagrangian approach. The influence of heat loss and radiation of the wall on the gas temperature have been found to be negligible in the low-temperature regions of the reactor. Fig.5.21 shows the temperatures in different points in the reactor. A number of other studies on gasification of coal and coke, such as the ones by Deng et al. (2008) and Tang et al. (2010), have reported using the P-1 radiation model; however most of these studies did not discuss the or validate the effect of radiation on the model predictions.



Fig. 6.4. Comparison of predicted and measured axial temperature of the gasifier ((Gao et al., 2012).

#### **6.1.4. Conclusion of the literature review**

The literature reviewed indicated that the combustion reactions are very important in modelling gasification of solid fuels; however there is little effort on systematic analysis or discussions on the importance or the model sensitivity towards the various reaction options. There is no clear agreement on what combustion reactions to include in the

gasification model, especially when the gasifying agent is steam/air mixture. Therefore, this study is looking at possibility of eliminating some of the combustion reactions in order to reduce computational time without jeopardizing the model validity.

Radiation models in the simulation of biomass gasification are rare due to the general belief that the heat of radiation only becomes important at high temperature well above  $>1000$  °C. Nevertheless, review of the literature indicate that some studies have been reported to include radiation term in the simulation model, but with the exception of Gräbner et al.(2007), none of these studies looked at the detailed effect of the radiation on the overall gasifier performance. In this study, comparative analysis is presented to study the effect of the heat of radiation on the reactor temperature and product gas quality.

## **6.2. Results of the model sensitivity analysis**

The model sensitivity towards the various options of combustion reactions, heat of radiation and type of devolatilization models used in the simulation has been carried out to compare the results obtained with the various options and to see the effect of these options on the product gas quality and the overall reactor performance. The geometry used was mentioned in Fig. 5.3.

### **6.2.1. Effect of combustion reactions**

The various combustion reactions reported in the literature were discussed in section 6.1.2. It is clear that the most commonly used combustion reactions are of C and CO, and the less common ones are of H<sub>2</sub> and CH<sub>4</sub>. In order to investigate the model sensitivity, Fig. 6.5 and Fig. 6.6 show the results of two simulations carried out with the inclusion of all four combustion reactions compared to the results of simulation without the inclusion of H<sub>2</sub> and CH<sub>4</sub> Combustions. The first condition is referred to by “full” and the second condition is referred to by “CO” and “C”. The operating conditions used for

the simulations results shown in Fig. 6.5 are given in Table 6.2. The air ratio in this case was 0.1 and the air/steam ratio was 0.6. According to this result, it is clear that the inclusion of H<sub>2</sub> and CH<sub>4</sub> combustion in the gasification model has a negligible effect on the overall gasifier performance, except for the tar yield.

Table 6.2 Operating conditions for the results shown in Fig. 6.5.

Biomass size (µm)	500
Sand size (µm)	200
Wood mass flow (g/s)	2
Sand mass flow rate (g/s)	20
Wood temperature (°C)	20
Sand temperature (°C)	900
Fluidization velocity (volume weighted and time average) (m/s)	2.73
Air temperature (°C)	20
Steam temperature (°C)	153
Biomass velocity (volume weighted and time average) (m/s)	1.53
Sand velocity (volume weighted and time average) (m/s)	1.73

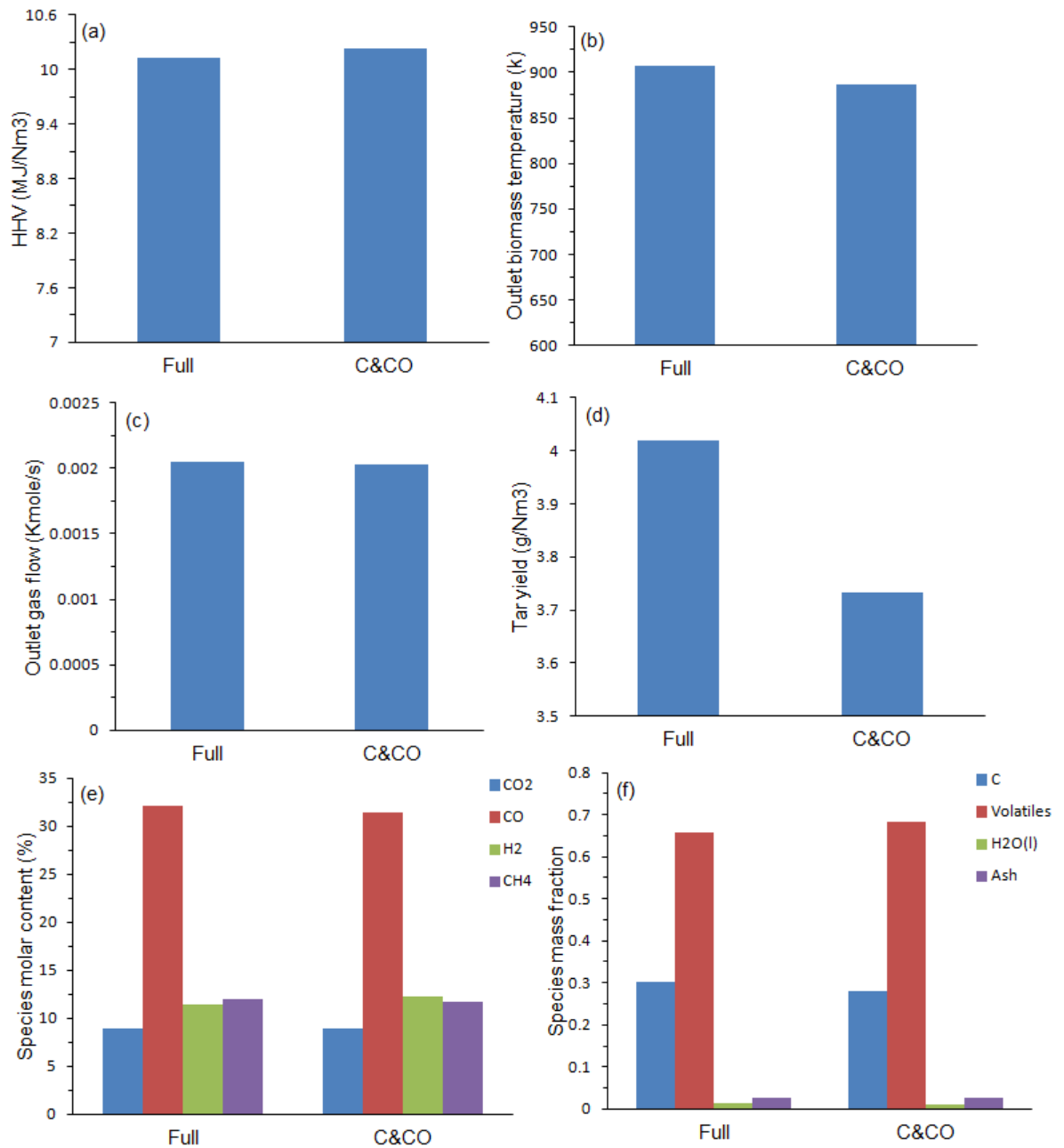


Fig. 6.5 . Comparison between the model predictions for the case of full combustion reactions (C, CO, H<sub>2</sub> and CH<sub>4</sub>) and the case of CO and C combustions only (ignoring H<sub>2</sub> and CH<sub>4</sub> combustion) using steam/air as fluidizing agent (a) HHV of the product gas in (b) outlet temperature of char (c) outlet gas flow (d) tar yield (e) gas species molar concentrations (f) species mass fractions in the outlet. The operating conditions used in the simulation are given in Table 6.2.

The simulation results when using pure air as a gasifying agent are shown in Fig. 6.6. The operating conditions for this case are given in Table 6.3. In this case, it is shown that there are significant differences between the two cases of full combustion and C and CO combustions only, especially in the HHV and tar yield. The tar yield decreased

when using full combustion reactions due to the increase in the gas temperature as shown in Fig. 6.6-b. It is also interesting to note the great sensitivity of tar yield with respect to temperature. The molar concentrations of the gases in the outlet are almost the same, except for H<sub>2</sub> gas, which is found to be lower in this case. This is expected, since some of the H<sub>2</sub> gas formed will be consumed by the excess O<sub>2</sub> gas available in the gasifying air. These results also emphasize on the importance of considering full range of combustion reactions (C, CO, H<sub>2</sub> and CH<sub>4</sub>) when excess air is used in the gasifier. However, for the case of steam/air gasification with low air to biomass ratio, the effects of H<sub>2</sub> and CH<sub>4</sub> combustion are negligible, and therefore, could be eliminated from the reaction mode to reduce computational time.

Table 6.3 operating conditions for the simulation results shown in Fig. 6.6. the velocities of gas sand and biomass were calculated using volume weighted and time average.

Operating condition	Full combustion reactions	C& CO combustion reactions
Initial air temperature (°C)	20	20
Initial sand temperature (°C)	900	900
Initial biomass temperature (°C)	20	20
Gas velocity (m/s)	3.09	3.04
Sand velocity(m/s)	1.76	1.71
Biomass velocity(m/s)	1.60	1.55
Gas residence time (s)	0.53	0.54
Sand residence time (s)	0.93	0.95
Biomass residence time (s)	1.02	1.05

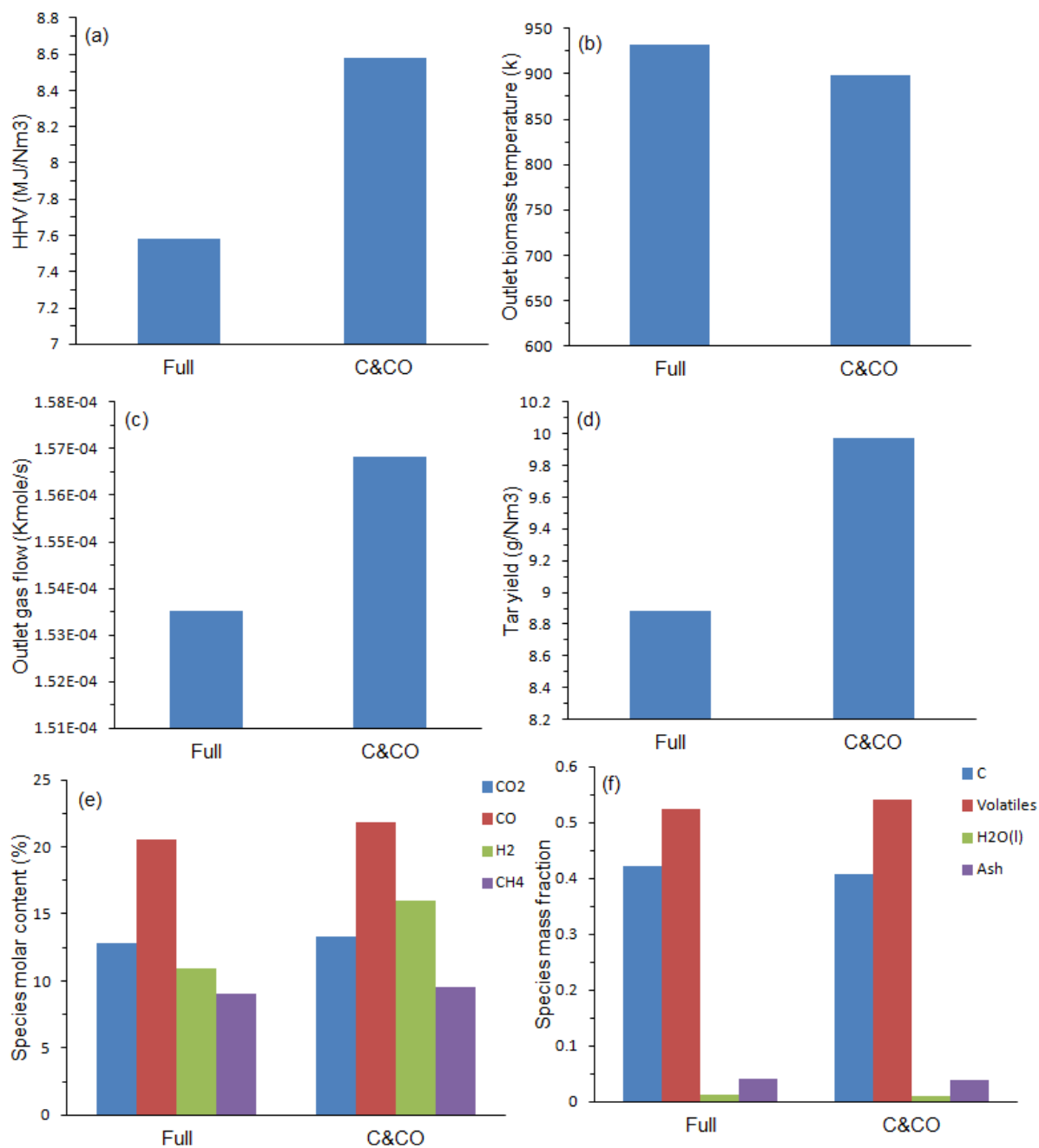


Fig. 6.6 . Comparison between the model predictions for the case of full combustion reactions (CO, CO<sub>2</sub>, H<sub>2</sub> and CH<sub>4</sub>) and the case of CO and H<sub>2</sub> combustions only using pure air as fluidizing agent. (a) The HHV of the product gas in (MJ/Nm<sup>3</sup>). (b) The outlet temperature of biomass (K). (c) Tar yield (g/Nm<sup>3</sup>) (e) Gas species molar concentrations. (f) Char species mass fractions in the outlet. The operating conditions used in the simulation are given in Table 6.4

### 6.2.2. Effect of radiation on the model predictions

The literature review shows that the effect of the radiation in biomass gasification has not received enough attention in the past. In this part of the study, the P-1 radiation model (available as an option in Fluent Ver. 12.1) has been employed in the heat transfer model to investigate the effect of the radiation from the hot solids to the gas phase on the overall gasifier performance. For details on the P-1 model formulation please refer to Chapter 4. Fig. 6.7 shows the temperature of the solid and gas phases, with and without taking into account the radiation effect in the model. The operating conditions used in these simulations are shown in Table 6.4. Fig. 6.7 (a, b and c) show that there is differences in the temperature (max of ~100 °C) in the bottom region of the riser, especially below 0.2 m height. This is the region where the solid concentration is high, and therefore, it appears that the radiation effect becomes important with the solid concentration. In fact, the absorption coefficient shown as contours in Fig 6.16-d confirms high radiation activities in this region. Effect of inclusion of the radiation term on the predicted gas quality and composition is shown in Fig. 6.8. The main effect was observed in the outlet gas temperature, tar yield and HHV. However, in quantified percentage difference the effect of radiation is clearly negligible.

Table 6.4 Operating conditions

Biomass size ( $\mu\text{m}$ )	500
Sand size ( $\mu\text{m}$ )	200
Wood mass flow (g/s)	5
Sand mass flow rate (g/s)	40
Wood temperature ( $^{\circ}\text{C}$ )	20
Sand temperature ( $^{\circ}\text{C}$ )	900
Fluidization velocity (volume weighted and time average) (m/s)	3.48
Air temperature ( $^{\circ}\text{C}$ )	20
Steam temperature ( $^{\circ}\text{C}$ )	153
Biomass velocity(volume weighted and time average) (m/s)	1.90
Sand velocity (volume weighted and time average) (m/s)	2.11

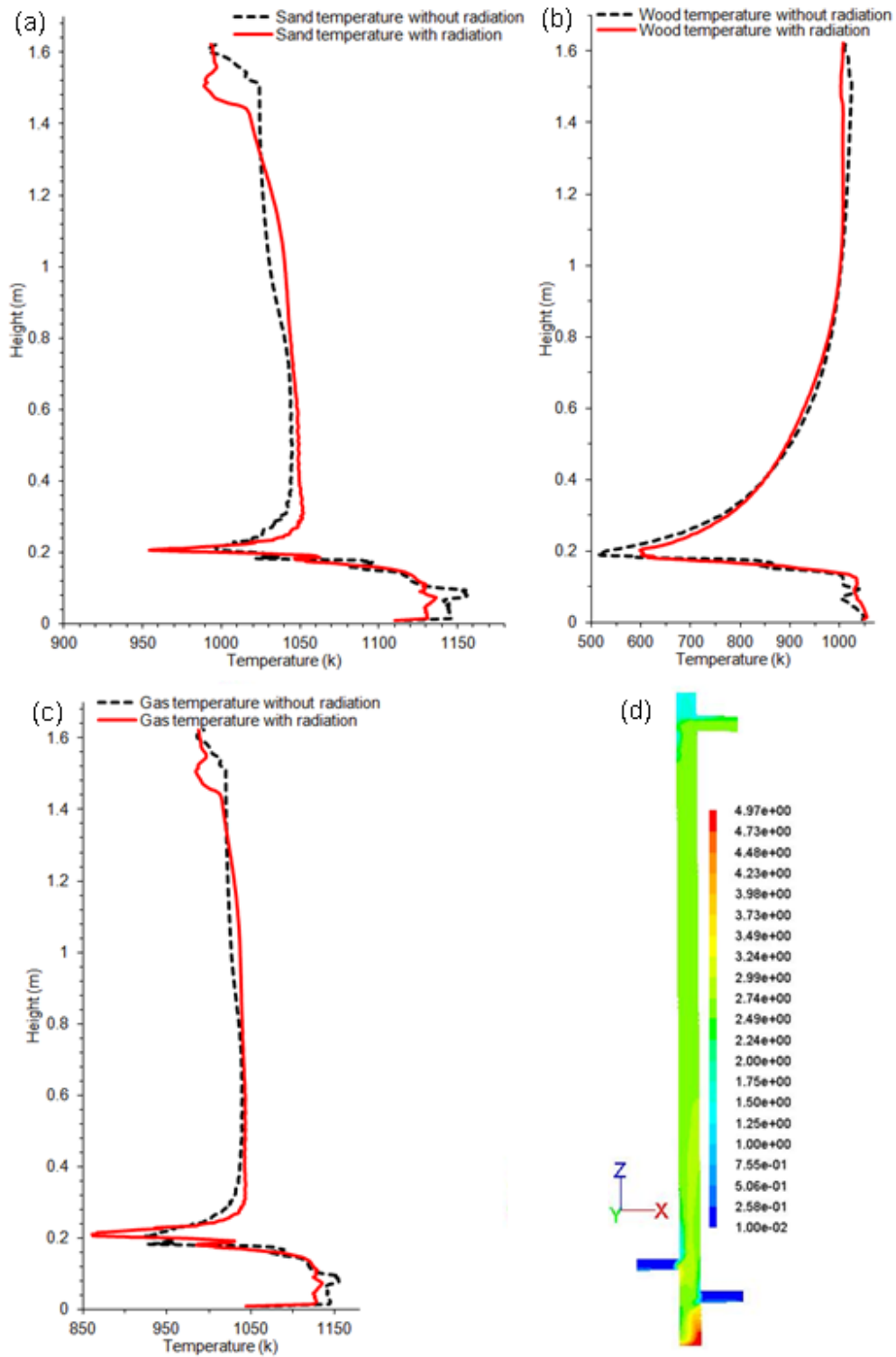


Fig. 6.7. Simulation results with and without inclusion of radiation term in the model (a) sand temperature (b) wood temperature (c) gas temperature (d) absorption coefficient contours (1/m)

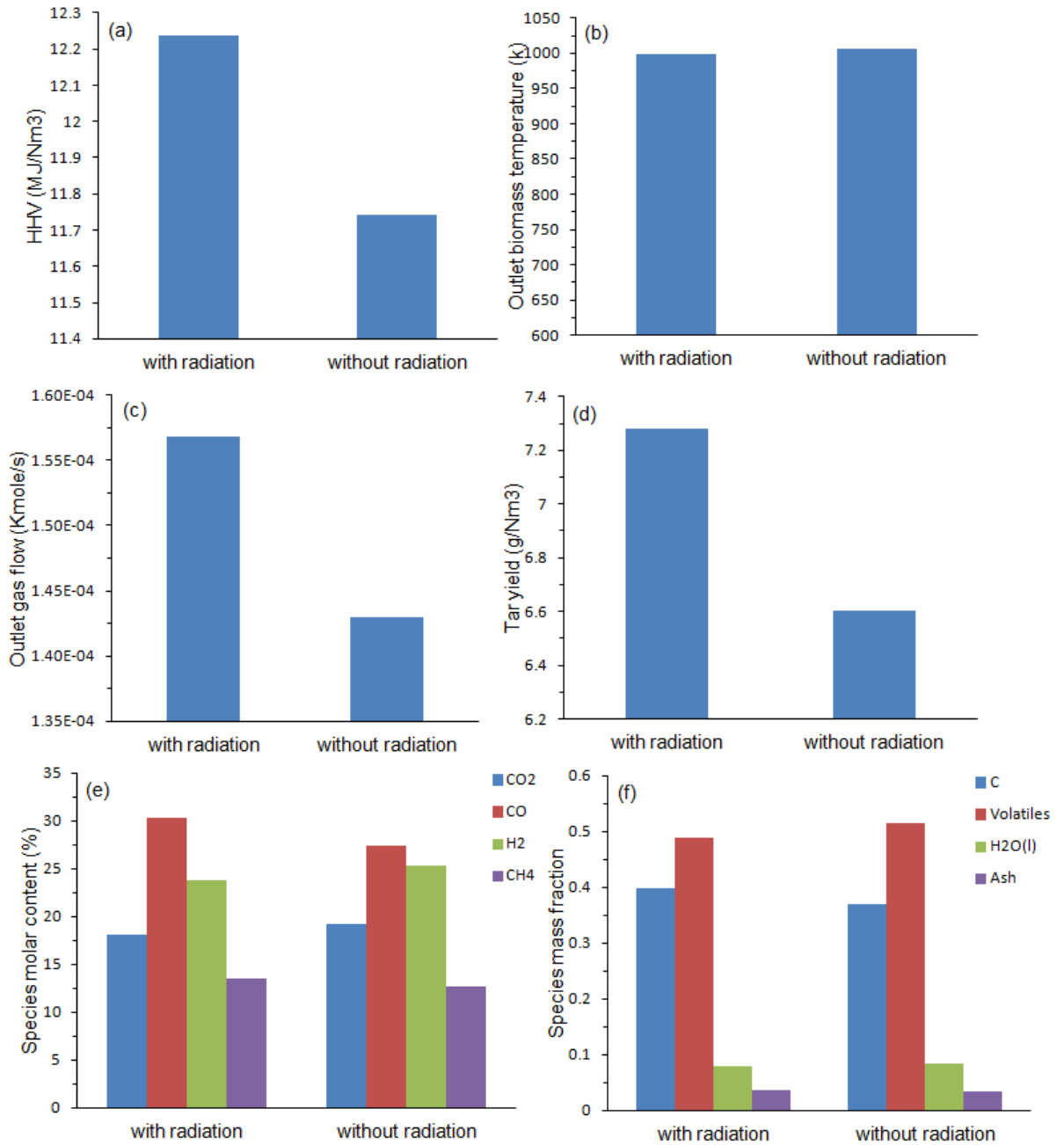


Fig. 6.8 . Comparison between the model predictions for the cases with and without taken consideration of radiation through PI radiation model (a) The HHV of the product gas in (MJ/Nm<sup>3</sup>). (b) The outlet temperature of biomass (the char) (K). (c) Tar yield (g/Nm<sup>3</sup>) (e) Gas species molar concentrations. (f) Char species mass fractions in the outlet.

### 6.3. Interim conclusion on the sensitivity analysis

Based on the above sensitivity analysis it has been concluded that:

- i. The full combustion reactions described in section 6.2.1 should be included in the model in order to correctly predict the product gas quality and overall

gasifier performance in highly oxidative environment. However, in steam gasification, with relatively low percentage of air or O<sub>2</sub> in the gasifier, it is safe to ignore the combustion of CO and CH<sub>4</sub> from the model formulations without losing accuracy, and with the added advantage of considerably reduced computational time.

- ii. Within the range of conditions considered in this study, it is safe to conclude that the effect of radiation on the gasification is negligible, and therefore could be eliminated from the model. However, if considering higher operating temperature or higher solid throughput (concentration), then it is recommended to include the radiation term in the simulation model.

The above conclusions have been taken into consideration in the model used in the comparisons section and also in the parametric analysis shown in Chapter 7.

#### **6.4. Results of model comparisons**

Most of the simulations carried out in this study using steam as gasifying agent and air as secondary agent. Few simulations were carried out using pure steam and pure air. For the model comparison, the results have been compared with the data obtained from the literature.

Simulation of pure air gasification was carried out using the operating conditions shown in Table 7.8 in pure air results section. For these operating conditions, the product gases in the outlet in dry basis consist of 20.58% CO, 10.91% H<sub>2</sub>, 9.02% CH<sub>4</sub>, 12.84% CO<sub>2</sub>, 37.17% N<sub>2</sub> and heating value of 7.58 MJ/Nm<sup>3</sup>. Despite the recognized differences in the reactor geometry and the solid fuel used, this data has been found to be in a very good agreement with the ranges of the data provided by Bingyan et al. (1994) (experiments in wood gasification using CFB), Li et al. (2004) (experiments and model in saw dust gasification using CFB), Gerber et al. (2010) (model validated using

experimental data for wood gasification in BFB. A graphical comparison with the data produced by the authors mentioned above is shown in Fig. 6.9.

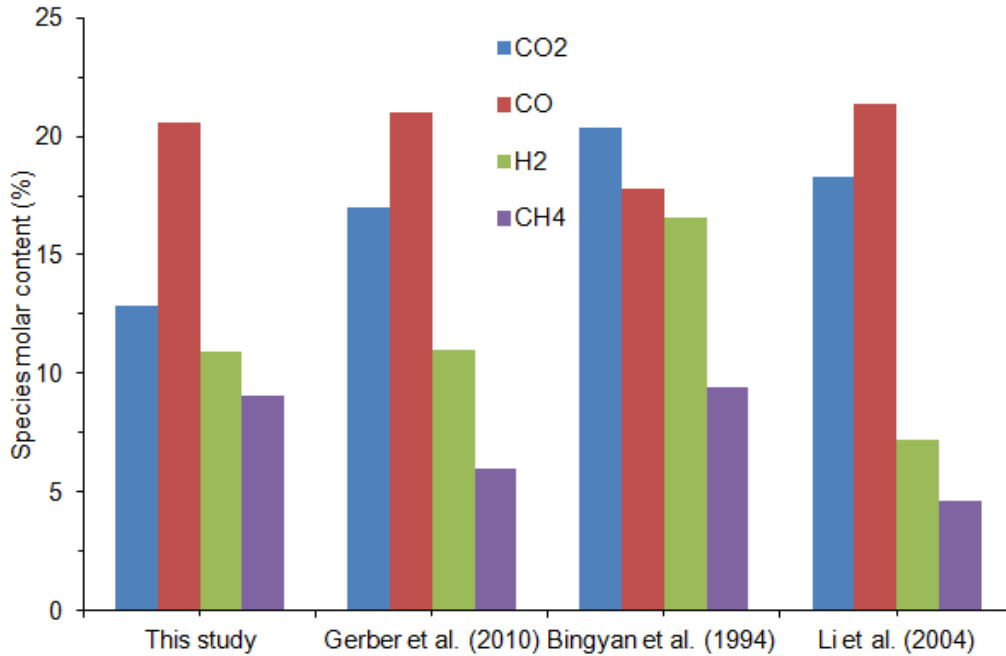


Fig. 6.9. Comparisons between the results of this study and studies by Gerber et al. (2010), Bingyan et al. (1994) and Li et al. (2004) using pure air as a fluidizing agent.

Simulations of pure steam gasification were carried out in this study using gasification average temperature in a range between 680-880°C and steam to biomass ratio of 0.28. The operating conditions and the results of this simulation are shown in Table 7.9 for 900°C sand. The ranges of product gases was as follow; CO<sub>2</sub> 17.96%-25.59%, CO 24.39%-35.6%, H<sub>2</sub> 26.81-30.00% and CH<sub>4</sub> 14.39%- 14.68%. These results also show good agreement with the experiments results of Ngo et al. (2011) as shown in Fig. 6.11. Ngo et al. (2011) carried out his experiments for wood gasification in a dual fluidized bed gasifier with steam to biomass ratio of 0.3 and temperature range of 700°C to 900°C.

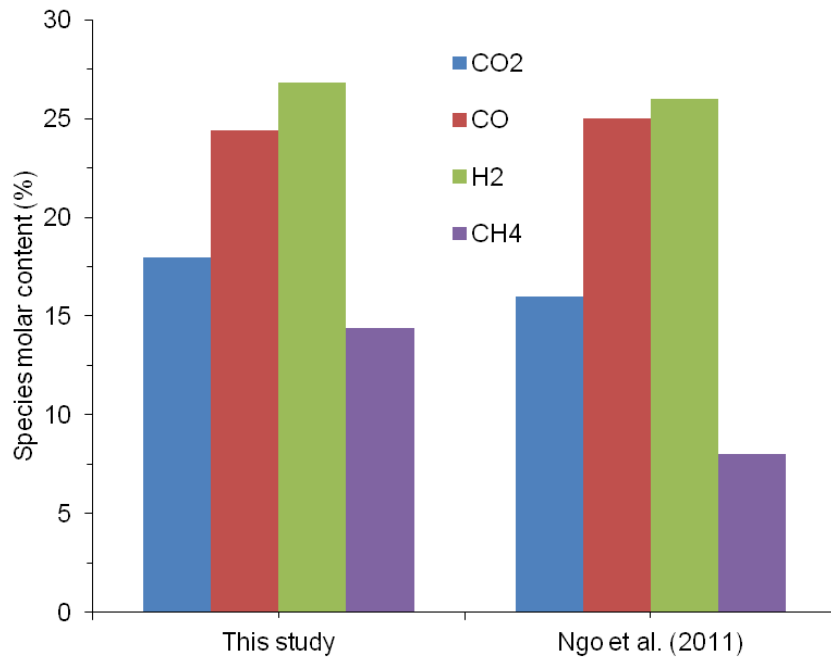


Fig. 6.10. Comparison of the model prediction of product gas composition for the case of pure steam gasification. The external data was obtained from (Ngo et al., 2011).

## 6.5. Conclusion

In this chapter the gasification model developed and presented in Chapter 4 has been further refined with respect to its sensitivity to various combustion reactions and inclusion of thermal radiation in the model formulation. An interim conclusion regarding sensitivity analysis was reported in section 6.3. The model was then validated using different experimental data from the literature. Good agreement was observed with a number of reported experimental and simulation data on wood gasification found in the open literature. This comparison provided confidence on the accuracy of the developed model and allowed for further parametric analysis of the CFB gasifier as discussed in Chapter 7.

## **7. Chapter 7: Parametric analysis of the gasifier model**

### **7.1. Introduction:**

This chapter presents results obtained from investigation on the effect of operational parameters on the gasifier performance in general and in the product gas quality in particular. The geometry used was presented in Fig. 5.3. The parameters investigated are:

- i. air ratio
- ii. biomass feed rate
- iii. heat carrier temperature and flow rate
- iv. biomass and heat carrier particle size
- v. steam to biomass ratio

This chapter also includes a review of the relevant literature.

### **7.2. Literature review**

In this literature review, the reported studies on parametric analysis of biomass gasification models for fluidized beds, with particular focus on CFB gasifiers has been covered. Summary of these studies is given in Table 7.1.

#### **7.2.1.1. Choice of the gasifying agent**

##### Air as a gasifying agent

Majority of the reported literature on modelling and simulation of biomass gasification are on using air as a gasifying agent (e.g. (Li et al., 2004); (Liu and Gibbs, 2003); (Petersen and Werther, 2005a, Petersen and Werther, 2005b); (Gungor and Yildirim, 2013); (Miao et al., 2013).

Li et al. (2004) studied experimentally the effect of air equivalence ratio (ER) in the product gases. The authors reported that the concentrations of CO<sub>2</sub> and H<sub>2</sub>O expected

to increase with increasing the air ratio while the concentrations of CO, H<sub>2</sub> and CH<sub>4</sub> decrease, also added that the carbon conversion improved at higher air ratio. The O/C molar ratio was varied between 1.1 and 2.1, and as a result more oxygen was supplied and more CO<sub>2</sub> formed, as consequence, the CO/CO<sub>2</sub> ratio decreased. Li et al. (2004) reported that the H<sub>2</sub>/CO ratio increased slightly with increasing the air ratio while CH<sub>4</sub>/H<sub>2</sub> molar ratio decreased. They concluded that air-blown gasification results in H<sub>2</sub>/CO ratio less than one, also added that the injection of steam increases the H<sub>2</sub>/CO ratio because steam enhances H<sub>2</sub> production through steam gasification and CO shift reactions.

Liu and Gibbs (2003) studied, through modelling, the effect of equivalence ratio (ER) on the gas product composition, heating value, tar emission and carbon conversion. The results shown in Fig. 7.1, were obtained in a fluidized bed temperature of 1123 K (850°C). The ER was manipulated by changing the biomass flow (2-4 kg/s) with fixed air flow (2.0 Nm<sup>3</sup>/s). It is shown that the CO<sub>2</sub> concentration, the gas yield and carbon conversion all increased with increasing ER, while the HHV, H<sub>2</sub> concentration and the tar are decreased.



Fig. 7.1. Predicted effects of equivalence ratio on (a) main gas composition, (b) NO, NH<sub>3</sub> and HCN emissions, (c) gas yield and high heating value of the product gas, (d) tar emission and carbon conversion (Liu and Gibbs, 2003).

A very recent study on modelling biomass gasification using air as gasifying agent has been reported by Gungor and Yildirim (2013). The authors looked at the effect of ER on the syngas composition. The authors presented their model results along with an experimental data taken from Li et al. (2004), as shown in Fig. 7.2. It is noted that H<sub>2</sub> and CO decreased while the CO<sub>2</sub> increased when the ER increased; the authors attributed that to the oxidation of the H<sub>2</sub> and CO to H<sub>2</sub>O and CO<sub>2</sub>. They concluded that at low values of ER small amount of CH<sub>4</sub> formed and then got oxidized as more air was supplied.



Fig. 7.2. Effects of equivalence ratio on syngas composition at gasifier output (a) hydrogen composition, (b) carbon monoxide composition, (c) carbon dioxide composition, and (d) methane composition. (Model simulation results are compared with Li et al. (2004) experimental data) (Gungor and Yildirim, 2013)

#### Steam as a gasifying agent

Compared to air gasification, steam gasification in CFBs is less reported and understood. Recently, there have been growing interests in this type of gasification due to its great potential in enhancing H<sub>2</sub> production. The current focus is on the use of dual fluidized bed technology as this allows satisfying the highly endothermic steam gasification reactions. Two recently published studies on using pure steam as gasifying agent in a dual CFB have been reported by Bi and Liu (2010) and Ngo et al. (2011). Bi and Liu (2010) examined the use of high density and high solids flux in a CFB risers for steam gasification of solid fuels like coal and biomass. The authors reported that the steam gasification requires operating at high solids fluxes in order to supply sufficient heat to the endothermic gasification reactions.

Ngo et al. (2011) studied the effect of temperature and steam to biomass ratio experimentally in a reactor of 3 m height and 0.15 m diameter with external heat supplier.



Fig. 7.3. Effect of steam to fuel ratio on final gas composition obtained from modelling in comparison with experiment data taken from the literature (Ngo et al., 2011).

The authors reported that the amount of the  $H_2$  and  $CO_2$  increase with the increase of the steam to biomass ratio while the  $CH_4$  and  $CO$  decreases as shown in Fig. 7.3 . They attributed this to the gas shift reaction.

Saw et al. (2012) studied the steam gasification of mixtures of wood pellets and biosolids (dried sewage sludge) using a dual fluidised bed gasifier. The authors reported that the syngas produced from the biosolids had a higher  $H_2$  content (28%) compared with that from pure wood (23%), with the  $H_2$  content increasing with biosolids fuel loadings. It is not only the type of feedstock that influences the  $H_2$  production. In a very recent study by Kern et al. (2013) it was shown that the position

of the feed stock inlet to the gasifier has also important effect on the product gas quality.

Kaushal et al. (2011) developed a steady state one dimensional model to simulate steam gasification of biomass in a dual fluidized bed. The authors validated their model with an experimental data obtained from a commercial power plant. The authors concluded that most of the gasification reactions takes place at the bottom dense bubbling zone. It was also noted that there are three parameters that had strong influence on the heating value of the product gas and its quality and these are the mass transfer between the bubble and emulsion, moisture content in biomass, and the average temperature of the gasifier.

A study on gasification of sugar cane bagasse was modelled using Aspen by Ardila et al. (2012). The model predictions were validated using to experiments results from Gabra et al. (2001). Among many other operating parameters the authors studied the effect of steam to biomass ratio on the gasification. It was found that the highest yield of product gas was obtained with steam to biomass ratio=0.4.

Nguyen et al. (2012) developed a three stage steady state model for biomass steam gasification. The authors assumed that the remaining char and unconverted fuel from the gasifier go to a combustor and the resulting hot solids (silica sand) circulate back to the gasifier to supply the required heat. The model was validated using experimental data from Wei et al. (2007). It was reported that the product gases are mainly produced from the primary pyrolysis and only a small amount converted from the gasification of the fixed carbon. The authors reported that the gasification temperature could be raised by adding air/steam ratio, but this will decrease the heat efficiency of the product gases, due to the increase in nitrogen coming with the air.

### *Air-steam and O<sub>2</sub>-steam as a gasifying agent*

As mentioned above, most of the reported gasification studies have been mainly focused on using air as a gasifying/fluidizing agent. This section includes review of studies on using air-steam or oxygen-steam as gasifying/fluidizing agent.

Li et al. (2004) carried out experimental investigation on biomass gasification using air as the main fluidizing agent with fraction injection of steam to enhance H<sub>2</sub> production through water gas shift reactions. The authors noticed that the steam injected (the steam to biomass ratio injected was between 0 to 0.22) resulted in enhancing the product gas quality and heating value but at the same time resulted in lowering the gasifier temperature, thus, external heating was required to maintain the gasifier temperature at the required level.

#### **7.2.2. Studies on the Effect of temperature**

Li et al. (2004) carried out experiments and simulations in a CFB biomass gasifier. The CFB riser was 6.5 m height and 0.1 m diameter, air blown and using different kinds of saw dust as a feed stock. The moisture content of the feed stock was in the range of 4.2 to 22% and the operating temperature was in the range of 700 to 850 °C. The CFB was connected to a burner to heat the equipment to the desired temperature. The air enters the riser through the burner. Then the preheated air and the hot gas mixture go from the burner to the riser to preheat the bed and then if needed to maintain the suspension temperature at a desired level. The ranges of the compositions of the gas produced in dry basis were 3 - 7.2% H<sub>2</sub>, 53.9 - 68.1% N<sub>2</sub>, 6.9 - 21.4% CO, 1.2 - 4.6% CH<sub>4</sub>, 14.5 - 18.3% CO<sub>2</sub> and the heating value was 1.72 - 6.13 MJ/Nm<sup>3</sup>. The authors discussed many parameters as summarized in Table 7.1, one of these parameters is the effect of the temperature. The authors indicated that the heating value increases with increasing the bed temperature because the temperature enhances the carbon conversion and increase the product gas yield (see Fig. 7.4).



Fig. 7.4. Effect of biomass gasifier operating temperature on dry gas heating value for the equivalence ratio in a range ( $a=0.22-0.47$ ) (Li et al., 2004).

Ngo et al. (2011) used quasi-equilibrium three-stage gasification model to evaluate the performance of a dual CFB biomass steam gasifier with external heating supply. The model was validated using experimental data obtained in a CFB riser of 0.15 m internal diameter and 3 m height. The biomass used was pine woodchips and the heat carrier was sand. The authors carried out three experiments using three different temperatures (700, 800 and 900°C) with fixed steam to biomass ratio (0.3) as shown in Fig. 7.5. It was noted the concentrations of the  $\text{CO}_2$  and  $\text{H}_2$  increase while the concentrations of the  $\text{CO}$  and  $\text{CH}_4$  decreases. The authors attributed that to the gas shift reaction since this reaction consumes the  $\text{CO}$  and increase the  $\text{CO}_2$  and  $\text{H}_2$  in the presence of the steam above 700°C. It was also noted that in high temperatures the gas shift reactions will be less important and the Boudourd and  $\text{C}+\text{H}_2\text{O}$  reactions will be more important. The experiment results showed the final gas composition ranges to be about 26 – 42%  $\text{H}_2$ , 25 – 37%  $\text{CO}$ , 16 – 19%  $\text{CO}_2$  and 8 – 11%  $\text{CH}_4$ . This result was obtained with steam to fuel ratio of 0.3 kg/kg and gasification temperature in the range

of 700°C to 900°C. The highest H<sub>2</sub> obtained was obtained when operating with temperature of 900°C as shown in Fig. 7.5.



Fig. 7.5. Effect of gasification temperature on the final gas composition obtained from a model in comparison with experiment data (Ngo et al., 2011).

### **7.2.3. Studies on the effect of biomass feed rate**

The effect of biomass feed rate on the gasifier performance has been studied by Sanz and Corella (2006). The authors studied the effect of the biomass feed rate on the temperature at the bottom part the gasifier, low heat value (LHV), tar content and the carbon content in the fly ash. The authors reported that the temperature in the bottom of the gasifier increases with the increasing the biomass flow rate, thus the tar content in the product gases decreases. The authors added that this trend has a limit and if the biomass flow exceeded this limit and the other parameters remain constant then the total gas flow and the superficial gas velocity will increase. Therefore, the gas residence time drops below the minimum required to obtain high tar conversion which then leads to high tar content in the outlet.

#### 7.2.4. Studies on the effect of inert solid and biomass size

The effect of the biomass size on the gasifier performance has been studied through modelling by Gungor (2011). The authors reported that using small biomass particle sizes in gasification improves the quality of the gas but at the same time increases the plant cost, due to the need of crushing and grinding. They added that big particle sizes reduce the pre-treatment cost but increase the devolatilization time, therefore the size of the gasifier increases. So, a balance between large sizes and small sizes has to be considered. The authors studied the effect of the biomass size on H<sub>2</sub> production and compared their results with experimental data from the literature as shown in Fig. 7.6.



Fig. 7.6. Effects of biomass particle size on H<sub>2</sub> composition (Gungor 2011). Validating data from (de Souza-Santos 1989).

Table 7.1 Summary of studies on parametric analysis of biomass gasification in circulating and bubbling fluidized beds (CFB and BFB)

Model and software used	Type of reactor	Parameters Studied	Source
Software: Aspen plus	Bubbling FB	<ul style="list-style-type: none"> <li>- Effect of temperature</li> <li>- Equivalence ratio</li> <li>- Steam-to-biomass ratio</li> </ul>	Nikoo and Mahinpey, 2008
Model: one-dimension steady state mathematical model based on two-phase theory of fluidization	Bubbling FB	<ul style="list-style-type: none"> <li>- Effect of temperature</li> <li>- Equivalence ratio</li> <li>- Steam-to-biomass ratio</li> <li>- Particle size</li> <li>- bed operational velocity</li> </ul>	Gungor, 2011
Model: two-phase (bubble and emulsion), two-zone (bottom dense bed and upper freeboard), steady state Software: Author mathematical model	Bubbling FB	- The effect of temperature in tar yield and product gas	Kaushal et al., 2010
Software: Aspen plus	Circulating FB	<ul style="list-style-type: none"> <li>- Effect of temperature</li> <li>- Equivalence ratio</li> <li>- Steam injection</li> </ul>	Ardila et al., 2012

Model: two-dimension Eulerian- Eulerian Software: MFIX	Bubbling FB	<ul style="list-style-type: none"> <li>- initial bed height</li> <li>- wood feeding rate</li> <li>- thermal boundary conditions</li> <li>- pyrolysis kinetics</li> </ul>	Gerber et al., 2010)
Model: two-dimension	Circulating FB	<ul style="list-style-type: none"> <li>- Effect of temperature</li> <li>- Equivalence ratio</li> </ul>	Gungor and Yildirim, 2013
Model: one-dimension model Software: Author mathematical model	Circulating FB	<ul style="list-style-type: none"> <li>- Temperature distribution</li> <li>- concentration and distribution of species</li> <li>- composition/heating value of produced gas</li> <li>- Gasification efficiency,</li> <li>- Overall carbon conversion</li> </ul>	Miao et al., 2013
Software: Aspen plus	Circulating FB	<ul style="list-style-type: none"> <li>- Effect of temperature</li> <li>- Equivalence ratio</li> <li>- Steam injection</li> <li>- Air preheating</li> <li>- Biomass moisture content</li> </ul>	Doherty et al., 2009
Model: non-stoichiometric equilibrium model	Circulating FB	<ul style="list-style-type: none"> <li>- Effect of temperature</li> </ul>	Li et al., 2004

		<ul style="list-style-type: none"> <li>- Equivalence ratio</li> <li>- Steam injection</li> <li>- Suspension density</li> <li>- Fly ash re-injection</li> </ul>	
Model: one-dimension	Bubbling FB	<ul style="list-style-type: none"> <li>- kinetic models for pyrolysis</li> <li>- Effect of temperature</li> <li>- Equivalence ratio</li> <li>- Steam-to-biomass ratio</li> <li>- Feed location</li> </ul>	Radmanesh et al., 2006
Model: three-dimension, Eulerian–Lagrangian Software: Fluent (Ver. 6.1)	Bubbling FB	<ul style="list-style-type: none"> <li>- Effect of temperature</li> <li>- Equivalence ratio</li> </ul>	Wang and Yan, 2008
Model: pseudo-rigorous, one-dimension steady state	Circulating FB	<ul style="list-style-type: none"> <li>- Equivalence ratio</li> <li>- Percentage of secondary air</li> <li>- Biomass moisture and flow rate</li> </ul>	Sanz and Corella, 2006
Model: An equilibrium modelling approach	Bubbling FB	<ul style="list-style-type: none"> <li>- Type of biomass</li> <li>- Effect of temperature</li> <li>- Steam-to-biomass ratio</li> </ul>	Loha et al., 2011

Model: a quasi-equilibrium three-stage gasification model	Circulating FB	<ul style="list-style-type: none"> <li>- biomass type</li> <li>- Effect of temperature</li> <li>- Steam-to-biomass ratio</li> </ul>	Ngo et al., 2011
Model: one-dimensional steady state	Dual FB	<ul style="list-style-type: none"> <li>- Mixing of devolatilized gas</li> <li>- temperature of incoming bed material</li> <li>- Effect of moisture content</li> <li>- Effect of steam to biomass ratio</li> </ul>	Kaushal et al., 2011
Model: one-dimensional steady state	Dual FB	<ul style="list-style-type: none"> <li>- Effect of temperature</li> <li>- Steam-to-biomass ratio</li> </ul>	Nguyen et al., 2012

### 7.2.5. Conclusion of the literature review

The literature reviewed indicates that there are no reported studies on three-dimensional CFD simulation of biomass gasification in a CFB, especially for the case where the reaction is driven by circulating solid heat carrier. Most of the literature has found to be mainly focused on simple two-dimensional models, majority on bubbling bed reactors.

In terms of the gasifying agent, the literature was arranged in three categories classified by the gasifying agent used. The main conclusions in this regard are as follows:

i. Gasification with air

When air is used as a gasifying agent, the product gas is of low calorific value (in the range of 4-7 MJ/Nm<sup>3</sup>). This is mainly due to the fact the product gas is diluted by the nitrogen in the air. This is the main reason why alternative technology using steam with or without air/O<sub>2</sub> is now receiving increasing attention.

ii. Gasification with pure steam

Review of the literature indicated that studies on pure steam gasification are rare. However, there is general agreement that using steam as a gasifying agent requires external heat supply to maintain the reactor at the required temperature. Using mixture of steam and air or oxygen is now the area of interest in the research as an alternative solution to generate heat through partial combustion of carbon. Alternatively, some recent studies are looking at dual circulating fluidized beds; where one of the beds is used as a gasifier while the second is used as a combustor to produce the required heat

iii. Gasification with steam-air or steam-O<sub>2</sub> mixture

Using steam with air or oxygen as gasifying agent is the most suitable option in gasification as mentioned in the literature reviewed. There are many reasons to declare that; using pure air gives very low gas calorific value, and using pure steam

needs an external heat supply. So, using steam with air or oxygen is the most appropriate option since the extra heat needed for gasification when pure steam is used can be covered with the combustion reactions; and the low calorific value when pure air has been used can be avoided.

The parameters analysis literature reviewed was mainly focused on the effect of gasification temperature; biomass feed rate, equivalence ratio, biomass and inert size and steam to biomass ratio. The effect of gasification temperature widely discussed in the literature but fewer studies have discussed the effect of biomass feed rate, biomass size and inert size.

### **7.3. Results of parameters variations**

In the following sections the influence of some important parameters on the product gas composition was investigated. The base case is taken as the reference solution in order to allow comparing with other simulation where only one parameter is changed at a time.

#### **7.3.1. Variations of the air ratio**

The simulation results of the gas yield with varying the air ratio from 0.1 to 0.4 is shown in Fig. 7.7. It is shown in Fig. 7.7-b that, the higher the air ratio the higher the gas outlet temperature. The temperature increased from around 900 k to 1040 k in the outlet. This trend is expected because by keeping the sand inlet temperature and increasing the supplied oxygen (for exothermic reactions) one would expect higher temperatures as a result of combustion reactions. On the contrary, Fig. 7.7-a show that the HHV is decreasing as a result of increasing the air ratio. This is believed to occur because of two reasons: (i) the amount of Nitrogen is increased so the percentages of the other gases decreased and (ii) the amount of the CO decreased as seen in Fig. 7.7-e. As

shown earlier in Eq. 5.6, the HHV depends on the amounts of the CO, H<sub>2</sub> and CH<sub>4</sub>, so if any of these components decreased without increasing of the other effective components then the heating value will be decreased. In regard to the tar content in the product gas (shown in Fig. 6.18-d), most of the literature reviewed, indicate that the tar decreases with increasing the temperature. This is not the same case here, because increasing the fuel to air ratio appear to cause more volatiles, and hence more tar. The corresponding increase in temperature does not seem to be sufficient enough to crack the increasing tar. Further comments about this is given in section 7.3.3, when discussing the effect of temperature.

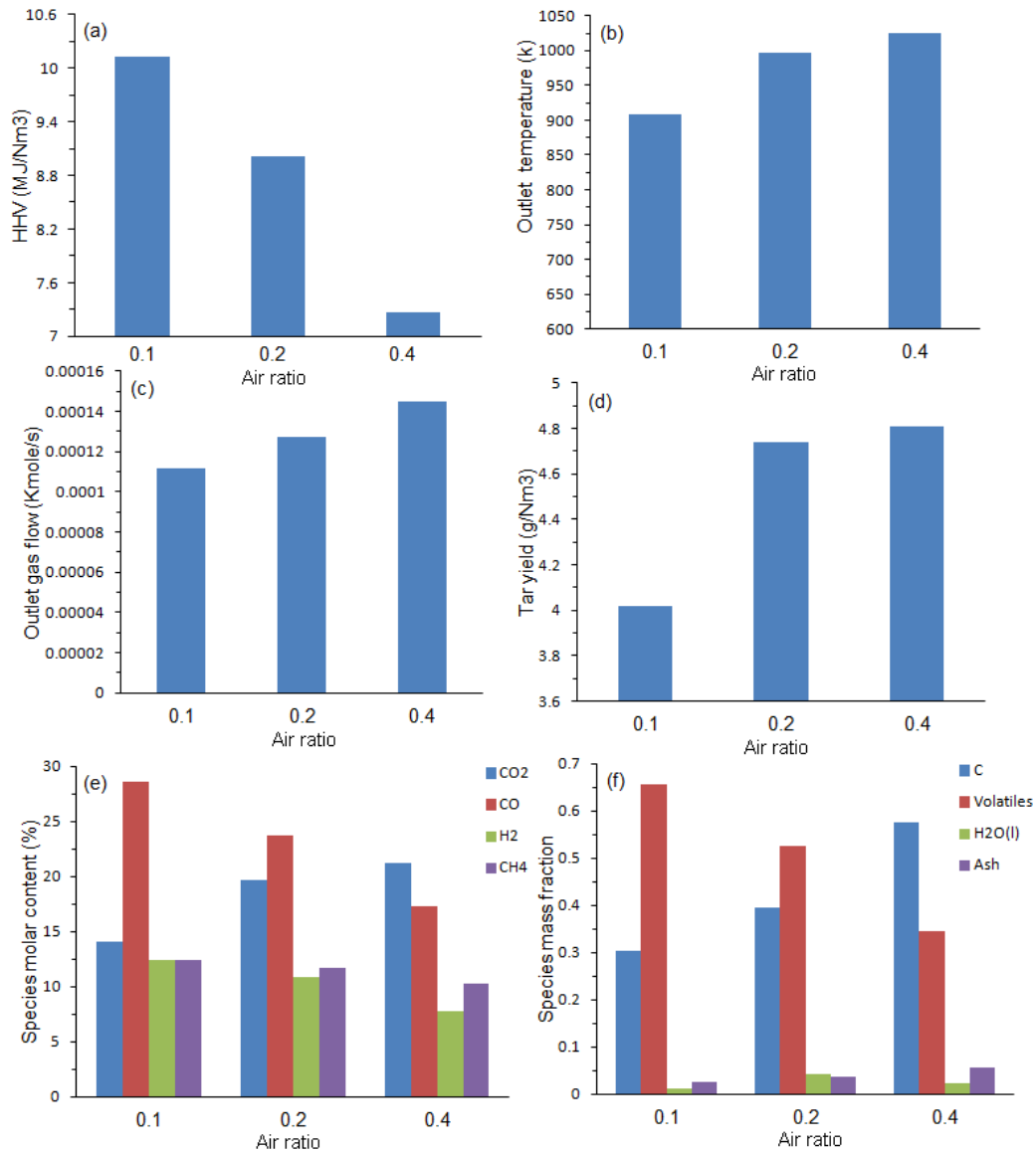


Fig. 7.7 . The effect of varying the air ratio (0.1-0.4) for the case of wood gasification using sand as bed material ( $d_{wood}= 500 \mu\text{m}$ ,  $d_{sand}= 200 \mu\text{m}$ ) with mass flow rate 2g/s and 20g/s respectively. Operating conditions were summarised in Table 7.2. The figures showing the effect of different air ratio in the following parameters: (a) The HHV of the product gas in (MJ/Nm<sup>3</sup>). (b) The outlet temperature (K). (c) Tar yield (g/Nm<sup>3</sup>) (e) Gas species molar concentrations. (f) Char species mass fractions in the outlet.

Table 7.2. Operating conditions for the simulation results shown in Fig. 7.7. The velocities of gas sand and biomass shown in this Table were calculated using volume weighted and time average.

Operating condition	Air ratio 0.1	Air ratio 0.2	Air ratio 0.4
Initial air temperature (°C)	20	20	20
Initial sand temperature(°C)	900	900	900
Initial biomass temperature(°C)	20	20	20
Gas velocity (m/s)	2.79	3.32	4.05
Sand velocity(m/s)	1.76	2.13	2.69
Biomass velocity(m/s)	1.56	1.91	2.42
Gas residence time (s)	0.58	0.49	0.40
Sand residence time (s)	0.93	0.77	0.61
Biomass residence time (s)	1.05	0.85	0.67

### 7.3.2. Variation of the biomass feed rate

The simulation results of varying the fuel mass flow from 2 to 10 g/s while keeping all other parameters fixed is shown in Fig. 7.8. The operating conditions used in producing these results are summarized in Table 7.3. In this figure it is shown that the HHV, product gas flow and tar yield, all have increased with increasing the biomass feed rate as shown in Fig. 7.8-a, c, d. On the contrary, Fig. 7.8-b shows that the outlet temperature decreases, which can be attributed to large amount of heat lost to drying and devolatilization as a result of increasing the biomass feed rate. Keeping fixed the sand inlet temperature and the air supplied one would expect lower temperatures as the amount of available heat is limited. This is indeed true as the outlet temperature decreased as shown in Fig. 7.8-b. In Fig. 6.16-a the HHV increased due to the considerable increase of H<sub>2</sub> content in the product gas while the amount of the gases also increased (Fig. 7.8-c) as more volatiles are released. The tar content also increased (Fig. 6.18-d) due to the clear decrease in the temperature.

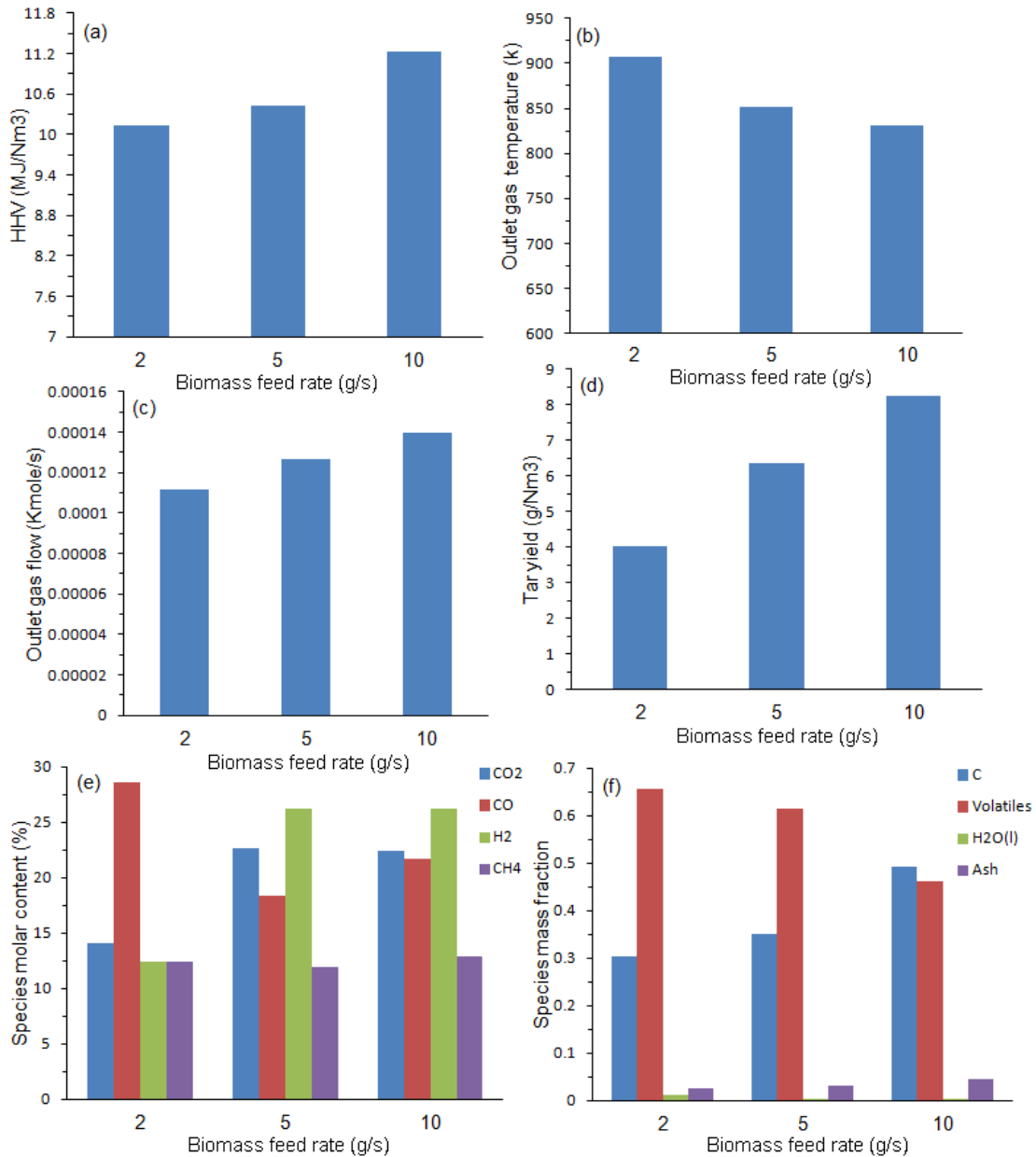


Fig. 7.8 . The effect of using different biomass mass flow rates (2-10g/s) for the case of wood gasification using sand as bed material ( $d_{wood}= 500 \mu\text{m}$ ,  $d_{sand}= 200 \mu\text{m}$ ) with sand mass 20g/s respectively. Operating conditions were summarised in Table 7.3. The figures showing the effect of different biomass mass flow rates in the following parameters: (a) The HHV of the product gas in (MJ/Nm<sup>3</sup>). (b) The outlet temperature of biomass (c) Tar yield (e) Gas species molar concentrations (f) species mass fractions in the biomass at outlet.

The biomass mass flow rate does not seem to play a major role on the overall hydrodynamics of the gasifier, mainly because the biomass flow is relatively less in quantity and density than the heat carrier sand. However, there is a slight increase in the solid and gas velocities with the increasing biomass flow rate, probably due to the

slight increase in the gas flow as shown in Fig. 7.8-c. Fig. 7.8-f shows the species mass fraction at outlet. The major effect of increasing the biomass feed rate is found to be in the carbon conversion. This appears to slow down as the biomass feed rate increases. This is expected, since with keeping all other parameters fixed, there will be no sufficient heat for biomass conversion, and this more carbon leaves with the char.

Table 7.3. operating conditions for Fig. 7.8. the velocities of gas sand and biomass were calculated using volume weighted and time average.

Operating condition	Biomass flow rate (g/s)		
	2	5	10
Initial air temperature (°C)	20	20	20
Initial sand temperature (°C)	900	900	900
Initial biomass temperature (°C)	20	20	20
Gas velocity (m/s)	2.79	2.95	2.99
Sand velocity (m/s)	1.76	1.72	1.70
Biomass velocity (m/s)	1.56	1.50	1.49
Gas residence time (s)	0.58	0.55	0.55
Sand residence time (s)	0.93	0.95	0.96
Biomass residence time (s)	1.05	1.09	1.09

### 7.3.3. Variations of gasifier temperature

The gasifier temperature has a significant effect on the composition of product gases. As understood, there are many endothermic reactions involved in the gasification process, specially the reforming reactions. The rate of these reactions increases with increasing the temperature. The main provider of the heat to the process in the simulations is the sand. In this analysis, the sand temperature was varied between 700 to 1200°C while fixing all the other operating conditions, to see its effect on the HHV, outlet gas temperature, outlet gas flow, tar yield, product gas species molar concentration and the biomass species mass fractions in the outlet as shown in Fig. 7.9.

Figs. 7.9-a and b show the effect of the sand temperature on HHV and the outlet temperature respectively. While the outlet temperature shows a steady and consistent increase with increasing sand temperature, which is expected, the HHV stayed almost constant beyond the temperature 1100 °C. The HHV increases from 10.5 to 13.5 MJ/Nm<sup>3</sup> and the main reason for this is the increase in CO. The outlet gas flow and the tar yield shown in Figs. 7.9-e and d, respectively, show increase up the temperature of 1100 °C, after which a slight decrease is noticed. Fig. 7.9-e shows the molar concentration of the product gas. It is clear that, while the H<sub>2</sub> and CH<sub>4</sub> concentrations almost remained constant, the CO and CO<sub>2</sub> are the most species affected by increasing the inlet sand temperature (i.e. gasification temperature). Fig.7.9-f shows the mass fractions of the char in the outlet. The volatiles were significantly affected with the increase of the temperature. At low sand temperature there seems to be very limited devolatilization as almost 70% of the volatiles leave with the char.

There is a general agreement that the tar in the product gas should decrease with the increase of temperature. But in this case the tar increased until 1100°C then decreased afterwards. The reason is, in the low temperature range the devolatilization did not reach its ultimate value or equilibrium, so the amount of the gases devolatilized is very low, and hence the amount of tar. Then as the devolatilization increases with the increasing the temperature up to 1100 °C, and where no more devolatilization takes place the temperature cracking effect appears, thus lowering the tar yield . It is therefore concluded that with increasing the gasification temperature there is an improvement in devolatilization and carbon conversion, but with the added problem of tar formation. However, there appear to be a critical temperature at which the tar cracking becomes dominant and has much effect than the opposing factor of devolatilization.

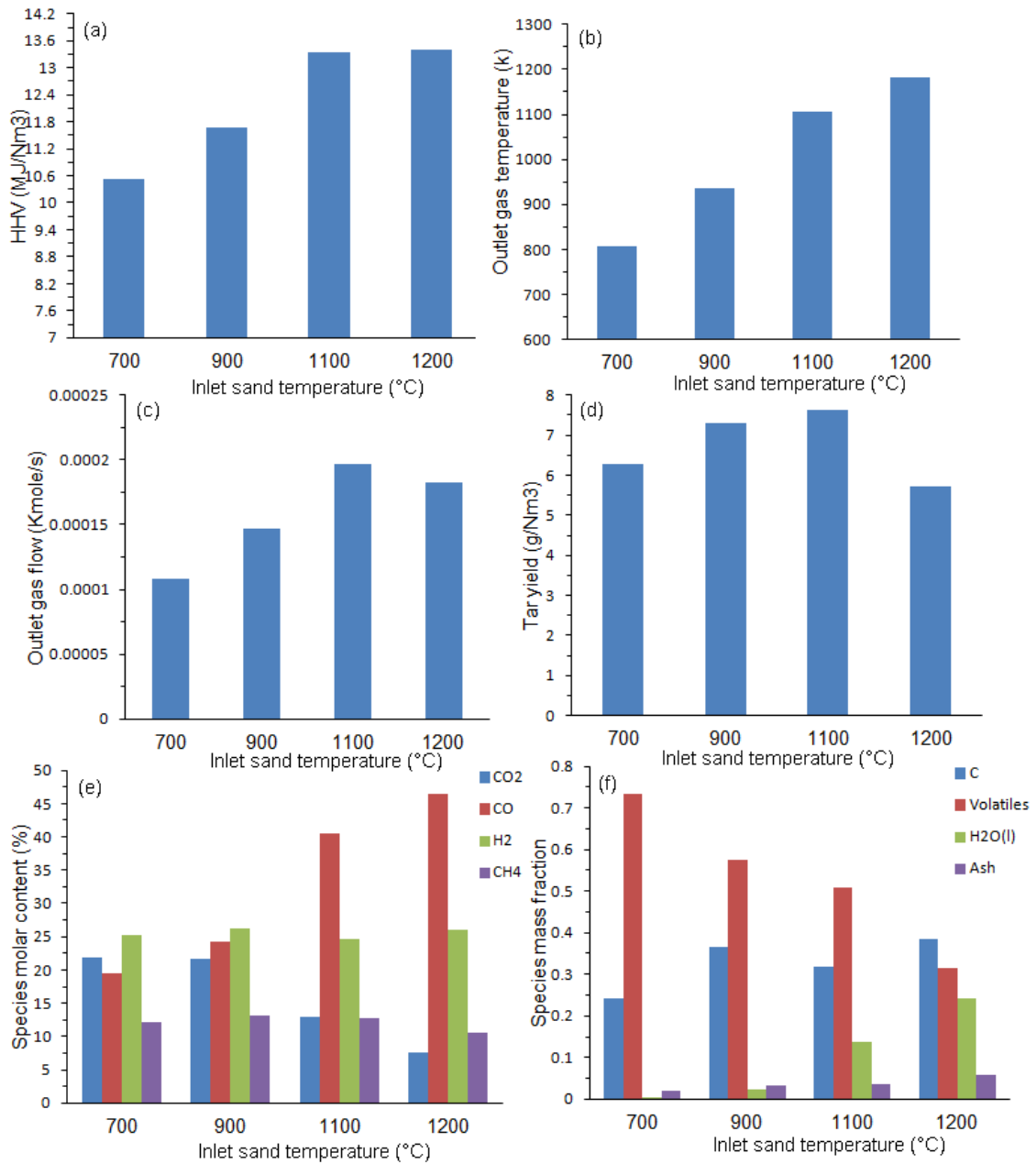


Fig. 7.9. Variation of the inlet sand temperature or the gasifier temperature between 700 and 1200°C for the case of wood gasification ( $d_{wood} = 500 \mu\text{m}$ ,  $d_{sand} = 200 \mu\text{m}$ ) at biomass flow rate of 5 g/s (20°C) and sand flow of 30 g/s. Detailed operating conditions are summarised in Table 7.4. (a) HHV of the product gas (b) outlet temperature of gas (c) Tar yield (e) gas species molar concentrations. (f) biomass species mass fractions at the outlet.

In looking at the data in Table 7.4, it is clear that hydrodynamics of the gasifier have been considerably affected by the change in the gasifier's temperature. The velocities and the residence times of the gas and solids phases for the simulations of different temperatures are notably increased with the increasing the temperature. The gas

velocity changed from 2.69 to 5.8 m/s when the sand temperature changed from 700 to 1200°C. As a result, the velocities of the biomass and the sand have also changed because both depend on the gas velocity. Accordingly, the residence time also changed, as seen in Table 7.4 because this is inversely proportional to the velocity. The effect of the residence time on the final product gas composition is shown in Fig. 7.10.

Table 7.4. Operating conditions for the results shown in Fig. 7.9. The velocities of gas, sand and biomass were calculated using volume weighted and time average.

Operating condition	Inlet sand temperature (°C)			
	700	900	1100	1200
Initial air temperature (°C)	20	20	20	20
Initial sand temperature(°C)	700	900	1100	1200
Initial biomass temperature(°C)	20	20	20	20
Gas velocity (m/s)	2.69	3.27	4.79	5.80
Sand velocity(m/s)	1.47	2.05	2.94	3.53
Biomass velocity(m/s)	1.30	1.82	2.63	3.20
Gas residence time (s)	0.61	0.50	0.34	0.28
Sand residence time (s)	1.11	0.80	0.55	0.46
Biomass residence time (s)	1.25	0.90	0.62	0.51

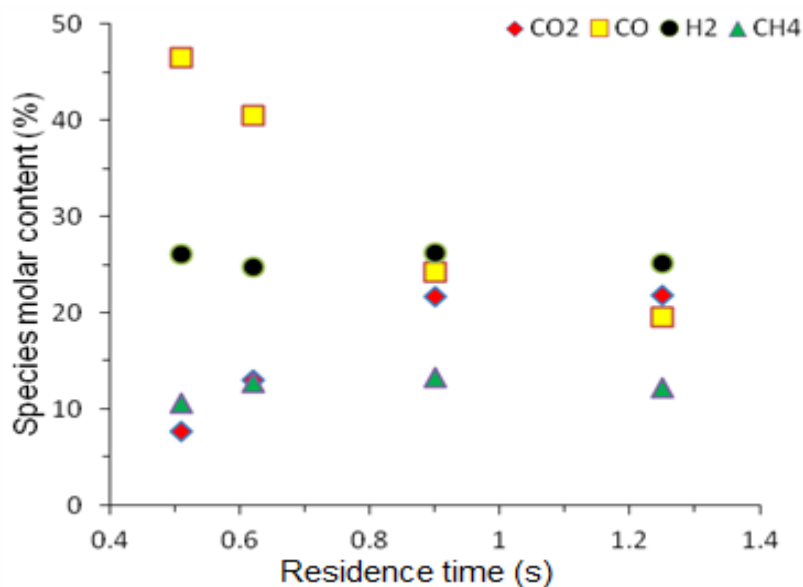


Fig. 7.10 The product gases molar contents against the biomass residence time for the operating conditions given in Table 7.4 and the data presented in Fig. 7.9.

#### 7.3.4. Variation of the sand (heat carrier) flow rate

Increasing the sand, or heat carrier, is another way of increasing the reactor temperature, however, with different effects on the reactor hydrodynamics, thus may result in changing the gasifier performance in a different way. One of the basic hydrodynamics effects is related to mixing and the heat transfer since more sand flow mains denser riser. The sand in these simulations was varied from 20 to 40 g/s while keeping all other operating parameters fixed. Simulations with higher sand flow were not successful due to the size and capacity of the CFB used in the simulation model.

The results of varying the sand flow rates is shown in Fig. 7.11. First it is interesting to not the clear similarity in terms of the overall trend when comparing the effect of increasing the sand temperature and increasing the sand flow rate. The HHV, the outlet temperature and the tar content in the product gas all have shown increase up to a certain limit of solid flow rate, after which a slight decrease is noticed. Also similar to the effect of increasing sand temperature, here the CO increased with the inreasing of the sand flow while the volatiles in the biomass leaving (thae char) is decreased.

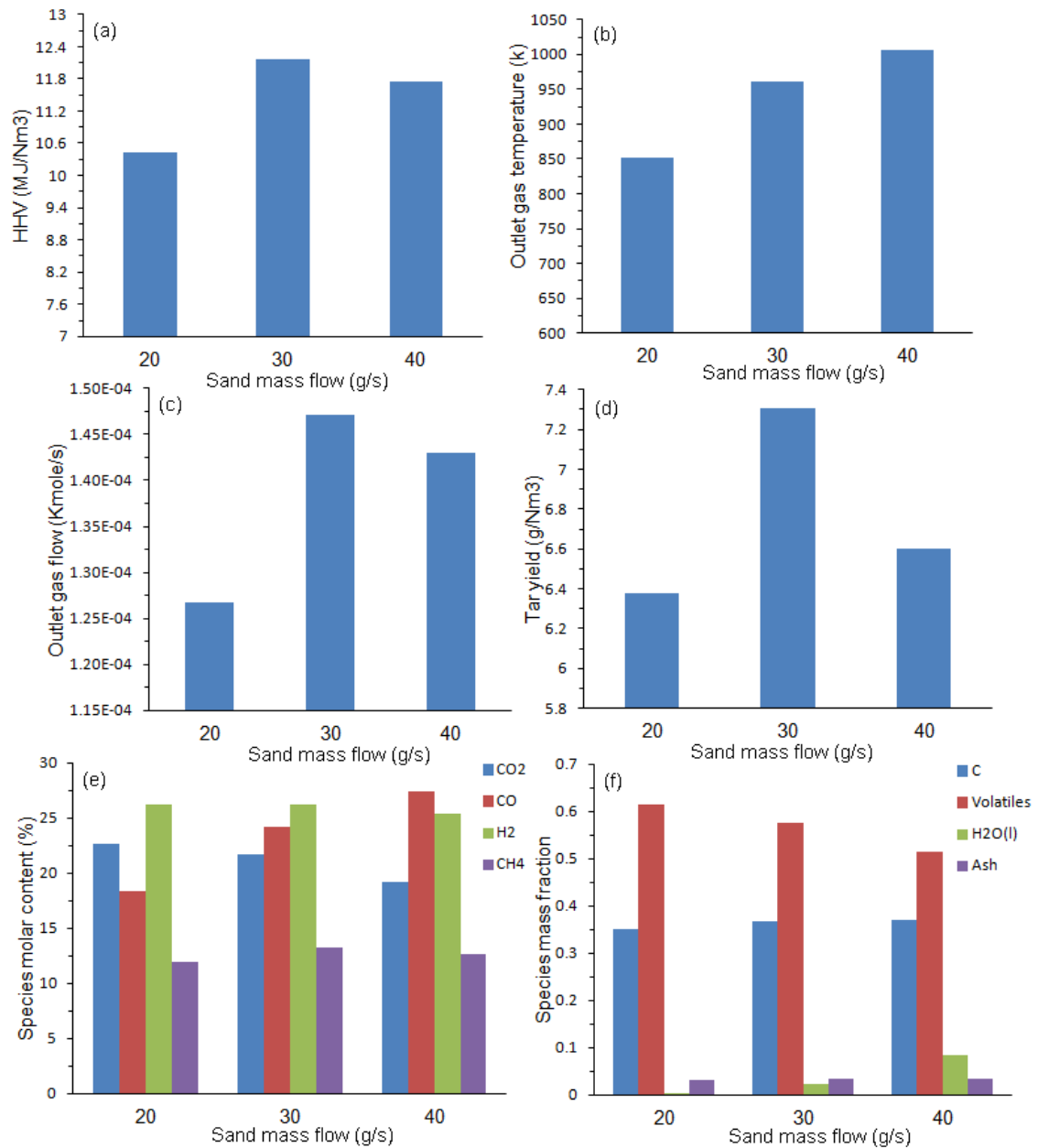


Fig. 7.11 . Variation of the sand (heat carrier) mass flow rate (20-40g/s) for the case of wood gasification ( $d_{wood}= 500 \mu\text{m}$ ,  $d_{sand}= 200 \mu\text{m}$ ) with biomass mass flow rate 5g/s (20°C). Operating conditions were summarised in Table 7.5. The figures showing the effect of different sand mass flow rate in the following parameters: (a) HHV of the product gas(b) outlet temperature of gas (c) Tar yield (e) Gas species molar concentrations (f) Char species mass fractions in the outlet.

Table 7.5 Operating conditions for the results shown in Fig. 7.11. The velocities of the gas, sand and biomass phases were calculated using volume weighted and time average.

Operating condition	Sand (heat carrier) flow rate (g/s)		
	20	30	40
Initial air temperature (°C)	20	20	20
Initial sand temperature(°C)	900	900	900
Initial biomass temperature(°C)	20	20	20
Gas velocity (m/s)	2.95	3.27	3.71
Sand velocity(m/s)	1.72	2.05	2.33
Biomass velocity(m/s)	1.50	1.82	2.11
Gas residence time (s)	0.55	0.50	0.44
Sand residence time (s)	0.95	0.80	0.70
Biomass residence time (s)	1.09	0.90	0.77

### 7.3.5. Variations of the sand size

The main effect of the sand size is in the hydrodynamics of the riser as bigger sand size requires higher gasifying agent velocity to allow entrainment and sand circulation. It is also understood that the smaller the particle size the higher heat transfer rate due to the increase in particle surface area.

In this part of the parametric analysis the sand size was varied from 150 to 300  $\mu\text{m}$ , while keeping all other operating conditions fixed. Summary of the operating conditions are given in Table 7.6. Fig. 7.12-a to d show that the HHV, the outlet temperature, the gas flow and the tar yield all decreased with increasing the particle size. The decreases in first three parameters (HHV, outlet temperature, and gas flow) are directly related to the expected decrease in heat transfer rate with increasing the particle size, the decrease in tar can only be explained by changes in the flow hydrodynamics. As shown in Table 7.6, the residence time of gas phase increased with increasing the sand size, this may have caused increased tar cracking as indicated by the increase in  $\text{H}_2$  content in the product gas (see Fig. 7.6-e). In terms of biomass species

concentration, the particle size do not seem to play a critical effect as shown in Fig. 7.122-f.

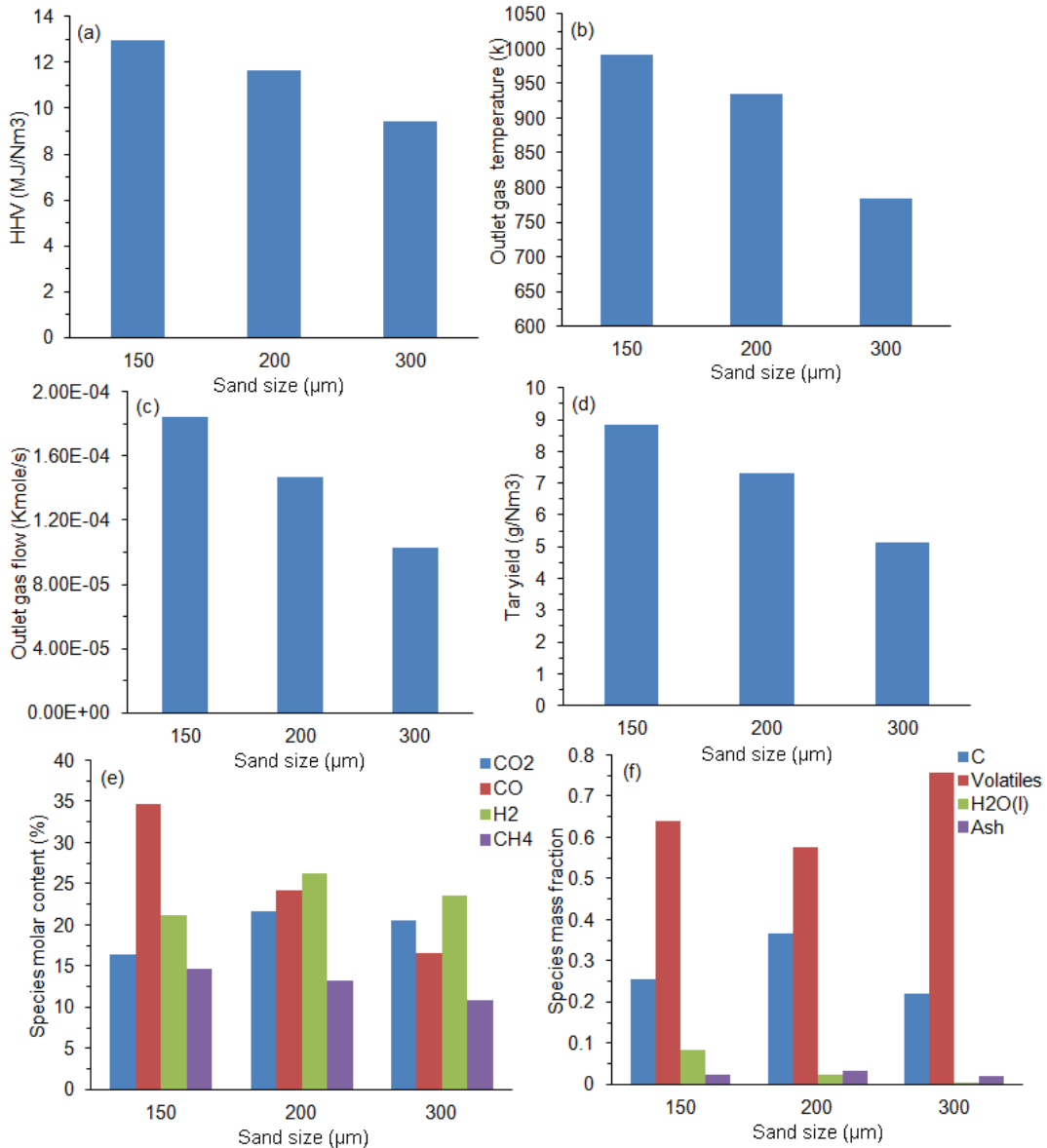


Fig. 7.12 . Variation of the sand (heat carrier) size (150 to 300μm) for the case of wood gasification ( $d_{wood} = 500 \mu\text{m}$ ) with biomass mass flow rate of 5 g/s (20°C) and sand flow rate of 30 g/s (900°C). The operating conditions for this case are summarised in Table 7.6. (a) HHV of the product gas (b) The outlet temperature of gas (c) Tar yield (e) product gas species molar concentrations (f) biomass species mass fractions at the outlet.

Table 7.6 operating conditions for Fig. 7.12 the velocities of gas sand and biomass were calculated using volume weighted and time average.

Operating condition	Sand (heat carrier) size ( $\mu\text{m}$ )		
	150	200	300
Initial air temperature ( $^{\circ}\text{C}$ )	20	20	20
Initial sand temperature( $^{\circ}\text{C}$ )	900	900	900
Initial biomass temperature( $^{\circ}\text{C}$ )	20	20	20
Gas velocity (m/s)	3.89	3.27	2.51
Sand velocity(m/s)	2.73	2.05	1.10
Biomass velocity(m/s)	2.31	1.82	0.91
Gas residence time (s)	0.42	0.50	0.65
Sand residence time (s)	0.6	0.80	1.48
Biomass residence time (s)	0.71	0.90	1.79

### 7.3.6. Variation of the biomass size

In biomass gasification, the literature generally agrees that smaller particle size the better quality the gas product. In this study the biomass particle size has been varied within a relatively narrow and small size range of 250 to 1000  $\mu\text{m}$ .

The quality and the quantity of the product gas (in term of heating value) poorer in the small sizes as seen in Fig. 7.13-a and c. Among the three sizes investigated, the biomass size of 500  $\mu\text{m}$  appear to give the best hydrogen production (see Fig. 7.13-e), reasonably good HHV and good biomass conversion (see Figs. 7.13-a and f). Despite of the clear change in the biomass residence time and velocity, the effect of biomass size is relatively weak, at least within the range studied here.

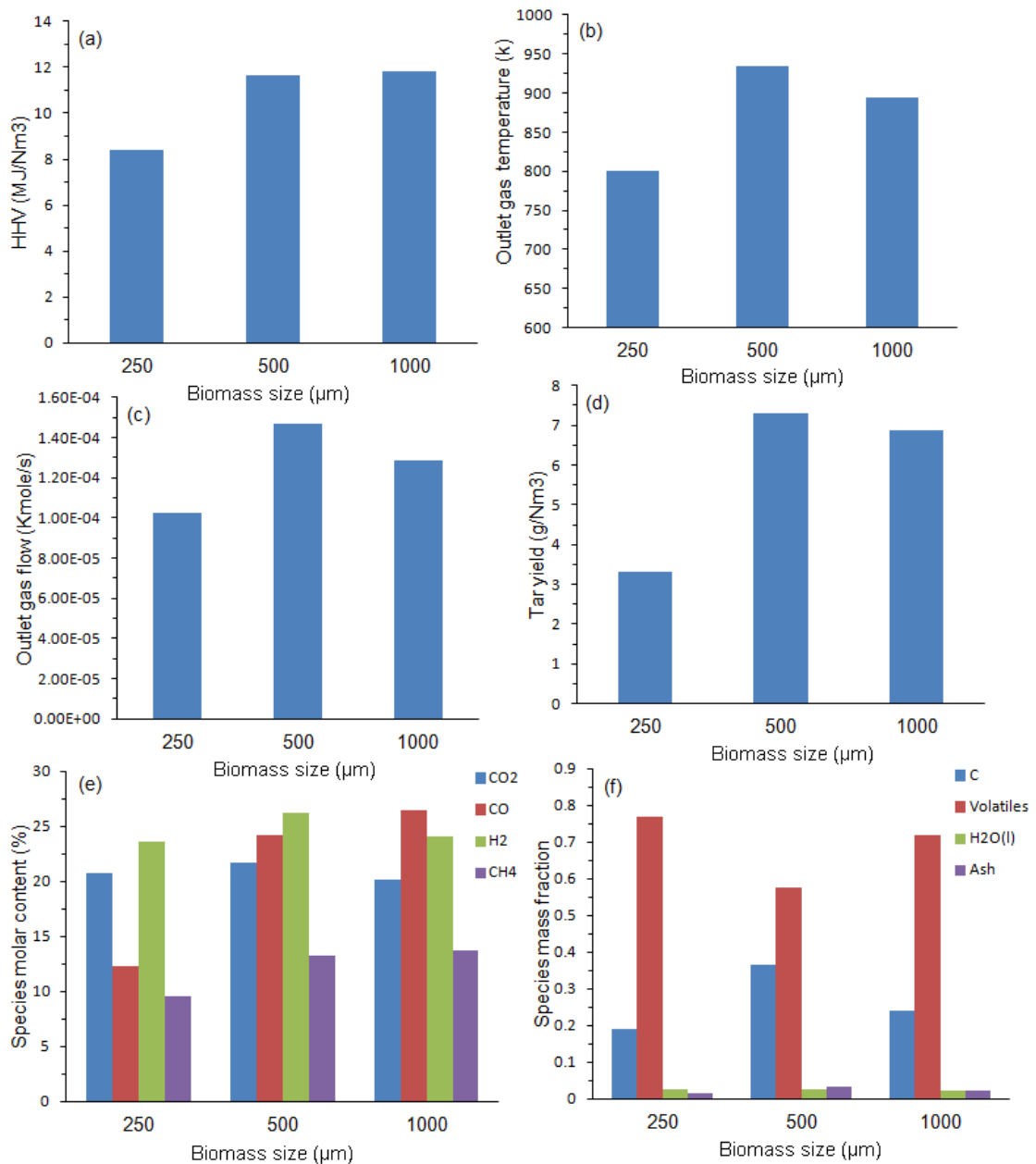


Fig. 7.13 . Variation of the biomass particle size (250-1000μm) for the case of wood gasification ( $d_{sand}= 200 \mu\text{m}$ ) with biomass mass flow rate of 5 g/s (20°C) and sand flow rate of 30 g/s (900 °C). The operating conditions used for these results are summarised in Table 7.7. (a) HHV of the product gas (b) outlet temperature of gas (c) Tar yield (e) Gas species molar concentrations at outlet (f) biomass species mass fractions in the outlet.

Table 7.7 operating conditions for Fig. 7.13. the velocities of gas sand and biomass were calculated using volume weighted and time average.

Operating condition	Biomass particle size ( $\mu\text{m}$ )		
	250	500	1000
Initial air temperature ( $^{\circ}\text{C}$ )	20	20	20
Initial sand temperature( $^{\circ}\text{C}$ )	900	900	900
Initial biomass temperature( $^{\circ}\text{C}$ )	20	20	20
Gas velocity (m/s)	2.71	3.27	3.21
Sand velocity(m/s)	1.75	2.05	2.02
Biomass velocity(m/s)	2.03	1.82	1.39
Gas residence time (s)	0.60	0.50	0.51
Sand residence time (s)	0.93	0.80	0.81
Biomass residence time (s)	0.80	0.90	1.17

### 7.3.7. Operating with pure air

The gas produced from air gasifying of biomass has broad range of applications, e.g. in combined heat and power (CHP) and as a starting agent for producing other chemicals. This section presents the simulation results of using pure air as gasifying agent in comparison with the results obtained when using air-steam mixture (with the ratio of 0.16). All the operating conditions have been kept exactly the same in the two cases, except that in case of air/steam mixture, the pure air was replaced by the same mass flow of the mixture

Fig. 7.14 clearly show that there are considerable differences between the two cases. The HHV extensively dropped from 12.3 to 8.5 when pure air is used as shown in Fig. 7.14-a. This is mainly attributed to the drop of CO, CO<sub>2</sub>, H<sub>2</sub> and CH<sub>4</sub> concentration in the product gas composition (see Fig. 7.14-e) due to the nitrogen associated with the gas in the outlet. Most important, Fig. 7.14-e show that the hydrogen mole fraction in the product gas increased from around 15% to almost 25%.

There are no significant differences in the outlet temperature and the species concentration in the outlet char as shown in Fig. 7.14-b and c, except that the volatiles in the outlet of the char, in the case of pure air, is higher. In terms of the tar content the product gas quality is decreased in the case of pure air since the tar yield increased and the molar contents of the combustible gases decreased as shown in Fig. 7.14.

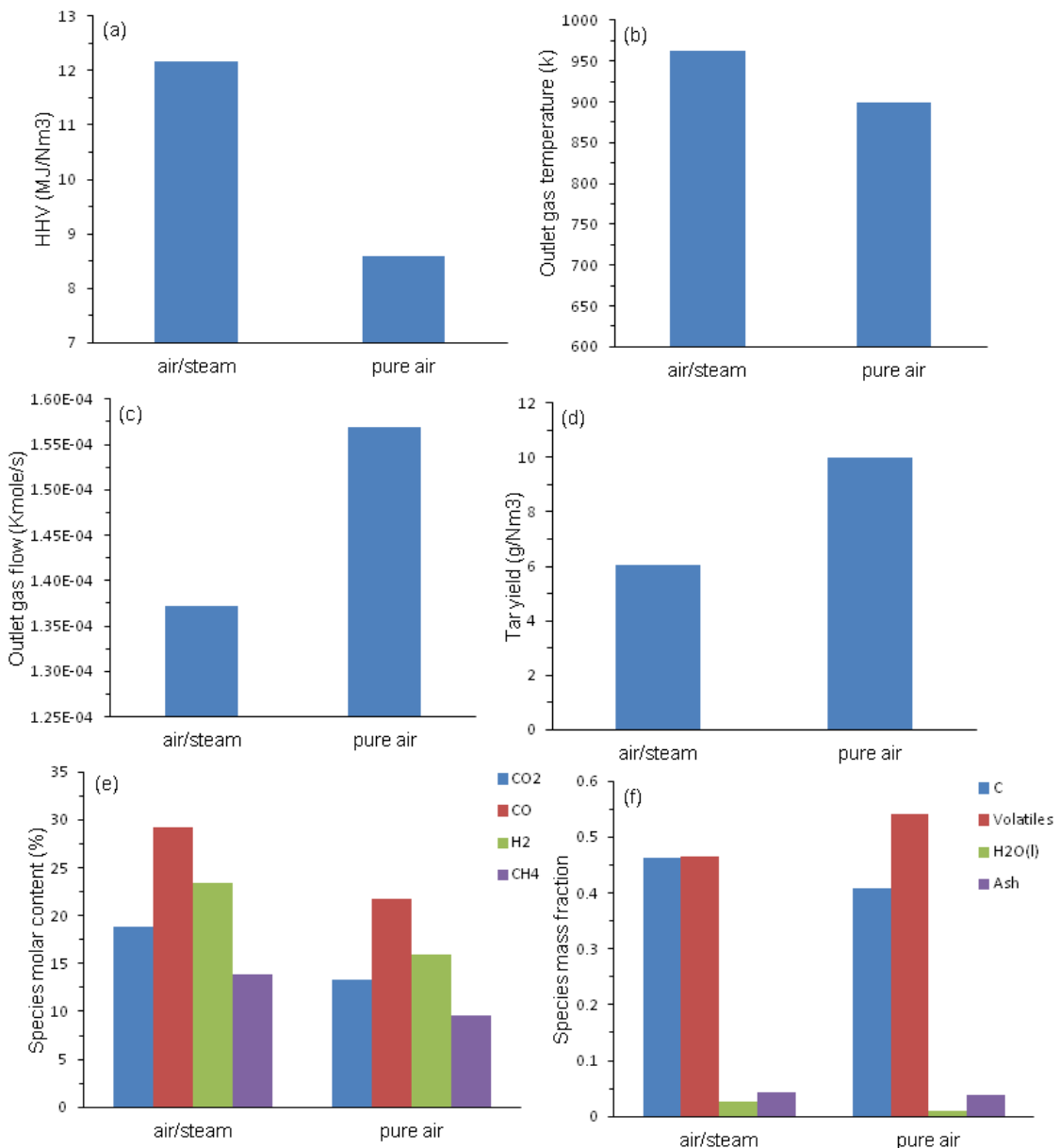


Fig. 7.14 . Comparison between using pure air and air/steam mixture (ratio of 0.16) as a gasifying agent for the case of wood gasification ( $d_{wood}= 500 \mu\text{m}$ ,  $d_{sand}= 200 \mu\text{m}$ ) with mass flow rate 5 g/s (20°C) and sand flow of 30 g/s (900°C). The operating conditions used are summarised in Table 7.8. (a) HHV of the product gas (b) outlet temperature of gas (c) Tar yield (e) gas species molar concentrations (f) char species mass fractions in the outlet.

Table 7.8 Operating conditions for the results shown in Fig. 7.14. The velocities of gas sand and biomass were calculated using volume weighted and time average.

Operating condition	Pure air	Air /Steam
Initial air temperature (°C)	20	20
Initial sand temperature(°C)	900	900
Initial biomass temperature(°C)	20	20
Gas velocity (m/s)	3.04	3.27
Sand velocity(m/s)	1.71	2.05
Biomass velocity(m/s)	1.55	1.82
Gas residence time (s)	0.54	0.50
Sand residence time (s)	0.95	0.80
Biomass residence time (s)	1.05	0.90

### 7.3.8. Operating with pure steam

Using pure steam in biomass gasification is not very common in the research or industry, as mentioned in the literature review in this chapter. This is mainly because such option requires careful setting and control of external heat supply to ensure maintain the reactor temperature at the desired level. Though, using pure steam is appreciated in the gasification of biomass and solid fuels in general because the product gas will be much cleaner and as a result of increasing the hydrogen content.

In this section, two cases of using pure steam as the gasifying agent have been compared; one for the case where in the inlet steam and sand temperature was within the standard case range of 153 °C and 900 °C respectively, and another case were the steam and sand temperature is raised to a higher level of 400 °C and 1200 °C respectively, as detailed in the operating conditions given in Table 7.9.

It can be clearly seen that in the low temperature case the gasification is very low as shown in Fig. 7.15. The amount of the gas flow rate and the tar in the outlet is very low

in low temperature case as shown in Fig. 7.15-c and d respectively. Very little devolatilization have taken place in the case of low temperature as indicated by the high percentage of volatiles in the outlet char as shown in Fig. 7.15-f. In terms of gas composition at the outlet, there are no critical differences, except in terms of the CO and CO<sub>2</sub> concentrations.

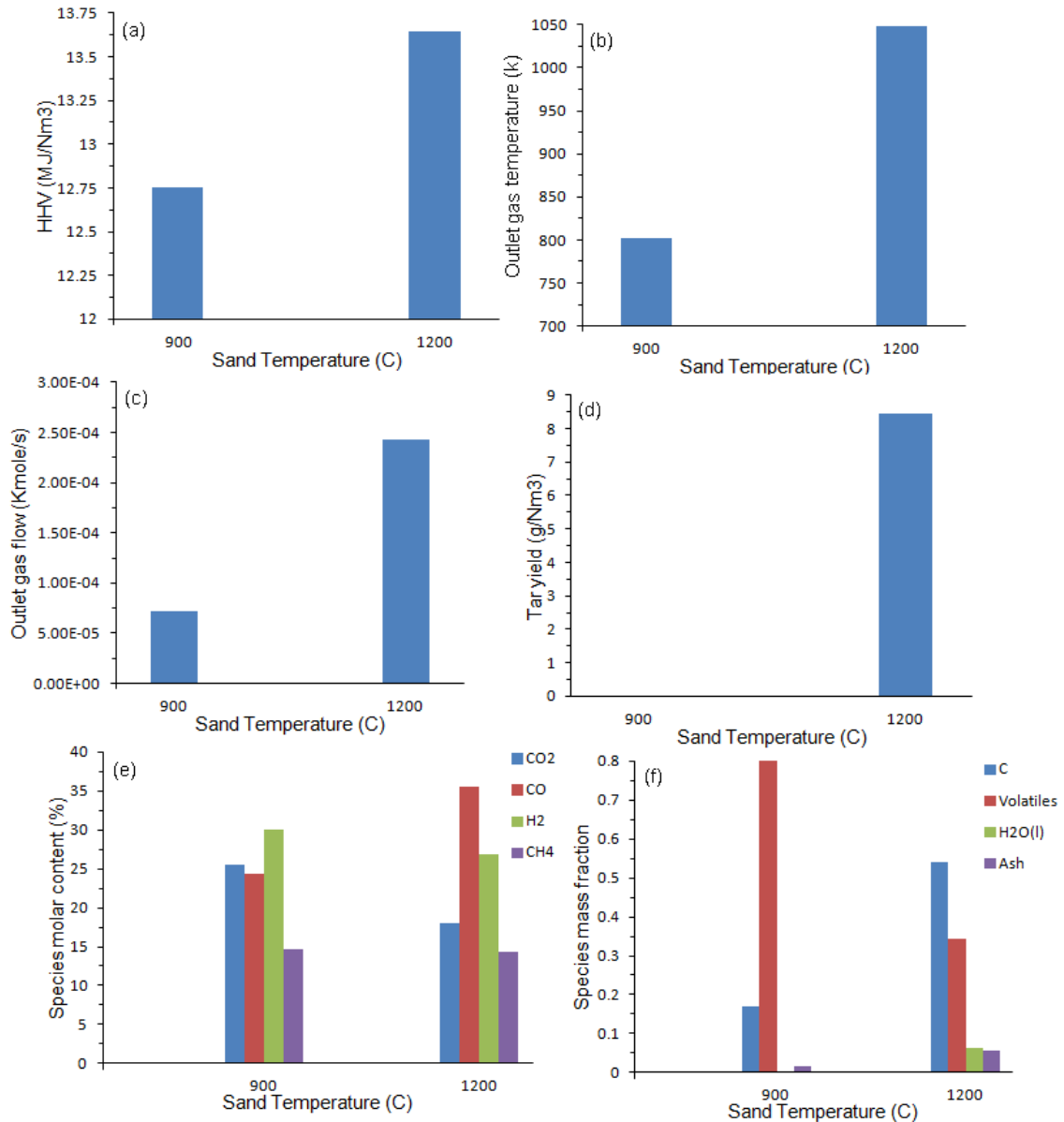


Fig. 7.15. Comparison between two different pure steam gasification at different gasification temperatures using with sand as bed material ( $d_{wood}= 500 \mu\text{m}$ ,  $d_{sand}= 200 \mu\text{m}$ ) with biomass mass flow rate of 5 g/s and sand of 30 g/s. The operating conditions are summarised in Table 7.9. (a) HHV of the product gas (b) Outlet temperature of gas (c) Tar yield (e) gas species molar concentrations (f) char species mass fractions in the outlet.

Table 7.9 operating conditions for Fig. 7.15 the velocities of gas sand and biomass were calculated using volume weighted and time average.

Operating condition	Sand 900°C	Sand 1200°C
Initial steam temperature (°C)	153	400
Initial sand temperature (°C)	900	1200
Initial biomass temperature (°C)	20	20
Gas velocity (m/s)	3.33	5.22
Sand velocity (m/s)	2.10	3.14
Biomass velocity (m/s)	1.92	2.83
Gas residence time (s)	0.49	0.31
Sand residence time (s)	0.78	0.52
Biomass residence time (s)	0.85	0.58

### 7.3.9. Variations of steam/biomass ratio

Different steam to biomass ratio was used to investigate the effect of this parameter on the product gas and the overall performance of the gasifier. The operating conditions of the simulation are given in Table 7.10. The steam to biomass ratio was varied from 0.1 to 0.8. The results are presented in Fig. 7.16. The volatiles in Fig. 7.16-f shows that the volatiles decreases with the decreasing of the steam to biomass ratio. The gas flow in the outlet increased with the increases of the steam to biomass ratio, as shown in Fig. 7.16-c, and that due to the increases of the amount of the steam involved in the operation. The tar in the outlet decreased with the increase of the steam to biomass ratio as shown in Fig. 7.16-d. The hydrogen in the outlet was expected to increase with the increase of the steam to biomass ratio but surprisingly Fig. 7.16-e shows that it decreased, however, not critically. This has been found to be related to the degree of devolatilization. In Fig. 7.16-f it is shown that the devolatilization decreases with increasing the steam to biomass ratio. This can mainly be attributed to the decrease in the biomass residence time and system temperature, up to the ratio of 0.6. However, using 0.8 steam to biomass ratio is showing a slight change in trend as the temperature and the hydrogen content starts to increase. The main reason for

increasing the temperature, in 0.8 steam to biomass ratio case, is the combustion reaction, as this occurred in the exit region (due to solid accumulation at the top when operating with high velocities).

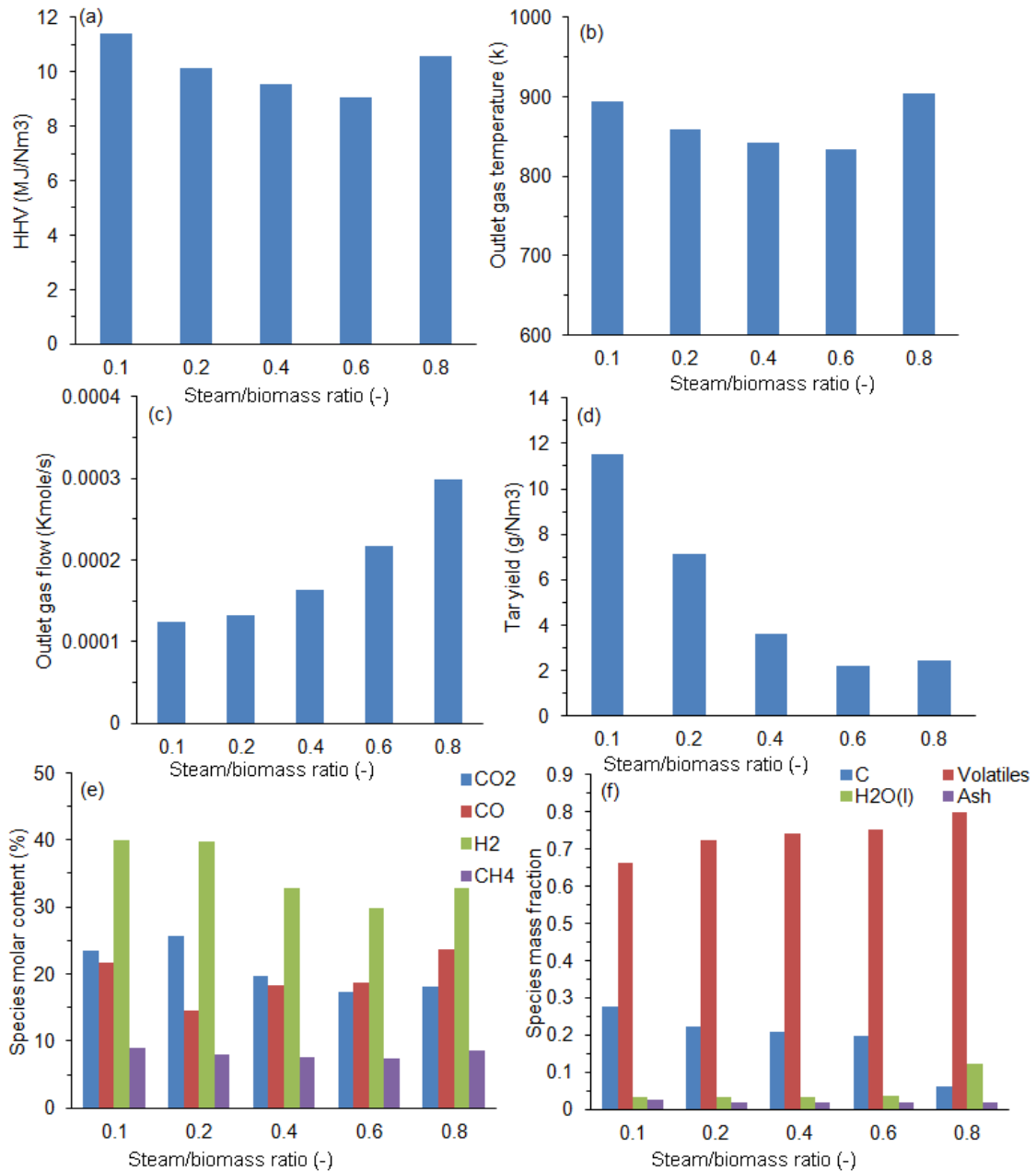


Fig. 7.16. Variation of steam to biomass ratio (0.1-0.8) for the case of wood gasification using sand as bed material ( $d_{wood} = 500 \mu\text{m}$ ,  $d_{sand} = 200 \mu\text{m}$ ) with biomass flow rate of 5 g/s and sand of 30 g/s. The operating conditions are summarised in Table 7.10 for 900°C sand temperature. T (a) HHV of the product gas (b) outlet gas temperature (c) Tar yield (e) gas species molar concentrations. (f) char species mass fractions in the outlet.

Table 7.10 Operating conditions for the simulation results shown in Fig. 7.16. The velocities of gas sand and biomass were calculated using volume weighted and time average.

Operating condition	Steam to biomass ratio				
	0.1	0.2	0.4	0.6	0.8
Initial air temperature (°C)	20	20	20	20	20
Initial sand temperature(°C)	900	900	900	900	900
Initial biomass temperature(°C)	20	20	20	20	20
Gas velocity (m/s)	2.78	2.96	4.36	5.60	7.82
Sand velocity(m/s)	1.74	1.82	2.74	3.73	4.98
Biomass velocity(m/s)	1.60	1.65	2.40	3.17	4.35
Gas residence time (s)	0.59	0.55	0.37	0.29	0.21
Sand residence time (s)	0.94	0.90	0.60	0.44	0.33
Biomass residence time (s)	1.02	0.99	0.68	0.51	0.38

The results obtained with 0.8 steam to biomass ratio appear to be interesting and therefore further investigation was considered by rising the reactor temperature through increasing the inlet solid temperature to 1200 °C. Fig. 7.17 shows that the main effect of the sand temperature was in the devolatilization process as the concentration of volatiles in the char outlet has been considerably decreased, as a result the product gas HHV and hydrogen content increased, however not significantly. The other parameters almost remained the same.

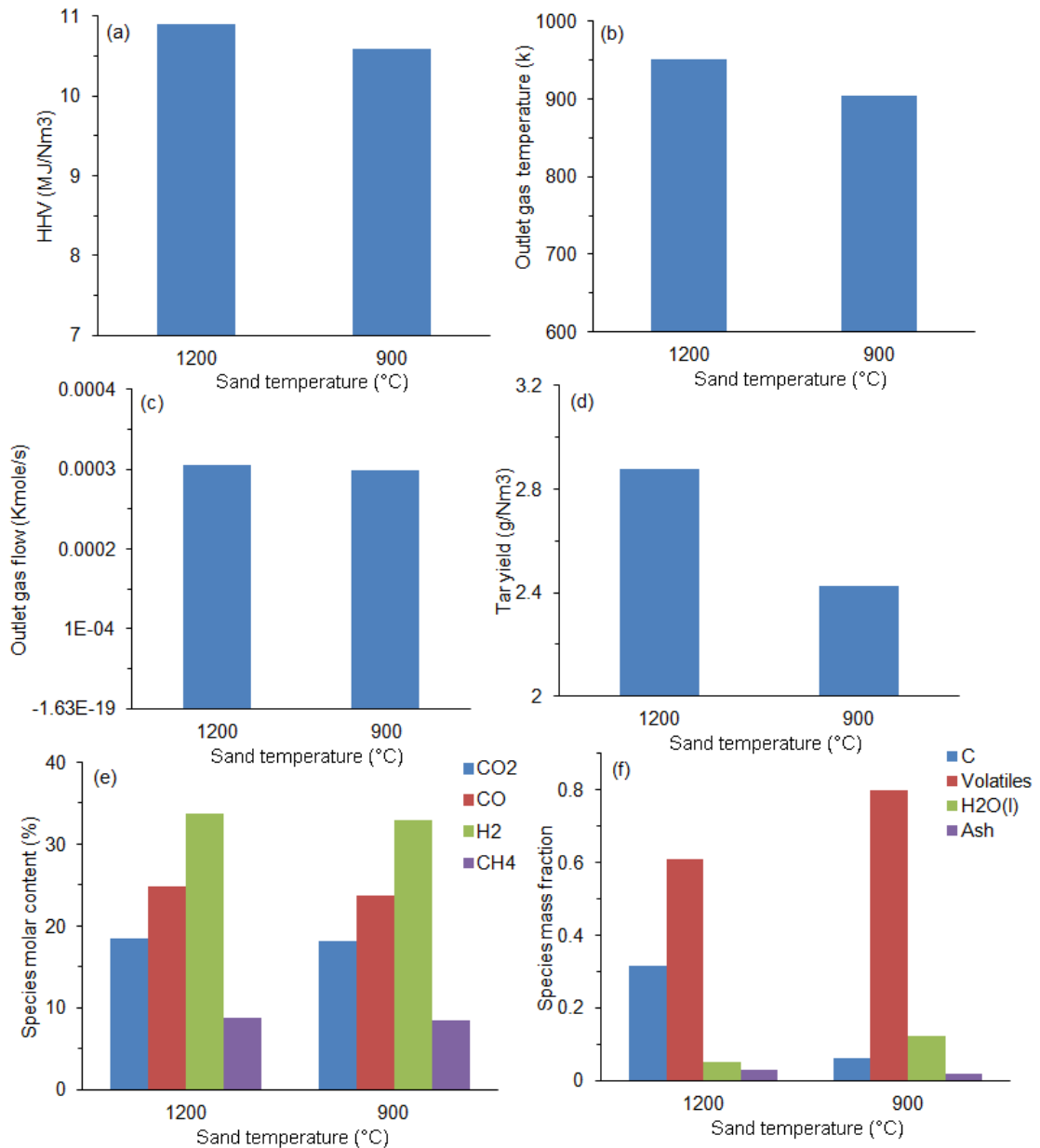


Fig. 7.17. The effect of different sand temperatures (900°C -1200°C) using steam to biomass ratio 0.8 for the case of wood gasification using sand as bed material ( $d_{wood}=500\ \mu\text{m}$ ,  $d_{sand}=200\ \mu\text{m}$ ) with mass flow rate 5g/s and 30g/s respectively. Operating conditions were summarised in Table 7.11. The figures showing the effect of steam to biomass ratio in the following parameters: (a) The HHV of the product gas in (MJ/Nm<sup>3</sup>). (b) The outlet temperature of gas (K). (c) Tar yield (g/Nm<sup>3</sup>) (e) Gas species molar concentrations. (f) Char species mass fractions in the outlet.

Table 7.11 operating conditions for Fig. 7.17. The velocities of gas sand and biomass were calculated using volume weighted and time average.

Operating condition	Inlet sand temperature °C	
	900	1200
Initial air temperature (°C)	20	20
Initial sand temperature (°C)	900	1200
Initial biomass temperature (°C)	20	20
Gas velocity (m/s)	7.82	9.27
Sand velocity (m/s)	4.98	5.62
Biomass velocity (m/s)	4.35	4.89
Gas residence time (s)	0.21	0.18
Sand residence time (s)	0.33	0.29
Biomass residence time (s)	0.38	0.33

#### 7.4. Conclusions

In this chapter a comprehensive parametric analysis of the gasifier has been performed and discussed. The parameters investigated are: air ratio, biomass feed rate, heat carrier temperature and flow rate, biomass and heat carrier particle size, and steam to biomass ratio. Also the literature was reviewed in this chapter. The literature reviewed indicates that there are no reported studies on three-dimensional CFD simulation of biomass gasification in a CFB, especially for the case where the reaction is driven by circulating solid heat carrier. Most of the literature has found to be mainly focused on simple two-dimensional models, majority on bubbling bed reactors.

The main conclusions are that the tar yield is very sensitive to the operating conditions. The reactor temperature is one of the most influential parameters, and this can be directly controlled through increasing the heat carrier (sand) flow rate or by increasing its inlet temperature. Changing the biomass flow rates and air ratio indirectly affect the operating temperature and hence the overall gasifier performance.

Using short CFB gasifier was not discussed before in the literature so identifying the optimum parameters for a short CFB gasifier was one of the objectives of this study and the other objective is to get syngas with high hydrogen content. So regarding the air ratio it was found that the best biomass conversion with using 0.4 air ratio but with the lowest HHV and hydrogen. On the other hand 0.1 air ratio gives the highest hydrogen content and HHV but with the lowest conversion. So, 0.1 air ratio was taken in the following simulation and more focus was done to increase the conversion. In the second step the biomass flow was increased to 5 and 10g/s with keeping the other parameters constant. The simulations showed that, increasing the biomass flow extremely affected the hydrogen generation. Better conversion was found in 10g/s case but 5g/s seems to be more cleaner because it has slightly higher hydrogen content and lower CO content so the 5g/s flow was taken forward and the air ratio in this case will be 0.04. Then the temperature was varied to increase the biomass conversion but it was found that the CO hugely increased with the increasing the reactors temperature and the hydrogen remains almost the same. So, the high heating value and the quantity of the product gas was increased but at the same time it became less clean. So, if the conversion of the biomass is needed regardless of the gas is clean or not then the high temperature is recommended but if we need clean gas then the 900 °C is recommended. So in this case we need the high amount of the hydrogen so the 900 °C will be taken forward. Then the sand flow rate was varied and it was found that increasing the sand flow will enhance the biomass conversion. It is also found that the 30 g/s gives the best situation with good conversion and high hydrogen content and if the sand increased further then the CO amount will increase. So 30 g/s was taken forward. The sand and the biomass sizes was varied and it was found that the best size gives best conversion and hydrogen content was 200 $\mu$ m for the sand and 500  $\mu$ m for the biomass. Then the steam to biomass ratio was varied between 0.1 to 0.8. it was found that the best steam to the biomass ratio is 0.1 where

the hydrogen, HHV and the conversion of the biomass in their highest level. Then there were more simulations were carried out using pure air and pure steam. It was found that using pure air lowers the HHV and in the case of using pure steam with the recommended temperature (900C), the conversion of the biomass will be very low. So it is recommended to use a mixture of air and steam.

So the optimum parameters recommended (for the CFB dimensions studied in this case) are as follow:

- air to biomass ratio 0.04
- Biomass flow 5 g/s
- Biomass to sand ratio 0.1
- Sand temperature 900 °C
- Steam to biomass ratio 0.1

## **8. Chapter 8: Achievements, conclusions and Recommendations**

### **8.1. Introduction:**

The use of CFD for modeling fluidized bed reactors is a very useful tool, especially for high temperature reactive mixture, such as in biomass gasification. This is mainly due to the recognized technical difficulties and cost associated with the set-up and operation of experimental investigation.

The conclusions and achievements of this study are summarised in this chapter, moreover recommendations for future extension are also discussed.

### **8.2. Summary of the achievements**

8.2.1. In this study a three dimensional predictive model, the first of its kind for biomass gasification in a CFB riser, has been developed using advanced Computational Fluid Dynamic (CFD). The model included formulations to predict details of the complex hydrodynamics, heat transfer, reaction and product gas quality.

The developed model has been successfully used to carry out sensitivity and parametric analysis. The sensitivity analysis included:

- Study of the effect of inclusion of various combustion reaction.
- Study of the effect of inclusion of Radiation.

The developed model was also used to carry out parametric analysis by changing the following gasifier operating conditions:

- air ratio
- biomass feed rate
- heat carrier temperature and flow rate
- biomass and heat carrier particle size

- steam to biomass ratio

8.2.2. Two different experiments techniques have been used simultaneously and complimentary to validate the hydrodynamic model, namely classical pressure measurement technique and the state of the art particle tracking technique. The pressure measurement is a very common and widely used technique in fluidized bed studies, while, particle tracking using PEPT, which was originally developed for medical imaging, is a relatively new technique in the engineering field. It is relatively expensive and only available at few research centres around the world. It is therefore one of the achievement in this study to successfully demonstrate the use of these two measuring techniques in CFB study.

8.2.3. The classic kinetic theory of granular flow has been implemented and validated for a binary solid flow mixture using two-fluid modelling. Studies on binary solid mixture modelling are rare in the literature. In this study the binary solid mixture was modelled and validated using experimental data from the both techniques mentioned above.

8.2.4. A new modelling approach have been developed to incorporate the various heterogeneous and homogeneous reaction in the gasification model. As a result, a new user defined function, in C++ programming language, has been developed and verified (see Appendix B). This new UDF will be available for the wider engineering community for future investigations on biomass gasification, particular that relay on using commercial codes, such as Fluent.

To be according to the general gasification steps the developed model has been separated into three main reaction steps; drying, devolatilization and tar cracking , and partial combustion and gasification.

The drying model was modelled as a mass transfer from solid phase to gas phase. The devolatilization and tar cracking model consist of two steps; the devolatilization of the biomass which is used as a single reaction to generate the biomass gases from the volatile materials and tar cracking. The latter is also modelled as one reaction to generate gases with fixed mass fractions. The first reaction was classified as a heterogeneous reaction while the second reaction was classified as homogenous reaction. The partial combustion and gasification model consisted of carbon combustion reactions and carbon and gas phase reactions. The partial combustion is for C, CO, H<sub>2</sub> and CH<sub>4</sub>. The carbon gasification reactions used in this is the Boudouard reaction with CO<sub>2</sub>, the reaction with H<sub>2</sub>O and Methanation (Methane forming reaction) reaction to generate methane. The other gas phase reactions considered in this study is the water gas shift reaction which modelled as a reversible reaction and the other reaction is methane steam reforming reaction.

8.2.5. The first, comprehensive sensitivity and parametric analysis of biomass gasification in a CFB has been studied through modelling. As far as I am aware, such a study particularly focused on CFB gasification driven by circulating heat carrier has not been reported so far.

### **8.3. Conclusions**

#### **8.3.1. The hydrodynamic and heat transfer models**

Based on the extensive experimental comparison the following constitutive relation and conditions are recommended for modelling and simulation of a CFB gasifier

Table. 8.1. Proposed hydrodynamic model constitutive relations

Model constitutive correlation	Model used
Turbulence model	Dispersed standard k- $\epsilon$ model
Drag force model	(Syamlal and O'Brien, 1989)
Granular Viscosity(kg/m s)	(Syamlal et al., 1993)
Granular Bulk Viscosity(kg/m s)	(Lun et al., 1984)
Granular temperature model	Algebraic
Friction	None
Radial distribution	(Lun et al., 1984)
Solids pressure (Pascal)	(Lun et al., 1984)

In regard to heat transfer modelling, the gas solid heat transfer can be modelled successfully using Gunn (1978) correlation. In terms of heat of radiation, the most important conclusion is that the radiation effect is mainly in the region where the solids have high volume fraction ( $>0.2$ ). This region is found to be at the bottom part of the CFB riser, however its influence on the overall heat transfer in the system is negligible.

### 8.3.2. The reactive model

8.3.2.1. Based on the literature review, a gasification reactive model has been developed with full details of the reactions involved. The reactions have been classified into homogenous and heterogeneous reactions. According to the general gasification steps the developed model has been separated into three main steps; drying, devolatilization and tar cracking, and partial combustion and gasification.

8.3.2.2. The drying steps can be modelled successfully using a mass transfer from solid phase to gas phase. The devolatilization and tar cracking model are divided into two steps; the devolatilization of the biomass which is used as a single reaction to generate the biomass gases from the volatile materials and tar cracking. The latter can also be modelled as one reaction to generate gases with fixed mass fractions. The first

reaction was classified as a heterogeneous reaction while the second reaction was classified as homogenous reaction.

8.3.2.2. The combustion of  $H_2$  and  $CH_4$  can be eliminated from the gasification model when using low fraction of air in the gasifying agent because they have no significant effect on the overall gasifier performance.

8.3.2.3. The partial combustion and gasification model consisted of carbon combustion reactions and carbon and gas phase reactions. The partial combustion involves C, CO,  $H_2$  and  $CH_4$ . In low steam to air ratio is concluded that the combustion of  $H_2$  and  $CH_4$  can be eliminated from the gasification model because both reactions have no significant effect on the overall gasifier performance. However, both reactions are critically important when considered using pure air gasification.

### **8.3.3. Parametric analysis**

8.3.3.1 The extensive parametric analyse have shown that there is a strong influence of the bed temperature on the overall gasifier performance, particularly on the product gas composition and tar yield.

8.3.3.2 Changing the biomass flow rates and air have indirect effect through the changing the gasifier temperature.

## **8.4. Recommendations**

### **8.4.1. The effect of the high temperature on the CFB hydrodynamics**

It is found that the temperature has a significant effect in the hydrodynamics of the CFB. High temperatures lowers the gas density therefore it increases its velocity so the solid velocities will increase due to increase of the gas velocity. So, a more detailed

study on the effect of the gasifier temperature on the flow hydrodynamics of the CFB riser is recommended.

#### **8.4.2. Developing new heat transfer coefficient for dilute gas-solid flow**

Different correlations are available in literature for the gas-solid heat transfer coefficient. There is generally good agreement to some extent between the experimental results and the data obtained from the simulations. However in the dilute zone there is partial divergence. The literature was reviewed to find heat transfer correlation describing dilute gas-solid flow, some of these correlations have been found give poor predictions. So, it is recommended to develop a new correlation to calculate the heat transfer in a dilute gas-solid flow systems. This correlation can be obtained by carrying out experiments using different solid sizes and shapes heated with different gas temperatures. The developed correlation can then be implemented, as a UDF in most available CFD codes or models.

#### **8.4.3. Modeling of devolatilization**

In developing the reaction model the devolatilization step was found to be the most important step in generating the product gas in CFBs biomass gasifier. In the literature there are different methods to model the pyrolysis of the biomass and different product results. So, this step has to be carefully modelled. The percentages of the gases produced from the gasification can be changed with changing the boundary conditions as example the temperature. Therefore, characterizing the biomass and developing specific models for each type is very important and it is recommended to do characterizing to the biomass used in simulations or carefully pick the information from the literature to match the required feed stock gasification.

## References

- Agarwal, P. K., Genetti, W. E. and Lee, Y. Y. (1986) 'Coupled drying and devolatilization of wet coal in fluidized beds', *Chemical Engineering Science*, 41(9), 2373-2383.
- Almuttahir, A. and Taghipour, F. (2008) 'Computational fluid dynamics of a circulating fluidized bed under various fluidization conditions', *Chemical Engineering Science*, 63(6), 1696-1709.
- Arastoopour, H., Pakdel, P. and Adewumi, M. (1990) 'Hydrodynamic analysis of dilute gas—solids flow in a vertical pipe', *Powder Technology*, 62(2), 163-170.
- Ardila, Y. C., Figueroa, J. E. J., Lunelli, B. H., Filho, R. M. and Wolf Maciel, M. R. (2012) 'Syngas production from sugar cane bagasse in a circulating fluidized bed gasifier using Aspen Plus™: Modelling and Simulation' in Ian David Lockhart, B. and Michael, F., eds., *Computer Aided Chemical Engineering*, Elsevier, 1093-1097.
- Basu, P. (2010a) 'Chapter 3 - Pyrolysis and Torrefaction' in *Biomass Gasification and Pyrolysis*, Boston: Academic Press, 65-96.
- Basu, P. (2010b) 'Chapter 5 - Gasification Theory and Modeling of Gasifiers' in *Biomass Gasification and Pyrolysis*, Boston: Academic Press, 117-165.
- Beetstra, R., van der Hoef, M. A. and Kuipers, J. A. M. (2007) 'Drag Force of Intermediate Reynolds Number Flow Past Mono- and Bidisperse Arrays of Spheres', *American Institute of Chemical Engineers (AIChE)*, 53(2), 489-501.
- Behjat, Y., Shahhosseini, S. and Marvast, M. A. (2011) 'Investigation of catalyst particle hydrodynamic and heat transfer in three phase flow circulating fluidized bed', *International Communications in Heat and Mass Transfer*, 38(1), 100-109.
- Benyahia, S., Arastoopour, H., Knowlton, T. M. and Massah, H. (2000) 'Simulation of particles and gas flow behavior in the riser section of a circulating fluidized bed using the kinetic theory approach for the particulate phase', *Powder Technology*, 112(1-2), 24-33.
- Bi, X. T. and Liu, X. (2010) 'High density and high solids flux CFB risers for steam gasification of solids fuels', *Fuel Processing Technology*, 91(8), 915-920.
- Bingyan, X., Zengfan, L., Chungzhi, W., Haitao, H. and Xiguang, Z. (1994) 'Circulating fluidized bed gasifier for biomass', [online], available: <http://www.fao.org/docrep/T4470E/T4470E00.htm> [accessed

- Boroson, M., Howard, J., Longwell, J. and Peters, A. (1989) 'Products Yields and Kinetics from the Vapor Phase Cracking of Wood Pyrolysis Tars', *AIChE Journal*, 35(1), 120-128.
- Broido, A. (1976) 'Kinetics Of Solid-phase Cellulose Pyrolysis' in Fred, S., ed. *Thermal Uses and Properties of Carbohydrates and Lignins*, Academic Press, 19-36.
- Chalermssinsuwan, B., Kuchonthara, P. and Piumsomboon, P. (2010) 'CFD modeling of tapered circulating fluidized bed reactor risers: Hydrodynamic descriptions and chemical reaction responses', *Chemical Engineering and Processing: Process Intensification*, 49(11), 1144-1160.
- Chan, C. W., Seville, J., Fan, X. and Baeyens, J. (2009a) 'Particle motion in L-valve as observed by positron emission particle tracking', *Powder Technology*, 193(2), 137-149.
- Chan, C. W., Seville, J., Fan, X. and Baeyens, J. (2009b) 'Solid particle motion in a standpipe as observed by Positron Emission Particle Tracking', *Powder Technology*, 194(1-2), 58-66.
- Chan, C. W., Seville, J., Yang, Z. and Baeyens, J. (2009c) 'Particle motion in the CFB riser with special emphasis on PEPT-imaging of the bottom section', *Powder Technology*, 196(3), 318-325.
- Chan, W.-C. R., Kelbon, M. and Krieger, B. B. (1985) 'Modelling and experimental verification of physical and chemical processes during pyrolysis of a large biomass particle', *Fuel*, 64(11), 1505-1513.
- Corella, J. and Sanz, A. (2005) 'Modeling circulating fluidized bed biomass gasifiers. A pseudo-rigorous model for stationary state', *Fuel Processing Technology*, 86(9), 1021-1053.
- Dalla Valle, J. (1948) *Micromeritics*, London Pitman.
- de Souza-Santos, M. L. (1989) 'Comprehensive modelling and simulation of fluidized bed boilers and gasifiers', *Fuel*, 68(12), 1507-1521.
- Deng, Z., Xiao, R., Jin, B., Huang, H., Shen, L., Song, Q. and Li, Q. (2008) 'Computational Fluid Dynamics Modeling of Coal Gasification in a Pressurized Spout-Fluid Bed', *Energy & Fuels*, 22(3), 1560-1569.
- Di Blasi, C. (1993) 'Modeling and simulation of combustion processes of charring and non-charring solid fuels', *Progress in Energy and Combustion Science*, 19(1), 71-104.

- Di Blasi, C. (2004) 'Modelling Wood Gasification in a Counter current Fixed-Bed Reactor', *American Institute of Chemical Engineers (AIChE Journal)*, 50, 2306-2319.
- Di Blasi, C. (2008) 'Modeling chemical and physical processes of wood and biomass pyrolysis', *Progress in Energy and Combustion Science*, 34(1), 47-90.
- Di Blasi, C., Buonanno, F. and Branca, C. (1999) 'Reactivities of some biomass chars in air', *Carbon*, 37(8), 1227-1238.
- Di Blasi, C., Signorelli, G. and Portoricco, G. (1999) 'Countercurrent Fixed-Bed Gasification of Biomass at Laboratory Scale', *Ind. Eng. Chem. Res.*, 38, 2571-2581.
- Ding, J. and Gidaspow, D. (1990) 'A bubbling fluidization model using kinetic theory of granular flow', *AIChE Journal*, 36(4), 523-538.
- Doherty, W., Reynolds, A. and Kennedy, D. (2009) 'The effect of air preheating in a biomass CFB gasifier using ASPEN Plus simulation', *Biomass and Bioenergy*, 33(9), 1158-1167.
- Dryer, F. (1972) *High Temperature Oxidation of CO and CH4 in a Turbulent Flow Reactor* unpublished thesis Princeton University.
- Dupont, C., Boissonnet, G., Seiler, J.-M., Gauthier, P. and Schweich, D. (2007) 'Study about the kinetic processes of biomass steam gasification', *Fuel*, 86(1-2), 32-40.
- Fletcher, D. F., Haynes, B. S., Christo, F. C. and Joseph, S. D. (2000) 'A CFD based combustion model of an entrained flow biomass gasifier', *Applied Mathematical Modelling*, 24(3), 165-182.
- Gabra, M., Pettersson, E., Backman, R. and Kjellström, B. (2001) 'Evaluation of cyclone gasifier performance for gasification of sugar cane residue—Part 1: gasification of bagasse', *Biomass and Bioenergy*, 21(5), 351-369.
- Gao, J., Zhao, Y., Sun, S., Che, H., Zhao, G. and Wu, J. (2012) 'Experiments and numerical simulation of sawdust gasification in an air cyclone gasifier', *Chemical Engineering Journal*, 213(0), 97-103.
- Garside, J. and Al-Dibouni, M. (1977) 'Velocity-Voidage Relationships for Fluidization and Sedimentation in Solid-Liquid Systems', *Industrial & Engineering Chemistry Research*, 16, 206-214.

- Gerber, S., Behrendt, F. and Oevermann, M. (2010) 'An Eulerian modeling approach of wood gasification in a bubbling fluidized bed reactor using char as bed material', *Fuel*, 89(10), 2903-2917.
- Gidaspow, Bezburuah and Ding (1992) *Hydrodynamics of circulating fluidized beds, kinetic theory approach*, translated by 75–82.
- Gräbner, M., Ogriseck, S. and Meyer, B. (2007) 'Numerical simulation of coal gasification at circulating fluidised bed conditions', *Fuel Processing Technology*, 88(10), 948-958.
- Grammelis, P. (2011) *Solid Biofuels for Energy*, Springer- Verlag London Limited.
- Grønli, M. (1996) *A theoretical and experimental study of the thermal degradation of biomass*, unpublished thesis The Norwegian University of Science and Technology.
- Grønli, M. and Melaaen, M. (2000) 'Mathematical Model for Wood Pyrolysis Comparison of Experimental Measurements with Model Predictions', *Energy & Fuels*, 14, 791-800.
- Gungor, A. (2011) 'Modeling the effects of the operational parameters on H<sub>2</sub> composition in a biomass fluidized bed gasifier', *International Journal of Hydrogen Energy*, 36(11), 6592-6600.
- Gungor, A. and Eskin, N. (2008) 'Two-dimensional coal combustion modeling of CFB', *International Journal of Thermal Sciences*, 47(2), 157-174.
- Gungor, A. and Yildirim, U. (2013) 'Two dimensional numerical computation of a circulating fluidized bed biomass gasifier', *Computers & Chemical Engineering*, 48(0), 234-250.
- Gunn, D. J. (1978) 'Transfer of heat or mass to particles in fixed and fluidised beds', *International Journal of Heat and Mass Transfer*, 21(4), 467-476.
- Hannula, I. and Kurkela, E. (2012) 'A parametric modelling study for pressurised steam/O<sub>2</sub>-blown fluidised-bed gasification of wood with catalytic reforming', *Biomass and Bioenergy*, 38(0), 58-67.
- Hartge, E.-U., Ratschow, L., Wischnewski, R. and Werther, J. (2009) 'CFD-simulation of a circulating fluidized bed riser', *Particuology*, 7(4), 283-296.
- Hobbs, M. L., Radulovic, P. T. and Smoot, L. D. (1992) 'Modeling fixed-bed coal gasifiers', *AIChE Journal*, 38(5), 681-702.

- Huynh, C. V. and Kong, S.-C. (2013) 'Performance characteristics of a pilot-scale biomass gasifier using oxygen-enriched air and steam', *Fuel*, 103(0), 987-996.
- Iddir, H. and Arastoopour, H. (2005) 'Modeling of Multitype Particle Flow Using the Kinetic Theory Approach', *AIChE Journal*, 51(6), 1620-1632.
- Jennen, T., Hiller, R., Köneke, D. and Weinspach, P. M. (1999) 'Modeling of Gasification of Wood in a Circulating Fluidized Bed', *Chemical Engineering & Technology*, 22(10), 822-826.
- Johnson, P. and Jackson, R. (1987) 'Frictional collisional constitutive relations for granular materials, with application to plane shearing', *Journal of Fluid Mechanics*, 176, 67-93.
- Johnsson, F., Zijerveld, R. C., Schouten, J. C., van den Bleek, C. M. and Leckner, B. (2000) 'Characterization of fluidization regimes by time-series analysis of pressure fluctuations', *International Journal of Multiphase Flow*, 26(4), 663-715.
- Kaushal, P., Abedi, J. and Mahinpey, N. (2010) 'A comprehensive mathematical model for biomass gasification in a bubbling fluidized bed reactor', *Fuel*, 89(12), 3650-3661.
- Kaushal, P., Proell, T. and Hofbauer, H. (2011) 'Application of a detailed mathematical model to the gasifier unit of the dual fluidized bed gasification plant', *Biomass and Bioenergy*, 35(7), 2491-2498.
- Kern, S., Pfeifer, C. and Hofbauer, H. (2013) 'Gasification of wood in a dual fluidized bed gasifier: Influence of fuel feeding on process performance', *Chemical Engineering Science*, 90(0), 284-298.
- Klass, D. L., Technology, I. o. G., Biomass, S. o. E. f., Wastes and .01.28-02.01 (1985) *Energy from Biomass and Wastes IX: Symposium Papers Presented January 28 - February 1, 1985, Lake Buena Vista, Florida*, Inst. of Gas Technology.
- Kunii, D. and Levenspiel, O. (1991) *Fluidization Engineering*, 2nd Edition ed., Butterworth-Heinemann.
- Larfeldt, J., Leckner, B. and Melaaen, M. C. (2000) 'Modelling and measurements of the pyrolysis of large wood particles', *Fuel*, 79(13), 1637-1643.
- Lauder, B. E. and Spalding, D. B. (1972) *Lectures in Mathematical Models of Turbulence*, London, England: Academic Press.

- Lee, W. (1979) *A Pressure Iteration Scheme for Two-Phase Flow Modeling*, Los Alamos Scientific Laboratory, Los Alamos, New Mexico.
- Li, T., Dietiker, J.-F. and Shahnam, M. (2012) 'MFIX simulation of NETL/PSRI challenge problem of circulating fluidized bed', *Chemical Engineering Science*, 84(0), 746-760.
- Li, X. T., Grace, J. R., Lim, C. J., Watkinson, A. P., Chen, H. P. and Kim, J. R. (2004) 'Biomass gasification in a circulating fluidized bed', *Biomass and Bioenergy*, 26(2), 171-193.
- Liden, A., Berruti, F. and Scott, D. (1988) 'A Kinetic Model for the Production of Liquids from the Flash Pyrolysis of Biomass', *Chemical Engineering Communications*, 65, 207-221.
- Lim, K. S., Zhu, J. X. and Grace, J. R. (1995) 'Hydrodynamics of gas-solid fluidization', *International Journal of Multiphase Flow*, 21, Supplement(0), 141-193.
- Liu, H. and Gibbs, B. M. (2003) 'Modeling NH<sub>3</sub> and HCN emissions from biomass circulating fluidized bed gasifiers☆', *Fuel*, 82(13), 1591-1604.
- Loha, C., Chatterjee, P. K. and Chattopadhyay, H. (2011) 'Performance of fluidized bed steam gasification of biomass – Modeling and experiment', *Energy Conversion and Management*, 52(3), 1583-1588.
- Lun, C., Savage, S., Jeffrey, D. and Chepurniy, N. (1984) 'Kinetic theories for granular flow : inelastic particles in Couette flow and slightly inelastic particles in a general flowfield', *J. Fluid Mech.*, 140, 223–256.
- Lv, P., Chang, J., Xiong, Z., Huang, H., Wu, C., Chen, Y. and Zhu, J. (2003) 'Biomass Air–Steam Gasification in a Fluidized Bed to Produce Hydrogen-Rich Gas', *Energy & Fuels*, 17(3), 677-682.
- Lv, P. M., Xiong, Z. H., Chang, J., Wu, C. Z., Chen, Y. and Zhu, J. X. (2004) 'An experimental study on biomass air–steam gasification in a fluidized bed', *Bioresource Technology*, 95(1), 95-101.
- Makkawi, Y. (2013) 'Reactor design and its impact on performance and products' in *Transformation of Biomass: Theory to Practice*, John Wiley & Sons.
- Mansaray, K. G., Ghaly, A. E., Al-Taweel, A. M., Hamdullahpur, F. and Ugursal, V. I. (1999) 'Air gasification of rice husk in a dual distributor type fluidized bed gasifier', *Biomass and Bioenergy*, 17(4), 315-332.

- Manyà, J. J., Sánchez, J. L., Gonzalo, A. and Arauzo, J. (2005) 'Air Gasification of Dried Sewage Sludge in a Fluidized Bed: Effect of the Operating Conditions and In-Bed Use of Alumina', *Energy & Fuels*, 19(2), 629-636.
- Melaaen, M. (1996) 'Numerical analysis of heat and mass transfer in drying and pyrolysis of porous media', *Numerical Heat Transfer, Part A: Applications: An International Journal of Computation and Methodology*, 29(4), 331-355.
- Miao, Q., Zhu, J., Barghi, S., Wu, C., Yin, X. and Zhou, Z. (2013) 'Modeling biomass gasification in circulating fluidized beds', *Renewable Energy*, 50(0), 655-661.
- Mitani, T. and Williams, F. A. (1980) 'Studies of cellular flames in hydrogen-oxygen-nitrogen mixtures', *Combustion and Flame*, 39(2), 169-190.
- Morf, P., Hasler, P. and Nussbaumer, T. (2002) 'Mechanisms and kinetics of homogeneous secondary reactions of tar from continuous pyrolysis of wood chips', *Fuel*, 81(7), 843-853.
- Ngo, S. I., Nguyen, T. D. B., Lim, Y.-I., Song, B.-H., Lee, U.-D., Choi, Y.-T. and Song, J.-H. (2011) 'Performance evaluation for dual circulating fluidized-bed steam gasifier of biomass using quasi-equilibrium three-stage gasification model', *Applied Energy*, 88(12), 5208-5220.
- Nguyen, T. D. B., Ngo, S. I., Lim, Y.-I., Lee, J. W., Lee, U.-D. and Song, B.-H. (2012) 'Three-stage steady-state model for biomass gasification in a dual circulating fluidized-bed', *Energy Conversion and Management*, 54(1), 100-112.
- Nikoo, M. B. and Mahinpey, N. (2008) 'Simulation of biomass gasification in fluidized bed reactor using ASPEN PLUS', *Biomass and Bioenergy*, 32(12), 1245-1254.
- Nunn, T. R., Howard, J. B., Longwell, J. P. and Peters, W. A. (1985) 'Product compositions and kinetics in the rapid pyrolysis of sweet gum hardwood', *Industrial & Engineering Chemistry Process Design and Development*, 24(3), 836-844.
- Petersen, I. and Werther, J. (2005a) 'Experimental investigation and modeling of gasification of sewage sludge in the circulating fluidized bed', *Chemical Engineering and Processing: Process Intensification*, 44(7), 717-736.
- Petersen, I. and Werther, J. (2005b) 'Three-dimensional modeling of a circulating fluidized bed gasifier for sewage sludge', *Chemical Engineering Science*, 60(16), 4469-4484.
- Pfeifer, C. and Hofbauer, H. (2008) 'Development of catalytic tar decomposition downstream from a dual fluidized bed biomass steam gasifier', *Powder Technology*, 180(1-2), 9-16.

- Radmanesh, R., Chaouki, J. and Guy, C. (2006) 'Biomass gasification in a bubbling fluidized bed reactor: Experiments and modeling', *AIChE Journal*, 52(12), 4258-4272.
- Ragland, K. W., Aerts, D. J. and Baker, A. J. (1991) 'Properties of wood for combustion analysis', *Bioresource Technology*, 37(2), 161-168.
- Rath, J. and Staudinger, G. (2001) 'Cracking reactions of tar from pyrolysis of spruce wood', *Fuel*, 80(10), 1379-1389.
- Roberts, A. F. and Clough, G. (1963) 'Thermal decomposition of wood in an inert atmosphere', *Symposium (International) on Combustion*, 9(1), 158-166.
- Sabbaghan, H., Sotudeh-Gharebagh, R. and Mostoufi, N. (2004) 'Modeling the acceleration zone in the riser of circulating fluidized beds', *Powder Technology*, 142(2-3), 129-135.
- Sánchez-Delgado, S., Almendros-Ibáñez, J. A., García-Hernando, N. and Santana, D. (2011) 'On the minimum fluidization velocity in 2D fluidized beds', *Powder Technology*, 207(1-3), 145-153.
- Sanz, A. and Corella, J. (2006) 'Modeling circulating fluidized bed biomass gasifiers. Results from a pseudo-rigorous 1-dimensional model for stationary state', *Fuel Processing Technology*, 87(3), 247-258.
- Saw, W., McKinnon, H., Gilmour, I. and Pang, S. (2012) 'Production of hydrogen-rich syngas from steam gasification of blend of biosolids and wood using a dual fluidised bed gasifier', *Fuel*, 93(0), 473-478.
- Saxena, S. C. (1990) 'Devolatilization and combustion characteristics of coal particles', *Progress in Energy and Combustion Science*, 16(1), 55-94.
- Schaeffer, D. G. (1987) 'Instability in the evolution equations describing incompressible granular flow', *Journal of Differential Equations*, 66(1), 19-50.
- Seebauer, V. (1999) *Experimentelle Untersuchungen zur Pyrolyse von Kohle und Holz*, unpublished thesis Graz University of Technology.
- Seo, M. W., Nguyen, T. D. B., Lim, Y. I., Kim, S. D., Park, S., Song, B. H. and Kim, Y. J. (2011) 'Solid circulation and loop-seal characteristics of a dual circulating fluidized bed: Experiments and CFD simulation', *Chemical Engineering Journal*, 168(2), 803-811.

- Shafizadeh, F. (1984) 'The Chemistry of Pyrolysis and Combustion' in *The Chemistry of Solid Wood*, American Chemical Society, 489-529.
- Shafizadeh, F. and Chin, P. (1977) 'Thermal Deterioration of Wood' in Goldstein, I. S., ed. *Wood Technology: Chemical Aspects*, 57-81.
- Shih, T.-H., Liou, W. W., Shabbir, A., Yang, Z. and Zhu, J. (1995) 'A new  $k-\epsilon$  eddy viscosity model for high reynolds number turbulent flows', *Computers & Fluids*, 24(3), 227-238.
- Siedlecki, M., Nieuwstraten, R., Simeone, E., de Jong, W. and Verkooijen, A. H. M. (2009) 'Effect of Magnesite as Bed Material in a 100 kWth Steam–Oxygen Blown Circulating Fluidized-Bed Biomass Gasifier on Gas Composition and Tar Formation', *Energy & Fuels*, 23(11), 5643-5654.
- Solomon, P. R., Hamblen, D. G., Carangelo, R. M., Serio, M. A. and Deshpande, G. V. (1988) 'General model of coal devolatilization', *Energy & Fuels*, 2(4), 405-422.
- Srivastava, A. and Sundaresan, S. (2003) 'Analysis of a frictional–kinetic model for gas–particle flow', *Powder Technology*, 129(1–3), 72-85.
- Syamlal, M. (1987) *The Particle-Particle Drag Term in a Multiparticle Model of Fluidization*, United States: EG and G Washington Analytical Services Center, Inc., Morgantown, WV (USA).
- Syamlal, M. and Bisset, L. (1991) *METC Gasifier Advanced Simulation (MGAS) Model*, U.S. Department of Energy Office of Fossil Energy, Morgantown Energy Technology Center P.O. Box 880, Morgantown, West Virginia 26507-0880.
- Syamlal, M. and O'Brien, T. (1987) *Derivation of a drag coefficient from velocity–voidage correlation*, U.S., Morgantown, West Virginia.: U.S. Department of Energy, Office of Fossil Energy, National Energy Technology Laboratory.
- Syamlal, M. and O'Brien, T. (1989) 'Computer Simulation of Bubbles in a Fluidized Bed', *AIChE Symp. Series*, 85, 22–31.
- Syamlal, M., Rogers, W. and O'Brien, T. (1993) *MFIX Documentation, Theory Guide*, U.S. Department of Energy, Office of Fossil Energy, Morgantown Energy Technology Center, Morgantown, West Virginia.
- Tang, Y.-l., Liu, D.-j., Liu, Y.-h. and Luo, Q. (2010) '3D Computational Fluid Dynamics Simulation of Natural Coke Steam Gasification in General and Improved Fluidized Beds', *Energy & Fuels*, 24(10), 5602-5610.

- Telmo, C., Lousada, J. and Moreira, N. (2010) 'Proximate analysis, backwards stepwise regression between gross calorific value, ultimate and chemical analysis of wood', *Bioresource Technology*, 101(11), 3808-3815.
- Tinaut, F. V., Melgar, A., Pérez, J. F. and Horrillo, A. (2008) 'Effect of biomass particle size and air superficial velocity on the gasification process in a downdraft fixed bed gasifier. An experimental and modelling study', *Fuel Processing Technology*, 89(11), 1076-1089.
- Van de Velden, M., Baeyens, J., Seville, J. P. K. and Fan, X. (2008) 'The solids flow in the riser of a Circulating Fluidised Bed (CFB) viewed by Positron Emission Particle Tracking (PEPT)', *Powder Technology*, 183(2), 290-296.
- van Ommen, J. R., Sasic, S., van der Schaaf, J., Gheorghiu, S., Johnsson, F. and Coppens, M.-O. (2011) 'Time-series analysis of pressure fluctuations in gas–solid fluidized beds – A review', *International Journal of Multiphase Flow*, 37(5), 403-428.
- Wang, L., Weller, C. L., Hanna, M. A. and American Institute of Chemical Engineers, M. (2005) 'An integrated mathematical model of fluid dynamics, heat transfer and reaction kinetics for fluidized bed gasification of sorghum DDG',
- Wang, Q., Lu, J., Yin, W., Yang, H. and Wei, L. (2013) 'Numerical study of gas–solid flow in a coal beneficiation fluidized bed using kinetic theory of granular flow', *Fuel Processing Technology*, 111(0), 29-41.
- Wang, Y. and Yan, L. (2008) 'CFD modeling of a fluidized bed sewage sludge gasifier for syngas', *Asia-Pacific Journal of Chemical Engineering*, 3(2), 161-170.
- Wei, L., Xu, S., Zhang, L., Liu, C., Zhu, H. and Liu, S. (2007) 'Steam gasification of biomass for hydrogen-rich gas in a free-fall reactor', *International Journal of Hydrogen Energy*, 32(1), 24-31.
- Wen, C., Chen, H. and Onozaki, M. (1982) *User's manual for computer simulation and design of the moving bed coal gasifier*, United States Department of Energy, Morgantown Energy Technology Center, Morgantown, West Virginia.
- Wen, C. and Yu, Y. (1966) 'Mechanics of Fluidization', *Chem. Eng. Prog. Symp. Series*, 62, 100-111.
- Westbrook, C. K. and Dryer, F. L. (1984) 'Chemical kinetic modeling of hydrocarbon combustion', *Progress in Energy and Combustion Science*, 10(1), 1-57.
- Wu, C.-z., Yin, X.-l., Ma, L.-l., Zhou, Z.-q. and Chen, H.-p. (2009) 'Operational characteristics of a 1.2-MW biomass gasification and power generation plant', *Biotechnology Advances*, 27(5), 588-592.

- Yakhot, V. and Orszag, S. (1986) 'Renormalization group analysis of turbulence. I. Basic theory', *Journal of Scientific Computing*, 1(1), 3-51.
- Yan, A., Pärssinen, J. H. and Zhu, J.-X. (2003) 'Flow properties in the entrance and exit regions of a high-flux circulating fluidized bed riser', *Powder Technology*, 131(2–3), 256-263.
- Yin, X. and Sundaresan, S. (2009) 'Fluid-particle drag in low-Reynolds-number polydisperse gas–solid suspensions', *AIChE Journal*, 55(6), 1352-1368.
- Zhong, H., Gao, J., Xu, C. and Lan, X. (2012) 'CFD modeling the hydrodynamics of binary particle mixtures in bubbling fluidized beds: Effect of wall boundary condition', *Powder Technology*, 230(0), 232-240.
- Zhou, W., Zhao, C. S., Duan, L. B., Qu, C. R. and Chen, X. P. (2011) 'Two-dimensional computational fluid dynamics simulation of coal combustion in a circulating fluidized bed combustor', *Chemical Engineering Journal*, 166(1), 306-314.
- Zimmermann, S. and Taghipour, F. (2005) 'CFD modeling of hydrodynamics and reaction kinetics of FCC fluidized bed reactors', *Industrial & Engineering Chemistry Research*, 44, 9818–9827.

## List of Publications

### Proposed journal papers:

1. **Makkawi, Y.** and Hassan, M., Computational fluid dynamic model for biomass gasification in a Circulating Fluidized Bed- I: Hydrodynamics.
2. **Makkawi, Y.** and Hassan, M., Computational fluid dynamic model for biomass gasification in a Circulating Fluidized Bed- II: Developing the reactive model, comparison and sensitivity analysis.
3. **Makkawi, Y.** and Hassan, M., Computational fluid dynamic model for biomass gasification in a Circulating Fluidized Bed- III: Parametric analysis.

### Conference papers:

1. **Makkawi, Y.**, Hassan, M., Modelling and simulation of biomass thermal conversion to hydrogen-rich gas in a short circulating fluidized bed riser. BioEnergy IV: Innovations in Biomass Conversion for Heat, Power, Fuels and Chemicals, June 2-7, 2013, Otranto, Italy.

## Appendix A: Sample of raw PEPT data

Time, ms	Pos X, mm	Pos Y, mm	Pos Z, mm	Vel X, mm/ms	Vel Y, mm/ms	Vel Z mm/ms
72.2	31.3	39.8	55.9	0.361686	0.367904	-0.039258
82.1	35.8	43.1	64	0.384552	0.364052	-0.036111
94.1	42.3	47.7	60	0.377185	0.357964	-0.024678
101.4	45.7	51.2	60.9	0.35164	0.350976	-0.040303
106.8	47	53.1	61	0.314449	0.355919	-0.107815
113.1	48.1	54.2	61.8	0.289349	0.369193	-0.209378
119.3	49.1	55.5	61	0.285939	0.395807	-0.344228
125.8	49.7	59.1	56.9	0.297994	0.426437	-0.428087
132.3	52.8	62.3	53	0.306791	0.448477	-0.475162
138.3	56.2	65.3	46.2	0.287991	0.440732	-0.475326
144.5	59.1	68.7	45.2	0.238163	0.399123	-0.439894
153.5	60.1	73.5	40.2	0.158723	0.326735	-0.418313
159.3	60.2	74.3	43.8	0.072343	0.23832	-0.412098
164.3	60.8	74.9	41.4	-0.010248	0.155106	-0.414006
170.4	59.4	74.5	31.8	-0.07205	0.091255	-0.399544
176.9	58.8	74.9	32.2	-0.121711	0.059258	-0.368798
179.7	58.4	75.4	30.8	-0.159784	0.047986	-0.305713
184.9	57.8	75.2	30.4	-0.193925	0.058297	-0.247963
191	56.1	75.3	30.2	-0.233699	0.070161	-0.210353
195.8	55.7	75.7	29	-0.27068	0.087383	-0.176576
200.8	53.6	77.2	26.8	-0.305606	0.102307	-0.159956
205.3	51.7	76.8	24.4	-0.328381	0.112246	-0.12933
210.9	50.5	77.4	27.5	-0.343826	0.115724	-0.09986
217	47.7	78.2	26	-0.348923	0.111118	-0.091266
222.2	45.3	80.1	24.5	-0.361406	0.103276	-0.095651
225.7	45	79.8	25.3	-0.384933	0.092258	-0.111103
230.1	44.5	79	25.5	-0.420901	0.08557	-0.125072
238.4	39.8	80	23.8	-0.465093	0.07655	-0.122064
242.6	37.4	81.4	19.5	-0.506178	0.070584	-0.095777
245.7	35.9	81.6	22.4	-0.529099	0.061516	-0.062192
250.4	32.9	80.8	25	-0.521703	0.053768	-0.025667
255	29.7	81.3	20.1	-0.487332	0.038816	0.001856
259.8	28.2	81.8	21.1	-0.427301	0.015766	-0.009091
265	25.4	82	23.8	-0.362809	-0.016423	-0.016294
267.4	24.8	81.8	23.6	-0.308887	-0.063017	-0.023378
272.6	24.6	82.3	21.3	-0.269717	-0.111872	-0.00772
278	23.1	80.8	21.4	-0.242267	-0.157192	0.05676
285.2	21	78.6	19.6	-0.217499	-0.187497	0.132686
288	19.7	79	22.1	-0.186997	-0.196212	0.209108
293	19.2	77.3	25.6	-0.151233	-0.181309	0.252296
296.7	18.9	76.3	26.6	-0.120996	-0.154256	0.248042
302.3	18.5	75.4	27.7	-0.095985	-0.109668	0.210696

## Appendix B: User Defined Function for the heterogeneous reactions

```
/******      Biomass Gasification Model      *****/
/*
          Version: 2.0

Programmer(s): Fluent
Date : 2009
Modified By: Mohamed Hassan
Reviewer(s): Dr Yassir Makkawi
Date : 2011

/* ----- */

#include "udf.h"
#include "stdio.h"
#include "time.h"

#define SMALL_S 1.e-29
#define eps_g_small 0.99999
#define spe_small 1.e-8
#define TMAX 2500.

static const real Arrhenius_devolatilization = 1.1e+5;
static const real E_Activation_devolatilization = 8.86e+7;
static const real Arrhenius_steamr = 3.42; /* From S. Gerber et al. / Fuel 89 (2010)
2903–2917 for C +H2O => CO + H2 */
static const real E_Activation_steamr = -15600.; /* From S. Gerber et al. / Fuel 89
(2010) 2903–2917 for C +H2O => CO + H2 */
static const real Arrhenius_steamr1 = 3.42; /* From S. Gerber et al. / Fuel 89 (2010)
2903–2917 for C +CO2 => 2CO*/
static const real E_Activation_steamr1 = -15600.; /* From S. Gerber et al. / Fuel 89
(2010) 2903–2917 for C +CO2 => 2CO */
static const real Arrhenius_steamr2 = 3.42e-3; /* From S. Gerber et al. / Fuel 89
(2010) 2903–2917 for C +2H2 => CH4 */
static const real E_Activation_steamr2 = -15600.; /* From S. Gerber et al. / Fuel 89
(2010) 2903–2917 for C +2H2 => CH4*/
static const real Arrhenius_tardevolatilization = 2.3000e+4;
static const real E_Activation_tardevolatilization = 8.0000e+4;

static const real c_devol_pre = 1., c_devol_exp = 1.;
static const real c_char_comb = 1; /* control the char combustion rate */

static cxboolean init_flag = TRUE;

/* Search the index for each species */
static real mw[MAX_PHASES][MAX_SPE_EQNS];
static int INDEX_PHASE_CH4 = 0, INDEX_SPECIES_CH4 = 0, INDEX_PHASE_CO =
0, INDEX_SPECIES_CO = 0,
      INDEX_PHASE_CO2 = 0, INDEX_SPECIES_CO2 = 0, INDEX_PHASE_H2 = 0,
INDEX_SPECIES_H2 = 0,
```

```

INDEX_PHASE_H2O = 0, INDEX_SPECIES_H2O = 0, INDEX_PHASE_O2 = 0,
INDEX_SPECIES_O2 = 0,
INDEX_PHASE_H2S = 0, INDEX_SPECIES_H2S = 0, INDEX_PHASE_CL2 = 0,
INDEX_SPECIES_CL2 = 0,
INDEX_PHASE_NH3 = 0, INDEX_SPECIES_NH3 = 0, INDEX_PHASE_N2 = 0,
INDEX_SPECIES_N2 = 0,
INDEX_PHASE_TAR = 0, INDEX_SPECIES_TAR = 0, INDEX_PHASE_C = 0,
INDEX_SPECIES_C = 0,
INDEX_PHASE_VOL = 0, INDEX_SPECIES_VOL = 0, INDEX_PHASE_TARINERT
= 0, INDEX_SPECIES_TARINERT = 0,
INDEX_PHASE_MOISTURE = 0, INDEX_SPECIES_MOISTURE = 0,
INDEX_PHASE_ASH = 0, INDEX_SPECIES_ASH = 0;

```

```

DEFINE_ADJUST(gasification, domain)

```

```

{

```

```

    int n, ns;
    Domain *subdomain;

```

```

    /*int n_phases = DOMAIN_N_DOMAINS(domain);*/

```

```

    if(init_flag)
    {

```

```

#ifdef IRP_HOST

```

```

    /* search all the species and saved the Molecular Weight */
    sub_domain_loop(subdomain, domain, n)

```

```

    {

```

```

        Material *m_mat, *s_mat;

```

```

        if (DOMAIN_NSPE(subdomain) > 0)

```

```

        {

```

```

            m_mat = Pick_Material(DOMAIN_MATERIAL_NAME(subdomain), NULL);
            mixture_species_loop(m_mat, s_mat, ns)

```

```

            {

```

```

                if (0 == strcmp(MIXTURE_SPECIE_NAME(m_mat, ns), "ch4"))

```

```

                {

```

```

                    INDEX_PHASE_CH4 = n;

```

```

                    INDEX_SPECIES_CH4 = ns;

```

```

                }

```

```

                else if (0 == strcmp(MIXTURE_SPECIE_NAME(m_mat, ns), "co"))

```

```

                {

```

```

                    INDEX_PHASE_CO = n;

```

```

                    INDEX_SPECIES_CO = ns;

```

```

                }

```

```

                else if (0 == strcmp(MIXTURE_SPECIE_NAME(m_mat, ns), "co2"))

```

```

                {

```

```

                    INDEX_PHASE_CO2 = n;

```

```

                    INDEX_SPECIES_CO2 = ns;

```

```

                }

```

```

                else if (0 == strcmp(MIXTURE_SPECIE_NAME(m_mat, ns), "h2"))

```

```

                {

```

```

                    INDEX_PHASE_H2 = n;

```

```

        INDEX_SPECIES_H2 = ns;
    }
else if (0 == strcmp(MIXTURE_SPECIE_NAME(m_mat,ns),"h2o"))
    {
        INDEX_PHASE_H2O = n;
        INDEX_SPECIES_H2O = ns;
    }
else if (0 == strcmp(MIXTURE_SPECIE_NAME(m_mat,ns),"o2"))
    {
        INDEX_PHASE_O2 = n;
        INDEX_SPECIES_O2 = ns;
    }
else if (0 == strcmp(MIXTURE_SPECIE_NAME(m_mat,ns),"h2s"))
    {
        INDEX_PHASE_H2S = n;
        INDEX_SPECIES_H2S = ns;
    }
else if (0 == strcmp(MIXTURE_SPECIE_NAME(m_mat,ns),"cl2"))
    {
        INDEX_PHASE_CL2 = n;
        INDEX_SPECIES_CL2 = ns;
    }
else if (0 == strcmp(MIXTURE_SPECIE_NAME(m_mat,ns),"nh3"))
    {
        INDEX_PHASE_NH3 = n;
        INDEX_SPECIES_NH3 = ns;
    }
else if (0 == strcmp(MIXTURE_SPECIE_NAME(m_mat,ns),"n2"))
    {
        INDEX_PHASE_N2 = n;
        INDEX_SPECIES_N2 = ns;
    }
else if (0 == strcmp(MIXTURE_SPECIE_NAME(m_mat,ns),"tar"))
    {
        INDEX_PHASE_TAR = n;
        INDEX_SPECIES_TAR = ns;
    }
else if (0 == strcmp(MIXTURE_SPECIE_NAME(m_mat,ns),"c"))
    {
        INDEX_PHASE_C = n;
        INDEX_SPECIES_C = ns;
    }
else if (0 == strcmp(MIXTURE_SPECIE_NAME(m_mat,ns),"volatile"))
    {
        INDEX_PHASE_VOL = n;
        INDEX_SPECIES_VOL = ns;
    }
else if (0 == strcmp(MIXTURE_SPECIE_NAME(m_mat,ns),"h2o<l>"))
    {
        INDEX_PHASE_MOISTURE = n;
        INDEX_SPECIES_MOISTURE = ns;
    }

```

```

else if (0 == strcmp(MIXTURE_SPECIE_NAME(m_mat,ns),"ash-
coal"))
    {
        INDEX_PHASE_ASH = n;
        INDEX_SPECIES_ASH = ns;
    }
else if (0 ==
strcmp(MIXTURE_SPECIE_NAME(m_mat,ns),"TARINERT"))
    {
        INDEX_PHASE_TARINERT = n;
        INDEX_SPECIES_TARINERT = ns;
    }

CX_Message ("\n --- %d %d, %d %d, %d %d, %d
%d,%d %d, %d %d, %d %d, %d %d, %d %d,%d %d, %d %d, %d %d,
%d %d\n",
INDEX_PHASE_CO2, INDEX_SPECIES_CO2,
INDEX_PHASE_H2, INDEX_SPECIES_H2,
INDEX_PHASE_CH4,
INDEX_SPECIES_CH4,INDEX_PHASE_CO, INDEX_SPECIES_CO,
INDEX_PHASE_H2O, INDEX_SPECIES_H2O,
INDEX_PHASE_O2, INDEX_SPECIES_O2,
INDEX_PHASE_H2S, INDEX_SPECIES_H2S,
INDEX_PHASE_CL2, INDEX_SPECIES_CL2,
INDEX_PHASE_NH3, INDEX_SPECIES_NH3,
INDEX_PHASE_N2, INDEX_SPECIES_N2,
INDEX_PHASE_TAR, INDEX_SPECIES_TAR,
INDEX_PHASE_C, INDEX_SPECIES_C,
INDEX_PHASE_VOL, INDEX_SPECIES_VOL,
INDEX_PHASE_TARINERT, INDEX_SPECIES_TARINERT,
INDEX_PHASE_MOISTURE, INDEX_SPECIES_MOISTURE,
INDEX_PHASE_ASH, INDEX_SPECIES_ASH);

mw[n][ns] = MATERIAL_PROP(s_mat,PROP_mwi);
}
}
else
{
s_mat = Pick_Material(DOMAIN_MATERIAL_NAME(subdomain),NULL);
mw[n][0] = MATERIAL_PROP(s_mat,PROP_mwi);
}
}

#endif

init_flag = FALSE;
/* to calculate some commonly used values here in order to save the CPU time */

}

}

```

```

DEFINE_HET_RXN_RATE(devolatilization,c,t,hr,mw,yi,rr,rr_t)
{
  Thread **pt = THREAD_SUB_THREADS(t);
  Thread *tp = pt[0]; /* gas phase */
  Thread *ts = pt[1]; /* solid phase */

  real prod;
  real x0_star = 0., x_star =0.;
  real T = MAX(273.,C_T(c,ts));
  real T_SAT = 373.15;

  *rr = 0;
  prod =0.;
  if(T>TMAX) T = TMAX;
  if(T > T_SAT)
  {
    if(C_VOF(c, tp) < eps_g_small &&
    yi[INDEX_PHASE_VOL][INDEX_SPECIES_VOL] > spe_small)
    {
      prod = (yi[INDEX_PHASE_VOL][INDEX_SPECIES_VOL]-
      x_star)*C_R(c,ts)/mw[INDEX_PHASE_VOL][INDEX_SPECIES_VOL];

      *rr = c_devol_pre * Arrhenius_devolatilization *
      exp(- c_devol_exp / (UNIVERSAL_GAS_CONSTANT*T)) *
      prod*C_VOF(c, ts); /* kmol/(m3.s) */ } }}

DEFINE_HET_RXN_RATE(char_combustion,c,t,hr,mw,yi,rr,rr_t)
{
  Thread **pt = THREAD_SUB_THREADS(t);
  Thread *tp = pt[0]; /* gas phase */
  Thread *ts = pt[1]; /* solid phase */

  real T = MAX(273.,C_T(c,tp));
  real T_s = MAX(273.,C_T(c,ts));
  real T_f;
  real Rgas = 82.06; /* atm.cm^3/mol.K */ /*UNIVERSAL_GAS_CONSTANT;*/

  real p_o2 = 0.;
  real k_f, k_a, k_r, diff, Sc1o3;
  real Pt = MAX(0.1, (op_pres+C_P(c,t))/101325);
  real Re, vrel, N_sherwood, rd;
  real D_p = C_PHASE_DIAMETER(c,ts); /* read in later ssp*/
  real y_carbon, y_ash;
  real ash_ar = 12., fc_ar = 45.;

  real factor;
  /* Void Fraction of Ash Layer */
  real ep_a = 0.25 + 0.75*(1-ash_ar/100.);
  real f_ep_a = pow(ep_a,2.5);

```

```

/*
!      2C + O2 --> 2CO      kg-mole/(m^3.s)
!
!      Wen at al. (1982), Syamlal and Bissett (1992), Syamlal (1993)
!      Intrinsic rate from Desai and Wen (1978), originally from
!      Sergeant and Smith (1973).
!
*/

*rr = 0;

T = MIN(T,TMAX);
T_s = MIN(T_s,TMAX);
if(C_VOF(c, tp) < eps_g_small && yi[INDEX_PHASE_C][INDEX_SPECIES_C] >
spe_small && yi[INDEX_PHASE_O2][INDEX_SPECIES_O2] > spe_small)
{
  y_carbon = yi[INDEX_PHASE_C][INDEX_SPECIES_C];
  y_ash = yi[INDEX_PHASE_ASH][INDEX_SPECIES_ASH];

  p_o2
C_R(c,tp)*UNIVERSAL_GAS_CONSTANT*C_T(c,tp)*yi[INDEX_PHASE_O2][INDEX_
SPECIES_O2]
  /mw[INDEX_PHASE_O2][INDEX_SPECIES_O2] / 101325.;

  if(fc_ar > 0.)
  {
    if (y_carbon > 0.)
    {
      rd = pow( (y_carbon * ash_ar/100.)/(y_ash * fc_ar/100.), (1./3.));
      rd = MIN(1., rd);
    }
    else rd = 0.;
  }
  else rd = 0.;

  diff =4.26 * pow((T/1800.),1.75)/Pt; /* cm^2/s */
  diff = MAX(diff, 1.e-10);
  Sc1o3 = pow(C_MU_L(c,tp)/(C_R(c,tp) * diff * 1.e-4), 1./3.);
  vrel = pow( ( (C_U(c,tp)-C_U(c,ts))*(C_U(c,tp)-C_U(c,ts)) +
(C_V(c,tp)-C_V(c,ts))*(C_V(c,tp)-C_V(c,ts)) +
(C_W(c,tp)-C_W(c,ts))*(C_W(c,tp)-C_W(c,ts)) ), 0.5);
  Re = C_VOF(c,tp) * D_p * vrel * C_R(c,tp)/(C_MU_L(c,tp)+SMALL_S);
  N_sherwood = 4.; /*(7. - 10. * C_VOF(c,tp) + 5. * C_VOF(c,tp) * C_VOF(c,tp) ) *
(1. + 0.7 * pow(Re, 0.2) * Sc1o3)
+
(1.33 - 2.4 * C_VOF(c,tp) + 1.2 * C_VOF(c,tp) * C_VOF(c,tp)) *
pow(Re, 0.7) * Sc1o3; */
  if ( rd <= 0. || C_VOF(c, ts) <= 0. )
  {
    *rr = 0.;
  }
  else
  {
    T_f = 0.5 * ( C_T(c,tp) + C_T(c,ts) );

```

```

T_f = MIN(T_f, TMAX);
k_f = diff * N_sherwood / (D_p * 1.e+2 *
Rgas/mw[INDEX_PHASE_O2][INDEX_SPECIES_O2] * T_f);
k_r = 8710. * exp( -27000/1.987/T_s ) * rd * rd;
if ( rd >= 1.)
{
*rr = 1. / (1./k_f + 1./k_r);
}
else
{
k_a = 2. * rd * diff * f_ep_a / (D_p * 1.e+2 * (1.-rd) *
Rgas/mw[INDEX_PHASE_O2][INDEX_SPECIES_O2] * T_s);
*rr = 1. / (1./k_f + 1./k_r + 1./k_a);
}
factor = y_carbon / (y_carbon + 1.e-6);
*rr = *rr * p_o2 * 6. * C_VOF(c,ts) * factor / (D_p * 1.e+2 * 32.); /* mol/(cm^3
.s) */
*rr = c_char_comb * *rr * 1000.; /* kmol/(m^3 .s) */ } }}

```

```

DEFINE_HET_RXN_RATE(steamr,c,t,hr,mw,yi,rr,rr_t)
{
Thread **pt = THREAD_SUB_THREADS(t);
Thread *tp = pt[0]; /* gas phase */
Thread *ts = pt[1]; /* solid phase */

real prodst;
real x0_star1 = 0., x_star1 =0.;
real T = MAX(273.,C_T(c,ts));
real T_SAT = 373.15;

*rr = 0;
prodst =0.;
if(T>TMAX) T = TMAX;
if(T > T_SAT)
{
if(C_VOF(c, tp) < eps_g_small &&
yi[INDEX_PHASE_H2O][INDEX_SPECIES_H2O] > spe_small)
{
prodst = (yi[INDEX_PHASE_H2O][INDEX_SPECIES_H2O]-
x_star1)*C_R(c,ts)/mw[INDEX_PHASE_H2O][INDEX_SPECIES_H2O];

*rr = T*Arrhenius_steamr *
exp(E_Activation_steamr/T)
* prodst*C_VOF(c, ts); /* kmol/(m3.s) */
}
}
}
}

```

```

DEFINE_HET_RXN_RATE(steamr1,c,t,hr,mw,yi,rr,rr_t)

```

```

{

Thread **pt = THREAD_SUB_THREADS(t);
Thread *tp = pt[0]; /* gas phase */
Thread *ts = pt[1]; /* solid phase */

real prodst1;
real x0_star1 = 0., x_star1 =0.;
real T = MAX(273.,C_T(c,ts));
real T_SAT = 373.15;

*rr = 0;
prodst1 =0.;
if(T>TMAX) T = TMAX;
if(T > T_SAT)
{
  if(C_VOF(c, tp) < eps_g_small &&
  yi[INDEX_PHASE_CO2][INDEX_SPECIES_CO2] > spe_small)
  {
    prodst1 = (yi[INDEX_PHASE_CO2][INDEX_SPECIES_CO2]-
x_star1)*C_R(c,ts)/mw[INDEX_PHASE_CO2][INDEX_SPECIES_CO2];

    *rr = T*Arrhenius_steamr1 *
    exp( E_Activation_steamr1/T)
    * prodst1*C_VOF(c, tp); /* kmol/(m3.s) */ }}

DEFINE_HET_RXN_RATE(steamr2,c,t,hr,mw,yi,rr,rr_t)
{

Thread **pt = THREAD_SUB_THREADS(t);
Thread *tp = pt[0]; /* gas phase */
Thread *ts = pt[1]; /* solid phase */

real prodst2;
real x0_star1 = 0., x_star1 =0.;
real T = MAX(273.,C_T(c,ts));
real T_SAT = 373.15;

*rr = 0;
prodst2 =0.;
if(T>TMAX) T = TMAX;
if(T > T_SAT)
{
  if(C_VOF(c, tp) < eps_g_small && yi[INDEX_PHASE_H2][INDEX_SPECIES_H2]
> spe_small)
  {
    prodst2 = (yi[INDEX_PHASE_H2][INDEX_SPECIES_H2]-
x_star1)*C_R(c,ts)/mw[INDEX_PHASE_H2][INDEX_SPECIES_H2];

    *rr = T*Arrhenius_steamr2 *
    exp( E_Activation_steamr2/T)
    * prodst2*C_VOF(c, tp); /* kmol/(m3.s) */ }}

```